



**Fakultät für Medizin**  
**Institut für Virologie**



## **Regulation of Hepatitis B virus X protein function by host SUMOylation processes as a basis for novel therapy approaches**

**Verena Alexandra Plank**

Vollständiger Abdruck der von der Fakultät für Medizin der Technischen Universität München zur Erlangung des akademischen Grades eines

**Doktors der Naturwissenschaften (Dr. rer. nat.)**

genehmigten Dissertation.

**Vorsitzender:** Prof. Dr. Dr. Stefan Engelhardt

**Prüfende/-r der Dissertation:**

1. Prof. Dr. Sabrina Schreiner
2. Prof. Dr. Percy Knolle

Die Dissertation wurde am 02.03.2021 bei der Technischen Universität München eingereicht und durch die Fakultät für Medizin am 08.06.2021 angenommen.



---

## Table of contents

Abbreviations.....	8
Abstract .....	13
Zusammenfassung .....	15
1. Introduction.....	17
1.1. Hepatitis B virus .....	17
1.1.1. Virus classification.....	17
1.1.2. Epidemiology and pathogenesis of Hepatitis B virus.....	18
1.1.3. Morphology and genome organization of Hepatitis B virus .....	19
1.1.4. Replication cycle of Hepatitis B virus .....	21
1.1.5. Formation and characterization of covalently closed circular DNA.....	24
1.1.6. Hepatitis B virus protein X (HBx).....	25
1.1.6.1. HBx putative protein domains and localization.....	27
1.1.6.2. HBx and viral replication .....	28
1.1.6.3. HBx promotes SMC5/6 degradation via CRL4 interaction .....	29
1.1.7. Current treatment approaches against HBV .....	30
1.2. PML-NBs comprise various biological processes.....	32
1.2.1. SUMO conjugating pathway .....	33
1.2.2. SUMO-targeted ubiquitin ligases RING-finger protein 4 .....	35
1.2.3. Arsenic trioxide .....	36
1.3. Aim of the study.....	38
2. Materials and Methods .....	39
2.1. Materials.....	39
2.1.1. Mammalian cell lines, cell culture media and bacterial strain .....	39
2.1.1.1. Mammalian cell lines.....	39
2.1.1.2. Cell culture media .....	40
2.1.1.3. Bacterial strain .....	42
2.1.2. Viruses .....	42
2.1.3. Nucleic acids .....	42
2.1.3.1. Recombinant plasmids.....	42
2.1.3.2. Oligonucleotides .....	47
2.1.4. Antibodies .....	49
2.1.4.1. Primary antibodies .....	49

---

2.1.4.2. Secondary antibodies .....	50
2.1.5. Enzymes and buffers .....	51
2.1.6. Chemicals and reagents .....	52
2.1.7. Laboratory equipment .....	55
2.1.8. Disposable laboratory equipment.....	58
2.1.9. Softwares and programs .....	59
2.2. Methods .....	61
2.2.1. Cell culture techniques.....	61
2.2.1.1. Maintenance of cell lines.....	61
2.2.1.2. Seeding of cells.....	61
2.2.1.3. Harvesting of cells.....	62
2.2.1.4. Storage of cells .....	62
2.2.1.5. Treatment with the proteasome inhibitor MG132 .....	63
2.2.2. Bacteria .....	63
2.2.2.1. Preparation of chemically competent bacteria .....	63
2.2.2.2. Heat shock transformation of chemically competent <i>E. coli</i> bacteria .	64
2.2.2.3. Storage and liquid bacterial culture.....	64
2.2.3. Hepatitis B virus infection.....	65
2.2.4. Protein biochemistry methods.....	65
2.2.4.1. Whole-cell protein lysates .....	65
2.2.4.2. Insoluble membranous fraction.....	66
2.2.4.3. Nickel-nitrilotriacetic acid (NiNTA) pulldown.....	66
2.2.4.4. Co-immunoprecipitation .....	68
2.2.4.5. Separating protein lysates by SDS-PAGE .....	69
2.2.4.6. Western blot.....	70
2.2.4.7. Immunofluorescence analysis.....	71
2.2.4.8. Determination of secreted HBeAg quantity by ELISA .....	71
2.2.4.9. Flow cytometry.....	72
2.2.4.10. Cell viability assay.....	72
2.2.5. DNA techniques .....	72
2.2.5.1. Polymerase chain reaction (PCR).....	72
2.2.5.2. Agarose gel electrophoresis and gel extraction of DNA.....	73
2.2.5.3 DNA precipitation .....	74

---

2.2.5.4. Digest of DNA .....	74
2.2.5.5. Ligation .....	74
2.2.2.6. Site-directed mutagenesis .....	75
2.2.2.7. Inverse PCR.....	75
2.2.5.8. Plasmid DNA preparation from <i>E.coli</i> .....	75
2.2.5.9. Sequencing of DNA .....	76
2.2.5.10. Plasmid transfection with Polyethylenimine .....	77
2.2.6. RNA techniques .....	77
2.2.6.1. Production of <i>in vitro</i> transcribed (IVT) mRNA .....	77
2.2.6.2. Lipofectamine transfection .....	78
2.2.7. DNA and RNA analysis .....	78
2.2.7.1. Preparation of total cellular DNA.....	78
2.2.7.2. RNA processing.....	79
2.2.7.2.1. Preparation of total cellular RNA .....	79
2.2.7.2.2. Reverse transcription of RNA into cDNA .....	79
2.2.7.3. Quantitative polymerase chain reaction .....	80
2.2.8. Statistical analysis.....	81
3. Results.....	82
3.1. <i>In silico</i> prediction and examination of HBx SUMO consensus motifs.....	82
3.2. Generation of HBx wt and SCM mutant expressing plasmids .....	84
3.3. Post-translational modification of HBx by SUMO2 moieties .....	88
3.3.1. HBx co-localizes with all SUMO paralogues in the hepatocyte nucleus....	88
3.3.2. HBx is a novel target for SUMO2 post-translational modification .....	90
3.3.3. SUMO2 dependent proteasomal degradation of HBx protein .....	91
3.4. Interplay between viral HBx proteins and PML.....	93
3.4.1. PML is a novel interaction partner of the HBx protein .....	93
3.4.2. HBx proteins alter PML-NB number and size.....	95
3.4.3. HBx protein is localized juxtaposed to transiently expressed single PML isoforms .....	98
3.4.4. Mutual shift of HBx proteins and PML isoforms to the insoluble matrix fraction concomitant with elevated expression of the viral factor .....	100
3.4.5. Increased HBx protein expression and mutual re-localization to the insoluble matrix fraction with PML isoforms in HepG2-NTCP-K7 shPML cell .....	102
3.4.6. Interaction between HBx proteins and PML isoforms.....	104

---

3.5. Crosstalk between viral HBx proteins and PML-NB associated host proteins .....	106
3.5.1. Sp100A represents a PML-NB component that binds HBx .....	106
3.5.2. Analysis of a novel crosstalk between the host STUbL RNF4 and viral HBx .....	108
3.5.2.1. RNF4 induces HBx localization to the membranous fraction .....	108
3.5.2.2. HBx protein expression affects RNF4 localization .....	109
3.5.2.3. RNF4 as a novel interaction partner of HBx.....	110
3.5.3. Novel interplay between the PML-NBs and the CRL4-HBx complex .....	112
3.5.3.1. Cellular Cul4 proteins are found within PML-NBs .....	112
3.5.3.2. Transiently expressed HBx modulated Cul4 nuclear localization.....	114
3.5.3.3. PML modulates HBx binding with DDB1 .....	117
3.6. Identification of the relevant HBx SUMO conjugation motif .....	119
3.6.1. Structure comparison of predicted HBx SUMO conjugation motif within HBx .....	119
3.6.2. HBx is efficiently SUMOylated at the SCM1/2.....	120
3.6.3. Re-localization of HBx SCM1/2 mutant from PML-NBs.....	122
3.6.4. Cul4 only co-localizes with SUMO conjugated HBx variants.....	126
3.6.5. HBx-DDB1 interaction is promoted by less SUMOylated HBx proteins...	129
3.6.6. HBx SUMOylation status irrelevant for alteration of endogenous protein expression levels .....	131
3.6.7. HBx SUMOylation is a prerequisite for cccDNA conversion and maintenance .....	133
3.7. ATO is a potential treatment candidate to reduce HBV chronic cccDNA reservoirs .....	135
3.7.1. ATO represses expression of Hepatitis B virus proteins .....	135
3.7.1.1. Cell viability assay during ATO administration .....	135
3.7.1.2. Dose-dependent elevation of HBx by ATO .....	136
3.7.1.3. Accumulation of nuclear HBx during ATO administration .....	137
3.7.1.4. ATO treatment induces dose-dependent reduction of transfected core .....	139
3.7.1.5. Re-localization of core during ATO application .....	141
3.7.1.6. Efficient core reduction by ATO in SUMO2 overexpressing cells.....	142
3.7.2. ATO counteracts acute HBV infections .....	145

---

3.7.2.1. ATO efficiently inhibits HBV core expression .....	145
3.7.2.2. ATO administration induces diminution of HBV core <sup>+</sup> cells and mean fluorescence intensity .....	146
3.7.2.3. Decreased core protein expression levels during ATO administration .....	147
3.7.2.4. Nuclear HBV core vanished during ATO application.....	149
3.7.2.5. Dose-dependent loss of HBV mRNA, DNA, cccDNA and HBeAg levels by ATO early and late after HBV infection .....	150
3.7.3. Established HBV infections suppressed during ATO administration .....	152
3.7.3.1. Dose-dependent reduction of established core protein by ATO administration .....	152
3.7.3.2. Re-localization of HBV core during ATO treatment.....	154
3.7.3.3. ATO induced reduction of HBV mRNA, DNA, cccDNA and HBeAg secretion .....	155
4. Discussion .....	157
4.1. <i>In silico</i> prediction and examination of HBx SUMO consensus motifs.....	157
4.2. Generation of expression plasmids encoding SUMOylation deficient HBx-variants.....	158
4.3. Post-translational modification of HBx by SUMO2 moieties .....	160
4.4. Interplay between viral HBx proteins and PML.....	160
4.5. Crosstalk between viral HBx proteins and PML-NB associated host proteins .....	162
4.6. Identification of the relevant HBx SUMO conjugation motif .....	164
4.7. Discovery of ATO as a novel treatment against HBV .....	167
4.8. Summary and concluding remarks .....	171
5. Addendum .....	173
5.1. Figure legend .....	173
5.2. Table legend.....	175
6. References .....	176

**Abbreviations**

3D	3-dimensional
μM	Micromolar
aa	Amino acid
AdV	Adenovirus
APS	Ammonium persulfate
ASPP	Apoptosis-stimulating protein of p53
ATF	Activating transcription factor
ATP	Adenosine triphosphate
ATRX	Alpha thalassemia/mental retardation syndrome X-linked
BSA	Bovine serum albumin
cccDNA	Covalently closed circular DNA
CREB	cAMP response element-binding protein
CMV	Cytomegalovirus
CRL4	Cullin 4A RING E3 ubiquitin ligase
DAPI	4',6-Diamidin-2-phenylindol dihydrochloride
Daxx	Death domain-associated protein
DCAF	DDB1 Cullin Accessory Factor
DDR	DNA damage response
DHBV	Duck Hepatitis B virus
DMEM	Dulbecco's Modified Eagle's Medium
DMSO	Dimethyl sulfoxide
DNA	Deoxyribonucleic acid
dpi	Days post-infection
DR1	Direct repeat 1
DR2	Direct repeat 2
dsDNA	Double-stranded DNA
DZIF	Deutsches Zentrum für Infektionsforschung
E. coli	Escherichia coli
ECL	Enhanced chemiluminescence
EDTA	Ethylenediaminetetraacetic acid
ELISA	Enzyme-linked immunosorbent assay

ERK	Extracellular signal-regulated kinases
EtOH	Ethanol
FBS	Fetal Bovium Serum
ffu	Fluorescence forming unit
FSC	Forwards Scatter
fwd	Forward
GAG	Glycosaminoglycans
GAPDH	Glyceraldehyde-3-phosphate dehydrogenase gene
GFP	Green fluorescent protein
h	Hour
HAdV	Human Adenovirus
HBc	Hepatitis B core antigen
HBeAg	Hepatitis B e antigen
HBsAg	Hepatitis B surface antigen
HBV	Hepatitis B virus
HBx	Hepatitis B x protein
HCC	Hepatocellular carcinoma
HCV	Hepatitis C virus
HIF	Hypoxia-inducible factor
HAdV	Human adenovirus
His	Histidine
IF	Immunofluorescence
IFN	Interferon
IL	Interleukin
IP	Immunoprecipitation
ITR	Inverted terminal repeat
IU	Infectious units
IVT	In vitro transcribed
K	Lysine
kb	Kilobase
kDa	Kilodalton
L protein, LHBs	Large HBV surface protein
LB	Luria-bertani

---

M protein, MHBs	Middle HBV surface protein
mA	Milliampere
MAPK	Mitogen activated protein kinase
mg	Milligram
min	Minute
ml	Milliliter
mM	Milimolar
MOI	Multiplicity of infection
mRNA	Messenger RNA
MVB	Multivesicular bodies
NaOAc	Sodium acetate
NaCl	Sodium chloride
NEAA	Non-essential amino acids
NES	Nuclear export signal
NF- $\kappa$ B	Nuclear factor kappa B
NiNTA	Nickel nitrilotriacetic acid
NLS	Nuclear localization site
nm	Nanometer
ns	Not significant
nt	Nucleotide
NTA	Nitrilotriacetic acid
NTCP	Sodium taurocholate co-transporting polypeptide
NUC	Nucleos(t)ide analogue
ORF	Open reading frame
P protein	Polymerase protein
p.i.	Post infection
p.t.	Post transfection
PAGE	Polyacrylamide gel electrophoresis
PBS	Phosphate buffered saline
PBS-T	Phosphate buffered saline Twen 20
PCAF	p300/CREB-binding protein-associated factor
PCR	Polymerase chain reaction
PEG	Polyethylene glycol

---

PEI	Polyethylenimine
PFA	Paraformaldehyde
pgRNA	Pregenomic RNA
PHH	Primary human hepatocytes
PIAS	Protein inhibitors of activated STAT
PKC	Protein kinase C
PML	Promyelocytic leukemia protein
PML-NB	Promyelocytic leukemia protein nuclear bodies
PMSF	Phenylmethylsulfonyl fluoride
PNK	Polynucleotide Kinase
PTM	Post-translational modification
qPCR	Quantitative polymerase chain reaction
RAR $\alpha$	Retino acid receptor $\alpha$
RBCC motif	RING, B-Box, coiled-coil domain
rcDNA	Relaxed-circular DNA
rev	Reverse
RING	Really interesting new gene
RIPA	Radioimmunoprecipitation assay
RNA	Ribonucleic acid
RNA pol II	RNA polymerase II
RNase	Ribonuclease
rpm	Rounds per minute
RT	Room temperature
s	Seconde
S protein, SHBs	Small HBV surface protein
SCM	SUMO consensus motif
SDS	Sodium dodecyl sulphate
SDS-PAGE	Sodium dodecyl sulfate polyacrylamide gel electrophoresis
SENP	SUMO-specific protease
shRNA	Short hairpin RNA
SIM	SUMO interacting motif
Smc	Structural maintenance of chromosomes
Sp100	Speckled protein 100

---

ss	Single-stranded
SSC	Sideward Scatter
STUbL	SUMO-targeted ubiquitin ligases
SUMO	Small ubiquitin-like modifier
SVP	Secretion of subviral particles
T	Thymine
TBS-BG	Tris-buffered saline with BSA and glycine
TEMED	N, N, N', N'-Tetra-methylethylenediamine
TGS	Tris, glycine, SDS
TP	Terminal Protein
Tris	Tris(hydroxymethyl)aminomethane
U	Unit
Ubc9	Ubiquitin carrier protein 9
UV	Ultraviolet
V	Volt
v/v	Volume per volume
vol	Volume
w/v	Weight per volume
wt	Wild type
YFP	Yellow fluorescent protein
µg	Microgram
µl	Microliter

## Abstract

Despite an available vaccination, still more than 257 million people worldwide are estimated to suffer from chronic hepatitis B infections, resulting in even more than 880.000 related deaths per year by liver cirrhosis or HCC. Since current treatments for chronic Hepatitis B virus (HBV) infection fail to eradicate the persistence reservoir, namely the covalently closed circular DNA (cccDNA) of HBV, novel treatment approaches are urgently required. Here, we suggest that the rcDNA to cccDNA conversion takes place at the SUMOylation hotspot foci in the cell nucleus, so-called PML-NBs. These multiprotein complexes are associated with host DDR proteins, which are required for cccDNA synthesis. Moreover, the HBx protein is mandatory factor for efficient cccDNA de-condensation and transcription. In a first part of this work, the post-translational modification of HBx by SUMO2 was shown. Furthermore, HBx was identified as a novel binding partner of PML, the PML-NB associated protein Sp100A and the SUMO-target ubiquitin ligase RNF4. Based on our work, we propose a model in which PML-NBs represent key factors during efficient HBV infection, whereupon Sp100A supports the HBx directed cccDNA opening and de-condensation. Moreover, the RING E3 ubiquitin ligase (CRL4) was discovered to also be associated with PML-NBs, which was already reported to mediate HBx-DDB1 interaction. Besides the important role of PML-NBs, SUMOylation of the HBx protein was shown and further investigated. We identified the potential SUMO conjugation motifs in the HBx open reading frame that might be conjugated with SUMO moieties. The HBx SCM1/2 was shown to be the main SUMOylation site within HBx, while at position SCM5 we discovered hyper-SUMOylation. Our data showed that HBx variants with a reduced SUMOylation elicited significantly lower cccDNA levels, revealing the importance of this post-translational modification for the HBV life cycle and persistence.

In the second part of this work, we focused on the treatment of HBV infections based on the novel findings we made in the first part and used arsenic trioxide (ATO) to specifically modulate PML-NBs and PML SUMOylation during HBV infection. ATO administration revealed efficient reduction of HBV parameters *in vitro*, such as HBV core protein levels, total HBV transcripts, HBeAg expression, total HBV DNA as well as cccDNA levels. The results of this thesis lead to the conclusion, that PML-NBs concomitant with post-translational modifications by SUMO have a fundamental impact

on HBx and the HBV infection processes since even the persistent cccDNA pool is affected. Moreover, the association of HBV components to PML-NBs permitted the successful treatment of HBV via ATO administration. Thus, ATO represents a promising novel antiviral therapy against acute and chronic HBV infections, which is urgently required.

## Zusammenfassung

Trotz einer wirkungsvollen Impfung gegen Hepatitis B Virus (HBV) leiden weltweit immer noch mehr als 257 Millionen Menschen an chronischen Hepatitis B Infektionen, was jährlich zu mehr als 880.000 Todesfällen durch HBV induzierte Leberzirrhose oder Hepatozelluläre Karzinomen führt. Da alle derzeitigen verfügbaren Behandlungsansätze die persistente DNA einer chronischen HBV Infektion, die kovalent geschlossene zirkuläre DNA (cccDNA) nicht bekämpfen können, sind neuartige Behandlungsansätze dringend erforderlich. Wir gehen davon aus, dass die Entstehung der cccDNA durch die Umwandlung der HBV rcDNA an PML-NBs stattfindet. Diese PML-NBs sind nukleäre Komplexe, auch SUMOylierungs Hotspots genannt, welche zahlreiche Proteine beinhalten wie zum Beispiel die SUMO Proteine selbst, aber auch Sp100 Proteine oder DANN Reparaturfaktoren, welche für die cccDNA Synthese unerlässlich sind. Darüber hinaus ist auch das HBx Protein ein obligatorischer Faktor für eine effiziente Öffnung der cccDNA und für die virale Transkription.

Im ersten Teil dieser Arbeit konnte die post-translationale Modifikation von HBx durch SUMO2 nachgewiesen werden. Des Weiteren konnte auch die Interaktion des HBx Proteins mit PML und dem PML-NB assoziierten Protein Sp100A festgestellt werden. Somit konnte gezeigt werden, dass PML-NBs eine wichtige Funktion während der HBV Infektion übernehmen, wobei das Protein Sp100A die HBx induzierte Öffnung der cccDNA für die darauffolgende Transkription unterstützt. Zudem konnte bewiesen werden, dass der Cullin 4A RING E3 ubiquitin ligase (CRL4) Komplex, welcher für die HBx-DDB1-Interaktion notwendig ist, auch mit PML-NBs assoziiert ist. Neben der wichtigen Rolle der PML-NBs wurde auch die SUMOylierung des HBx Proteins analysiert. Die HBx SCM 1/2 konnte dabei als SUMOylierungsstelle des HBx Proteins identifiziert werden, wobei die HBx-Mutante SCM5 hyper-SUMOyliert wird. Aufgrund dieser Ergebnisse wurde außerdem der Einfluss mutierter HBx SCM Stellen auf HBV Infektionen untersucht. Die HBx SUMOylierungs Mutante führte dabei zu signifikant niedrigeren cccDNA Mengen, als das wildtyp HBx Protein, was die große Bedeutung dieser post-translationalen Modifikation für die HBV Infektion und dessen Persistenz unterstreicht. Zusätzlich wurde gezeigt, dass die SUMO abhängige Ubiquitinligase RNF4 mit HBx interagiert.

Der zweite Teil dieser Arbeit konzentrierte sich, basierend auf den vorhergehenden neuen Erkenntnissen, auf die Behandlung von HBV Infektionen mit Arsentrioxid (ATO). Dabei konnte gezeigt werden, dass die Verabreichung von ATO zahlreiche HBV-Parameter wie Proteinmengen, Transkriptionsraten, HBeAg Sekretion, Gesamt-DNA sowie cccDNA Mengen effizient reduziert.

Zusammenfassend konnte in dieser Arbeit gezeigt werden, dass PML-NBs die mit post-translationalen Modifikationen durch SUMO einhergehen, einen großen Einfluss auf das HBx Protein selbst, als auch die gesamte HBV Infektion und die persistierende cccDNA betroffen haben. Darüber hinaus ermöglichte die Organisation von HBV Bestandteilen an PML-NBs die erfolgreiche Behandlung von HBV mit dem Medikament ATO. Somit stellt ATO eine vielversprechende und neue Therapie gegen akute und chronische HBV Infektionen dar, welche dringend im Kampf gegen chronische HBV und seine Folgen erforderlich ist.

# 1. Introduction

## 1.1. Hepatitis B virus

Since the present study focuses on the molecular mechanisms of Hepatitis B virus (HBV) infections, the following chapters introduce the basic molecular biology, characteristics, and therapeutic approaches of HBV.

### 1.1.1. Virus classification

Human Hepatitis B virus was described for the first time in 1967, by discovering the Hepatitis B surface (HBs) antigen in the blood of Australian aboriginal inhabitants [3]. Three years later David Dane was capable of visualizing the HBV virions, also called “Dane particles”, by electron microscopy and in 1986 the whole viral genome was already completely sequenced [4-7].

HBV in general represents a small enveloped hepatotropic DNA virus, designated as Para-retrovirus and classified as a member of the Hepadnaviridae family [8-10]. This family comprises two genera, the *Orthohepadnaviridae* and the *Avihepadnaviridae* sharing several common features, like a narrow host specificity, liver tissue tropism and similar genome organizations [8, 11, 12]. Members of the *Avihepadnaviridae* infect birds such as herons, snow geese and ducks, whereas *Orthohepadnaviridae* include viruses infective for mammals such as the ground squirrel, orangutan, or woolly monkey Hepatitis B virus, as well as the human HBV [8, 11, 13-18]. Nevertheless, no Hepatitis B virus infection was ever discovered in mice or other experimental animal models. Human HBV is phylogenetically subdivided into nine genotypes A-J, defined by more than 7.5% genome sequence divergence, varying clinical outcomes and geographic incidences (Table 1) [19-27]. These depicted genotypes can be further divided in sub-genotypes, characterized by variations in their genome of more than 4% [19, 20, 28].

**Table 1: Worldwide geographic incidences of HBV genotypes. [19-27].**

genotype	incidence
A	Africa, Europe, Central America
B	predominantly Asia, Oceania, Australia
C	predominantly Asia, Oceania, Australia
D	worldwide
E	predominantly Western, Central Africa
F	Central and South America
G	America, Europe
H	Central and South America
I	most frequently in Asia
J	single patient in Japan

### 1.1.2. Epidemiology and pathogenesis of Hepatitis B virus

HBV is a highly contagious virus, whose transmission occurs via blood as well as all other body fluids [29-34]. Further transfer pathways can proceed either vertical from an infected mother to her child or parenteral [29, 30]. Overall, the incubation period can last from 1-6 months, whereupon first symptoms like jaundice, nausea and fever appear on average 2-3 months post infection [35-39]. Ordinarily, two thirds of all HBV infections in adults proceed asymptotically [35, 39]. Consequently, one third suffer from an acute, icteric infection and approximately 1% evolve a fulminant infection including liver failure and jaundice [35, 40]. During an acute HBV infection, markers for liver inflammation (alanine aminotransferase) increase simultaneously to symptoms and HBV core antibodies 1-2 weeks after the onset of HBsAg [41]. After a few weeks, HBsAg antibodies rise, alanine aminotransferase levels decline again and symptoms as well as viral indicators vanish [41].

An HBV infection is considered as chronic, when the HBsAg persists for more than six months in the patients' blood, which is caused by the failure of the immune system to clear the viral infection [37, 42]. Chronic HBV infections are characterized by a high replicative phase, decreased HBV DNA levels and elevated alanine aminotransferase levels [41]. Transition into the viral inactive phase occurs, enclosed the absence of immune system activation, followed by HBeAg seroconversion, decreased HBV DNA

levels and normalized alanine aminotransferase levels [41]. Moreover, in 20-30% of all cases a viral re-activation takes place, characterized by HBeAg seroconversion followed by increased HBV DNA levels and/or alanine aminotransferase concentrations [41]. Overall, 5-10% of all adults suffering from HBV evolve a chronic hepatitis infection, whereas the number rises to 30-90% in immune suppressed patients and 90% in early childhood within 0-6 months [43, 44]. Despite an effective vaccine and an available post-exposure prophylaxis, administering antibodies against HBs, still 257 million individuals worldwide are estimated to be chronically infected with HBV [37, 45-49]. Indeed, the HBV infection itself is not directly cytopathic, liver damage originates by the host immune response acting as a defense mechanism against the virus, causing more than 800.000 annually deaths due to accompanied diseases, such as liver cirrhosis or hepatocellular carcinoma (HCC) [37, 45-53].

### **1.1.3. Morphology and genome organization of Hepatitis B virus**

Hepatitis B viruses constitute enveloped particles with a size of approximately 42 nm in diameter [7]. Figure 1 A depicts the schematic Hepatitis B virion structure. The outer virion envelope incorporates the small (S), middle (M) and large (L) surface proteins (HBs; S) embedded in a lipid bilayer [2, 54]. The inner nucleocapsid consists of 120 dimers of 180 (T=3) or 240 (T=4) HBV core protein (HBc) subunits, constituting the characteristic icosahedral shape [2, 55]. This nucleocapsid harbors the small, partially double-stranded relaxed-circular DNA (rcDNA) with a size of ~3.2 kb and 5' end that is covalently bound to the terminal protein (TP) section of the viral polymerase protein (P protein) [2, 35, 56, 57]. In total, the rcDNA genome is tightly organized and harbors four overlapping open reading frames (ORFs) encoding for all seven viral proteins (surface variants, core, precore, e antigen, polymerase, and X protein) (Fig. 1 B) [58, 59]. All three structural surface (HBs; S) proteins share the same carboxy-terminus, whereas the small S protein is encoded by the S domain, the middle M protein by the S and additional preS2 domain and the large L protein is even more prolonged by the preS1 domain [54, 60, 61]. The HBV core protein (HBc; C) constitutes the structural nucleocapsid by self-assembly as described previously [62-64]. However, the core sequence can be extended with an additional N-terminal peptide (precore, preC)

resulting in the proteolytically altered and secreted immunomodulatory protein, the Hepatitis B e antigen (HBeAg) [50, 65-67]. Furthermore, the P protein contains three functional domains: the ribonuclease H (RNase H), the reverse transcriptase and the terminal protein (TP) serving as a primer during rcDNA synthesis [68]. Finally, the small multifunctional non-structural HBV X protein (HBx; X) is particularly mandatory for the initiation and maintenance of viral transcription [69]. Further characteristics of this protein are described in the following chapters. Moreover, several regulatory elements like transcription initiators, transcriptional enhancers (EnhI/II), direct repeats (DR1, DR2) and an RNA primer are located on the rcDNA [2, 70-73].

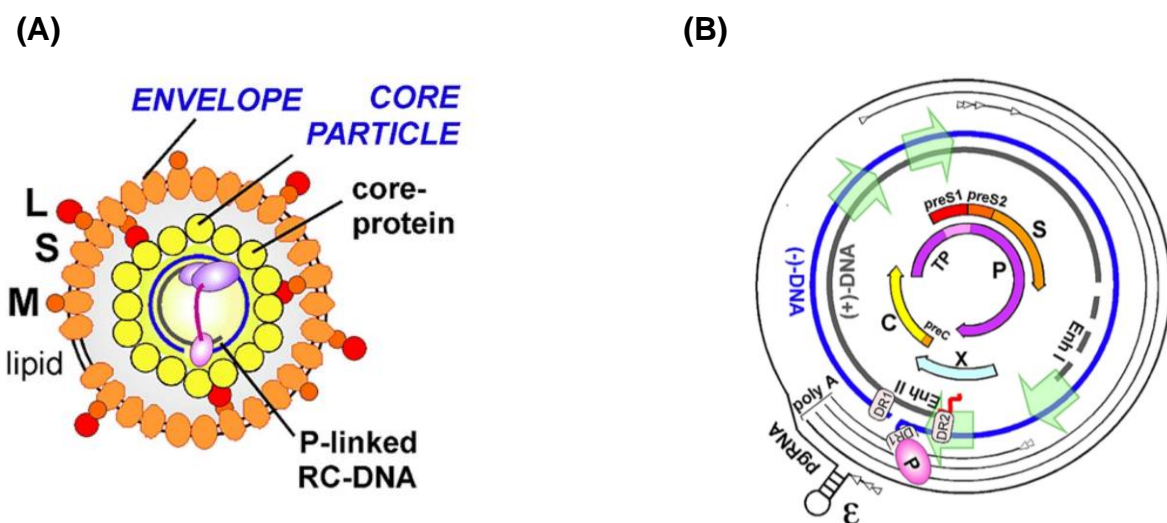


**Figure 1: Molecular characteristics of Hepatitis B virus.** (A) Virion structure of Hepatitis B virus. The outer envelope of the infectious virion consists of surface proteins S (small), M (middle) and L (large) embedded in a lipid layer. The icosahedral inner nucleocapsid composes of HBV core proteins and harbors the relaxed-circular DNA (rcDNA) HBV genome, which is bound to the polymerase protein (P). (B) Genome organization of Hepatitis B virus. The outer lines depict viral transcripts with white arrowheads indicating transcriptional start.  $\epsilon$  represents the RNA stem-loop for the encapsidation signal on the pregenomic RNA (pgRNA) initiating co-encapsidation of pgRNA and P protein. The (+)- and (-)-DNA strands are illustrated with the transcriptional enhancers EnhI/II and direct repeat DR1/DR2. Green arrows indicate the promoters, and the wiggly red line denotes the RNA primer on (+)-DNA. The inner circles show the four viral RNAs encoding the open reading frames (ORFs) transcribed from the cccDNA. Modified from [2].

#### 1.1.4. Replication cycle of Hepatitis B virus

The HBV replication cycle is schematically depicted in Figure 2. The viral infection is initiated by the attachment of the virions to particular susceptible hepatocytic cells [74, 75]. Here, the envelope L HBs protein of the infectious particles interacts via an antigenic loop with the glycosaminoglycan (GAG) side chains of the cellular heparan sulfate proteoglycan (HSPG) [76]. Next, the myristoylated and acylated preS1 domain of L HBsAg establishes a strong binding to the cellular bile acid transporter sodium taurocholate co-transporting polypeptide (NTCP), which serves as a functional receptor for HBV infection [77-82]. In addition, clathrin-mediated endocytosis was found to be mandatory for total HBV entry [83]. Thereafter, the viral nucleocapsid gets disassembled within the nuclear basket, rcDNA is released subsequently translocated through the nuclear pore complex by the nuclear localization signal (NLS) of HBV core [2, 84-88].

Here, the rcDNA is then converted into the double-stranded covalently closed circular DNA (cccDNA), residing in the nucleus as an episomal, nucleosome-bound minichromosome associated with histone and non-histone proteins [56, 64, 89-91]. The cccDNA represents the transcription template for the host RNA polymerase (Pol) II for the viral RNAs, comprising the three subgenomic mRNAs for HBs, HBx and precore, as well as concomitant the pregenomic RNA (pgRNA) [2]. The RNA then gets shifted into the cytoplasm, translated and protein synthesis is conducted [2, 92]. Whereat, the subgenomic RNAs are prerequisite for the translation of the surface HBs proteins and HBx, the precore RNA is translated, processed and finally secreted as HBeAg. [2, 50, 93]. The pgRNA is responsible for the translation of the HBV core as well as the P protein and additionally serves as a template for reverse transcription [2, 50, 93-97]. Here, the viral pgRNA, is enveloped by the nucleocapsid and the transcriptional process is initiated by the binding of the P protein to the  $\epsilon$  stem-loop, resulting in a  $\epsilon$ -templated DNA oligo whose 5' terminal is covalently linked to the P protein tyrosine residue of terminal protein (TP) domain [2, 93, 97]. Based on the C-terminal domain of the HBV core protein, this binding induces the co-packaging of the pgRNA complex into newly formed viral nucleocapsids [2, 98-100]. This is followed by a translocation of the TP protein and covalently bound DNA to the pgRNA DR1, inducing an extension of (-)-strand DNA with a redundancy (r) [2, 98, 101]. Meanwhile

the whole pgRNA apart from the 5' end is degraded via the P protein RNaseH activity, resulting in a single-stranded DNA (ssDNA) [2, 102-106]. The remaining 5' end serves as a (+)-strand primer, for the extension of a double-stranded linear DNA (dsL-DNA) starting at the DR1 [2, 98, 102, 107-109]. After the translocation of the RNA primer to the DR2 reaching the 5' end of the (-)-strand, the r enables an exchange with r from the 3' end, the (+)-strand synthesis proceeds and the DNA ends ligate for the finale rcDNA, remaining in an incomplete partially double-stranded DNA [2, 98, 107, 109-112]. Mature nucleocapsids containing rcDNA are either re-transported into the nucleus to enrich the cccDNA pool or are finally enveloped by HBs proteins at the endoplasmic reticulum and released [2, 113-117]. The secretion of mature virions out of the cells is at this juncture mediated by the host multivesicular bodies (MVB) [2, 118, 119]. Additionally, HBeAg and DNA-free subviral particles (SVPs) lacking rcDNA were found to be secreted via the endoplasmic reticulum and Golgi complex [9, 120-128]. These SVPs outnumber the DNA-containing virions by a factor of up to  $10^6$  and consist basically of HBsAg as well as derived lipids [9, 115, 123, 129-132]. SVPs can be subdivided in filaments, consisting of the viral envelope and nucleocapsid, or spheres, solely composed of envelope proteins [9, 115, 123, 129-132].

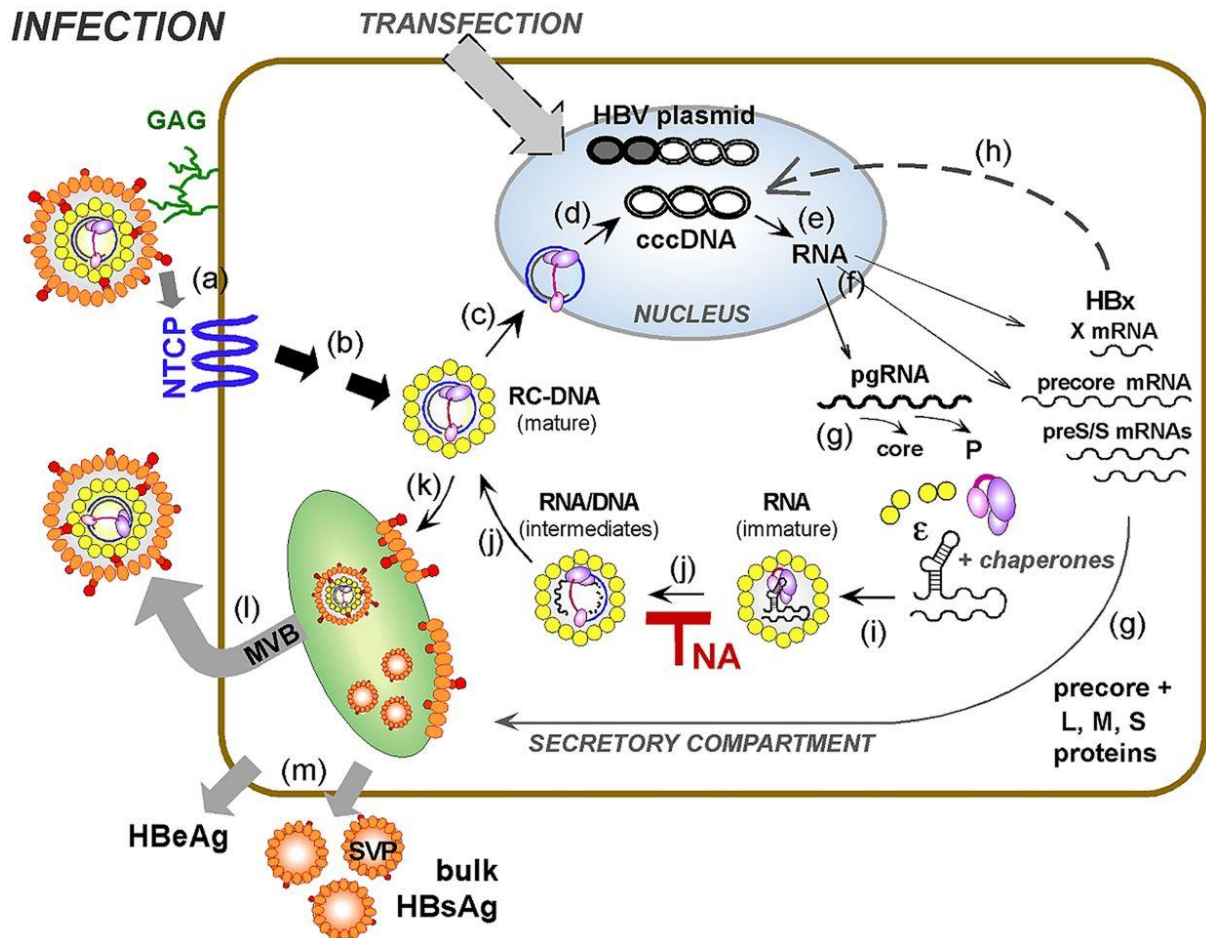


**Figure 2: Replication cycle of Hepatitis B virus infection.** (a) Initial attachment of virions followed by the interaction with the NTCP receptor and viral entry. (b) Viral nucleocapsid release into cytoplasm. (c) Nucleocapsid-mediated transport of rcDNA to the nucleus and release through the nuclear pore into the nucleus. (d) Conversion of rcDNA to covalently closed circular DNA (cccDNA) conversion. (e) Viral RNA transcription. (f) Nuclear export of viral RNAs. (g) Translation of viral RNAs. (h) Prevention of cccDNA silencing by Hepatitis B virus X protein (HBx). (i) Co-packaging of polymerase (p) and pregenomic RNA (pgRNA) in newly synthesized nucleocapsids. (j) First-strand DNA synthesis, pgRNA degradation and second-strand DNA synthesis resulting in rcDNA formation (k) Envelopment of nucleocapsids containing mature rcDNA. (l) Secretion of newly synthesized virions assisted by MVB. (m) Secretion of SVPs and HBeAg. L, large; M, middle; S, small Modified from [2].

### 1.1.5. Formation and characterization of covalently closed circular DNA

During HBV infection, the rcDNA is converted into the stable, nuclear persistent minichromosome, the cccDNA [2, 133]. The cccDNA copy number varies between 1-9 in HepG2-NTCP cells, whereupon the half-life of cccDNA comprises approximately 40 days [134]. The persistent cccDNA, thus, is the major therapeutic target in chronic Hepatitis B virus infection. Upon cccDNA formation, the tyrosyl-DNA-phosphodiesterase (TDP)2 removes the viral polymerase P from the rcDNA, by cleaving the phosphodiester linkage between the terminal protein and the 5' end of the (-)-strand [135-137]. However, TDP2 was shown to be not essential for cccDNA formation [2, 136, 138-140]. The redundant sequence of the rcDNA (-)-strand and the RNA primer of the (+)-strand are detached [50, 71, 107, 135, 139, 141]. Further, unresolved repair mechanisms, filling the nick and gap regions of the protein-free DNA are performed [2, 135, 141-143]. These repair processes are presumably conducted primarily by cellular host repair mechanisms, comprising >250 endogenous factors for DNA damage recognition, independent of the viral polymerase [2, 84, 135, 139, 141, 144, 145]. Moreover, the DNA polymerase  $\kappa$  was identified to be a mandatory factor for filling the gaps [146]. After replenishing the gaps, the DNA is ligated and supercoiled via topoisomerase to reduce torsional stress [2, 139, 145, 147, 148]. Finally, various proteins and histones (H1, H2A, H2B, H3 and H4) are associated to the cccDNA, to reduce nucleosomal spacing, resulting in a viral minichromosome, acquiring a chromatin-like structure [2, 64, 89, 135, 149-151]. Overall, several dynamic post-translational modifications (PTM) of the cccDNA histones regulate the transcriptional process such as phosphorylation, acetylation but also methylation modulate the epigenetic permissiveness of cccDNA [149, 152-155]. Moreover, the viral HBx protein modulates the epigenetic status of cccDNA for transcriptional activities [2, 69, 135, 150, 156, 157]. Following chapters focus in more detail on the functions of HBx.

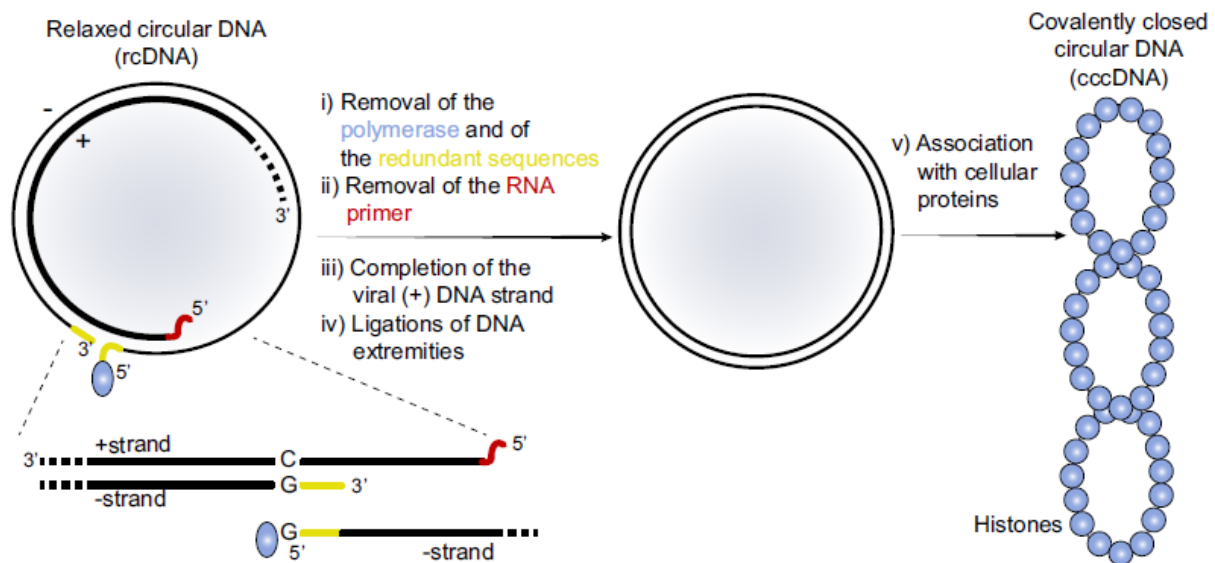


**Figure 3: Schematic representation of rcDNA to cccDNA conversion.** Removal of the (-)-strand 5'-end polymerase protein (blue) and the redundant sequences (yellow). Removal of the (+)-strand 5'-end RNA primer (red) and completion of the (+)-strand. Ligation of both (+)- and (-)-strands. Supercoiling of the newly synthesized DNA and protein association with proteins such as histones to form the cccDNA minichromosome. Modified from [135].

### 1.1.6. Hepatitis B virus protein X (HBx)

The regulatory multifunctional protein HBx comprises a size of 154 amino acids with a molecular weight of approximately 17 kDa [158, 159]. It is highly conserved among all mammalian hepadnaviruses, nevertheless avian hepadnaviruses do not encode the HBx protein [158, 160, 161]. Interestingly, in contrast to mammals, avians never develop HCC after a hepatitis infection, presuming an oncogenic potential of the HBx protein [161-163]. Meanwhile, interplay of the p53 protein and various other tumor suppressors with HBx was observed in HCC, supporting this hypothesis [164-169]. Since HBx interacts with more than 100 proteins, one major function is its ability to bind *inter alia* transcription factors, whereupon HBx transactivates several promoters, enhancers, and cellular genes, leading to the activation of diverse cellular signal transduction pathways [162, 170-178]. Several involved transcription factors are for instance the cAMP response element-binding protein (CREB), the nuclear factor kappa B (NF- $\kappa$ B) or the transcriptional factor IIB and IIH (TFIIB, TFIIH) [168, 169, 179-183]. Further modulating signal transduction pathways like the Ras-Raf-mitogen activated

protein kinase (Ras-Raf-MAPK) or the Janus kinase/signal transducers and activators of transcription (JAK/STAT) [168, 169, 179, 180, 184-192]. Besides, HBx affects the cellular DNA repair and the cell cycle regulation whereas HBx was found to induce cells from phase G0 to G1, remaining them in the G1/S phase [193-199]. Accessorily, HBx impinges the mitochondrial antiviral signaling proteins during the cellular immune response, provoking their degradation, and thus impeding the induction of IFN- $\beta$  [200]. In addition, HBx was reported to be able to sustain several post-translational modifications, comprising disulfide bond formation constituted by nine conserved cysteine residues, acetylation as well as phosphorylation, however their functions remains unclear [201-205].

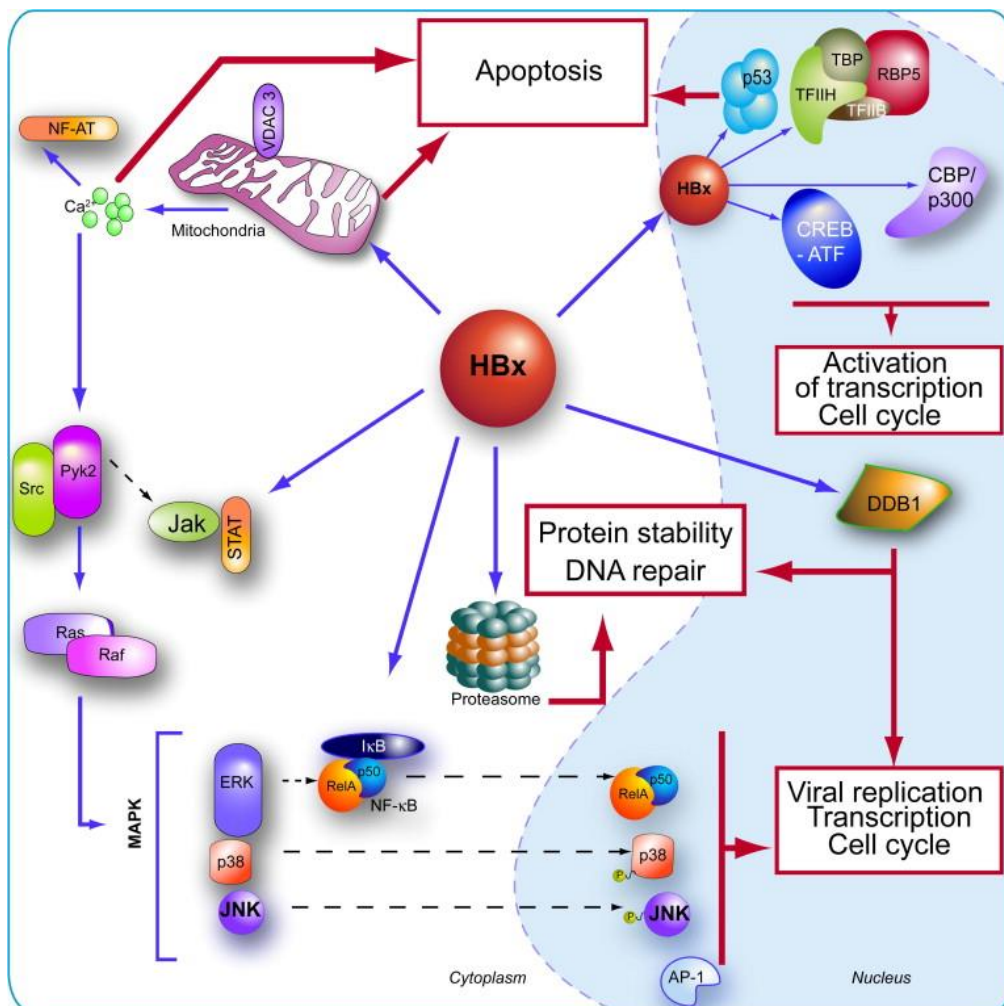


**Figure 4: Overview of multiple HBx functions.** HBx interferes with numerous transcription factors, co-activators as well as components of the basal transcription machinery. HBx can also modify transcriptional processes indirectly by altering cellular signaling pathways such as NF- $\kappa$ B, MAPK or JAK/STAT. Moreover, the HBx protein may affect protein degradation, apoptosis, mitochondrial proteins, DDB1 as well as the tumor suppressor protein p53. Modified from [206].

### 1.1.6.1. HBx putative protein domains and localization

The HBx protein consists of two different functional domains, whereas the amino acids (aa) 43-154 are essential for viral replication, in contrast aa 1–42 are dispensable [207, 208]. The N-terminal regulatory (trans-repression) domain comprising aa 1-50, including the dimerization region (21-50 aa) as well as the 14-3-3-binding motif (26-31 aa) [176, 204, 209-211]. The HBx trans-activation domain covers aa 51-154, harbors the p53 binding region (101-154 aa), the mitochondrial targeting region (111-116 aa) and the minimal DDB1 binding region (88-100 aa) [166, 168, 176, 200, 207, 208, 211-215].

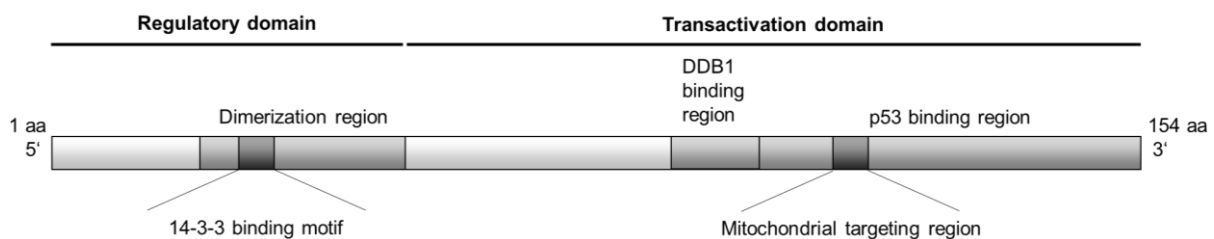


**Figure 5: Schematic representation of HBx regions.** HBx harbors two functional domains, the N-terminal regulatory domain (1-50 aa) comprising the dimerization region (21-50 aa), the 14-3-3-binding motif (26-31 aa) and the C-terminal transactivation domain (51-154 aa) including the minimal DDB1 binding motif (88-100 aa), the p53 binding region (101-154 aa) as well as the mitochondrial targeting region (111-116 aa) [166, 168, 176, 200, 204, 207-215].

The HBx protein localizes to the soluble as well as cytoskeletal fraction within the cell [216-218]. In the nucleus, HBx binds the HBV minichromosome, modulates the cccDNA and finally induces the regulation of transcriptional processes, even though conflicting results concerning the direct localization of HBx at the cccDNA were published [201, 216, 219]. Moreover, HBx was discovered to stimulate signal transduction pathways in the cytoplasm [178, 201, 216, 219-223]. Furthermore, HBx localizes to the mitochondrial membrane, reducing mitochondrial enzymes, resulting in an elevation of the reactive oxygen species and lipid peroxide production [183, 216, 224, 225]. A fraction of HBx in the endoplasmic reticulum alters the maintenance of liver proliferation and inflammation [226, 227]. Despite this, many functions of the HBx protein still remain unacquainted.

### 1.1.6.2. HBx and viral replication

In the course of an HBV infection, HBx represents an essential regulating factor. In the absence of HBx no viral RNAs are detectable, nevertheless cccDNA is formed [69, 162, 228]. Indicating that HBx is not important for the early steps of viral replication, though it is required to initiate and maintain viral replication from the cccDNA minichromosome [69, 162, 228]. During HBV replication, HBx promotes the opening of cccDNA by activating histone modifiers, PTMs as well as chromatin remodelers, leading to a transcriptionally active state of the HBV minichromosome [2, 69, 149, 156, 201]. The HBx protein interacts with several cellular proteins comprising the basal transcriptional machinery, co-activators like CBP/p300 and p300/CREB-binding protein-associated factor (PCAF) and promoters of CREB-regulated genes, resulting in transcription of the viral cccDNA by the cellular RNA polymerase (Pol) II [2, 69, 145, 150, 201, 210, 229, 230]. In contrast, HBx can suppress the gene expression of tumor suppressor promoters like E-cadherin by hyper-methylation via increased DNA methyltransferase activity [158, 231-237]. Synoptically, the lack of HBx induces the silencing of viral transcription as well as replication, by blocking cellular factors, initiating the cccDNA into a closed and repressed state [2, 69, 150, 238]. Overall, the bulk of mechanisms and binding partners of HBx during viral replication remain unexplored and have to be elucidated.

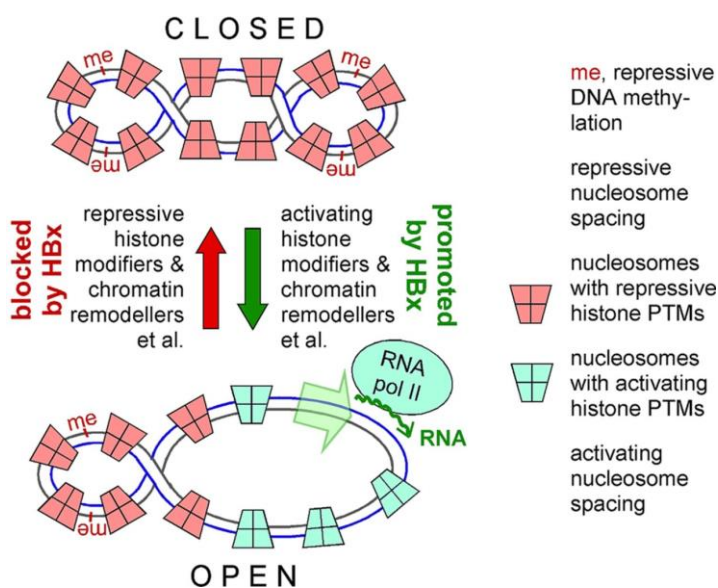


**Figure 6: Epigenetic modulation of cccDNA.** The nucleosome associated cccDNA consists of histones, post-translational modifications (PTM) and DNA methylation (me) regulating the epigenetic permissiveness. HBx regulates the epigenetic status of cccDNA and thus the transcription of cccDNA by RNA Pol II. HBx promotes de-silencing (open state, green), either by activating histone modifications and chromatin remodelers, and/or by blocking repressive modifications. Otherwise cccDNA is silenced (closed state, red). Modified from [2].

### 1.1.6.3. HBx promotes SMC5/6 degradation via CRL4 interaction

Besides all these findings, HBx was disclosed to bind and mediate the cellular DNA binding protein 1 (DDB1) early after infection, promoting structural maintenance of chromosomes 5 and 6 (Smc5/6) degradation, and thereby enabling gene expression from the cccDNA [1, 201, 212, 216, 239-242]. DDB1 was primarily identified as a factor for the recognition of nucleotide-excision repair [216, 243, 244]. In detail, DDB1 represents an adaptor protein of the Cullin 4A RING E3 ubiquitin ligase (CRL4), which interferes with DDB1 Cullin Accessory Factor (DCAF) receptors, recruiting substrates for ubiquitinylation and proteasomal degradation [1, 212, 216, 241, 245, 246]. The viral HBx epitomizes such a DCAF receptor and thus, interacts with the cellular DDB1 protein [207, 212, 216, 241]. Thereupon, the CRL4-HBx E3 ubiquitin ligase complex targets Smc5 and Smc6 for ubiquitinylation concomitant subsequent proteasomal degradation [1]. Smc5/6 usually directly bind the cccDNA, restricting the transcription from the cccDNA template, whereas the degradation of Smc5/6 antagonizes this repression, finally conducting cccDNA transcription [208, 242, 247]. Accessorily, Smc5/6 depletion was recently also found to induce genomic instability in dividing cells as well as genetic errors in mice harboring chronic HBV which could be then related to increased cancer incidence [208, 248-251]. In conclusion, these data led us to the hypothesis that HBx-promoted loss of Smc5/6 may also affect the probability for HCC during chronic HBV infections. In line with this, hijacking cellular antiviral processes by interfering with CRL4 E3 ubiquitin ligase in order to degrade host proteins were also reported for other viruses such as Human immunodeficiency virus, Paramyxovirus simian virus and simian immunodeficiency virus [252-255].

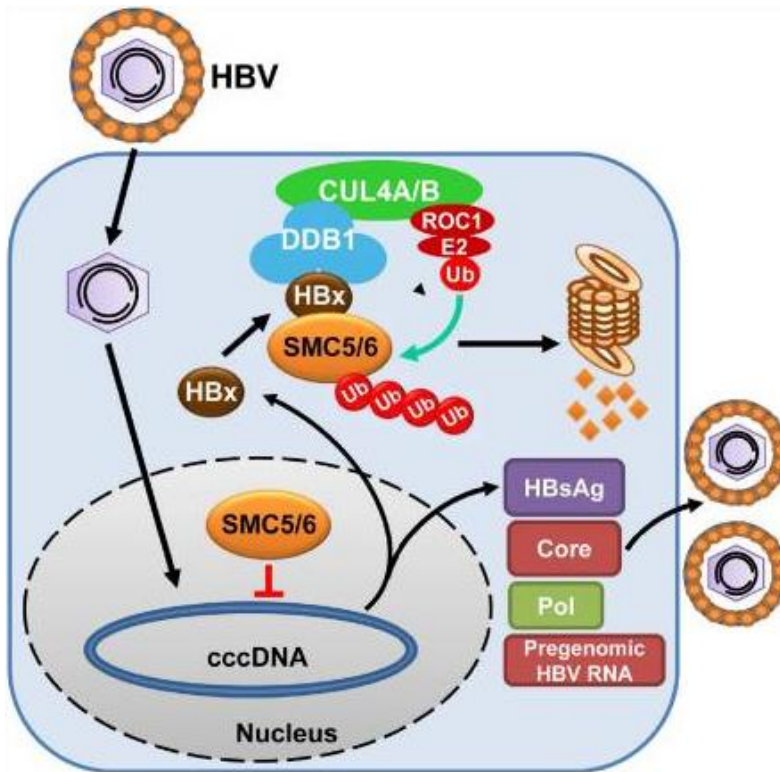


**Figure 7: HBx dependent SMC5/6 degradation via CUL4 E3 ubiquitin ligase complex.** The viral cccDNA is restricted by the cellular structural maintenance of chromosomes complex SMC5/6, inhibiting the HBV replication. HBx interacts with the DDB1-CUL4-ROC1 (CRL4) E3 ligase complex, targeting the SMC5/6 for ubiquitination and subsequent degradation by the proteasome, activating the gene expression from the cccDNA. Modified from [1].

### 1.1.7. Current treatment approaches against HBV

Actual problems of the current clinical therapeutic approaches to treat HBV infections are mainly high costs, patient adherence, drug resistance after a short medication period and especially the rare purge of total HBsAg [2, 41, 256-260]. Re-activation of an HBV infection can also be developed, due to cellular *de novo* infections by remaining virions in the blood stream, representing a severe treatment problem after liver transplantation [261-264]. Currently, the therapeutic options are mainly based on life-long administration of antivirals, whereupon seven against chronic HBV are approved: interferon (IFN)-a2b, (PEGylated) IFN-a2α and/or nucleos(t)ide analogues (NUCs) [41, 265, 266]. The (PEGylated) IFN-α treatment enhances immunomodulatory and concomitant antiviral effects against HBV and induces the hypoacetylation of cccDNA-associated histones, preventing cccDNA transcription [41, 157, 267, 268]. However, the dosing is still challenging and often causes various side effects, like depression, fatigue or bone marrow suppression [41, 265, 269-274]. In addition, PEGylated IFN-α is relatively inefficient, accomplishing merely successful

response rates of <10% [275]. Another commonly utilized medication against HBV infection is the administration of previously mentioned NUCs Lamivudine, Adefovir, Entecavir, Telbivudine and Tenofovir [41, 265, 266]. These substances target the viral polymerase, whereupon the HBV replication cycle is inhibited [265, 276, 277]. Consequently, the inhibition of viral reverse transcription provokes reduced viral loads in patients, however the viral cccDNA is unaffected resulting in incomplete eradication of the virus [2, 41, 278-280]. Lamivudine represents one of the oldest NUCs, though more than 50% of patients evolve a drug resistance within three years of treatment [281-283]. Based on this issue further alternative NUCs must be administered to develop much lower resistance rates in patients, like Adefovir an acyclic phosphonate, Entecavir a cyclopentane, Tenofovir an acyclic nucleotide or Telbivudine a L-nucleoside [284-290]. Nevertheless, those compounds still not directly target the persistent cccDNA and do not eradicate the virus, evoking viral relapse after ending the medication [41, 278, 291]. Novel therapeutic approaches include for instance small molecules, directly intercepting with HBV core proteins to either prevent or accelerate their assembly [292]. Thereby, inducing a cccDNA amplification block by yielding empty, aberrant, or non-infective HBV nucleocapsids but not affecting the established nuclear cccDNA pool [292, 293]. A further recent therapeutic approach is Myrcludex B, blocking the HBV entry into the cell by interference with the NTCP receptor [79, 82, 294]. Since all currently available treatment options fail to clear HBV infections, continuing research is indispensable to find a cure for chronic HBV, emphasizing the urgent therapeutic need for novel and innovative treatment concepts. Eradication of the stable nuclear cccDNA by non-cytolytic removal or exterminations of cells harboring the cccDNA would be imperative to terminate the long-term persistence of HBV in the liver [2, 291, 295-297]. Here, ideal solutions might be the inhibition of rcDNA import into the nucleus, the suppression of rcDNA to cccDNA conversion or cell division of proliferating HBV infected hepatocytes [2]. In the end, a functional cure should optimally accomplish demands by loss of HBsAg including seroconversion, HBV DNA and transcriptionally inactive cccDNA [291, 298, 299].

## 1.2. PML-NBs comprise various biological processes

PML-NBs (Promyelocytic leukemia nuclear bodies) are dynamic, nuclear matrix associated, multiprotein complexes, comprising a size of 0.1-1 $\mu$ m [300-302]. The functional integrity of PML-NBs is mediated by proteins covalently conjugated with the small ubiquitin-related modifier (SUMO) proteins that either constitutively or non-constitutively complex [300, 302-306]. PML-NBs are *inter alia* regulated by cellular stress, modulate the DNA damage response (DDR) and are implicated in antiviral defense [300, 307-311]. PML-NBs are known to be targeted by various viruses to alter or suppress cellular defense mechanisms for viral benefits, such as Herpes simplex viruses, Epstein-Barr virus, Papovaviruses and Adenovirus [312].

Seven different PML isoforms are disclosed until now, namely PML-I to PML-VII [313]. These different isoforms originate from variegating alternative splicing of the *pml* gene, whereupon the C-terminal region is accountable for the isoforms and various functions [313-320]. All isoforms embody the consistent N-terminal RBCC motif which is responsible for the homo-multimerization of PML proteins, comprising of a RING-finger (R), two B-Boxes (B) and a coiled-coil (CC) domain [300, 313, 321, 322]. PML-I to PML-VI own multiple SUMO consensus motifs and a nuclear localization site (NLS) whereas isoforms up to PML-V comprise an additional SUMO-interaction motif (SIM) [314, 323, 324]. In contrast, PML-VII localizes in the cellular cytoplasm, lacking the NLS and SIM but also harboring SUMO motifs [300, 314, 323]. PML-NBs affect numerous cellular mechanisms like transcriptional processes, apoptosis, and senescence by recruiting specific proteins and/or modifying them via post-translational modification (PTM) such as phosphorylation, acetylation, ubiquitylation, and SUMOylation (Small ubiquitin-like modifier) [300-302, 322, 325-331].

Sp100 (speckled protein 100) is another main component of PML-NBs and expresses four alternatively spliced isoforms Sp100A, Sp100B, Sp100C, and Sp100HMG [300, 302-306, 332-336]. Sp100A could be shown to elevate chromatin de-condensation by promoting the recruitment of histone acetyltransferase, whereas the SAND domain (named after Sp100, AIRE-1, NucP41/45, and DEAF-1) containing isoforms Sp100B, C, and HMG promote chromatin condensation by having a high affinity for DNA with unmethylated CpGs [305, 332, 335-341]. Here, Sp100 can form a SUMO-dependent chromatin-associated complex with the heterochromatin protein 1 (HP1), representing

a non-histone chromosomal protein and regulate chromatin remodeling [336, 342-345]. More in detail, the presence of SUMOylated KAP1 (KRAB-associated protein 1) binds the Histone-lysine N-methyltransferase SETDB1, leading to the induction of the methylating activity towards histone H3 [346-348]. HP1 proteins then bind the methylated H3-lysine 9 (H3K9), resulting in HP1 protein recruitment, heterochromatin formation and gene silencing [346-348].

Furthermore, it was recently reported that also the Smc5/6 complex, repressing HBV cccDNA transcription, is found juxtaposed to PML-NBs [349]. Suggesting, that also the viral cccDNA concomitant the HBx protein are associated to these intracellular structures [216, 349].

### **1.2.1. SUMO conjugating pathway**

SUMO proteins are the prerequisites for the PML-NB formation, as indicated above [303, 350]. SUMO proteins were identified in 1996, comprise a size of ~11 kDa and are part of the ubiquitin-like protein family, due to 18% sequence identity and a comparable conjugation pathway [351-356]. The SUMO conjugation pathway represents an enzymatic multistep process, initiated by the cleavage and maturation of the SUMO protein from its substrate by SUMO specific endopeptidases (SENPs) generating a di-glycine residue at the C-terminus of the SUMO protein [357-359]. Followed by an ATP-dependent activation of SUMO by the activating enzyme E1, a heterodimer consisting of SAE1 and SAE2 (SUMO-activating enzyme), via thioester binding between the di-glycine remnant of the SUMO protein and the SAE2 cysteine residue [360-367]. The E2 conjugation enzyme ubiquitin carrier protein 9 (Ubc9), links the SUMO protein via a thioester-binding to its cysteine residue [353, 368-370]. Then the E3 ligase initiates an isopeptide bond at the C-terminal SUMO to the SUMO consensus motif (SCM) of the target proteins [353, 357, 371-373]. This binding occurs precisely at the  $\epsilon$ -amino residue of the lysine within the SCM  $\psi$ KxE/D ( $\psi$  large hydrophobic residue, K lysine, x any amino acid, E glutamic acid, D aspartic acid) [353, 374-377]. Finally, the SUMOylation of substrates can be withdrawn by seven different SENPs, inducing de-conjugation of SUMO proteins from substrates as well as the maturation of the SUMO precursor at the outset of the SUMO conjugation pathway

[359, 361, 378-382]. Besides this specific SUMOylation cascade, SUMOylation also appears in around 26% of all cases at proteins lacking such SCMs, indicating that this motif is not crucial for the attachment of SUMO proteins [383]. Furthermore, the discrimination between the covalent interaction and a non-covalent conjugation at a SUMO interaction motif (SIM) of SUMO proteins is possible [384, 385]. Overall, SUMO proteins can be divided into five paralogues. The SUMO1 paralogue functions as monomer and shares amino acid sequence identity of around 50% with SUMO2 and SUMO3 [353, 386-388]. SUMO2/3 themselves differ marginal with 95% sequence consistency and are able to form poly-SUMO chains of certain SUMO proteins, which can be terminated by a SUMO1 modification [353, 387, 389-392]. SUMO4 is exquisitely homologue to SUMO2/3, sharing 87% sequence equality and is supposed to be a pseudogene [393, 394]. Recently, the controversially discussed species-specific SUMO5 paralogue was identified to modulate the PML-NBs and associated proteins [395]. Overall, PTM by SUMO is used in eukaryotes to modulate protein functions, stability and/or localization [352, 357, 361, 396-402]. SUMO proteins influence DNA repair mechanisms and have a crucial role in genomic integrity and chromosome maintenance via modification of histones [352, 360, 403]. Moreover, SUMOylation of transcription factors affect their activities and subsequent gene expression [352, 360, 403-409]. Recent studies additionally revealed that the loss of post-translational modification by SUMO alters cancer cells, supporting tumor proliferation [410]. In addition, several viruses interfere with the post-translational SUMO conjugation to either avoid antiviral defense mechanisms *inter alia* like Adenovirus or to benefit their viral replication like Dengue virus [371, 411, 412].

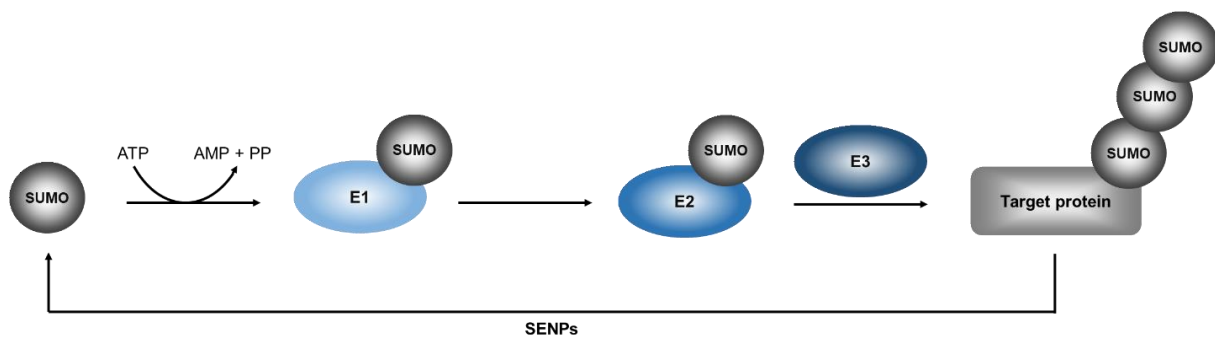


**Figure 8: The small ubiquitin like modifier (SUMO) Conjugation pathway.** The SUMO precursor protein is matured by the SUMO specific endopeptidases (SENPs). The SUMO protein is activated by the E1 activating enzyme (SAE1/SAE2), conjugated to the E2 enzyme (Ubc9) and finally attached by the E3 enzyme (PIAS or RANBP2) to the lysine residue (K) of the SUMOylation consensus motif  $\psi$ KxD/E ( $\psi$  large hydrophobic residue, K lysine, x any amino acid, E glutamic acid, D aspartic acid) of the target protein. Finally, the SUMO conjugation is variable and can be reversed by SENPs.

### 1.2.2. SUMO-targeted ubiquitin ligases RING-finger protein 4

The previously explained SUMO conjugation pathway can be even more extended by so called SUMO-targeted ubiquitin ligases (STUbLs) which function as E3 ubiquitin ligases for SUMO-modified proteins, leading to the ubiquitylation of SUMOylated proteins followed by proteasomal degradation [413]. Until now, two different human STUbLs the RING-finger protein 4 (RNF4) and the RING-finger protein 111 (RNF111) are known [413-416]. RNF4 comprises a size of 190 aa, including several N-terminal SUMO interacting motif (SIM) domains (SIM1-SIM4), a C-terminal RING domain, as well as a SIM5 which is unlikely to be a genuine functional SIM [414, 417]. The RING domain is decisive for the dimerization and thus the active state of RNF4 [418]. On this occasion, RNF4 is able to bind the E2 loaded ubiquitin and activate its catalysis for the transfer of ubiquitin to SUMO modified proteins [419-422]. In detail, RNF4 is capable to bind poly-SUMO chains via tandem SIM, inducing ubiquitylation and proteasomal degradation [304, 417, 423].

Furthermore, RNF4 can interact with phosphorylated proteins via an arginine rich motif triggering proteasomal degradation [424]. Overall, more than 300 target proteins of RNF4 were discovered, for instance during DNA repair or metabolic pathways [425]. Additionally, RNF4 was also found to play an important role during viral infections of Human Adenovirus (HAdV), promoting viral gene expression [426]. Here, RNF4 is

recruited by an early adenoviral protein (E1B-55K) to the insoluble nuclear matrix, causing the ubiquitylation and proteasomal degradation of a PML-NB associated cellular antiviral factor (Daxx) [426]. Previously, (SUMOylated) PML and the oncogenic fusion PML/retino acid receptor  $\alpha$  (RAR $\alpha$ ) proteins were also discovered as targets of RNF4 for proteasomal degradation [423, 427]. This process can be even strengthened in the presence of a compound called Arsenic trioxide [423, 428, 429].

### **1.2.3. Arsenic trioxide**

Arsenic trioxide (ATO/As<sub>2</sub>O<sub>3</sub>) represents an ancient compound which was already identified in traditional medicine 2400 years ago and first described to induce a complete clinical remission in patients suffering from acute promyelocytic leukemia (APL) in 1992 [430-432]. First evidence of ATO potency against leukemia was only reported in 1882 [433]. Thereupon, the admission for ATO as a treatment for APL was preserved by the U.S. Food and Drug Administration and reintroduced into current medicine (Cell Therapeutics, Inc., Application No.: 21-248, Approval Date: 9/25/2000) [434, 435]. During the genetic disorder APL, PML fuses with the RAR $\alpha$ , resulting in an altered myeloid differentiation at the promyelocytic stage and loss of PML functionality [317, 319, 436-438]. However, treatment with ATO induces a direct binding with the cysteine residues within the RBCC motif of PML, evoking PML oxidation [439, 440]. Subsequently, ATO binds PML, inducing hyper-SUMOylation of PML and PML associated proteins by SUMO2/3, followed by SUMO-dependent E3 ubiquitin ligase RNF4 ubiquitylation and eventual proteasomal degradation of PML/RAR $\alpha$  [310, 428, 429, 439-442]. ATO is able to affect all stages of APL disease, involving first-line acute treatment, remission induction of relapsed cases and the maintenance of treatment [430, 443-447]. PML-NBs represent also a possible therapeutic target to counteract several viral infections. For instance, our lab recently reported that treatment with ATO efficiently counteract HAdV by inducing re-localization of PML tracks into nuclear bodies and modulation of the host cell SUMO pool [448]. However, clearance of further PML-NB associated viral infections by ATO, and arsenicals have to be elucidated in the future. Even though controversial initial findings for HBV and HCC were published, studies in transgenic HBsAg expressing mice demonstrated reduced incidence for

HCC during ATO treatment, however the overall survival rates were not affected [449]. Another study revealed drinking water containing  $\pm 300$  mg/L arsenic to have a significantly increased impact on the risk for hepatitis or cirrhosis in healthy people, whereas levels of arsenic  $\pm 100.0$  mg/L significantly reduce the risk of chronic Hepatitis or cirrhosis in people harboring chronic Hepatitis [450]. Thereupon, elevated urinary arsenic exposure was associated with a higher risk for past natural and chronic HBV infections [451, 452].

### 1.3. Aim of the study

Worldwide 250 million humans are estimated to suffer from chronic HBV infection and more than 880.000 people die annually due to chronic HBV related diseases such as liver cirrhosis or HCC. Emphasizing the urgent need for novel therapeutic approaches since all current treatments fail to clear the persistent cccDNA reservoir of HBV. Here we hypothesized that cccDNA and HBx associate with PML-NBs, as several factors required for cccDNA synthesis and HBx mediated epigenetic opening of cccDNA for efficient transcription are found at those nuclear foci within the hepatocyte.

Thus, the primary aim of this thesis was to investigate the intracellular localization of HBx with regard on PML-NBs and SUMO conjugation to the viral regulator prior to dissection of PML associated functions of HBx. The second part of this work focused on the post-translational modification of HBx, whereupon the specific HBx SUMO conjugation site should be determined. Therefore, the generation of several HBx SCM mutants was required. Additionally, the impact of SUMO deficient HBx variants concerning HBx functions as well as the whole HBV infection should be analyzed. In the last part of this thesis, we investigated the potential treatment of HBV with the compound ATO *in vitro*. Since this chemical was discovered to reduce hyper-SUMOylate PML-NBs, leading to ubiquitinylation and proteasomal degradation, we suggested that ATO also counteracts HBV infection, which we hypothesized to be at least partially associated with PML-NBs.

## 2. Materials and Methods

### 2.1. Materials

In the following chapters, used materials and applied methods are described. This section gives an overview of the used laboratory materials, machines, and software applications.

#### 2.1.1. Mammalian cell lines, cell culture media and bacterial strain

##### 2.1.1.1. Mammalian cell lines

**Table 2: Used cell lines with database number, genotype, and reference.**

No.	Cell line	Genotype	Reference
1	HepaRG	Human hepatoma cells derived from HCV infected tissue (“pseudo-primary”) which can be differentiated into hepatocyte- and biliary-like cells	[453]
7	HeLa SUMO2-His	Human cervical carcinoma cells with HPV-18 genome integration, stably expressing 6xHis tagged SUMO2	[454]
12	HepaRG SUMO2-His/HA	Primary human hepatocytes, stably expressing 6xHis-tagged SUMO2	[455]
14	HepG2-NTCP-K7	Human liver carcinoma cell clone, overexpressing NTCP receptor	[134]
15	H1299	p53 negative human lung cell carcinoma cell line derived from metastatic lymph node	[456]
20	HepaRG His/HA	Primary human hepatocytes, stably expressing 6xHis-tag	[455]

<b>49</b>	HepaRG shCTR	Primary human hepatocytes, knock-down control cell line	Database [457]
<b>51</b>	HepaRG shPML	Primary human hepatocytes, knock-down against PML	Database [457]
<b>74</b>	HepG2 NTCP-K7 shPML	Human liver carcinoma cell clone, overexpressing NTCP receptor, knock-down against PML	Database unpublished
<b>81</b>	HepaRG shSp100	Primary human hepatocytes, knock-down against Sp100	Database [457]

### 2.1.1.2. Cell culture media

**Table 3: Media composition for H1299 and HeLa-SUMO2-His cell lines.**

<b>Chemical</b>	<b>Amount</b>
Dulbecco's Modified Eagle's Medium (DMEM) – high glucose (4500 mg/l glucose, L-glutamine, sodium pyruvate, sodium bicarbonate, liquid, sterile-filtered, suitable for cell culture)	500 ml
Heat-inactivated fetal bovine serum (FBS)	5% (v/v)
Penicillin/streptomycin (1000 U/ml penicillin, 10 mg/ml streptomycin in 0.9% NaCl)	1% (v/v)

**Table 4: Media composition for all HepG2 cell lines.**

<b>Chemical</b>	<b>Amount</b>	<b>Amount</b>
	Standard	Differentiation
Dimethyl sulfoxide (DMSO)	-	2.5% (v/v)
Dulbecco's Modified Eagle's Medium (DMEM) - high glucose (4500 mg/l glucose, sodium bicarbonate without L-glutamine and sodium pyruvat, liquid, sterile-filtered, suitable for cell culture, suitable for hybridoma)	500 ml	500 ml
Glutamine	2 mM	2 mM
Heat-inactivated fetal bovine serum (FBS)	10% (v/v)	10% (v/v)
NEAA	1 x	1 x
Penicillin/streptomycin (1000 U/ml penicillin, 10 mg/ml streptomycin in 0.9% NaCl)	1% (v/v)	1% (v/v)
Sodium pyruvate	1 mM	1 mM

**Table 5: Media composition for all HepaRG cell lines.**

<b>Chemical</b>	<b>Amount</b>	<b>Amount</b>
	Standard	Differentiation
Dimethyl sulfoxide (DMSO)	-	2.5% (v/v)
Dulbecco's Modified Eagle's Medium (DMEM) – high glucose (4500 mg/l glucose, L-glutamine, sodium pyruvate, sodium bicarbonate, liquid, sterile-filtered, suitable for cell culture)	500 ml	500 ml
Heat-inactivated fetal bovine serum (FBS)	10% (v/v)	10% (v/v)
Hydrocortison	0.5 µM	0.5 µM
Insulin	5 µg/ml	5 µg/ml
Penicillin/streptomycin (1000 U/ml penicillin, 10 mg/ml streptomycin in 0.9% NaCl)	1% (v/v)	1% (v/v)

### 2.1.1.3. Bacterial strain

**Table 6: Bacterial strain with phenotype and reference.**

Bacterial strain	Phenotype	Reference
Escherichia coli DH5 $\alpha$	supE44, $\Delta$ lacU169, ( $\phi$ 80dlacZ $\Delta$ M15), hsdR17, recA1, endA1, gyrA96, thi-1, relA1	[458]

### 2.1.2. Viruses

**Table 7: Used viral strains with database number, genotype and reference.**

Virus	Characteristics	Reference
HBV HBx-	HBx deficient Hepatitis B virus genotype D Including stop codon mutations in HBx ORFs at aa 5 (kindly provided by Prof. Dr. Ulrike Protzer, TUM)	[69]
HBV wt	Wild-type Hepatitis B virus purified from Ad38 cell line genotype D (kindly provided by Prof. Dr. Ulrike Protzer, TUM)	[459]

### 2.1.3. Nucleic acids

#### 2.1.3.1. Recombinant plasmids

**Table 8: Plasmids including database number, description, and reference.**

No.	Plasmid	Description	Reference
12	pcDNA3 empty	Empty pcDNA3 vector	Database
18	pcDNA3-HA	Empty pcDNA3 vector with CMV promoter and N-terminal HA tag	Database
21	pEYFP-C1	Empty pEYFP vector	Invitrogen, Karlsruhe, Germany

<b>72</b>	pLKO-pgD-EYFP empty	pLKO-pgD-EYFP empty vector (kindly provided by Prof. Roger Everett, Glasgow)	[460]
<b>73</b>	pLKO-pgD-EYFP-PML-I	pLKO-pgD-EYFP encoding PMLI (kindly provided by Prof. Roger Everett, Glasgow)	[460]
<b>74</b>	pLKO-pgD-EYFP-PML-II	pLKO-pgD-EYFP encoding PMLII (kindly provided by Prof. Roger Everett, Glasgow)	[460]
<b>75</b>	pLKO-pgD-EYFP-PML-III	pLKO-pgD-EYFP encoding PMLIII (kindly provided by Prof. Roger Everett, Glasgow)	[460]
<b>76</b>	pLKO-pgD-EYFP-PML-IV	pLKO-pgD-EYFP encoding PMLIV (kindly provided by Prof. Roger Everett, Glasgow)	[460]
<b>77</b>	pLKO-pgD-EYFP-PML-V	pLKO-pgD-EYFP encoding PMLV (kindly provided by Prof. Roger Everett, Glasgow)	[460]
<b>78</b>	pLKO-pgD-EYFP-PML-VI	pLKO-pgD-EYFP encoding PMLVI (kindly provided by Prof. Roger Everett, Glasgow)	[460]
<b>383</b>	empty pCMX3b-Flag	Empty vector pCMX3b-Flag	Database
<b>399</b>	SUMO1 HA	pcDNA3-HA vector encoding SUMO1 (kindly provided by Prof. Ron Hay, Glasgow)	[369, 397]
<b>400</b>	SUMO2 HA	pcDNA3-HA vector encoding SUMO2 (kindly provided by Prof. Ron Hay, Glasgow)	[369, 387]
<b>401</b>	SUMO3 HA	pcDNA3-HA vector encoding SUMO3 (kindly provided by Prof. Ron Hay, Glasgow)	[369, 387]
<b>440</b>	pENTRY HBx	pENTRY vector encoding HBV HBx with CMV promoter (kindly provided by Prof. Ulrike Protzer, TUM)	AG Protzer unpublished
<b>450</b>	pcDNA3-HA HBx	pcDNA3 vector encoding HBV HBx with CMV promoter and N-terminal HA-tag	This work

<b>451</b>	pcDNA3-HA HBx V5	pcDNA3 vector encoding HBV HBx with CMV promoter and N-terminal HA-tag and C-terminal V5-tag	This work
<b>452</b>	pCMX3b-Flag HBx V5	pCMX3b vector encoding HBV HBx with CMV promoter and N-terminal Flag-tag and C-terminal V5-tag	This work
<b>453</b>	pCMX3b-Flag HBx	pCMX3b vector encoding HBV HBx with CMV promoter and N-terminal Flag-tag	This work
<b>454</b>	pCMX3b-Flag HBx V5	pCMX3b vector encoding HBV HBx with CMV promoter and C-terminal V5-tag	This work
<b>455</b>	pCMX3b HBx	pCMX3b vector encoding HBV HBx with CMV promoter	This work
<b>456</b>	pLENTI HBx V5	pLenti vector encoding HBV HBx with CMV promoter (kindly provided by Prof. Ulrike Protzer, TUM)	AG Protzer unpublished
<b>461</b>	pcDNA3-HA HBx SCM1/2	pcDNA3 vector encoding HBV HBx SCM at aa position 91/95 with CMV promoter and N-terminal HA-tag	This work
<b>462</b>	pcDNA3-HA HBx SCM3/4	pcDNA3 vector encoding HBV HBx SCM at aa position 113/118 with CMV promoter and N-terminal HA-tag	This work
<b>463</b>	pcDNA3-HA HBx SCM5	pcDNA3 vector encoding HBV HBx SCM at aa position 130 with CMV promoter and N-terminal HA-tag	This work
<b>464</b>	pcDNA3-HA HBx SCM6.	pcDNA3 vector encoding HBV HBx SCM at aa position 140 with CMV promoter and N-terminal HA-tag	This work
<b>465</b>	pcDNA3-HA HBx V5 SCM1/2	pcDNA3 vector encoding HBV HBx SCM at aa position 91/95 with CMV promoter and N-terminal HA-tag and C-terminal V5- tag	This work

<b>466</b>	pcDNA3-HA HBx V5 SCM3/4	pcDNA3 vector encoding HBV HBx SCM at aa position 113/118 with CMV promoter and N-terminal HA-tag and C-terminal V5-tag	This work
<b>467</b>	pcDNA3-HA HBx V5 SCM5	pcDNA3 vector encoding HBV HBx SCM at aa position 130 with CMV promoter and N-terminal HA-tag and C-terminal V5 tag	This work
<b>468</b>	pcDNA3-HA HBx V5 SCM6	pcDNA3 vector encoding HBV HBx SCM at aa position 140 with CMV promoter and N-terminal HA-tag and C-terminal V5 tag	This work
<b>469</b>	RNF4-Flag	Unkown vector encoding RNF4 (kindly provided by Dr. Junjie Chen)	Dr. Junjie Chen
<b>512</b>	pcDNA3 core-HA	pcDNA3-HA vector encoding HBV core	PhD thesis Samuel Hofmann, AG Schreiner
<b>582</b>	pCMX3b-empty	Empty pCMX3b vector	Database
<b>777</b>	pcDNA3 DDB1-HA2	pcDNA3-HA2 encoding DDB1	Addgene, Watertown, USA
<b>779</b>	pYFP-Sp100A	pYFP vector encoding Sp100A	Database, [332]
<b>780</b>	pYFP-Sp100B	pYFP vector encoding Sp100B	Database
<b>781</b>	pYFP-Sp100C	pYFP vector encoding Sp100C	Database
<b>782</b>	pYFP-Sp100HMG	pYFP vector encoding Sp100HMG	Database
<b>784</b>	pCMX3b-Flag HBx SCM1/2	pCMX3b vector encoding HBV HBx SCM at aa position 91/95 with CMV promoter N-terminal Flag-tag	This work

<b>785</b>	pCMX3b-Flag HBx SCM3/4	pCMX3b vector encoding HBV HBx SCM at aa position 113/118 with CMV promoter and N-terminal Flag-tag	This work
<b>786</b>	pCMX3b-Flag HBx SCM5	pCMX3b vector encoding HBV HBx SCM at aa position 130 with CMV promoter and N-terminal Flag-tag	This work
<b>787</b>	pCMX3b-Flag HBx SCM6	pCMX3b vector encoding HBV HBx SCM at aa position 140 with CMV promoter and N-terminal Flag-tag	This work
<b>788</b>	pCMX3b-Flag HBx-V5 SCM1/2	pCMX3b vector encoding HBV HBx SCM at aa position 91/95 with CMV promoter and N-terminal Flag-tag and C-terminal V5-tag	This work
<b>789</b>	pCMX3b-Flag HBx-V5 SCM3/4	pCMX3b vector encoding HBV HBx SCM at aa position 113/118 with CMV promoter and N-terminal Flag-tag and C-terminal V5-tag	This work
<b>790</b>	pCMX3b-Flag HBx-V5 SCM5	pCMX3b vector encoding HBV HBx SCM at aa position 130 with CMV promoter and N-terminal Flag-tag and C-terminal V5-tag	This work
<b>791</b>	pCMX3b-Flag HBx-V5 SCM6	pCMX3b vector encoding HBV HBx SCM at aa position 140 with CMV promoter and N-terminal Flag-tag and C-terminal V5-tag	This work

### 2.1.3.2. Oligonucleotides

All oligonucleotides were obtained from Metabion (Planegg, Germany).

**Table 9: Primers including database number, sequence, and purpose.**

No.	Primer	Sequence	Purpose
71	366CMV/fwd	CCCACTGCTTACTGGC	sequencing
72	675pCMX3Brev	CCAATTATGTCACACCA	sequencing
92	pcDNA fwd	TAATACGACTCACTATAGGG	sequencing
92	pcDNA fwd	TAATACGACTCACTATAGGG	sequencing
93	pcDNA rev	GGCACCTTCCAGGGTCAAG	sequencing
104	PrP fwd	TGCTGGGAAGTGCCATGAG	qPCR
105	PrP rev	CGGTGCATGTTTTACGATAGTA	qPCR
106	cccDNA fwd	GCCTATTGATTGGAAAGTATGT	qPCR
107	cccDNA rev	AGCTGAGGCGGTATCTA	qPCR
108	HBV DNA fwd	GTTGCCCGTTTGTCTCTAATTC	qPCR
109	HBV DNA rev	GGAGGGATACATAGAGGTTCCCTTG A	qPCR
187	qPCR 18S fwd	CGGCTACCACATCCAAGGAA	qPCR
188	qPCR 18S rev	GCTGGAATTACCGCGGCT	qPCR
197	qPCR GAPDH fwd	CATCCTGGGCTACACTGA	qPCR
198	qPCR GAPDH rev	TTGACAAAGTGGTCGTTG	qPCR
387	pLENTI HBx fwd	GTGGTGAATTCATGGCTGC	cloning
388	HBx-V5 rev D	ATAGAATTCTTAACCGGTACGCGT AGAATC	cloning
389	HBx rev D	ATAGAATTCTTAGGCAGAGGTGAA AAAGTTGC	cloning
390	PML1 rev	CAGAACTGGAACCTCCTCCTC	sequencing
391	PML1 fwd	GTGCCGGACGTGACAAACG	sequencing
394	pLKO.neo fwd	CATGGAGAGCTGTACAAGTCC	sequencing
394	pLKO.neo fwd	CATGGAGAGCTGTACAAGTCC	sequencing
395	pLKO.neo rev	CTGGATCTCTGCTGTCCCTG	sequencing

<b>395</b>	pLKO.neo rev	CTGGATCTCTGCTGTCCCTG	sequencing
<b>398</b>	HBx 140 fwd	GGAGGCTGTAGGCATAGATTGGTC TGCGCACC	cloning
<b>399</b>	HBx 140 rev	GGTGCGCAGACCAATCTATGCCTA CAGCCTCC	cloning
<b>400</b>	HBx 130 fwd D	GAGGAGATTAGGTTAGAGGTCTTT GTATTAGG	cloning
<b>401</b>	HBx 130 rev D	CCTAATACAAAGACCTCTAACCTAA TCTCCTC	cloning
<b>404</b>	HBx 113/118 fwd D	GTGTTTtagggactgggaggagct GGG	cloning
<b>405</b>	HBx 113/118 rev D	ACAGTCTCTGAAGTAGGCCTCAAG GTCG	cloning
<b>408</b>	HBx 91/95 fwd D	GTCTTACATAGGAGGACTCTTGGA CTCCCAG	cloning
<b>409</b>	HBx 91/95 rev D	CCTGGGCAGGATCTGATGGGCG	cloning
<b>469</b>	pcDNA3/pCMX3b- 798fwd	GGTAGGCGTGTACGGTGG	sequencing
<b>858</b>	DDB1/BamHI/fwd	ATAGGATCCCCAAGCTTGGTACCG GGTATG	cloning
<b>859</b>	DDB1/XbaI/rev	TATTCTAGACTAGAGGATCCGAGT TAGCTC	cloning
<b>860</b>	HBV1805fw total HBV transcripts	TCACCAGCACCATGCAAC	qPCR
<b>861</b>	HBV1896rev total HBV transcripts	AAGCCACCCAAGGCACAG	qPCR

## 2.1.4. Antibodies

### 2.1.4.1. Primary antibodies

**Table 10: Primary antibodies including database number, properties, and company.**

Database No.	Antibody	Properties	Company [Reference]
AG Protzer	Core	anti-rabbit	CellMarque, Rocklin, USA
16	PML	anti-rabbit	Novus Biologicals, Abingdon, UK
17	PML	anti-mouse	Santa Cruz, Dallas, USA
19	Flag-M2	anti-mouse	Sigma Aldrich, Hamburg, Germany
21	HA	anti-rat	kindly provided by Elisabeth Kremmer
33	V5	anti-mouse	Abcam, Cambridge, UK
39	GFP	anti-rabbit	Abcam, Cambridge, UK
41	6-His	anti-mouse	Clontech, Mountain View, USA
46	HBx (X36C)	anti-mouse	Invitrogen, Karlsruhe, Germany
47	Sp100	anti-rabbit	kindly provided by Hans Will
54	Ubiquitin (P4D1)	anti-mouse	Cell Signaling Technology, Cambridge, UK
57	DDB1	anti-mouse	Santa Cruz, Dallas, USA
61	$\beta$ -actin (AC-15)	anti-mouse	Sigma Aldrich, Hamburg, Germany
67	Core	anti-mouse	Santa Cruz, Dallas, USA
79	Smc5 (B-11)	anti-mouse	Santa Cruz, Dallas, USA
100	Flag	anti-rabbit	Cell Signaling Technology, Cambridge, UK
133	SUMO	anti-mouse	Abcam, Cambridge, UK
140	PML	anti-rabbit	Novus Biologicals, Abingdon, UK
145	Cul4 (H11)	anti-mouse	Santa Cruz, Dallas, USA
167	SAF-A	anti-rabbit	Merck, Darmstadt, Germany

AG Protzer	HBV core (216A-14ASR)	anti-rabbit	Cell marque, Rockin, USA
AG Protzer	Smc6 (M01)	anti-mouse	Acepta, San Diego, USA

#### 2.1.4.2. Secondary antibodies

**Table 11: Secondary antibodies for western blot analysis including dilution, properties, and company.**

Antibody	Dilution	Properties	Company
HRP-anti-mouse IgG	1:10000	Horseradish peroxidase conjugated AffiniPure F(ab') <sub>2</sub> fragment goat anti-mouse IgG	Dianova/Jackson Immunoresearch, Hamburg, Germany
HRP-anti-rabbit IgG	1:10000	Horseradish peroxidase conjugated AffiniPure F(ab') <sub>2</sub> fragment goat anti-rabbit IgG	Dianova/Jackson Immunoresearch, Hamburg, Germany
HRP-anti-rat IgG	1:10000	Horseradish peroxidase conjugated AffiniPure F(ab') <sub>2</sub> fragment goat anti-rat IgG	Dianova/Jackson Immunoresearch, Hamburg, Germany

**Table 12: Secondary antibodies for immunofluorescence stainings including dilution, properties, and company.**

Antibody	Dilution	Properties	Company
647-anti-mouse	1:200	Alexa-647 conjugated goat-anti-mouse-antibody	Dianova/Jackson Immunoresearch, Hamburg, Germany
488-anti-rabbit	1:200	Alexa-488 conjugated goat-anti-rabbit-antibody	Dianova/Jackson Immunoresearch, Hamburg, Germany
578-anti-rabbit	1:1000	PE F(ab') <sub>2</sub> donkey anti-rabbit IgG 578	BD Biosciences, Franklin Lakes, USA

## 2.1.5. Enzymes and buffers

**Table 13: Enzymes and buffers including the indicated company.**

<b>Enzyme</b>	<b>Company</b>
Antarctic phosphatase	New England BioLabs, Ipswich, USA
Antarctic phosphatase reaction buffer (10 x)	New England BioLabs, Ipswich, USA
BamHI	New England BioLabs, Ipswich, USA
BEP II	Siemens Molecular Diagnostics, Marburg Germany
Buffer 3.1	New England BioLabs, Ipswich, USA
CutSmart buffer	New England BioLabs, Ipswich, USA
DpnI (20000 U/ml)	New England BioLabs, Ipswich, USA
EcoRI	New England BioLabs, Ipswich, USA
FIX&PERM	eBioscience, San Diego, USA
NcoI	New England BioLabs, Ipswich, USA
NEBuffer EcoRI	New England BioLabs, Ipswich, USA
PfuUltra II Fusion HS DNA Polymerase	Agilent Technologies, Santa Clara, US
PfuUltra II Fusion Reaction buffer (10 x)	Agilent Technologies, Santa Clara, US
Proteinase K	Sigma-Aldrich, St. Louis, USA
RNase A	Roth, Karlsruhe, Germany
T4 DNA ligase (400000 U/ml)	New England BioLabs, Ipswich, USA
T4 DNA Ligation buffer, 2 x conc.	New England BioLabs, Ipswich, USA
T4 ligase buffer (10X)	Roche, Basel, Switzerland
T4 Polynucleotide Kinase, PNK	New England BioLabs, Ipswich, USA
T5 exonuclease	New England Biolabs, Ipswich, USA
XhoI	New England BioLabs, Ipswich, USA

## 2.1.6. Chemicals and reagents

Table 14: Chemicals and reagents including the indicated company.

Substance	Company
2-Propanol	Roth, Karlsruhe, Germany
30% acrylamide/bisacrylamide mixture	Roth, Karlsruhe, Germany
6x DNA loading dye	New England BioLabs, Ipswich, USA
Agarose	Biozym, Hessisch Oldendorf, Germany
AGFA-GEVAERT G15 Developing solution	Valmex Medical Imaging, Hamburg, Germany
AGFA-GEVAERT G35 Fixation solution	Valmex Medical Imaging, Hamburg, Germany
Ampicillin	Sigma-Aldrich, St. Louis, USA
Aprotinin	Sigma-Aldrich, St. Louis, USA
APS	AppliChem, Darmstadt, Germany
Arsenic	Sigma-Aldrich, St. Louis, USA
Boric acid > 99,8%	Sigma-Aldrich, St. Louis, USA
Bovine serum albuminates (BSA)	New England BioLabs, Ipswich, USA
Bradford reagent	AppliChem, Darmstadt, Germany
Bromphenol blue	Roth, Karlsruhe, Germany
CaCl <sub>2</sub>	Roth, Karlsruhe, Germany
CellTiter-Blue Cell Viability Assay system	Promega, Madison, USA
Collagen R	Serva Electrophoresis, Heidelberg, Germany
DAPI	Sigma-Aldrich, St. Louis, USA
Dimethyl sulfoxide (DMSO) ≥ 99.5%	Roth, Karlsruhe, Germany
DMEM	Sigma-Aldrich, St. Louis, USA
dNTP mix (100 mM)	New England BioLabs, Ipswich, USA
EDTA	AppliChem, Darmstadt, Germany
Ethanol	Roth, Karlsruhe, Germany
Ethidium bromide	Sigma-Aldrich, St. Louis, USA

Fetal Bovine Serum (FBS) Gibco	Thermo Fisher Scientific, Waltham, USA
Formaldehyde	Thermo Fisher Scientific, Waltham, USA
Glycerol	AppliChem, Darmstadt, Germany
Glycine	AppliChem, Darmstadt, Germany
Guanidine hydrochloride	AppliChem, Darmstadt, Germany
H <sub>2</sub> O <sub>2</sub>	Sigma-Aldrich, St. Louis, USA
HCl	Roth, Karlsruhe, Germany
HiScrib T7 ARCA mRNA Kit (with tailing)	New England BioLabs, Ipswich, USA
Hydrocortisone	Sigma-Aldrich, Darmstadt, Germany
Imidazole	AppliChem, Darmstadt, Germany
Insulin	Sigma-Aldrich, Darmstadt, Germany
Iodacetamide	Sigma-Aldrich, St. Louis, USA
Isopropanol	Roth, Karlsruhe, Germany
KCl	Roth, Karlsruhe, Germany
KOAc	Merck, Darmstadt, Germany
Leupeptin	Roche, Basel, Switzerland
L-Glutamine	Sigma-Aldrich, Steinheim, Germany
LightCycler 480 SYBR Green I Master mix	Roche, Basel, Switzerland
Lipofectamine MessengerMax	Invitrogen/Thermo Fisher Scientific, Carlsbad, USA
Luminol sodium salt	Sigma-Aldrich, St. Louis, USA
Methanol	Roth, Karlsruhe, Germany
MG132	Sigma-Aldrich, St. Louis, USA
MgCl <sub>2</sub>	AppliChem, Darmstadt, Germany
MnCl <sub>2</sub>	Roth, Karlsruhe, Germany
Mowiol 4-88	Roth, Karlsruhe, Germany
Na <sub>2</sub> HPO <sub>4</sub>	VWR International, Darmstadt, Germany
NaCl	Roth, Karlsruhe, Germany
NaH <sub>2</sub> PO <sub>4</sub>	Merck, Darmstadt, Germany

NaOH	Roth, Karlsruhe, Germany
NEAA (100 x)	Gibco/Life Technologies, Carlsbad, USA
N-ethylmaleimide	Sigma-Aldrich, St. Louis, USA
NiNTA resin	Thermo Scientific, Waltham, USA
Nonidet-P40	AppliChem, Darmstadt, Germany
NucleoSpin Tissue Kit	Macherey-Nagel, Düren, Germany
PageRuler prestained protein ladder plus	Thermo Scientific, Waltham, USA
Pansorbin	Calbioche, Merck, Darmstadt, Germany
PBS	Biochrom, Berlin, Germany
p-Coumaric acid	Sigma-Aldrich, Darmstadt, Germany
PEG6000	Sigma-Aldrich, Darmstadt, Germany
PEI	Polxsciences, tebu-bio, Sigma-Aldrich, St. Louis, USA
Penicillin/streptomycin	Sigma-Aldrich, St. Louis, USA
Pepstatin	AppliChem, Darmstadt, Germany
Phenol/chloroform/isoamyl alcohol	Roth, Karlsruhe, Germany
Phenylmethylsulfonyl fluoride (PMSF)	Sigma-Aldrich, St. Louis, USA
Plasmid Maxi kit	QIAGEN, Hilden, Germany
Polyacrylamide	Roth, Karlsruhe, Germany
Quick-Load® 1 kb DNA Ladder	New England BioLabs, Ipswich, USA
RbCl <sub>2</sub>	AppliChem, Darmstadt, Germany
Reverse Transcription System	Promega, Madison, USA
RNA Clean & Concentrator-25	Zymo Research, Irvine, USA
Saccharose	Loewe Biochemica, Sauerlach, Germany
SDS ultrapure	AppliChem, Darmstadt, Germany
Sepharose A beads	Sigma-Aldrich, St. Louis, USA
Skim milk powder	Sigma-Aldrich, St. Louis, USA
Sodium acetate	Roth, Karlsruhe, Germany
Sodium azide	AppliChem, Darmstadt, Germany

Sodium deoxycholate	Roth, Karlsruhe, Germany
Sodium pyruvat	Gibco/Life Technologies, Carlsbad, USA
Sodiumacetate	Sigma-Aldrich, St. Louis, USA
TEMED	AppliChem, Darmstadt, Germany
Tris	Roth, Karlsruhe, Germany
Triton X-100	Sigma-Aldrich, Darmstadt, Germany
Trypan blue	Gibco/Life Technologies, Carlsbad, USA
Trypsin/EDTA	Sigma-Aldrich, St. Louis, USA
Tween-20	AppliChem, Darmstadt, Germany
Urea	AppliChem, Darmstadt, Germany
$\beta$ -mercaptoethanol	AppliChem, Darmstadt, Germany

### 2.1.7. Laboratory equipment

**Table 15: Laboratory equipment including the indicated supplier.**

<b>Equipment</b>	<b>Supplier</b>
Accu-jet pro pipette controller	Sigma-Aldrich, Darmstadt, Germany
Architect i2000SR System	Abbott, Chicago, USA
Avanti Je centrifuge	Beckman Coulter, Brea, USA
Axiovert 200 M microscope	Zeiss, Oberkochen, Germany
Branson Ultrasonics Analog Sonifier 450-CE	Thermo Fisher Scientific, Waltham, USA
Concentrator 5301	Eppendorf, Hamburg, Germany
Curix 60	AGFA, Mortsel, Belgium
CytoFLEX Flow Cytometer	Beckman Coulter, Brea, USA
Freezer, -20°C	Liebherr, Kempten, Germany
Frosty freezing container	Thermo Fisher Scientific, Waltham, USA
Gel chambers (agarose gel electrophoresis)	Peqlab, Erlangen, Germany

Gel Doc XR+ Gel Documentation System	Bio-Rad, München, Germany
Glass Micro Pipette	Hamilton Company, Reno, US
Heracell 150 CO <sub>2</sub> incubator	Thermo Fisher Scientific, Waltham, USA
Heraeus BB16 Function Line CO <sub>2</sub> incubator	Heraeus Instruments, Hanaua, Germany
Heraeus Fresco 17 Microcentrifuge	Heraeus Instruments, Hanaua, Germany
Heraeus Fresco 21 Microcentrifuge	Heraeus Instruments, Hanaua, Germany
Heraeus Herafreeze HFU 586 Basic	Heraeus Instruments, Hanaua, Germany
Heraeus Laminair HLB 2448 GS	Heraeus Instruments, Hanaua, Germany
Heraeus Megafuge 40 centrifuge	Heraeus Instruments, Hanaua, Germany
Heraeus: Herasafe HSP 12	Heraeus Instruments, Hanaua, Germany
Incubation Shaker Multitron Standard	Infors HT, Bottmingen, Switzerland
Incubator model 200	Memmert, Büchenbach, Germany
Inverted Research Microscope ECLIPS Ti	Nicon, Minato, Japan
LightCycler 480 Instrument II	Roche, Basel, Switzerland
Mastercycler Gradient	Eppendorf, Hamburg, Germany
Microwave 9029GD	Privileg, Stuttgart, Germany
ML-DNY-43 NewClassic	Mettler Toledo, Columbus, USA
MS 3 basic vortexer	IKA®-Werke & Co. KG, Staufen im Breisgau, Germany
Multigel electrophoresis chamber	Biometra, Jena, Germany
Multipette Plus	Eppendorf, Hamburg, Germany
Multitron incubation shaker	Infors HT, Bottmingen, Switzerland
NanoDrop 2000c Spectrophotometer	Thermo Fisher Scientific, Waltham, USA
Neubauer counting chamber (improved)	Assistent Hecht, Sondheim v. d. Rhön, Germany
No frost refrigerator and freezer CUN 3523	Liebherr, Kempten, Germany
Power Pac Standard P25	Biometra, Jena, Germany
PowerPac Basic Power Supply	Bio-Rad, München, Germany

PowerPac Universal Power Supply	Bio-Rad, München, Germany
Primover light microscope	Zeiss, Oberkochen, Germany
Reciprocating Shaker 3016	GFL Gesellschaft für Labortechnik, Burgwedel, Germany
Research plus pipette, 100-1000 µl	Eppendorf, Hamburg, Germany
Research plus pipette, 10-100 µl	Eppendorf, Hamburg, Germany
Research plus pipette, 20-200 µl	Eppendorf, Hamburg, Germany
Rotina 420R centrifuge	Hettich, Tuttlingen, Germany
Rotina 50RS centrifuge	Hettich, Tuttlingen, Germany
Sartorius portable	Sartorius AG, Göttingen, Germany
SmartSpec Plus Spectrophotometer	Bio-Rad, München, Germany
Sprout Mini Centrifuge	Heathrow Scientific, Vernon Hills, USA
Tecan Infinite M200 Multimode Reader	Tecan, Männedorf, Germany
Test Tube Rotating Shaker 3025	GFL Gesellschaft für Labortechnik, Burgwedel, Germany
Heraeus Incubator Thermo Scientific BB 15 CO <sub>2</sub>	Thermo Fisher Scientific, Waltham, USA
Thermocycler peqSTAR 96x universal gradient	VWR International, Darmstadt, Germany
Thermomixer Comfort 5355	Eppendorf, Hamburg, Germany
Trans-Blot Cell chamber	Bio-Rad, München, Germany
Unitwist RT	UniEquip Laborgerätebau- und Vertrieb, Planegg, Germany
Universal Hood II Gel Doc	Bio-Rad, München, Germany
Vacusaft vacuum pump	Integra, Biosciences, Zizers, Switzerland
Vortex-Genie 2T	Scientific Industries, Inc., Bohemia, US
VWR® Horizontal Gel Electrophoresis Systems	VWR International, Darmstadt, Germany
0.2 µm cell strainer	Corning, New York City, USA
Research plus pipette, 2-20 µl	Eppendorf, Hamburg, Germany
Research plus pipette, 0.1-2.5 µl	Eppendorf, Hamburg, Germany
Research plus pipette, 0.5-10 µl	Eppendorf, Hamburg, Germany

## 2.1.8. Disposable laboratory equipment

Table 16: Laboratory equipment including the indicated company.

Equipment	Company
96-multiwell plate black	Greiner, Sigma-Aldrich, Darmstadt, Germany
Aspiration pipette	Greiner, Sigma-Aldrich, Darmstadt, Germany
Blotting paper 460x570 mm, 195 g/m <sup>2</sup>	Hartenstein, Würzburg, Germany
Cell scraper	Sarstedt, Nürnbrecht, Germany
Cover slides 12 mm	Hartenstein, Würzburg, Germany
Cryo vial	Nunc/ Thermo Scientific, Waltham, USA
Eppendorf Combitips advanced® pipette tips	Eppendorf, Hamburg, Germany
Falcon polypropylene round-bottom tube 2059	Fisher Scientific Company LLC, Pittsburgh, US
FrameStar 96 well semi-skirted PCR plates	4titude, Berlin, Germany
Greiner CELLSTAR serological pipette, 10 ml	Greiner, Sigma-Aldrich, Darmstadt, Germany
Greiner CELLSTAR serological pipette, 25 ml	Greiner, Sigma-Aldrich, Darmstadt, Germany
Greiner CELLSTAR serological pipette, 5 ml	Greiner, Sigma-Aldrich, Darmstadt, Germany
Kimtech Science Purple Nitrile gloves	Kimberly-Clark Worldwide, Inc., Irving, USA
Micro tube 1.5 ml	Sarstedt, Nürnbrecht, Germany
Microscope slides	Hartenstein, Würzburg, Germany
Multiply-Pro tube 0.2 ml	Sarstedt, Nürnbrecht, Germany
Nitril NextGen gloves, small	Meditrade, Kiefersfelden, Germany

Nitrocellulose membrane 0.45 µm NC, Amersham™ Protran™	GE Healthcare, Chicago, USA
96 well platte	Sarstedt, Nürnberg, Germany
Parafilm M All-Purpose Laboratory Film	Bemis Company, Inc., Neenah, USA
Pipette filter tips 100-1000 µl	Sarstedt, Nürnberg, Germany
Pipette filter tips 1-10 µl	Sarstedt, Nürnberg, Germany
Pipette tips 2-100 µl	Sarstedt, Nürnberg, Germany
Semi-micro cuvette, acrylic	Sarstedt, Nürnberg, Germany
Sterile filter 0.45 µm	Merck, Darmstadt, Germany
Tissue culture dish 100, standard 83.3902	Sarstedt, Nürnberg, Germany
Tissue culture dish 150, standard 83.3903	Sarstedt, Nürnberg, Germany
Tissue culture plate 12 well, standard F 83.3921	Sarstedt, Nürnberg, Germany
Tissue culture plate 6 well, standard F 83.3920	Sarstedt, Nürnberg, Germany
Tube 15 ml, 62.554.502	Sarstedt, Nürnberg, Germany
Tube 50 ml, 62.547.254	Sarstedt, Nürnberg, Germany
X-ray films	Consumer Electronics Association, Arlington, USA

### 2.1.9. Softwares and programs

**Table 17: Softwares and programs with including the indicated publisher and purpose.**

<b>Software</b>	<b>Publisher</b>	<b>Purpose</b>
Adobe Photoshop CS5	Adobe, San José, USA	Image and Layout processing
Adobe Reader XI	Adobe, San José, USA	PDF data processing
BLAST	National Center for Biotechnology Information National Library of	Basic Local Alignment Search Tool

	Medicine, Rockville Pike, USA	
CLC Sequence Viewer 6	CLC bio, Aarhus, Denmark	Genome and Sequencing analysis
Endnote X8	Thomson Reuters, Toronto, Canada	Reference organization
Excel 2010	Microsoft, Redmond, USA	Data and table processing
Filemaker Pro 14	Claris International Inc., Cupertino, USA	Database management
FlowJo, LLC BD	BD, Franklin Lakes, USA	Flow cytometry analysis
GPS-SUMO 2.0 [461, 462]	The CUCKOO Workgroup, Wuhan, China	Prediction of potential SUMOylation and SUMO interacting motifs
GraphPad Prism 5.01	GraphPad Software Inc., San Diego, USA	Figure processing and statistical analysis
ImageJ [463]	NIH, Rockville, USA	Signal intensity calculations
PyMOL viewer 1.8.6.0	Schrödinger, Python License, New York, USA	Molecular Graphics System
Quantity One software 4.6.9 basic	Bio-Rad, München, Germany	Imaging and analyzing electrophoresis gels
<i>Serial Cloner 2.6.1</i>	Franck Perez, Serial Basics	Molecular biology software
Volocity 6.3.0	PerkinElmer Inc., Waltham, USA	Image acquisition and processing
Windows 7/8/10	MS Office Microsoft, Redmond, USA	Processing of text and images

## **2.2. Methods**

### **2.2.1. Cell culture techniques**

#### **2.2.1.1. Maintenance of cell lines**

All utilized human adhesive cells were generally propagated as monolayers on polystyrene tissue culture dishes (12-well, 6-well, 100 mm, 150 mm) under standard sterile cell culture conditions at 37°C, 5% CO<sub>2</sub> and 95% humidity (Heracell 150 CO<sub>2</sub> Incubator, Thermo Scientific; Heraeus Incubator BB 15 CO<sub>2</sub>, Thermo Scientific) in the cell line dependent standard media (Table 3, 4, 5). HepG2-derived cells were cultures on tissue culture dishes additionally coated with Collagen (1:10 in ddH<sub>2</sub>O) for 20 min at room temperature and washed with 1x phosphate buffered saline PBS (3 mM KCl, 1.5 mM KH<sub>2</sub>PO<sub>4</sub>, 4 mM Na<sub>2</sub>HPO<sub>4</sub>, 140 mM NaCl, pH 7.4, autoclaved). Mycoplasma tests were performed frequently and cell culture experiments were exclusively carried out with mycoplasma-negative cells.

For subculturing, confluent cells were washed with an appropriate amount of 1x PBS and detached by adding Trypsin/EDTA for 5-12 min at 37 °C. Trypsin activity was blocked by standard propagation medium, cells were rinsed, transferred into a 50 ml tube and centrifuged at 2000 rpm for 3 min (Heraeus Megafuge 40, Thermo Fisher Scientific). The cell pellet was resuspended in an appropriate amount of supplemented standard media dependent on the cell line. Cells were distributed in dilutions of 1:2–1:10 on tissue culture dishes for further propagation or counted and seeded for further experiments.

#### **2.2.1.2. Seeding of cells**

For comparable experiments, determination of cell number was indispensable. As described in 2.2.1.1.. Cells were detached from the tissue culture dish, centrifuged, and resuspended in standard media. 10 µl of this cell suspension were diluted 1:2 in Trypan blue and cells were counted in a hemocytometer Neubauer counting chamber with the Primovert light microscope. The calculation average number of 2 quadrants,

each containing 16 small squares, multiplied with dilution factor 2 and  $10^4$  results in the number of cells in 1 ml of the cell suspension.  $4 \times 10^6$  cells were seeded for a 100 mm dish,  $4 \times 10^5$  cells/ well for a 6-well plate and  $1.2 \times 10^5$  cells/well for a 12-well plate were seeded. For immunofluorescence staining, glass cover slides were additionally placed into the tissue culture dish. After 24 h further experiments were performed. For HBV infection experiments, HepG2-NTCP-K7 cells or HepaRG cells were seeded and subsequently differentiated in the appropriate differentiation media (Table 4, 5) for 2 days or 14 days respectively.

### **2.2.1.3. Harvesting of cells**

At a selected time point after transfection and/or infection, cultivated cells were detached from the tissue culture dish using a cell scraper. The plates were washed once with 1x PBS and the suspension was transferred in an appropriate tube. After centrifugation at 2000 rpm for 3 min (Heraeus Megafuge 40, Thermo Fisher Scientific) the pellet was washed with 5 ml 1x PBS and centrifuged again. The pelleted cells were frozen at  $-20^{\circ}\text{C}$  immediately for following experiments.

### **2.2.1.4. Storage of cells**

For long-term storage of cells, the cell pellet (described in 2.2.1.1.) was resuspended in FBS supplemented with 10% dimethyl sulfoxide (DMSO). This suspension was transferred into a cryo vial and frozen using a Frosty freezing container for at least 6 h at  $-80^{\circ}\text{C}$ .

For further use frozen cells were thawed at  $37^{\circ}\text{C}$  in a water bath and transferred in a 15 ml tube containing media. The suspension was centrifuged at 2000 rpm for 3 min (Heraeus Megafuge 40, Thermo Fisher Scientific), the cell pellet was resuspended in pre-warmed standard cultivation media and transferred on a tissue culture dish.

#### **2.2.1.5. Treatment with the proteasome inhibitor MG132**

Cells were seeded (2.2.1.2.) as described previously and transfected (2.2.5.10., 2.2.5.11.). 10  $\mu$ M MG132 (dissolved in DMSO) were added to the standard cultivation medium 16 h before harvesting (2.2.1.3.). DMSO served as a treatment control. Following experiments were performed as described.

#### **2.2.2. Bacteria**

##### **2.2.2.1. Preparation of chemically competent bacteria**

Chemically competent *Escherichia coli* DH5 $\alpha$  (*E. coli*) bacteria were plated on a LB agar plate and incubated overnight at 37°C (Incubator model 200, Memmert). A single colony was picked and inoculated in 10 ml LB medium (5 g/l NaCl, 10 g/l Trypton, 5 g/l Yeast extract) overnight at 37°C and 220 rpm (Incubation Shaker Multitron Standard, Infors HT). 2 ml of this liquid culture were transferred into 200 ml LB medium and incubated at 37°C with 220 rpm until an OD<sub>600</sub>=0.43 (SmartSpec Plus Spectrophotometer, Bio-Rad) was reached. The liquid culture was cooled on ice water for 20 min, transferred in a 50 ml tube and centrifuged for 5 min at 3000 rpm at 4°C (Rotina 50RS, Hettich centrifuge). The cell pellet was resuspended in 15 ml transformation buffer I (TFBI: 15% (v/v) glycerol, 10 mM calcium chloride (CaCl<sub>2</sub>), 30 mM potassium acetate (KOAc), 50 mM manganese(II) chloride tetrahydrate (MnCl<sub>2</sub>), ddH<sub>2</sub>O fill until 500 ml, pH=5.8) centrifuged and the pellet was dissolved in 4 ml transformation buffer II (TFB II: 15% (v/v) glycerol, 75 mM calcium chloride (CaCl<sub>2</sub>), 10 mM 3-(*N*-morpholino)propanesulfonic acid pH=7.0, 10 mM rubidium chloride (RbCl<sub>2</sub>), ddH<sub>2</sub>O fill until 500 ml, pH=5.8). Aliquots of 100  $\mu$ l DH5 $\alpha$  *E. coli* bacteria were pipetted in pre-cooled 1.5 ml micro tubes, frozen in liquid nitrogen and stored at -80°C.

### **2.2.2.2. Heat shock transformation of chemically competent *E. coli* bacteria**

Heat shock transformation of 0.5 µg plasmid DNA for re-transformation or 10 µl for freshly ligated DNA was performed with 100 µl chemically competent DH5α *E. coli* bacteria in a Falcon polypropylene tube. This suspension was incubated for 30 min on ice, followed by a heat shock for 40 s in the water bath (42°C) while shaking the Falcon polypropylene tube. The tube was immediately put back on ice and 1 ml LB medium was added. After incubation for 60 min at 37°C with 220 rpm (Incubation Shaker Multitron Standard, Infors HT) an appropriate amount was plated on a LB plate containing the appropriate antibiotic (100 µg/ml ampicillin or 25 µg/ml kanamycin) depending on the plasmid resistance. The solid bacterial culture LB plate was incubated at 37°C overnight (Incubator model 200, Memmert).

### **2.2.2.3. Storage and liquid bacterial culture**

For long-term storage of bacteria, glycerol stocks were produced. 5 ml of the liquid DH5α *E.coli* cultures were centrifuged at 4500 rpm for 10 min (Rotina 420R, Hettich centrifuge), the pellet was resuspended in 1 ml solution containing LB medium and 87% glycerol in ratio 1:1. The cell suspension was stored in a cyro vial at -80°C. A solid bacterial culture from either a bacterial transformation or from a glycerol stock was grown. For liquid bacterial culture, a single bacteria colony was inoculated in LB medium containing antibiotic (100 µg/ml) depending on the plasmid resistance. The amount of LB medium was dependent on the prospective techniques (Maxi-preparation 500 ml, TIP20 55 ml, Mini-preparation 5 ml). All cultures were incubated over night at 37°C with 150 rpm (Incubation Shaker Multitron Standard, Infors HT) and could be stored for one week at 4°C for further experiments.

### 2.2.3. Hepatitis B virus infection

Cells were seeded and differentiated as described in 2.2.1.2.. Hepatitis B virus infection was performed in differentiation media supplemented with 4% PEG6000 and the appropriate amount of virus, which was calculated with the following formula.

$$\text{Volume virus stock solution} = \frac{\text{cell number} * \text{MOI} * \text{number of plates/wells}}{\text{viral titer}}$$

The suspension was added to differentiated cells and incubated for 16-24 h post infection at 37°C (Heracell 250 CO<sub>2</sub> Incubator, Thermo Scientific) until the HBV containing medium was removed. Cells were washed three times with 1x PBS and the corresponding differentiation medium was added. The differentiation medium was changed 4 days post infection (d.p.i.). Cells were harvested after 4 or 7 days (2.2.1.3.).

### 2.2.4. Protein biochemistry methods

#### 2.2.4.1. Whole-cell protein lysates

The cells were harvested, as described previously (see 2.2.3.7.). The following steps were performed on ice to counteract degradation processes. The cell pellet was resuspended in 50-300 µl RIPA buffer (5 mM EDTA, 1% (v/v), 150 mM NaCl, 1% Nonidet-P40, 0.1% (w/v) SDS, 0.5% Sodium-deoxycholate, 50 mM Tris-HCl pH=8.0) freshly supplemented protease inhibitors (1:1000 PMSF, 1:100 Leupeptin, 1:100 Pepstatin A and 1:100 Aprotinin) depending on the pellet size. This suspension was incubated for 30 minutes, while it was vortexed every 10 minutes. After 30 seconds of sonification with 40 pulses, 80% output and 0.8 pulses/s at 5°C using a Branson Ultrasonics Analog Sonifier 450-CE (Thermo Fisher Scientific), the sample was centrifuged at 11000 rpm for 3 min at 4°C (Heraeus Fresco 17 Microcentrifuge, Thermo Fisher Scientific). The supernatant was transferred into a new, pre-cooled micro tube and the protein concentration was determined by performing an Bradford Assay [464]. Therefore 800 µl H<sub>2</sub>O, 1 µl of the sample and 200 µl Bradford reagent were pipetted

into a semi-micro acrylic cuvette and mixed. The absorbance of the BSA dilution row concomitant of the lysate was measured at 595 nm by a SmartSpec Plus Spectrophotometer (Bio-Rad). Finally, the protein concentration could be determined in relation to the BSA standard curve. The lysate was diluted with H<sub>2</sub>O and 5x Laemmli buffer (3.75% β-mercaptoethanol, 0.5% (w/v) bromphenole blue, 10% (w/v) SDS, 250 mM Tris-HCl pH=6.8), boiled for 3 min at 95°C (Thermomixer Comfort 5355, Eppendorf), cooled on ice and subsequently stored at -20°C.

### **2.2.4.2. Insoluble membranous fraction**

Cells were harvested, resuspended in 50-300 µl RIPA buffer with freshly supplemented protease inhibitors, incubated for 30 minutes as described previously for whole-cell protein lysates (2.2.4.1.). After centrifugation at 11000 rpm for 3 min at 4°C (Heraeus Fresco 17 Microcentrifuge, Thermo Fisher Scientific) the supernatant was utilized for whole-cell protein lysate preparation (2.2.4.1.), whereas the remaining cell pellet was used for the insoluble matrix fraction. For this, 50-300 µl 2x Laemmli (1.43% β-mercaptoethanol, 0.2% (w/v) bromphenol blue, 20% (v/v) glycerol, 4% (w/v) SDS, 100 mM Tris-HCl pH=6.8) were added to the pellet. This suspension was resuspended by pipetting and boiled for 10 min at 95°C and 1400 rpm (Thermomixer Comfort 5355, Eppendorf), cooled on ice and subsequently stored at -20°C.

### **2.2.4.3. Nickel-nitrilotriacetic acid (NiNTA) pulldown**

Cells were seeded, transfected or infected and harvested as described previously. The harvested cell pellet was resuspended in 5 ml 1x PBS, of which 1 ml was separated for the whole-cell protein lysate as an input control (see 2.2.4.1), while the remaining 4 ml were centrifuged at 2000 rpm for 3 min (Heraeus Megafuge 40, Thermo Fisher Scientific). The pellet was resuspended in 5 ml Guanidinium lysis buffer B1 and either stored in -80°C or immediately homogenized by sonification for 30 s with 40 pulses, 80% output and 0.8 pulses/s at 5°C (Branson Ultrasonics Analog Sonifier 450-CE, Thermo Fisher Scientific). 30 µl NiNTA beads per sample were centrifuged at 4°C and

600 x g for 3 min (Heraeus Fresco 21 Microcentrifuge, Thermo Fisher Scientific) and washed twice with B1. The NiNTA beads were added to the sonified sample and incubated at 4°C on the Test Tube Rotating Shaker 3025 overnight to bind the His<sub>6</sub>-tagged proteins. The sample was centrifuged for 10 min at 4000 rpm at 4°C (Rotina 420R, Hettich centrifuge). The NiNTA beads were transferred to a 1.5 ml micro tube and were washed successively with Guanidinium lysis buffer B1, buffer B2 and buffer B3. The supernatant was removed after centrifugation and 20 µl elution buffer were added to the NiNTA beads. The suspension was incubated 10 min at room temperature, boiled for 3 min at 95°C (Thermomixer Comfort 5355, Eppendorf), cooled on ice and stored at -20°C.

**Table 18: Composition of the utilized buffers for NiNTA pull down.**

<b>Buffer</b>	<b>Chemical</b>	<b>Concentration</b>
<b>B1 (guanidinium lysis buffer)</b>	Guanidinehydrochloride	6 M
	Na <sub>2</sub> HPO <sub>4</sub>	100 mM
	NaH <sub>2</sub> PO <sub>4</sub>	100 mM
	Tris-HCl, pH 8.0	10 mM
	Imidazole	20 mM
	β-mercaptoethanol	5 mM
<b>B2 (wash buffer, pH 8.0)</b>	Urea	8 M
	Na <sub>2</sub> HPO <sub>4</sub>	100 mM
	NaH <sub>2</sub> PO <sub>4</sub>	100 mM
	Tris-HCl, pH 8.0	10 mM
	Imidazole	20 mM
	β-mercaptoethanol	5 mM
<b>B3 (wash buffer, pH 6.3)</b>	Urea	8 M
	Na <sub>2</sub> HPO <sub>4</sub>	100 mM
	NaH <sub>2</sub> PO <sub>4</sub>	100 mM
	Tris-HCl, pH 6.3	10 mM
	Imidazole	20 mM
	β-mercaptoethanol	5 mM

---

<b>Elution buffer</b>	Imidazole	200 mM
	SDS	0.1% (w/v)
	Tris-HCl, pH 6.3	150 mM
	Glycerol	30% (v/v)
	$\beta$ -mercaptoethanol	720 mM
	Bromphenol blue	0.01% (w/v)

#### 2.2.4.4. Co-immunoprecipitation

The co-immunoprecipitation assay (IP) was performed to investigate the interaction of proteins. All following steps were performed on ice. Whole-cell protein lysates were prepared according to 2.2.4.1.. 1-3 mg of the protein lysate were pre-cleared with 30  $\mu$ l Pansorbin solution in 1 ml RIPA buffer at 4°C on a Test Tube Rotating Shaker 3025. After incubation for 1-2 hour, the sample was centrifuged for 2 min at 6000 rpm at 4°C (Heraeus Fresco 21 Microcentrifuge, Thermo Fisher Scientific) and the supernatant was transferred in new micro tube.

In parallel, 3 mg Sepharose A beads per sample were swollen in 1 ml of RIPA buffer for at least 20 min at 4°C on the spinning shaker. After centrifugation at 6000 rpm for 2 min at 4°C (Heraeus Fresco 21 Microcentrifuge, Thermo Fisher Scientific) the pellet was washed three times with RIPA buffer. 0.3-0.5  $\mu$ l monoclonal antibody per sample were then attached to the swollen Sepharose A beads for at least 1-2 hour on the spinning shaker at 4°C. The sample was centrifuged, and the pellet was washed twice with RIPA buffer freshly supplemented with protease inhibitors. The antibody coupled Sepharose A beads were added to the pre-cleared lysate and incubated for 1-2 hour on the spinning shaker at 4°C. The suspension was centrifuged, and the beads were washed with RIPA buffer supplemented with freshly added protease inhibitors. 20-40  $\mu$ l of 2x Laemmli were added to the Sepharose A beads, boiled for 5 min at 95°C (Thermomixer Comfort 5355, Eppendorf) and stored at -20°C.

### 2.2.4.5. Separating protein lysates by SDS-PAGE

Sodiumdodecyl sulfate polyacrylamide gel electrophoresis (SDS-PAGE) was utilized to separate protein samples on the basis of their molecular protein weight. For this, 7 ml per separating gel were prepared like indicated in (Table 19) and covered with 2-propanol to even the border to the stacking gel. As soon as the separating gel dried, the 2-propal was removed, 2 ml 5% stacking gel (Table 19) were added and a comb, containing either 11 or 24 pockets, was inserted. The dried gel was clamped in a Multigel electrophoresis chamber following the manufacturer's instructions and filled with TGS buffer (Tris 25 mM, 200 mM glycine, 0.1% (w/v) SDS). Meanwhile, the protein samples were thawed ant heated for 3 min at 95°C (Thermomixer Comfort 5355, Eppendorf), vortexed shortly, centrifuged (Heraeus Fresco 21 Microcentrifuge, Thermo Fisher Scientific) and loaded into the gel pocked using a Hamilton, Glass Micro pipette. Molecular sizes were indicated by using the PageRuler pre-stained protein ladder. The gel was run at 15-20 mA per gel for 1.5-2 hours.

**Table 19: Composition of 10 ml stacking and 2 ml separating gel.**

	<b>10%</b>	<b>12%</b>	<b>Stacking 5%</b>
<b>ddH<sub>2</sub>O</b>	4.0 ml	3.3 ml	1.38 ml
<b>30% Acrylamide/bisacrylamide</b>	3.3 ml	4.0 ml	0.35 ml
<b>Tris-HCl, pH 8.0</b>	2.5 ml	2.5 ml	-
<b>Tris-HCl, pH 6.8</b>	-	-	0.254 ml
<b>10% SDS</b>	0.1 ml	0.1 ml	0.02 ml
<b>10% APS</b>	0.1 ml	0.1 ml	0.02 ml
<b>TEMED</b>	0.004 ml	0.004 ml	0.002 ml

### 2.2.4.6. Western blot

Proteins were separated during SDS-PAGE as described previously (2.2.4.5.) and immediately blotted on a 0.45  $\mu\text{m}$  nitrocellulose membrane for 1.5 h at 400 mA. Therefore, a membrane and 4 blotting papers were soaked with Towbin buffer (200 mM glycine, 20% (v/v) methanol, 0.05% (w/v) SDS, 25 mM Tris/HCl pH 8.3) and placed in a plastic cassette as followed: 2 layers of blotting paper, SDS-PAGE gel, membrane and 2 layers of blotting paper. The cassette was put into a Trans-Blot Cell chamber filled with Towbin buffer according to the manufacturer's instructions. After the electrophoretic transfer, the membrane was blocked for 30-90 min in 5% skim milk powder in 1x PBS. The membrane was washed three times in 1x PBS-T (0.1% (v/v) Tween-20 in 1x PBS) and incubated in primary antibodies diluted in PBS-T, according to the manufacturers protocol, at 4°C on the orbital shaker overnight (Reciprocating Shaker 3016). Primary antibodies were removed the next day and stored at 4°C for further usage. After washing with 1x PBS-T for three times, the membrane was incubated in secondary antibody conjugated to horseradish peroxidase (HRP) (1:5000-1:10000) in 3% skim milk powder in 1x PBS-T for at least 2 h on the orbital shaker. The membrane was washed three times with 1x PBS-T.

Following steps were performed under red light in a dark chamber. The protein bands were visualized by chemiluminescence of the developing solution consisting of 10 ml enhanced chemiluminescence (ECL) A (250  $\mu\text{g}/\text{ml}$  Luminol sodium, 100 mM Tris/HCl, pH 6.8), 100  $\mu\text{l}$  ECL B (1.25 mg/ml p-Coumaric acid in DMSO) and 10  $\mu\text{l}$   $\text{H}_2\text{O}_2$ . The membrane was shortly incubated in the developing solution and placed in a developing cassette. Chemiluminescence was visualized on X-ray films (CEA) by the binding of the  $\text{H}_2\text{O}_2$  to the secondary antibody during developing (Curix 60, AGFA). The X-ray films were labelled, scanned, and further prepared for figures.

### **2.2.4.7. Immunofluorescence analysis**

Cells were cultured on glass cover slides, transfected or infected as described and subsequently fixed with 4% paraformaldehyde (PFA) for 5-10 min at room temperature. The fixed slides could be stored in 1x PBS at 4°C. After washing with 1x PBS, cells were permeabilized with PBS containing 0.5% (v/v) Triton-X-100 for 5 min and unspecific antibody binding was blocked by 1x TBS-BG (20 mM Tris/HCl, pH 7.6, 137 mM NaCl, 3 mM KCl, 1.5 mM MgCl<sub>2</sub>, 0.05% (v/v) Tween-20, 0.05% (w/v) sodium azide, 5% (w/v) glycine, 5% (w/v) BSA) for 1 hour. To stain specific cellular factors, all antibodies were diluted in PBS according to manufacturer's datasheet. Cover slides were incubated in primary antibody dilutions for 1-16 h at 4°C in a wet and dark environment and washed three times 1x TBS-BG. After cover slides incubated for at least 1 h at room temperature in secondary antibody in a dark and wet environment, the washing steps were repeated and the glass cover slides were mounted on microscope glass slides with Mowiol solution (6 g glycerol, 2.4 g Mowiol, 12 ml, 0.2 M Tris/HCl, pH 8.5, 0.1% (v/v) DABCO). The slides were dried overnight at room temperature and stored at 4°C. A confocal laser-scanning microscope (Nikon Inverted Research Microscope ECLIPS Ti) was utilized to generate digital images, which were processed and quantified using the *Volocity* program (64x, PerkinElmer).

### **2.2.4.8. Determination of secreted HBeAg quantity by ELISA**

The qualitative measurement of secreted HBeAg from HBV infected cells was performed according to the manufacturers protocol of the HBeAg BEP II (Siemens). The sample/cutoff was determined utilizing the internal cutoff value. The measurement of quantitative amounts of HBeAg was performed utilizing the Architect i2000SR System.

### 2.2.4.9. Flow cytometry

For flow cytometry analysis of HBc expression of HBV infected cells, cells were washed with 1x PBS, detached with trypsin and versene (1:1) and resuspended in 1x PBS with 1% FBS. HBc positive cells were stained according to the manufacturer's instructions of the FIX&PERM kit using the monoclonal rabbit anti-HBc (Cell marque 1:1000) and the donkey-anti mouse IgG-PE 548 antibody (BD, 1:10). The fluorescence analysis was performed using a CytoFLEX Flow Cytometer with following gating strategy: FSC-A-SSC-A (for cell population), FSC-A: FSC-H (for single cells), SSC-A: PE-A (for Atto<sub>594</sub>), respectively. Data processing was performed using *FloJow* software.

### 2.2.4.10. Cell viability assay

Differentiated HepG2-NTCP-K7 cells were infected with HBV (MOI 200) and treated with the indicated ATO concentration for 4 or 7 days. Cell viability was determined with the CellTiter-Blue Cell Viability Assay system (Promega, Madison, USA) according to the manufacturer's instructions. Fluorescence readouts were measured using an Infinite 200M plate reader and normalized to untreated, infected cells.

## 2.2.5. DNA techniques

### 2.2.5.1. Polymerase chain reaction (PCR)

Polymerase chain reaction was used to amplify DNA of interest or to generate point mutations within the DNA, induced by primers containing an exchanged complementary base. Therefore, 2.5 µl of 100 mM dNTP mix, 2 µl polymerase PfuUltra II Fusion HS DNA Polymerase, 10 µl 10x PfuUltra II reaction buffer were mixed with 25–100 ng DNA template and 125 ng forward and reverse primer in a total volume of 50 µl in a 0.2 ml PCR tube. The PCR was performed with following parameters (Table 20) in a Mastercycler Gradient (Eppendorf). 5-10 µl of the PCR reaction were loaded on an agarose gel (3.4.2.) to analyze the amount of PCR amplicon.

**Table 20: PCR cycling parameters.**

	Temperature [°C]	Time [min]	Cycles
<b>Prim. Denaturation</b>	98	2	1
<b>Denaturation</b>	95	1	24-27
<b>Annealing</b>	55	1	
<b>Elongation</b>	72	30 s/1 kb	
<b>Final Elongation</b>	68	10	1
<b>Storage</b>	4	∞	

### 2.2.5.2. Agarose gel electrophoresis and gel extraction of DNA

Agarose gel electrophoresis was utilized to analyze restriction digests or to estimate amounts of DNA for ligations. For analytical gel 0.66% agarose and for preparative gel 0.60% agarose were dissolved and melted in 1x TBE buffer (5x TBE buffer: 0.45 M boric acid 10 mM EDTA, Tris 0.45 M pH=7.8) by using a microwave. 0.5 µg/ml ethidium bromide were added to the agarose gel before pouring it in a gel tray with inserted combs. For preparative gel additionally 1 mM guanosin was added to protect DNA from UV-damage [465]. 6x loading dye (0.25% (w/v) bromphenol blue, 25% (v/v), saccharose in 10 mM Tris/HCl) was added to the DNA sample before loading on the gel. A DNA ladder (100µl 100 bp or 1 kb ladder, 100 µl 6 x loading dye, 400 µl ddH<sub>2</sub>O) was used to indicate the fragment sizes. The gel ran in 1x TBE buffer for 1-4 h at 90-130 V. The analytical gel was then monitored with the Universal Hood II Gel Doc (Bio-Rad) and *Quantity One* software at. The DNA bands of the preparative gel were visualized under UV light at 312 nm and cut out with a scalpel. The band was transferred to a micro tube and centrifuged for 90 min at 2000 rpm at 10°C (Beckman coulter, Avanti Je centrifuge). The supernatant was transferred in a fresh Eppendorf tube and DNA extraction was performed.

### 2.2.5.3 DNA precipitation

The DNA containing solution was transferred in a fresh 1.5 ml micro tube and 0.9 volumes 2-propanol as well as 0.1 volumes of 3 M NaOAc were added. The mixture was centrifuged for 10 min at 5000 rpm (Heraeus Fresco 21 Microcentrifuge, Thermo Fisher Scientific) and the supernatant was removed. 400  $\mu$ l 75% ethanol were added to the pellet, centrifuged for 3 min at 14800 rpm and the supernatant was discarded. The DNA pellet was dried for 10 min at 42°C (Thermomixer Comfort 5355, Eppendorf) and dissolved in 30  $\mu$ l 10 mM Tris (pH=8.0).

### 2.2.5.4. Digest of DNA

The restriction digest was performed to verify the DNA due to their fragment size or to cut specific sites out of a plasmid DNA. A total volume of 20  $\mu$ l was used containing 0.5  $\mu$ l enzyme, 10x buffer and 1  $\mu$ g DNA. The DNA digest was performed at 37°C with 300 rpm (Thermomixer Comfort 5355, Eppendorf) for at least 1.5 hours. To prevent the re-ligation of the vector backbone for further usage, 5  $\mu$ l Antarctic phosphatase and 10  $\mu$ l 10x buffer were added and incubated at 37°C for 2 h (Thermomixer Comfort 5355, Eppendorf) as a dephosphorylation step. The sample was then loaded on preparative or analytical agarose gel for further experiments as described (2.2.5.2.).

### 2.2.5.5. Ligation

The ligation of the viral insert into the vector backbone was performed with an appropriate amount of DNA, estimated by agarose gel analysis (1:7; insert:vector). 21  $\mu$ l were used as a final volume for the ligation reaction, containing 1  $\mu$ l of T4 DNA ligase and 10  $\mu$ l of 2x DNA ligation buffer. The reaction was incubated at 13°C overnight (Thermomixer Comfort 5355, Eppendorf) and at 37°C for 1 hour. 10  $\mu$ l of this ligation mix were transformed into DH5 $\alpha$  *E. coli* described in 2.2.2.2. followed by plasmid DNA preparation (2.2.5.8.) and DNA sequencing (2.2.5.9.).

### 2.2.2.6. Site-directed mutagenesis

Site-directed mutagenesis was used to generate HBx SCM point mutations. Therefore, the required oligonucleotides containing the mutation were designed and a PCR reaction was run according 2.2.5.1. as a control 10 µl of the newly synthesized PCR product were loaded on an 0.6% agarose gel (2.2.5.2.). A *DpnI* digest was performed to remove the parental, methylated DNA using 1 µl *DpnI* and 4 µl Cutsmart Buffer. The insert was then ligated into a vector backbone (2.2.5.5.) and transformed into *E.colis* (2.2.2.2.).

### 2.2.2.7. Inverse PCR

Point mutations in HBx SCM can also be inserted by another common method, the inverse PCR. The PCR reaction was performed with newly designed primers (Table 9), the PCR product was loaded on a preparative 0.66% agarose gel and the corresponding bands were extracted out of the gel (2.2.5.2.). A *DpnI* digest was performed for at least 1 hour in 34 µl H<sub>2</sub>O, 4 µl Cutsmart buffer and 2 µl *DpnI* (2.2.5.4.). For further construct phosphorylation 10 µl DNA were added to 8 µl ddH<sub>2</sub>O, 2 µl 10x ligase buffer and 1 µl PNK. The construct was ligated and transformed into *E.coli* (2.2.2.2.).

### 2.2.5.8. Plasmid DNA preparation from *E.coli*

A single colony was picked from the solid agarose plate, inoculated in a defined amount of LB-medium, containing appropriate antibiotics (Maxi-preparation 500 ml, Midi-preparation 55 ml) and incubated at 37°C at 150 rpm (Incubation Shaker Multitron Standard, Infors HT). After 12-18 h of incubation, the suspension was centrifuged for 20 min at 4500 rpm (Rotina 50R, Hettich centrifuge) and plasmid DNA was extracted utilizing the QIAGEN Plasmid DNA Purification Kits (Plasmid Maxi Kit, Plasmid Midi Kit) according to the manufacturer's instructions. Briefly, the bacterial cells were centrifuged and resuspended in several buffers (P1, P2, P3). The lysed cells were

centrifuged again, and the supernatant was loaded on the column. The plasmid DNA was eluted, washed, dried and dissolved in 10 mM Tris (pH=8.0). The received DNA was quantified and sequenced or digested dependent on the following experiments. To identify correct plasmid DNA during cloning processes, Mini-preparation was performed. Reagents of the Plasmid Maxi Kit were utilized, therefore. A single bacterial colony was inoculated in 5 ml LB medium containing the appropriate antibiotic for an overnight incubation at 37°C (Incubation Shaker Multitron Standard, Infors HT). 500 µl of the liquid bacterial culture, were transferred in a 1.5 ml micro tube and centrifuged for 10 min at 14800 rpm at 10 °C (Heraeus Fresco 21 Microcentrifuge, Thermo Fisher Scientific). The cell pellet was resuspended in 300 µl RNase containing resuspension buffer P1 followed by 300 µl of pre-warmed lysis buffer P2 and finally 300 µl neutralization buffer P3 were added to renature the DNA. The sample was again centrifuged for 10 min at 14800 rpm. 800 µl of the supernatant were transferred in a new 1.5 ml micro tube and the DNA was precipitated as described previously. The pellet was dissolved in an appropriate amount of 10 mM Tris (pH=8.0), the concentration was determined (2.2.5.3.) or a restriction digest was performed (2.2.5.4.).

DNA concentration was determined by a NanoDrop 2000c Spectrophotometer measuring the wavelength at 260nm. As a blank for the optical density measurement, 10 mM Tris (pH=8.0) were used. The ratio of OD260/OD280 indicated the purity of the DNA and the values for reliable measurements were set between 1.8-1.9.

### **2.2.5.9. Sequencing of DNA**

Sequencing of a DNA samples was performed by Eurofins Genomics (Ebersberg, Germany). For this, a premixed solution was prepared, containing 1 µg DNA, 30 pmol appropriate sequencing primer and ddH<sub>2</sub>O for a final volume of 17 µl. The obtained results were analyzed utilizing the programs BLAST and Serial Cloner.

### 2.2.5.10. Plasmid transfection with Polyethylenimine

The cationic polymer Polyethylenimine (PEI) was utilized to transfect DNA into 70-90% confluent cells. PEI owned a concentration of 1 mg/ml (pH=7.2) and sterile filtered. Aliquots were stored at -80°C. For transfection, the desired amount of DNA was pipetted into 2 ml micro tubes, 1.8 ml of pre-warmed DMEM without supplements and pre-warmed and vortexed PEI in a ratio of 1:10 based on the DNA amount were added. The maximum used volume of PEI was 150 µl. The mixture was vortexed and incubated at room temperature for 20-35 min. Meanwhile, the cultivation medium was changed from standard to 3 ml DMEM without supplements.

The DNA transfection mixture was pipetted on the tissue culture dish and incubated for 3-4 h (Heracell 250 CO<sub>2</sub> Incubator, Thermo Scientific). The DMEM transfection mixture was removed and standard cultivation medium appropriate to the cell line was added. When Hepatitis B virus infection was performed additionally (2.2.3.), this was carried out 3-4 h post DNA transfection. Cells were harvested as described (2.2.1.3.).

### 2.2.6. RNA techniques

#### 2.2.6.1. Production of *in vitro* transcribed (IVT) mRNA

*In vitro* transcription of T7 promoter containing plasmid DNAs was initiated by linearization of 10 µl of plasmid DNA (concentration 1 µg/µl) mixed with 2 µl Buffer (10x), 5 µl *Xho*I restriction enzyme and 3 µl ddH<sub>2</sub>O. After incubation for 1 h at 37°C, the digest was verified on an Agarose gel as previously described. The linearized plasmid was precipitated by adding 1:20 v/v 0.5 M EDTA, 1:10 v/v 5M NH<sub>4</sub>OH and 2 volumes of 100% ethanol. The purified DNA was pelleted for 15 min at 14800 rpm (Heraeus Fresco 21 Microcentrifuge, Thermo Fisher Scientific), washed twice with 100% ethanol and resuspended in 25 µl nuclease-free ddH<sub>2</sub>O. The production of *in vitro* transcribed (IVT) mRNA was performed with HiScribe T7 ARCA mRNA Kit (with tailing) according to the manufacturer's instructions including 30 min synthesis and 25 min poly(A)-tailing steps. The mRNA was further modified with Pseudo-UTP (Ψ-UTP) and 5-Methyl-CTP (m<sup>5</sup>CTP) which was additionally added to the reaction. IVT

mRNA was purified by utilizing the RNA Clean&Concentrator-25 according to the manufacturer's instructions. To ensure synthesis and poly(A)-tailing, samples were verified by agarose gel analysis. Therefore, 0.5  $\mu$ l of untailed and tailed IVT mRNA were mixed with 5.5  $\mu$ l nuclease-free ddH<sub>2</sub>O and 6  $\mu$ l RNA loading dye (2x), heated at 60 °C for 10 min and loaded on 2% agarose gel. Finally, the concentration of was determined via NanoDrop 2000c Spectrophotometer.

### **2.2.6.2. Lipofectamine transfection**

For mRNA transfection into cells, Lipofectamine MessengerMax was used according to manufacturer's protocol. For all transfection experiments mRNA and Lipofectamine were used in a 1:3 ratio. To transfect a 100 mm cell culture dish, two separate master mix were prepared containing either 5  $\mu$ g mRNA or 15  $\mu$ l Lipofectamine supplemented with 275  $\mu$ l DMEM without supplements, mixed and incubated for 10 min. Meanwhile, the cultivation medium was changed to 3 ml cultivation media. The mRNA mix was then added to the Lipofectamine mix, mixed and incubated again for 5 min before distributing the mRNA-lipid complex onto the cells. The transfected cells were harvested and used for further experiments after 24 h.

### **2.2.7. DNA and RNA analysis**

#### **2.2.7.1. Preparation of total cellular DNA**

Cellular DNA was isolated utilizing the NucleoSpin Tissue kit following the manufacturer's protocol except an additional incubation with prewarmed elution buffer for 5 min before the final elution. Furthermore, the protocol for covalently closed circular DNA (cccDNA) selectivity was optimized by a prior T5 exonuclease digestion of extracted DNA removing linear DNA, rcDNA or nicked DNA. 8.5  $\mu$ l extracted DNA were digested with 1  $\mu$ l NEB buffer 4 or CutSmart buffer and 0.5  $\mu$ l T5 exonuclease (10 U/ $\mu$ l) for 30 min at 37°C with subsequent inactivation at 99°C for 5 min (Mastercycler

Gradient). cccDNA was diluted 1:4 with nuclease-free water for further quantitative polymerase chain reaction analysis [466].

### **2.2.7.2. RNA processing**

#### **2.2.7.2.1. Preparation of total cellular RNA**

Preparation of cellular RNA was performed continuously on ice, using filtered tips. Cells were harvested as described (2.2.1.3.) and the cell pellet was resuspended in 600  $\mu$ l Trizol. 200  $\mu$ l chloroform were added, the sample was vortexed for 15 s and centrifuged for 15 min at 14800 rpm at 4°C (Heraeus Fresco 21 Microcentrifuge, Thermo Fisher Scientific). The clear phase was transferred in a new micro tube, 600  $\mu$ l isopropanol were added and mixed thoroughly. The sample was centrifuged again and the isopropanol was removed. The pellet was washed with 75% ethanol, dried for 5 min at 42°C (Thermomixer Comfort 5355, Eppendorf) and dissolved in 30  $\mu$ l nuclease-free water. The amount of RNA was measured with a NanoDrop 2000c Spectrophotometer. As a blank for the optical density measurement, 1  $\mu$ l nuclease-free ddH<sub>2</sub>O was used. The ratio of OD<sub>260</sub>/OD<sub>280</sub> for reliable measurements was set to ~2.0, indicating the RNA purity. The obtained RNA was either stored at -20°C or directly used for cDNA reverse transcription.

#### **2.2.7.2.2. Reverse transcription of RNA into cDNA**

The Reverse Transcription System (Promega) was utilized to reverse transcribe RNA into cDNA. Therefore, 1  $\mu$ g RNA was filled with nuclease-free water to 13  $\mu$ l and a master mix containing 0.7  $\mu$ l AMV reverse transcriptase, 2  $\mu$ l 10 mM dNTP mixture 4  $\mu$ l 25 mM MgCl<sub>2</sub>, 1  $\mu$ l oligo(dT)<sub>15</sub> random primers, 0.5  $\mu$ l recombinant RNasin ribonuclease inhibitor and 2  $\mu$ l 10x reverse transcription buffer was added. The suspension was incubated at 42°C for 1 hour (Thermomixer Comfort 5355, Eppendorf) and heat inactivated at 95°C for 5 min, followed by 5 min on ice. The obtained cDNA

was diluted 1:10 for further quantitative polymerase chain reaction analysis and stored at -20°C.

### 2.2.7.3. Quantitative polymerase chain reaction

Quantitative polymerase chain reaction (qPCR) was utilized to monitor the amplification of DNAs. All qPCRs were performed with a LightCycler 480 Instrument II (Roche) in FrameStar 96 well semi-skirted PCR plate. For HBV relative quantification of intracellular DNA (primers: HBV DNA fwd, HBV DNA rev) and cccDNA (primers: cccDNA fwd, cccDNA rev) PrP was used as a reference gene (primers: PrP fwd, PrP rev). 4 µl extracted DNA with 0.5 µl fwd primer (20 µM), 0.5 µl rev primer (20 µM) and 5 µl LightCycler 480 SYBR Green I Master mix (Roche) were analyzed per well. Obtained qPCR data were analyzed by advanced relative quantification considering primer efficiency normalized to the house-keeping gene PrP. Technical triplicates were performed and the following qPCR program were used for all analysis.

**Table 21: qPCR cycling parameters for HBV DNA, HBV cDNA and PrP.**

	T [°C]	t [s]	Ramp [°C/s]	Acquisition mode	Cycles
<b>Denaturation</b>	95	300	4.4		1
<b>Amplification</b>	95	25	4.4		40
	60	10	2.2		
	72	30	4.4	single	
<b>Melting</b>	95	1	4.4		1
	65	60	2.2		
	95		0.11	continuous: 5/°C	
<b>Cooling</b>	40	30	2.2		1

**Table 22: qPCR cycling parameters for HBV cccDNA.**

	T [°C]	t [s]	Ramp [°C/s]	Acquisition mode	Cycles
<b>Denaturation</b>	95	600	4.4		1
<b>Amplification</b>	95	15	4.4		50
	60	5	2.2		
	72	45	4.4		
	88	2	4.4	single	
<b>Melting</b>	95	1	4.4		1
	65	15	2.2		
	95		0.11	continuous: 5/°C	
<b>Cooling</b>	40	30	2.2		1

### 2.2.8. Statistical analysis

Statistically significant evaluations of *p*-values were calculated with unpaired Student's two-tailed *t*-test with Welch's correction using GraphPad Prism 5.01 software. Numeric values are presented as mean values including indication of standard deviation (SD).

### 3. Results

The HBx protein represents a mandatory factor for efficient HBV infection by enabling viral transcription from the cccDNA [2]. The formation of stable viral cccDNA requires multiply DNA repair response (DDR) factors of the host cell [2, 135, 467, 468]. As, the bulk of these factors is associated with PML-NBs, we hypothesized that cccDNA as well as HBx might co-localize with those nuclear multiprotein complexes [469]. Since PML-NBs are SUMO hotspots and SUMOylation is a prerequisite for PML-NB association, we investigated the post-translational SUMO modification of HBx by SUMO proteins

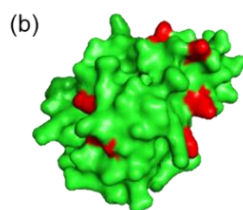
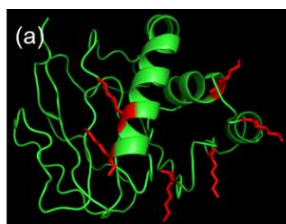
#### 3.1. *In silico* prediction and examination of HBx SUMO consensus motifs

As the SUMOylation dependent PML-NBs are multifunctional complexes harboring and recruiting numerous cellular as well as viral proteins, we were keen to identify the role of SUMO and PML-NBs during HBV infections with focus on the HBx protein [300-302]. Therefore, we initiatively performed *in silico* prediction analysis of the HBx sequence via an online software tool called *GPS-SUMO* [461, 462]. This tool identifies potential SUMOylation sites by screening the protein sequence for the SUMOylation sequence motif ( $\psi$ -K-x-D/E), leading to the identification of six putative SCM within HBx open reading frame with similar prognosis scores (Fig. 9 A). The predicted SCM1 localized at the lysine position 91 aa, SCM2 at 95 aa, SCM3 at 113 aa, SCM4 at 118 aa, SCM5 at 130 aa and SCM6 at 140 aa within the HBx sequence. In a next step, we examined the localization and the accessibility for theoretical SUMO modifications of these SCM sites by tertiary and surface structure analysis by comparing with a previously published HBx structure (Fig. 9 B, C) [470]. The structure analyses revealed feasible access for SUMO at all HBx SCM. Finally, the predicted HBx SCM sites were delineated in a schematic scale representation of the HBx sequence including published functional sites, illustrating that all SCMs located either within the reported DDB1 binding region (SCM1, 2) or the p53 binding region (SCM3, 4, 5, 6) (Fig. 9 D).

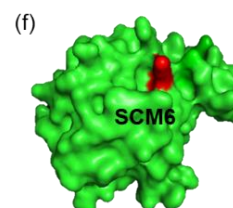
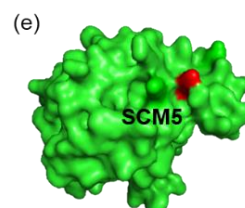
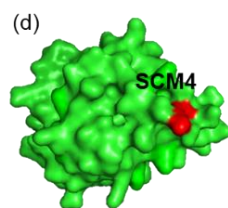
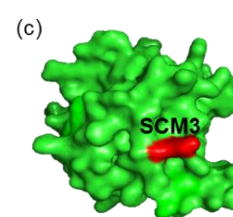
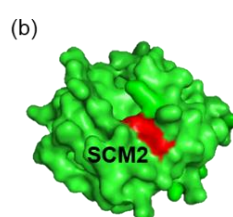
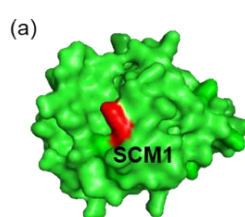
(A)

Name	Position	Sequence motif ( $\psi$ -K-x-D/E)	Score
SCM1	91	NAHQILPKVLHKRTL	17.872
SCM2	95	ILPKVLHKRTLGLPA	20.918
SCM3	113	TDLEAYFKDCVFKDW	21.152
SCM4	118	YFKDCVFKDWEELGE	22.604
SCM5	130	LGEEIRLKVFLGGC	25.732
SCM6	140	VLGGCRHKLVCAPAP	18.992

(B)



(C)



(D)

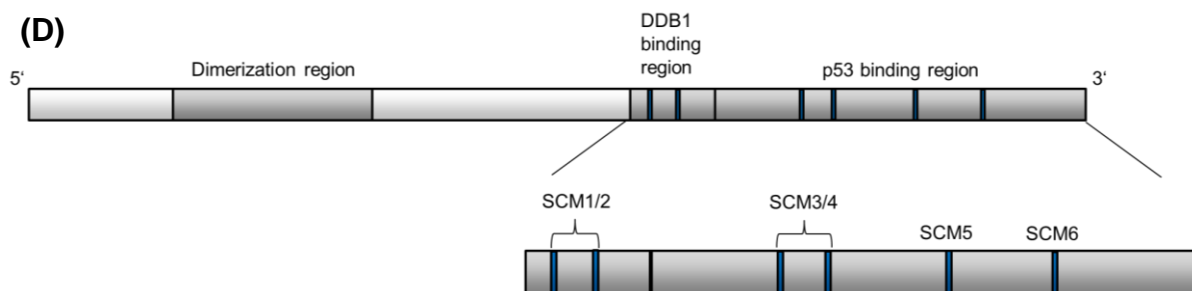


**Figure 9: *In silico* analysis of predicted HBx SUMO consensus motifs.** (A) Prediction of HBx SUMO consensus motifs (SCM) via GPS-SUMO. (B) Graphical representation of all predicted SCMs in HBx (red) (a) tertiary and (b) surface structure including predicted SCM. (C) Detailed graphical surface representation of each predicted SCM (red) within HBx (green). Modified from [470]. (D) Schematic depiction of HBx functional sites including novel predicted SCMs.

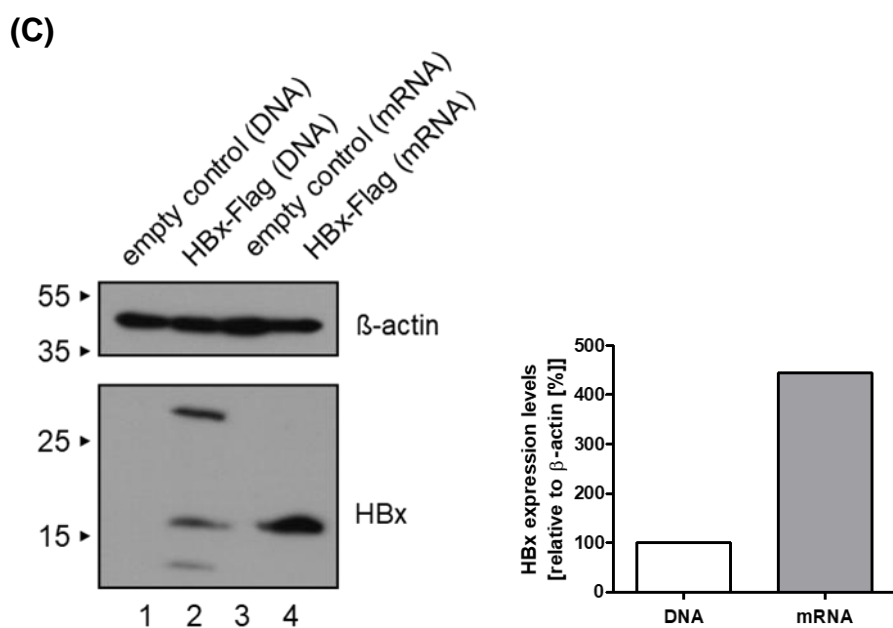
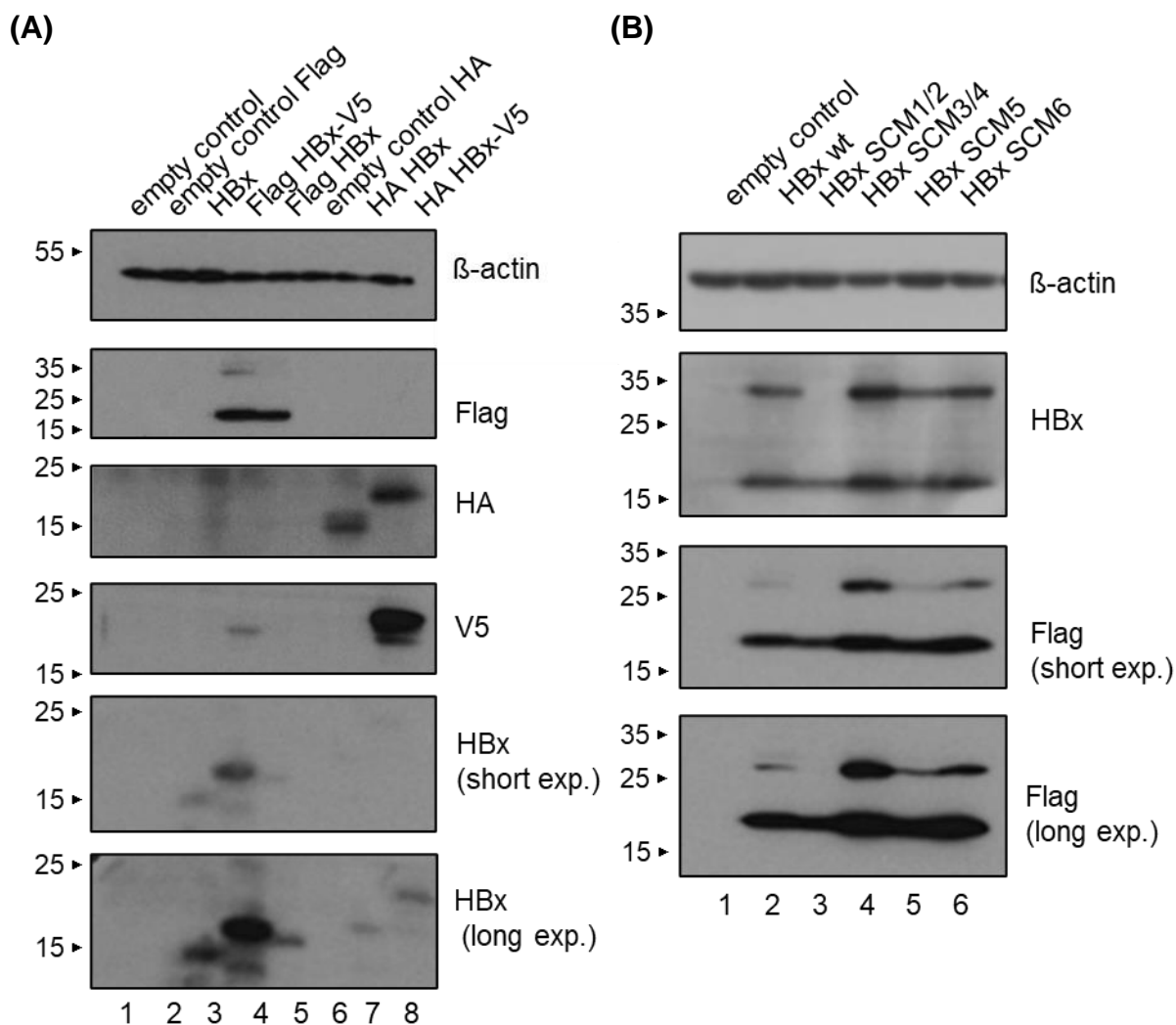
### 3.2. Generation of HBx wt and SCM mutant expressing plasmids

Prior to further investigations on the HBx protein and its SUMO modification, we generated a toolbox containing various DNA plasmids and mRNAs encoding for different tagged HBx constructs as well as HBx variants. Primary, the HBx sequence with and without V5 tag (kindly provided by AG Protzer) was cloned via *EcoRI* restriction into pcDNA3-HA or pCMX3b-Flag DNA plasmid vectors. The expression of these constructs was confirmed by transfection into HepaRG cells. Cells were harvested 24 h.p.t. and whole-proteins lysates were prepared. To determine efficient protein expression SDS-PAGE, western blot and immunostainings using HA, Flag, V5, HBx and  $\beta$ -actin were performed (Fig. 10 A). HBx staining detected bands for all constructs at around 15-20 kDa. These variations in size can be explained by the attached epitope tags to the HBx protein. Furthermore, pCMX3b-Flag HBx-V5 expression was higher than the other constructs and displayed an additional higher and lower migrating band.

Since all constructs expressed the HBx protein and the appropriate tags, we continued with the generation of HBx SCM mutant constructs. Here, the lysine (K) residue responsible and essential for the SUMO consensus motif of all predicted HBx SCM were exchanged to an arginine (R), resulting in a non-functional SUMO consensus motif. Due to the fact, that the predicted SCM1 and SCM2 are in close proximity within the HBx sequence, they were combined in one HBx mutant called SCM1/2. The same was also applied for HBx SCM3 and SCM4 merged to HBx mutant SCM3/4. Cloning was performed by site directed mutagenesis or inverse PCR for pcDNA3 HBx, pCMX3b-Flag HBx, pCMX3b-Flag HBx-V5, pcDNA3-HA HBx and pcDNA3-HA HBx-V5. All constructs were verified by transfection into HepG2-NTCP-K7 cells followed by protein lysis, SDS-PAGE, western blot analysis and immunoblotting (Fig. 10 B), which showed strong protein expression 24 h post transfection.

Since plasmid transfection efficiency especially in HepG2 and HepaRG cells is quite low we also generated IVT mRNA encoding for HBx to achieve higher transfection rates for later experiments [471]. To compare the transfection efficiency between our DNA and IVT mRNA, both constructs were transfected and harvested after 24 h. Whole-cell lysates were generated, analyzed by SDS-PAGE and western blot using immunostainings for HBx and  $\beta$ -actin were performed. Figure 10 C revealed a

4.45-fold higher expression of HBx using IVT mRNA than for DNA transfection. Furthermore, just one specific band for HBx appeared, whereas DNA transfection led to a lower band as well as a higher migrating band already mentioned in Figure 10 A. Besides the significantly increased number of HBx transfected cells per vision field, also the localization of HBx was more distinct in the nucleus using IVT mRNA (Fig. 10 D). In contrast, HBx transfected by DNA localized in the nucleus as well as in the cytoplasm. We further generated IVT mRNAs for HBx SCM mutants. These constructs were examined via transfection into HepG2-NTCP-K7, harvested after 24 h and whole-cell lysis, SDS-PAGE, western blot and immunostainings for HBx and  $\beta$ -actin were performed.



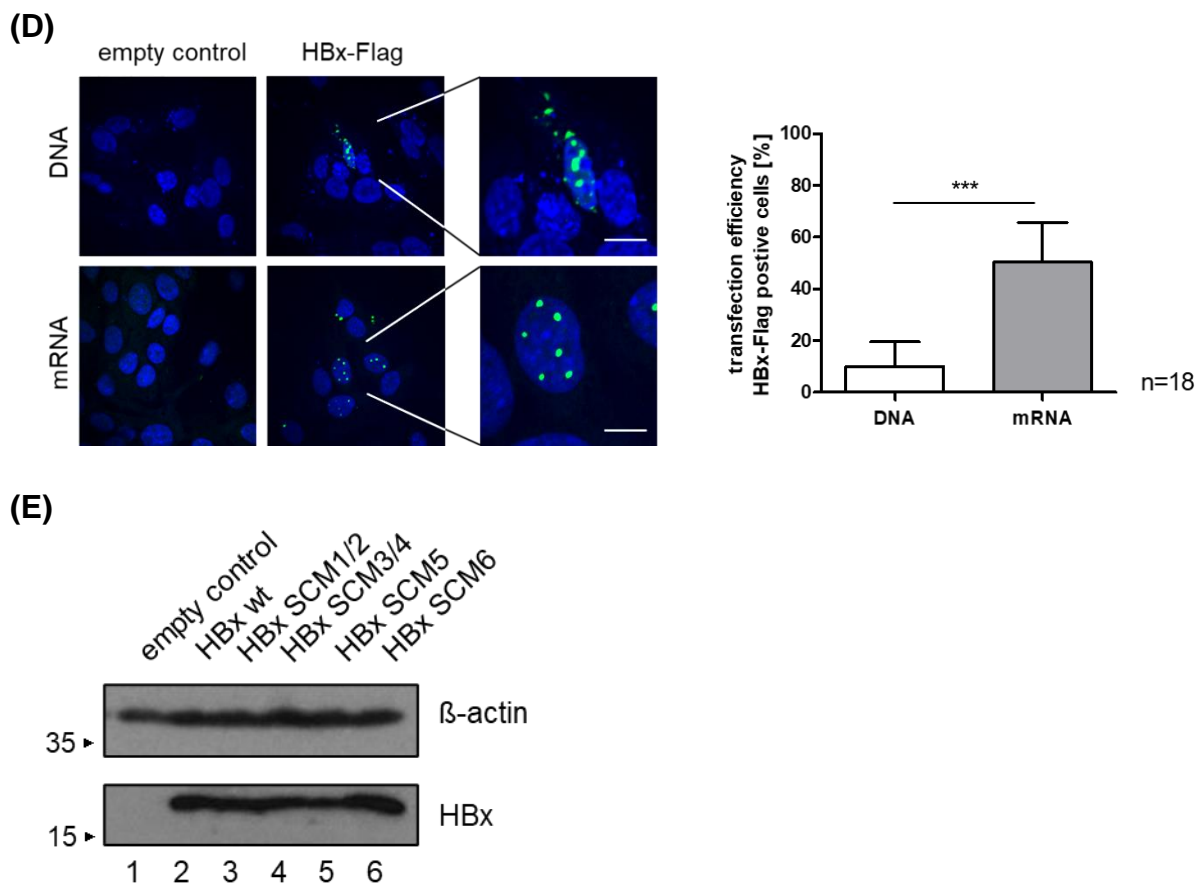


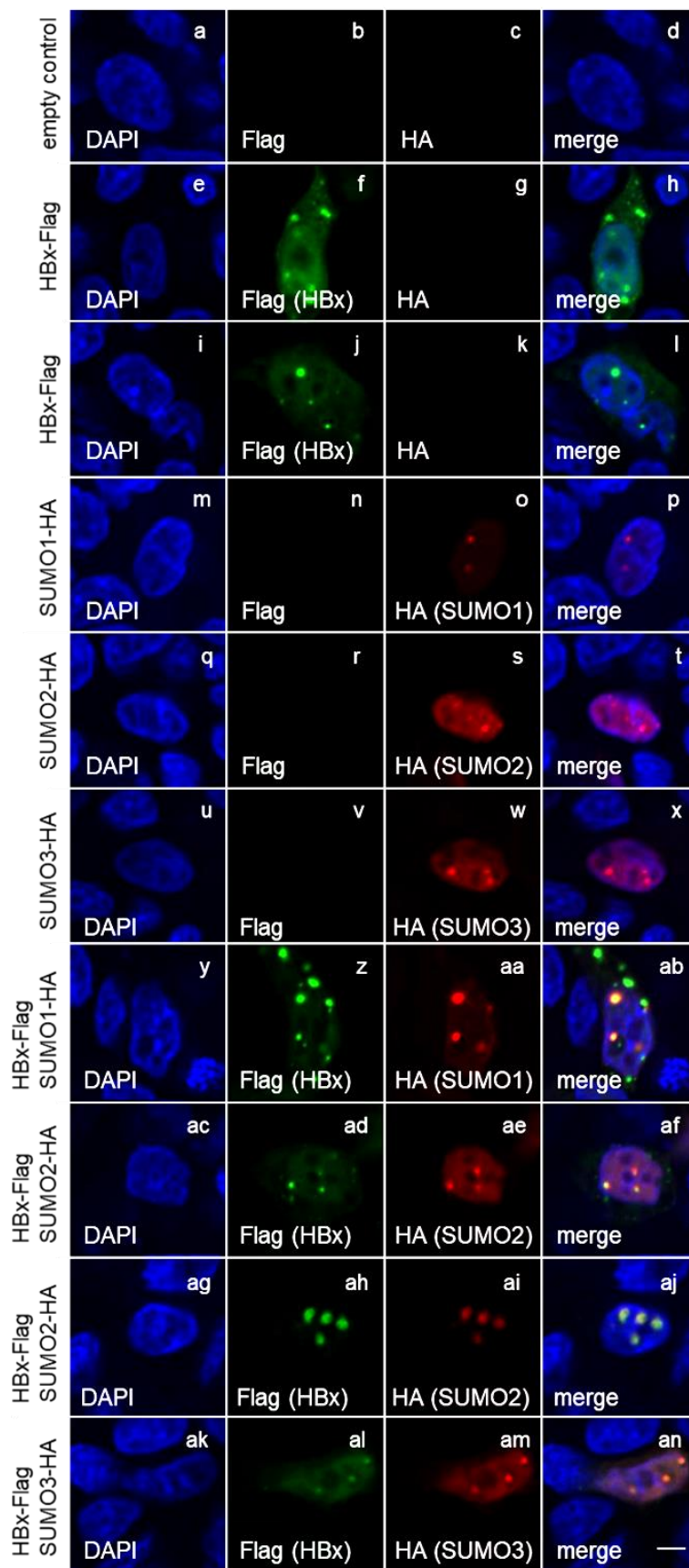
**Figure 10: Generation of a HBx plasmid toolbox.** HepG2-NTCP-K7 cells were transfected with the respective construct and harvested after 24 h. For immunodetection, proteins were lysed, separated by SDS-PAGE, subjected to western blot, and detected with the corresponding antibodies HBx,  $\beta$ -actin and the corresponding tags HA, Flag as well as V5. Stained proteins are depicted on the right, appendant molecular weights are indicated in kDa on the left, respectively. (A) Cells were transfected with pcDNA3, pCMX3b, pcDNA3 HBx, pCMX3b-Flag HBx, pCMX3b-Flag HBx-V5, pcDNA3.HA, pcDNA3-HA HBx and pcDNA3-HA HBx-V5 DNA. (B) Cells were transfected with pCMX3b-Flag HBx-V5 wt, SCM1/2, SCM3/4, SCM5 and SCM6. (C) Cells were transfected with pCMX3b-Flag HBx-V5 (DNA) or HBx (IVT mRNA). Protein levels were quantified via *ImageJ*. (D) Cells were transfected with pCMX3b-Flag HBx-V5 (DNA) or HBx (IVT mRNA) and fixed 24 h.p.t. with 4% PFA and stained with Flag (HBx) primary antibody detected by conjugated secondary antibody Alexa488. Nuclei were labeled with DAPI. Scale bar indicating 7  $\mu$ m. Depicted bar charts including standard deviation represent the percentage of transfected cells with HBx within a vision field. (E) Cells were transfected with IVT mRNA HBx wt, SCM1/2, SCM3/4, SCM5 and SCM6. Statistically significant differences were determined using Welch-corrected Student's t-test. \*:  $p \leq 0.05$ , \*\*:  $p \leq 0.01$ , \*\*\*:  $p \leq 0.001$ , \*\*\*\*:  $p \leq 0.0001$ .

### 3.3. Post-translational modification of HBx by SUMO2 moieties

#### 3.3.1. HBx co-localizes with all SUMO paralogues in the hepatocyte nucleus

Since the online prediction program *GPS-SUMO* confirmed HBx as a possible SUMOylation target, we examined the localization of co-transfected pCMX3b-Flag HBx-V5 and pcDNA3-HA SUMO paralogues SUMO1, SUMO2 or SUMO3, respectively. Cells were fixed with 4% PFA 48 h.p.t. and stained with Flag (HBx, green, 488 nm), HA (SUMO, red, 647 nm) and DAPI (nucleus, 405 nm) to detect immunofluorescence signal. Single transfection of HBx led to localization in the nucleus as well as in the cytoplasm, as previously mentioned. All transfected SUMO paralogues were found in the nucleus. HBx together with SUMO1, SUMO2 or SUMO3 exhibited distinct co-localizing dots within the cellular nucleus (Fig. 11 A, panel ab, af, aj, an). These findings were further supported by the quantification of the Pearson correlation coefficient (PC) with the *Volocity* software, since PC-values above 0.5 are known to indicate a direct localization of proteins [472]. Quantification of HBx with all three different SUMO paralogues revealed strong and distinct co-localization, emphasized by mean PC-values 0.79 for HBx-SUMO1, 0.82 for HBx-SUMO2 and 0.87 for HBx-SUMO3. These results provided indication of mixed SUMO2/3 chains terminated by SUMO1 [353, 387, 389-392]. Moreover, similar results could be generated in H1299 cells stably expressing SUMO1-, SUMO2- or SUMO3-GFP with transfected pCMX3b-Flag HBx-V5 (data not shown here). Summarized, HBx showed strong co-localization with all three SUMO paralogues, supporting the hypothesis of a post-translational modification of HBx with SUMO.

(A)



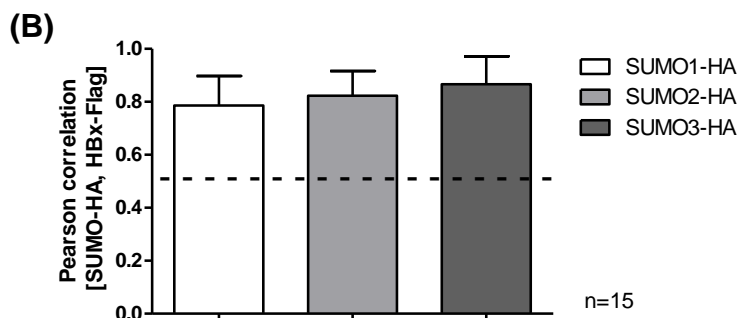


**Figure 11: Co-localization of transfected HBx with all SUMO paralogues.** (A) HepG2-NTCP-K7 cells were co-transfected with pCMX3b-Flag HBx-V5 and pcDNA3-HA SUMO1, SUMO2 and SUMO3. Cells were fixed with 4% PFA 48 h.p.t. and stained with Flag and HA primary antibodies detected by conjugated secondary antibodies Alexa488 (Flag (HBx), green) and Alexa647 (HA (SUMO), red). Nuclei were labeled with DAPI. Representative pictures as well as 3D Z-stack images are shown. Scale bar indicating 3  $\mu$ m. (B) Pearson correlation coefficient (PC) was quantified via *Volocity* software. Depicted bar charts represent the average PC values including standard deviations.

### 3.3.2. HBx is a novel target for SUMO2 post-translational modification

To substantiate our previous data, NiNTA assays for SUMOylation were performed. Since HBx localized at SUMO paralogous we proposed to demonstrate the specific SUMOylation of HBx. HeLa SUMO2-His stably overexpressing 6xHis-SUMO2 cells were transfected with pCMX3b-Flag HBx-V5, harvested after 30 h and whole-cell protein lysis as well as the NiNTA assay were conducted. SDS-PAGE and western blot were performed, followed by immunostainings of HBx, His (SUMO2) and  $\beta$ -actin (Fig. 12). Input controls and HBx protein displayed the correct migration pattern. Furthermore, the SUMO2 modification of HBx could be shown in the NiNTA assay. A single band for HBx alone was stained at ~15 kDa and in addition several upcoming bands could be detected. The band at ~35 kDa indicated a single SUMO2 modification of HBx, whereas all further upcoming bands (>35 kDa) exhibit poly-SUMO2 modifications of the HBx protein. In summary, these data revealed for the first time the post-translational SUMO modification of HBx by single as well as poly-SUMO2.

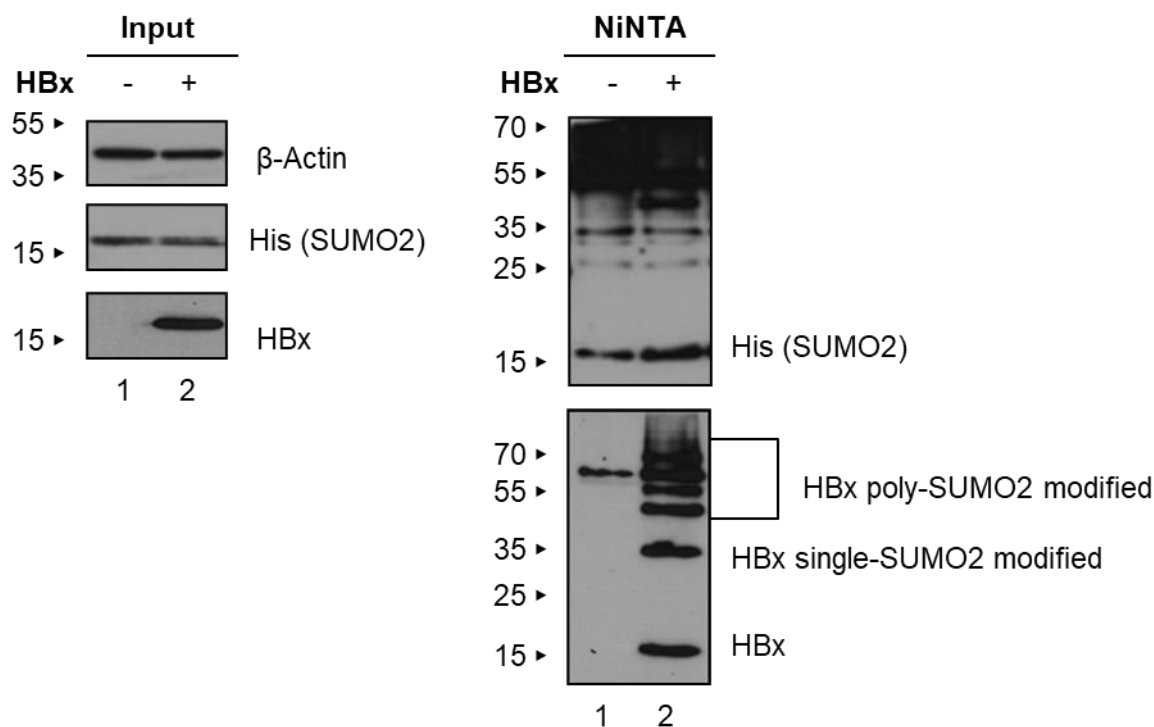


**Figure 12: HBx is post-translationally SUMO2 modified.** HeLa SUMO2-His cells were transfected with pCMX3b-Flag HBx-V5 and harvested 30 h.p.t., protein lysates and the corresponding NiNTA assay were prepared, separated by SDS-PAGE, subjected to western blot and immunodetection using His, HBx and  $\beta$ -actin as loading control. Stained proteins are depicted on the right, appendant molecular weights are indicated in kDa on the left, respectively.

### 3.3.3. SUMO2 dependent proteasomal degradation of HBx protein

We were able to disclose the post-translational modification of HBx by SUMO2, however the functional mechanism was not investigated yet. Since SUMOylation is published to trigger poly-ubiquitylation and proteasomal degradation, we were inquisitive to investigate the proteasomal degradation of HBx with regard on SUMO proteins [473]. Since, MG132 is known to inhibit proteasomal degradation, cells were treated with this compound 32 h.p.t. of pCMX3b-Flag HBx plasmid transfection into HepaRG His/HA or HepaRG SUMO2-His/HA cells and harvested after 48 h [474]. Whole-protein lysates, SDS-PAGE and western blot were conducted prior to immunoblotting using His (SUMO2), HBx, ubiquitin as well as  $\beta$ -actin antibodies (Fig. 13). Ubiquitin was used as MG132 treatment control since it is accumulated during this treatment [474]. Untreated HBx protein expression levels could be shown

to be lower in HepaRG SUMO2-His/HA compared to HepaRG His/HA cells. Moreover, MG132 treatment strongly inhibited the proteasomal degradation of HBx in HepaRG SUMO2-His/HA cells, resulted in increased HBx protein levels of almost 3-fold, whereas in HepaRG His/HA cells HBx protein levels were not altered. These data indicated a SUMO2 dependent proteasomal degradation of HBx.

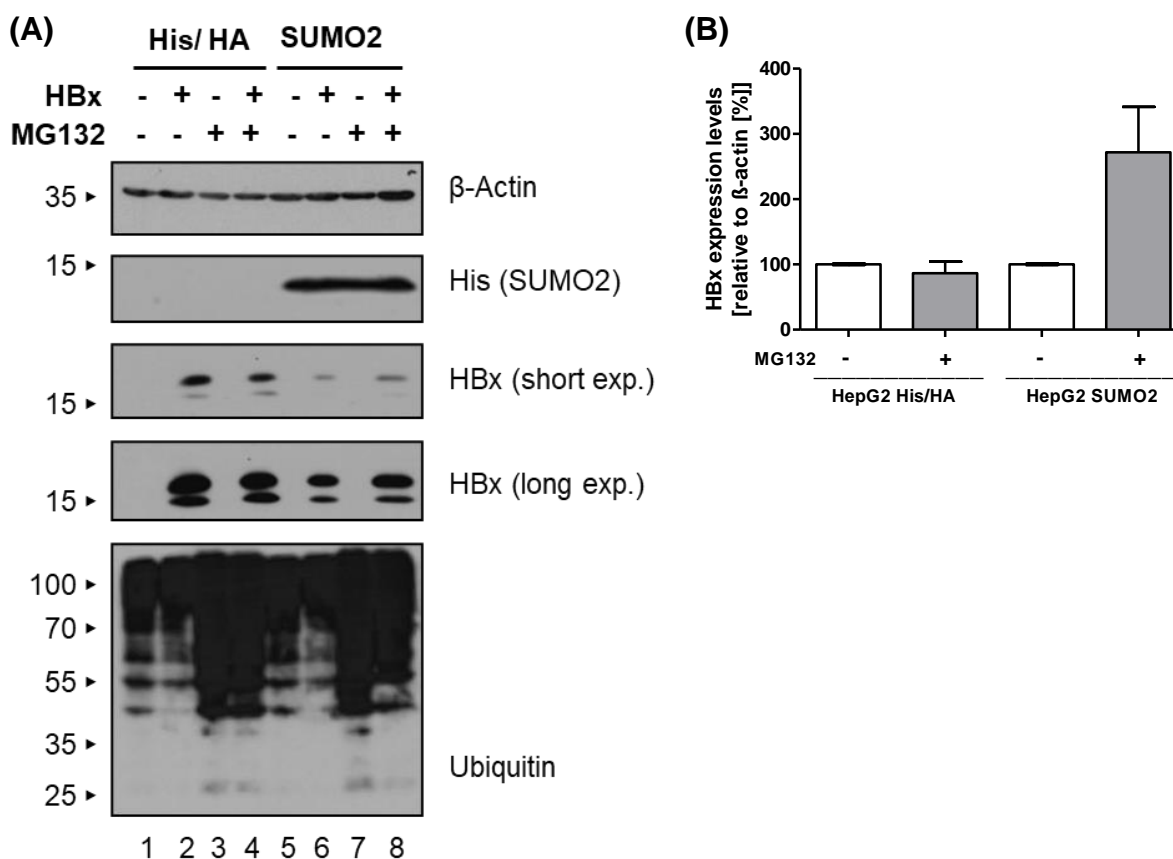


**Figure 13: Proteasomal degradation of HBx depends on SUMO2.** (A) HepG2-NTCP-K7 cells were transfected with pCMX3b-Flag HBx and treated 32 h.p.t. with MG132 to inhibit proteasomal degradation. Cells were harvested 48 h.p.t., protein lysates were generated, separated by SDS-PAGE, subjected to western blot and stained for His (SUMO2), HBx, ubiquitin as well as  $\beta$ -actin. Proteins are depicted on the right, molecular weights are indicated in kDa on the left, respectively. (B) Corresponding protein expression levels were quantified by densitometric analysis via *ImageJ*. Protein expression levels were normalized to  $\beta$ -actin. Depicted bar charts represent the average protein expression including standard deviations (n=2).

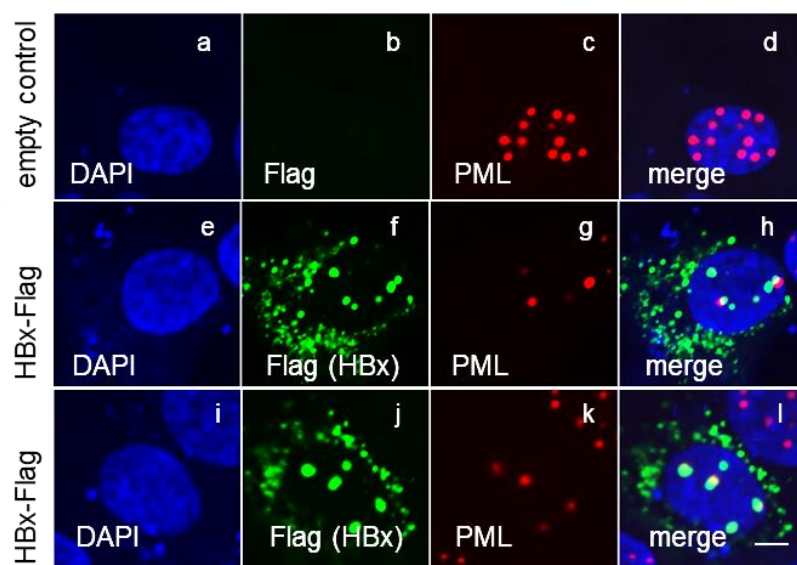
### 3.4. Interplay between viral HBx proteins and PML

#### 3.4.1. PML is a novel interaction partner of the HBx protein

Our previous investigations disclosed HBx as a SUMOylation target. Since PML-NBs represent SUMOylation hotspot, we were interested whether HBx also localizes and interacts with endogenous PML-NBs as a novel SUMOylation substrate. To analyze this, immunofluorescence stainings were performed. HepG2-NTCP-K7 cells were transfected with pCMX3b-Flag HBx-V5, fixed with 4% PFA after 48 h and stained with Flag (HBx, green, 488 nm), PML (red, 647 nm) and DAPI (nucleus, 405 nm) visualized in Figure 14 A. As previously shown, HBx localized in dot-like structures within the nucleus as well as diffusely distributed in the cytoplasm. Direct localization of transfected HBx with endogenous PML-NBs could be revealed in the nucleus (panel l), nevertheless also a minor proportion of HBx was found to localize juxtaposed to the PML-NBs (panel h). Besides, the number of PML-NBs was tremendously reduced in the presence of HBx compared to the empty control.

The localization of HBx served as a first indication for an interaction between HBx and PML, which was further validated via co-immunoprecipitation. Cells were transfected with pCMX3b-Flag HBx-V5, harvested after 48 h.p.t. and whole-protein lysis as well as co-immunoprecipitation pulled with PML were performed. SDS-PAGE, western blot and immunoblotting using PML, HBx and  $\beta$ -actin were conducted (Fig. 14 B). Protein input displayed the transfected HBx as well as PML levels for both conditions, whereat PML was increased in the presence of HBx. This experiment further exhibited an interaction of transiently expressed HBx protein with endogenous PML, demonstrating for the first time the localization as well as the interaction of HBx with endogenous PML.

(A)



(B)

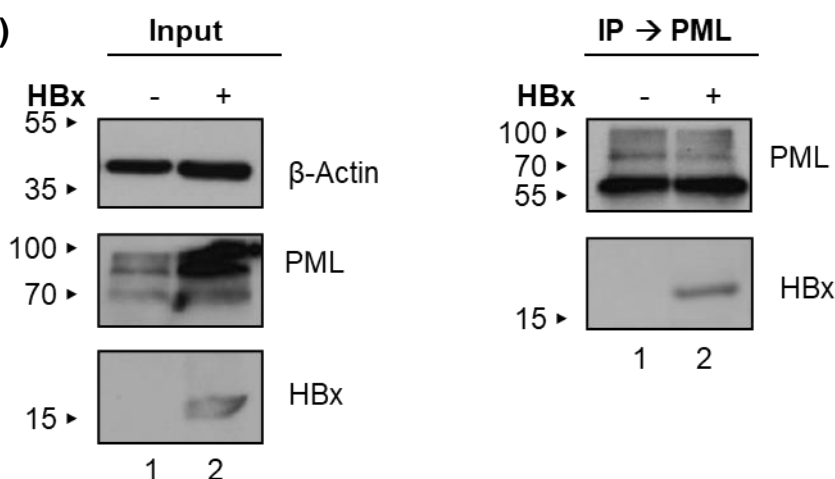
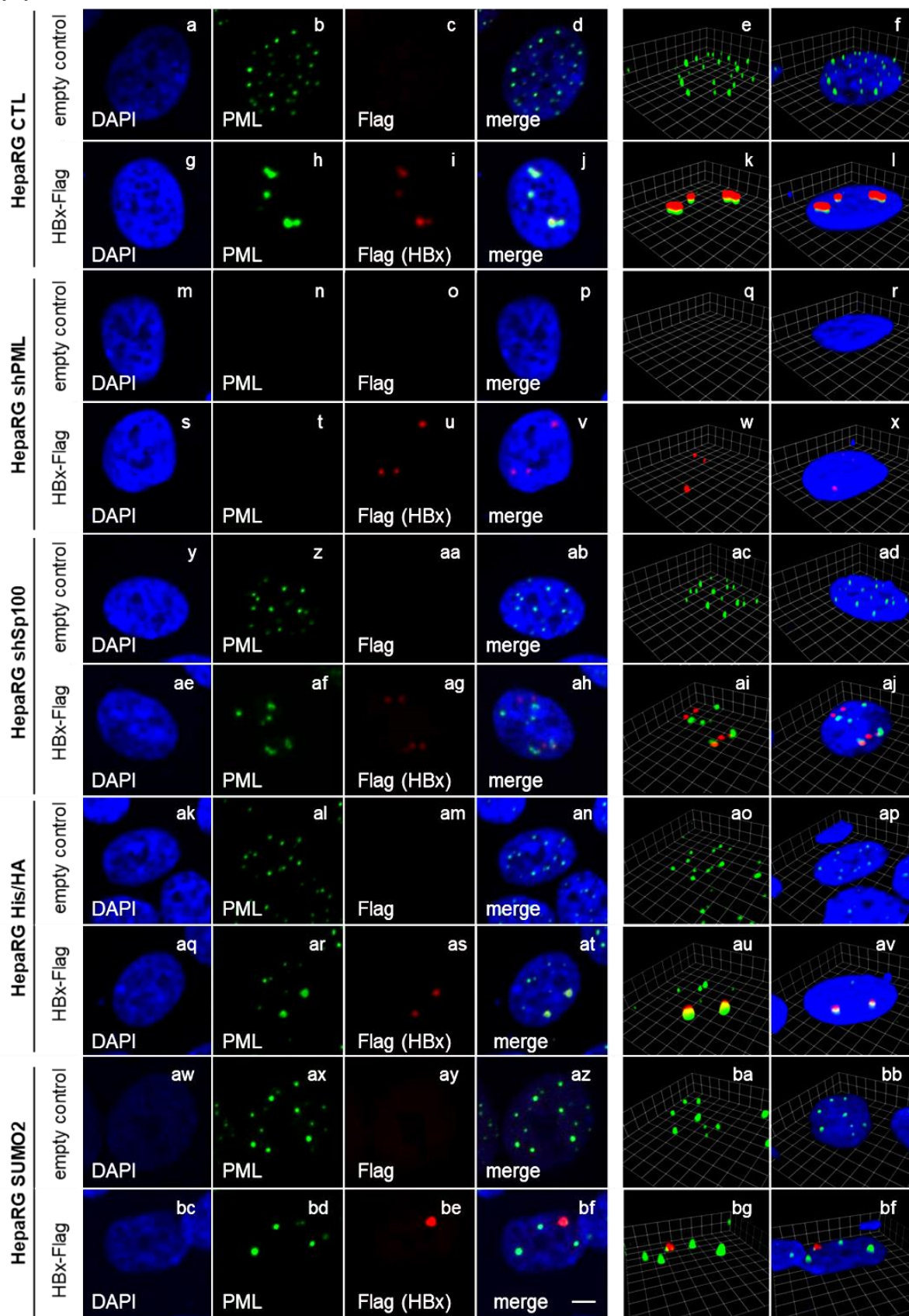


**Figure 14: Interaction between transfected HBx and endogenous PML.** (A) HepG2-NTCP-K7 cells were transfected with pCMX3b-Flag HBx-V5 fixed with 4% PFA 48 h.p.t. Cells were stained with PML and Flag (HBx) primary antibodies and detected by conjugated secondary antibodies Alexa488 (PML, green) and Alexa647 (Flag, red). Nuclei were labeled with DAPI. Representative pictures as well as 3D Z-stack images are depicted. (B) Protein lysis as well as co-immunoprecipitation (pulled endogenous PML) were implemented, separated by SDS-PAGE and subjected to western blot. Immunodetection was performed by using PML, HBx as well as  $\beta$ -actin as loading control. Stained proteins are depicted on the right, appendant molecular weights are indicated in kDa on the left, respectively. Scale bar indicating 3  $\mu$ m.

### 3.4.2. HBx proteins alter PML-NB number and size

To extend our findings on HBx localization at PML-NBs a different HepaRG cell lines (CTL, shPML, shSp100, His/HA and SUMO2-His/HA) were transfected with HBx IVT mRNA and analyzed by immunofluorescence analysis. Cells were stained for PML (green, 488 nm), Flag (HBx, red, 647 nm) and DAPI (nucleus, blue 405 nm) (Fig. 15 A). Representative pictures and 3D Z-Stack images were rendered. Interestingly, IVT mRNA transfected HBx localized solely in the nucleus. All images displayed a distinct co-localization of HBx with PML in HepaRG CTL, HepaRG shSp100, HepaRG His/HA and HepaRG SUMO2-His/HA cells (panel j, ah, at, bf). This could be also visualized by Z-stacks (panel k, ai, au, bg) and was confirmed via PC quantification higher than 0.5, with no significant differences between cell lines (Fig. 15 B). Additionally, the number and size of HBx aggregates as well as PML-NBs was assessed and measured in *Volocity*. The number and size of nuclear HBx dots did not change significantly between the different cell lines. Contrary, PML-NB number and size was altered significantly between the different cell lines between empty transfection *versus* HBx transfected cells (panel b, h, n, t, z af, al, ar, ax, bd). In detail, the number of PML-NBs was significantly reduced in HepaRG shSp100 cells (panel z) compared to HepaRG CTL cells (panel b) as well as in HepaRG His/HA cells (panel al) compared to HepaRG His-SUMO2 cells (panel ax). Since HepaRG shPML cells lack endogenous PML, no conclusions could be drawn here. Furthermore, the number of PML-NBs was significantly decreased in the presence of HBx protein expression, independent of the cell line examined. Regarding the size of PML-NBs, transient HBx expression induced significant enlargement of the NB diameter. Moreover, the size of PML-NBs was increased in cells stably overexpressing SUMO2 compared to His/HA, emphasizing the current knowledge of SUMO being an essential factor for PML-NBs. Taken together, HBx expression resulted in significantly reduced PML-NB number whereas the size of PML-NBs increased. Concluding, less but bigger PML-NBs were assembled within HepaRG cells, when HBx protein was expressed in transfected.

(A)



(B)

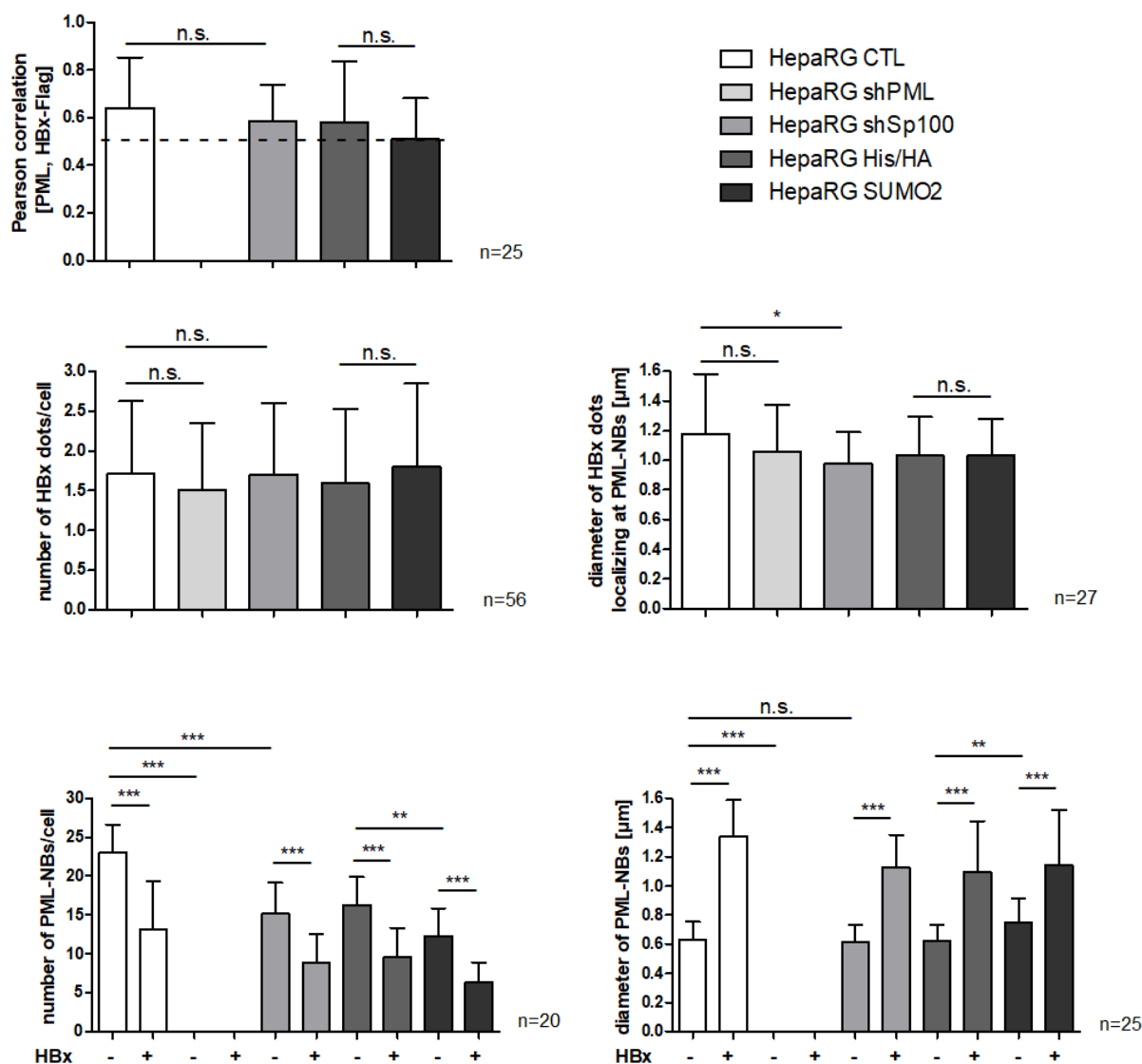
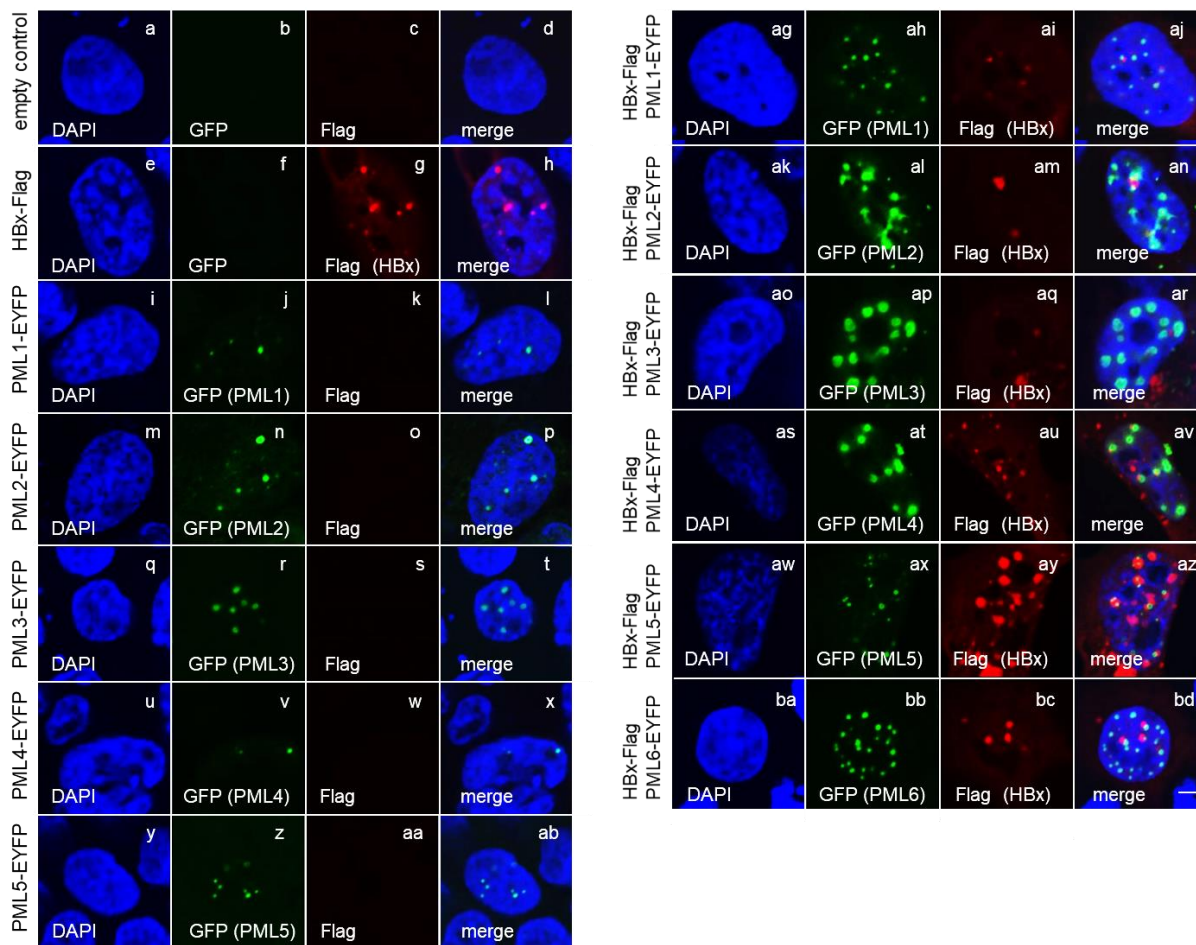


**Figure 15: Transfected HBx modulated PML-NB number and size.** (A) HepaRG CTL, HepaRG shPML, HepaRG Sp100, HepaRG His/HA and HepaRG SUMO2-His/HA cells were transfected with HBx IVT mRNA, fixed with 4% PFA 24 h.p.t. and stained with and PML and Flag primary antibodies detected by conjugated secondary antibodies Alexa488 (PML, green) and Alexa647 (Flag (HBx), red). Nuclei were labeled with DAPI. Representative pictures as well as 3D Z-stack images are depicted. Scale bar indicating 3 μm. (B) Pearson correlation coefficients (PC) as well as dot diameters were quantified via *Volocity* software. Depicted bar charts represent PC values, PML-NB size, HBx size or number of PML-NB or HBx per cell including standard deviations. Statistically significant differences were determined using Welch-corrected Student's t-test. \*:  $p \leq 0.05$ , \*\*:  $p \leq 0.01$ , \*\*\*:  $p \leq 0.001$ , \*\*\*\*:  $p \leq 0.0001$ .

### 3.4.3. HBx protein is localized juxtaposed to transiently expressed single PML isoforms

Since PML-NBs can compose of several different PML isoforms as well as various additional proteins, we were interested to identify specific PML isoforms regulating HBx co-localization or interaction [313]. First, immunofluorescence analysis was conducted in HepG2-NTCP-K7 shPML cells, which were successfully depleted for endogenous PML expression. Cells were co-transfected with pCMX3b-Flag HBx-V5 and pLKO-pgD-EYFP PML isoforms I-VI, fixed with 4% PFA after 48 h and stained for GFP (PML, green, 488 nm), Flag (HBx, red, 647 nm) and DAPI (nucleus, blue, 405 nm). Co-localization of HBx with all PML isoforms could be detected for a minor proportion of cells, whereas the majority of cells displayed HBx juxtaposed or in close proximity to the appropriate PML isoform (Fig. 16 A, panel j, an, ar, av, az, bd). This result could be substantiated by the quantification of PC values by *Velocity* (Fig. 16 B). All mean PC values were determined to be lower than 0.5, representing the threshold for co-localization. Based on these data, no specific PML isoform could be determined as single partner for HBx. Thus, various PML isoforms might act simultaneously to regulate HBx protein binding and co-localization.

(A)



(B)

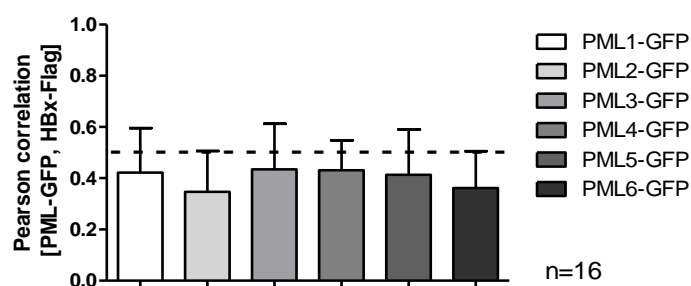
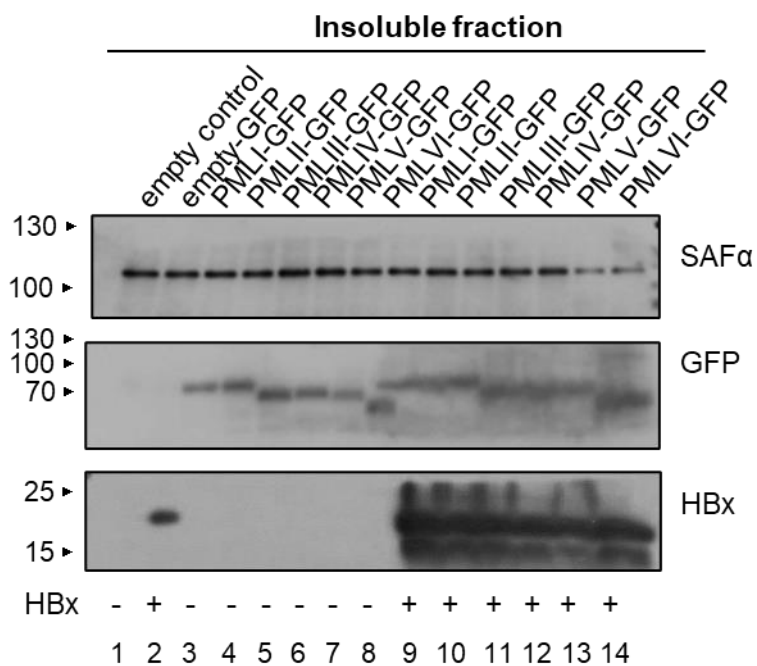
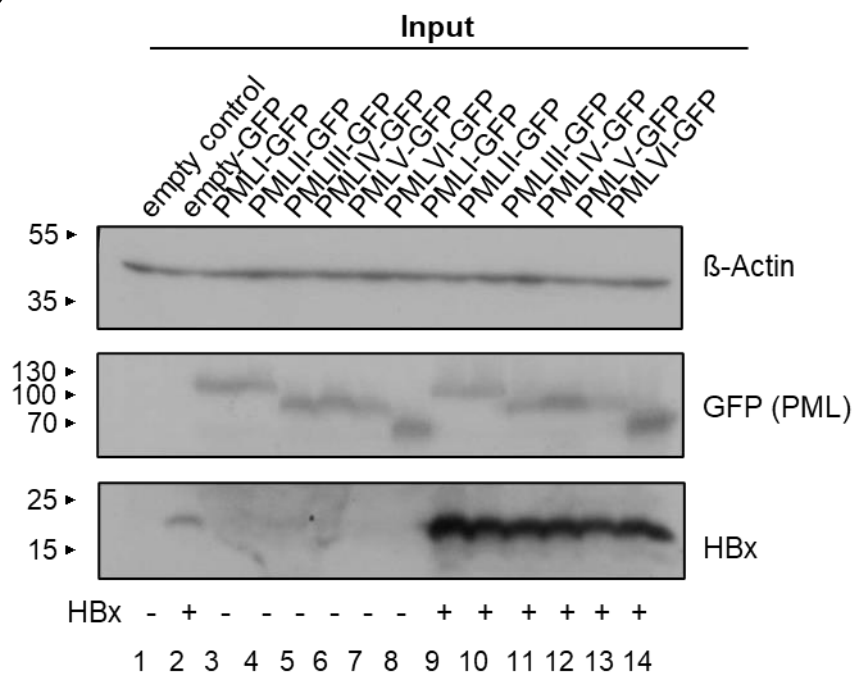


**Figure 16: HBx localizes juxtaposed to all PML isoforms in HepG2-NTCP-K7 shPML cells.** Cells were co-transfected with pCMX3b-Flag HBx-V5 and pLKO-pgD-EYFP PML isoforms I-VI, fixed 48 h.p.t. with 4% PFA and stained with GFP (PML) and Flag (HBx) primary antibodies detected by conjugated secondary antibodies Alexa488 (GFP (PML), green) and Alexa647 (Flag (HBx), red). Nuclei were labeled with DAPI. (A) Representative pictures as well as 3D Z-stack images are depicted. Scale bar indicating 3  $\mu$ m. (B) Pearson correlation coefficient (PC) was quantified via *Volocity* software. Depicted bar charts represent the PC values including standard deviations.

#### **3.4.4. Mutual shift of HBx proteins and PML isoforms to the insoluble matrix fraction concomitant with elevated expression of the viral factor**

Even though no prime candidate of PML isoforms could be determined for HBx localization, we were further interested in the impact of PML isoforms on HBx protein expression levels. During this experimental setup, HepG2-NTCP-K7 cells were co-transfected with pCMX3b-Flag HBx-V5 and pLKO-pgD-EYFP single PML isoforms. Cells were harvested after 48 h and whole-protein lysis as well as the membranous associated fraction were conducted. SDS-PAGE, western blotting as well as immunoblotting staining of GFP (PML), HBx, SAF $\alpha$  and  $\beta$ -actin were performed. Regarding the HBx protein levels, a considerably increased amount could be detected in the presence of PML isoforms for the soluble as well as insoluble fraction without significant changes between various PML isoforms (Fig. 17, lane 9-14). Moreover, a similar effect could be detected for the insoluble PML. Here, HBx also induced increased PML magnitude in the insoluble membranous fraction, however this effect was lower than observed *vice versa*. Furthermore, PMLV and PMLVI displayed to be less affected by HBx than the remaining isoforms. Nevertheless, this impact of HBx on PML could not be shown in the input fraction. Taken together, a reciprocal increase of HBx and single PML isoforms could be detected in the insoluble membranous fraction, whereas HBx was solely elevated by PML in the input fraction.

(A)



(B)

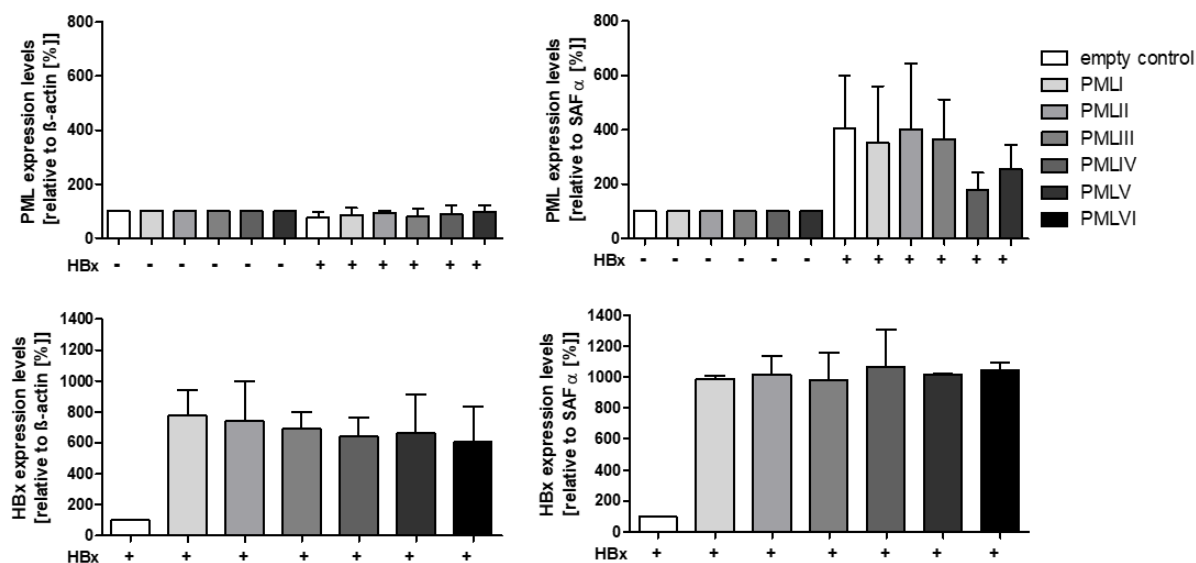
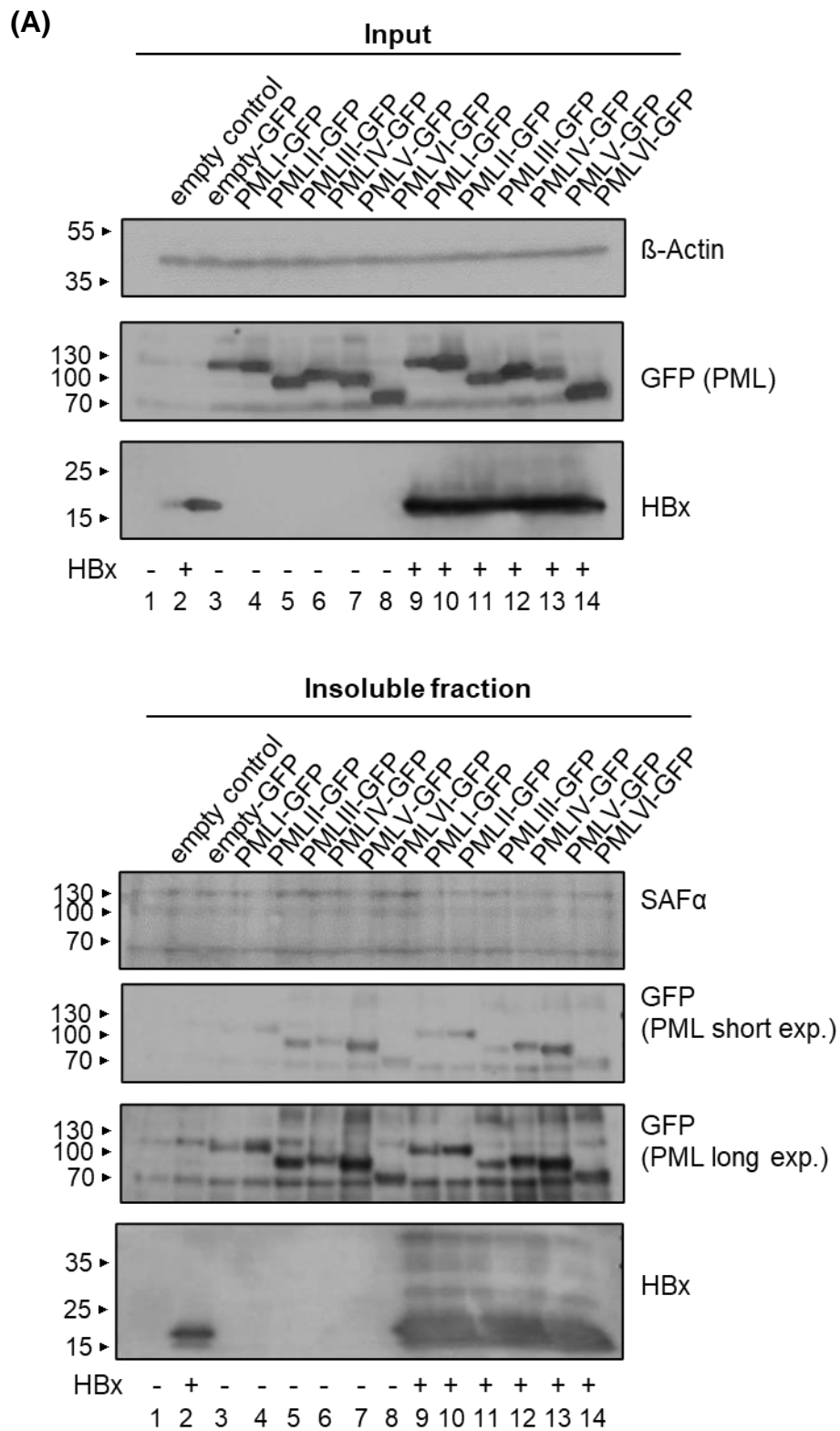


**Figure 17: Increased protein expression levels and mutual shift to the insoluble membranous fraction of transfected HBx in the presence of PML isoforms.** (A) HepG2-NTCP-K7 cells were co-transfected with pCMX3b-Flag HBx-V5 and PML isoforms I-VI in pLKO-pgD-EYFP and harvested 48 h.p.t.. Protein lysates as well as cellular insoluble fraction were generated, separated by SDS-PAGE, subjected to western blot and immunodetected using antibodies for GFP (PML), HBx, SAF $\alpha$  as well as  $\beta$ -actin. Stained proteins are depicted on the right, appendant molecular weights are indicated in kDa on the left, respectively. (B) Corresponding protein expression levels were quantified by densitometric analysis of the detected bands by *ImageJ*. Protein expression levels were normalized to the loading control  $\beta$ -actin. Depicted bar charts represent the average protein expression values including standard deviations (n=2).

### 3.4.5. Increased HBx protein expression and mutual re-localization to the insoluble matrix fraction with PML isoforms in HepG2-NTCP-K7 shPML cell

As the previous experiment was conducted in HepG2-NTCP-K7 cells expressing endogenous PML, this experiment was repeated in HepG2-NTCP-K7 shPML cells to exclude the impact of endogenous PML. In accordance with our previous results HBx was similarly elevated in both fractions in the presence of PML isoforms, whereas this effect was slightly pronounced in the insoluble membranous fraction (Fig. 18, lane 9-14). PML isoform expression was, as previously shown, unaffected by HBx in the input fraction but increased in the insoluble fraction. Here, no significant difference between the single isoforms could be detected (Fig. 18 B). Summarized, the impact of PML isoforms on HBx and *vice versa* further substantiate our previous findings in

parental HepG2-NTCP-K7 cells and emphasize the observed effect to be independent of endogenous PML.



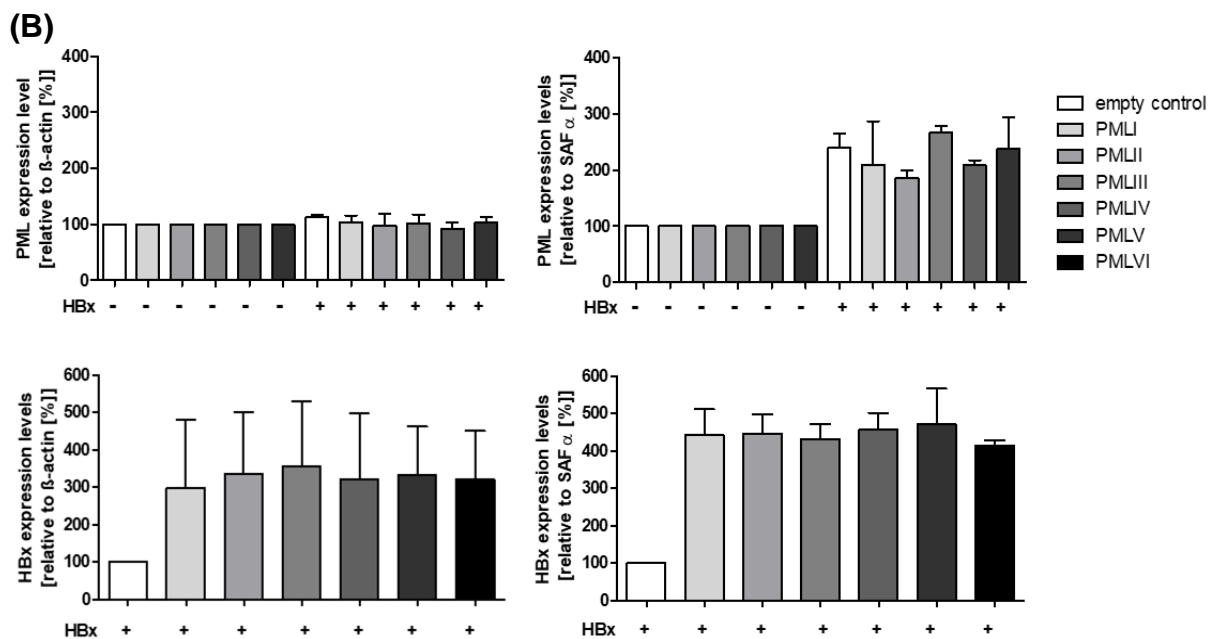


**Figure 18: Increased protein HBx expression levels as well as mutual shift to the insoluble membranous fraction of HBx in the presence of PML isoforms in HepG2-NTCP-K7 shPML cells.** (A) HepG2-NTCP-K7 shPML cells were co-transfected with pCMX3b-Flag HBx-V5 and PML isoforms I-VI in pLKO-pgD-EYFP and harvested 48 h.p.t.. Protein lysates as well as cellular insoluble fraction were generated, separated by SDS-PAGE, subjected to western blot and immunodetection to stain GFP (PML), HBx as well as  $\beta$ -actin. Stained proteins are depicted on the right, appendant molecular weights are indicated in kDa on the left, respectively. (B) Corresponding protein expression levels were quantified by densitometric analysis of the detected bands via *ImageJ*. Protein expression levels were normalized to the loading control  $\beta$ -actin. Depicted bar charts represent the average protein expression values including standard ( $n=2$ ).

### 3.4.6. Interaction between HBx proteins and PML isoforms

Even though no single PML isoform co-localized with HBx, we saw explicit impact of PML isoforms on HBx protein levels. Thus, we transfected and harvested cells 48 h.p.t. to analyze binding affinity between viral and host factors. Protein lysates as well as co-immunoprecipitation (pulled with HBx) were implemented, separated by SDS-PAGE and subjected to western blot. Immunodetection was performed for GFP (PML), HBx and  $\beta$ -actin (Fig. 19). The input control showed GFP signals for all PML isoforms, however HBx protein expression was strongly increased in the presence of the respective single PML isoforms. This HBx pattern was also displayed during the co-immunoprecipitation assay. Nevertheless, interactions of co-transfected HBx with all single PML isoforms could be detected between 70-100 kDa to the isoform (lane

3-8), respectively. These data indicate no specific PML isoform interaction for HBx. Since HBx did not co-localize with these PML isoforms it is likely that an additional host protein bridges HBx to PML.

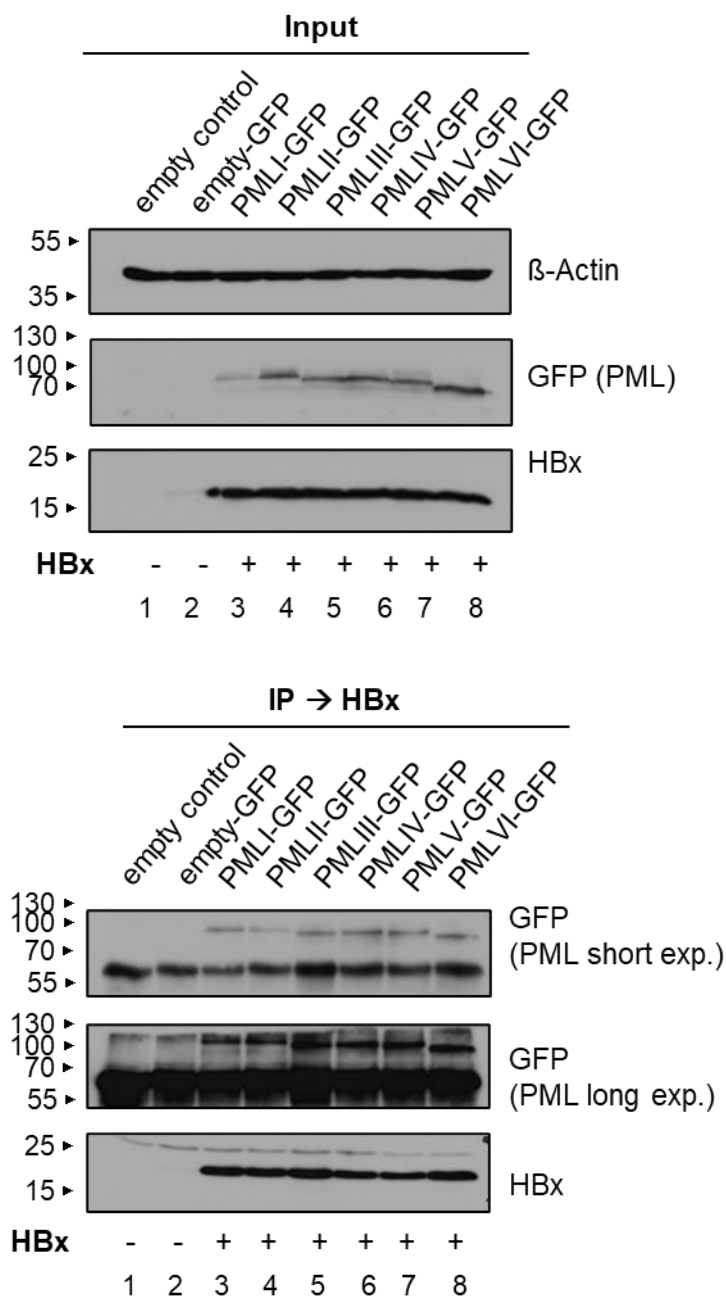


**Figure 19: HBx interacts with all co-transfected PML isoforms.** (A) HepG2-NTCP-K7 cells were co-transfected with pCMX3b-Flag HBx-V5 and PML isoforms I-VI in pLKO-pgD-EYFP and harvested 48 h.p.t.. Protein lysates as well as co-immunoprecipitation (pulled HBx) were implemented, separated by SDS-PAGE and subjected to western blot. Immunodetection was performed for GFP (PML), HBx as well as  $\beta$ -actin as loading control. Stained proteins are depicted on the right, appendant molecular weights are indicated in kDa on the left, respectively.

### **3.5. Crosstalk between viral HBx proteins and PML-NB associated host proteins**

#### **3.5.1. Sp100A represents a PML-NB component that binds HBx**

To find the potential linker protein for the HBx/PML interaction, we screened for Sp100, another main PML-NB component. Sp100 encodes four isoforms A, B, C and HMG, which we analyzed in the following experiment. All Sp100 isoforms were co-transfected with HBx plasmids and harvested 48 h.p.t; whole-protein lysis as well as co-immunoprecipitation assay (pulled with HBx) were conducted followed by SDS-PAGE, western blot and immunoblotting for GFP, HBx and  $\beta$ -actin. Western blot results indicated strong protein expression for all Sp100 isoforms, although the HBx protein levels declined in the presence of all Sp100 isoforms (Fig. 20, input, lane 3-6). Moreover, the co-immunoprecipitation revealed a specific interaction of HBx with Sp100A isoform indicated by an upcoming band at ~95 kDa (Fig. 20, IP, lane 3). Interestingly, this isoform is known to promote cellular chromatin de-condensation and affect transcriptional activation [337]. Taken together, all Sp100 proteins are capable to reduce HBx protein levels and Sp100A was found to interact with transiently expressed HBx, being the host candidate that bridges the viral regulator to PML-NB structures.

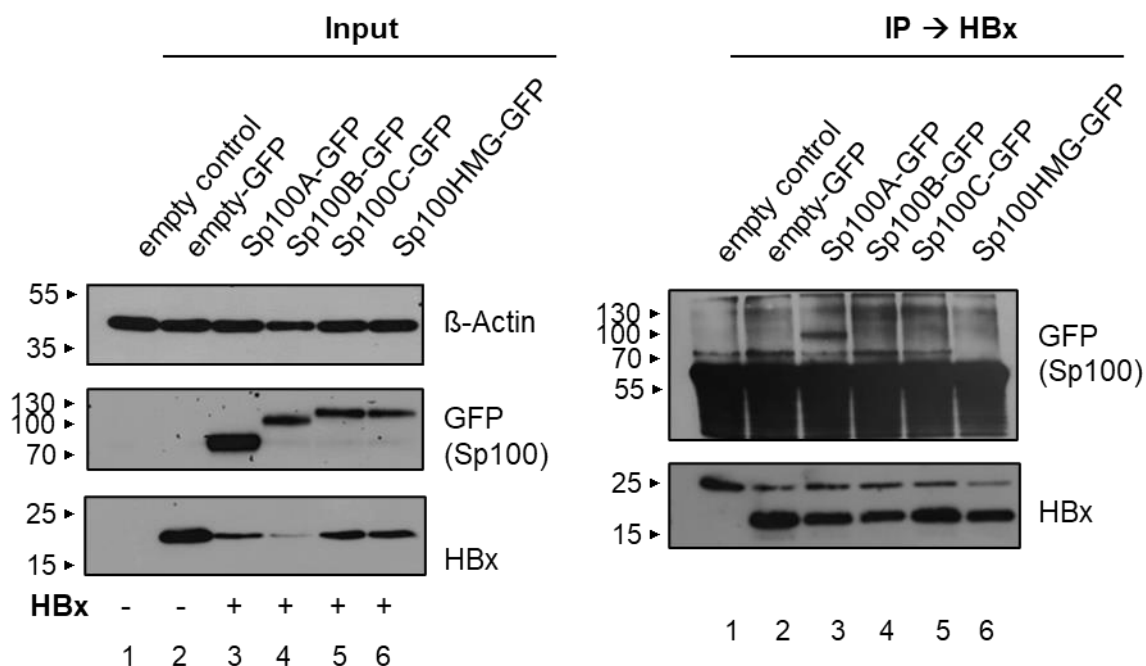


**Figure 20: Interaction of Sp100 isoform A with HBx.** H1299 cells were co-transfected with pCMX3b-Flag HBx-V5 and pYFP Sp100 isoforms A, B, C, HMG and harvested 48 h.p.t..(A) Protein lysates as well as co-immunoprecipitation (pulled HBx) were implemented, separated by SDS-PAGE and subjected to western blot. Immunodetection was performed using antibodies for GFP (Sp100A, B, C, HMG), HBx as well as  $\beta$ -actin as loading control. Stained proteins are depicted on the right, appendant molecular weights are indicated in kDa on the left, respectively.



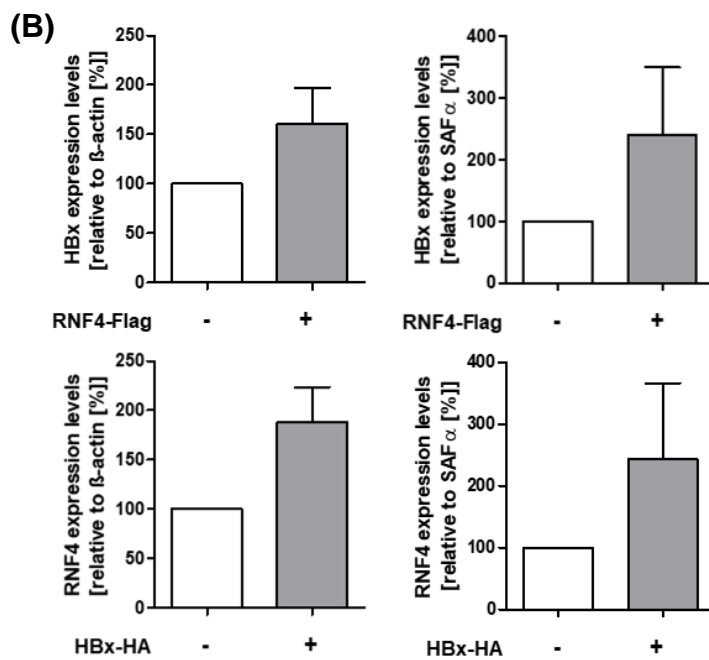


**Figure 21: Mutual re-localization of HBx and RNF4 to the insoluble membranous fraction.** (A) HepG2-NTCP-K7 cells were transfected with pcDNA3-HA HBx and pCMX3b-Flag RNF4 and harvested 48 h.p.t.. Protein lysates as well as the insoluble membranous fraction were implemented, separated by SDS-PAGE, subjected to western blot and immunodetection using HA (HBx), Flag (RNF4), and  $\beta$ -actin antibodies. Stained proteins are depicted on the right, appendant molecular weights are indicated in kDa on the left, respectively. (B) Corresponding protein expression levels were quantified by densitometric analysis of the detected bands via *ImageJ*. Protein expression levels were normalized to the loading control. Depicted bar charts represent the average protein expression values including standard deviations (n=2).

### 3.5.2.2. HBx protein expression affects RNF4 localization

In a next step, the localization of transfected pcDNA3-HA HBx and pCMX3b-Flag RNF4 was investigated. HepG2-NTCP-K7 cells were fixed 48 h.p.t. with 4% PFA, immunofluorescence stainings were performed for Flag (RNF4, 488 nm, green), HA (HBx, 647 nm, red) and DAPI (405 nm, nucleus, blue). Distribution of RNF4 was mainly displayed diffuse in the whole nucleus (Fig. 22, panel j), whereas a minor number of cells showed RNF4 preferentially located at the nuclear membrane (panel f). Transfected HBx alone located in the nucleus and in the cytoplasm of the cell. The combination of both proteins did not change the localization of HBx, however the majority of cells displayed RNF4 re-location to the nuclear membrane. Taken together, the nuclear localization of HBx was not affected by co-transfected RNF4, but RNF4 localization was altered by HBx.

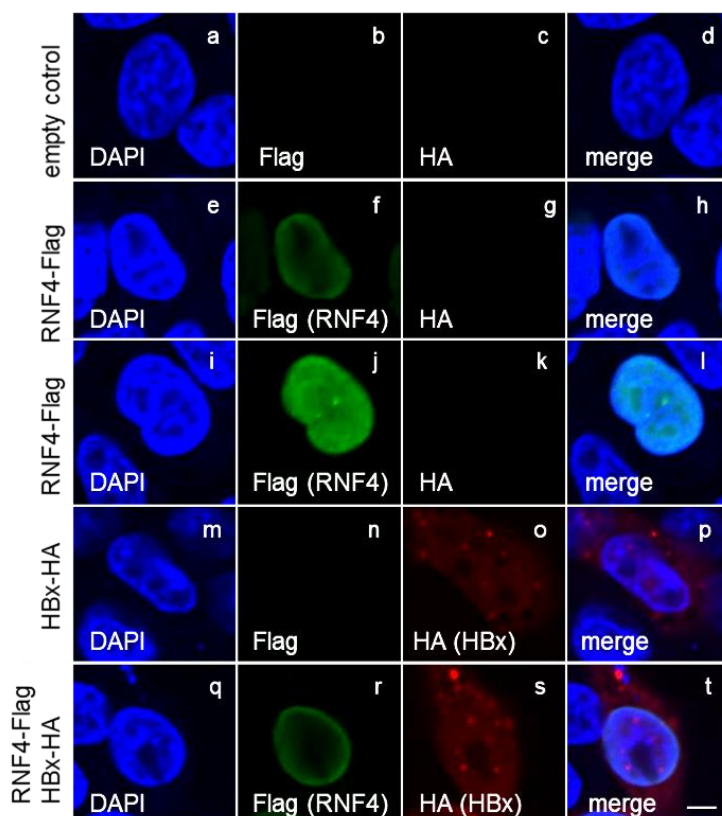


**Figure 22: RNF4 localization shifted to the nuclear membrane by co-transfected HBx.** HepG2-NTCP-K7 cells were co-transfected with pcDNA3-HA HBx and pCMX3b-Flag RNF4. Cells were fixed 48 h.p.t. with 4% PFA and stained with HA (HBx) and Flag (RNF4) primary antibodies detected by conjugated secondary antibodies Alexa488 (Flag (RNF4), green) and Alexa647 (HA (HBx), red). Nuclei were labeled with DAPI. Representative pictures as well as 3D Z-stack images are depicted. Scale bar indicating 3  $\mu$ m.

### 3.5.2.3. RNF4 as a novel interaction partner of HBx

Based on our previous findings, we were keen to examine the interaction between RNF4 and HBx. Therefore, cells were co-transfected again with pcDNA3-HA RNF4 and pCMX3b-Flag HBx-V5. Cells were harvested 48 h.p.t., whole-cell lysates and co-immunoprecipitation via HBx pull-down were performed, followed by SDS-PAGE and western blot analysis using immunoblotting for HA (HBx), Flag (RNF4) and  $\beta$ -actin (Fig. 23 A). Input levels confirmed former findings, showing elevated HBx protein levels in the presence of RNF4. Moreover, the co-immunoprecipitation displayed a specific interaction of HBx with RNF4. Taken together, these data revealed RNF4 as a novel interaction partner of the HBx protein, and that HBx might either function as a linker between substrates and RNF4 or HBx promotes SUMOylation of substrates, to be

recognized by the RNF4 STUbL, resulting in the ubiquitinylation and proteasomal degradation.

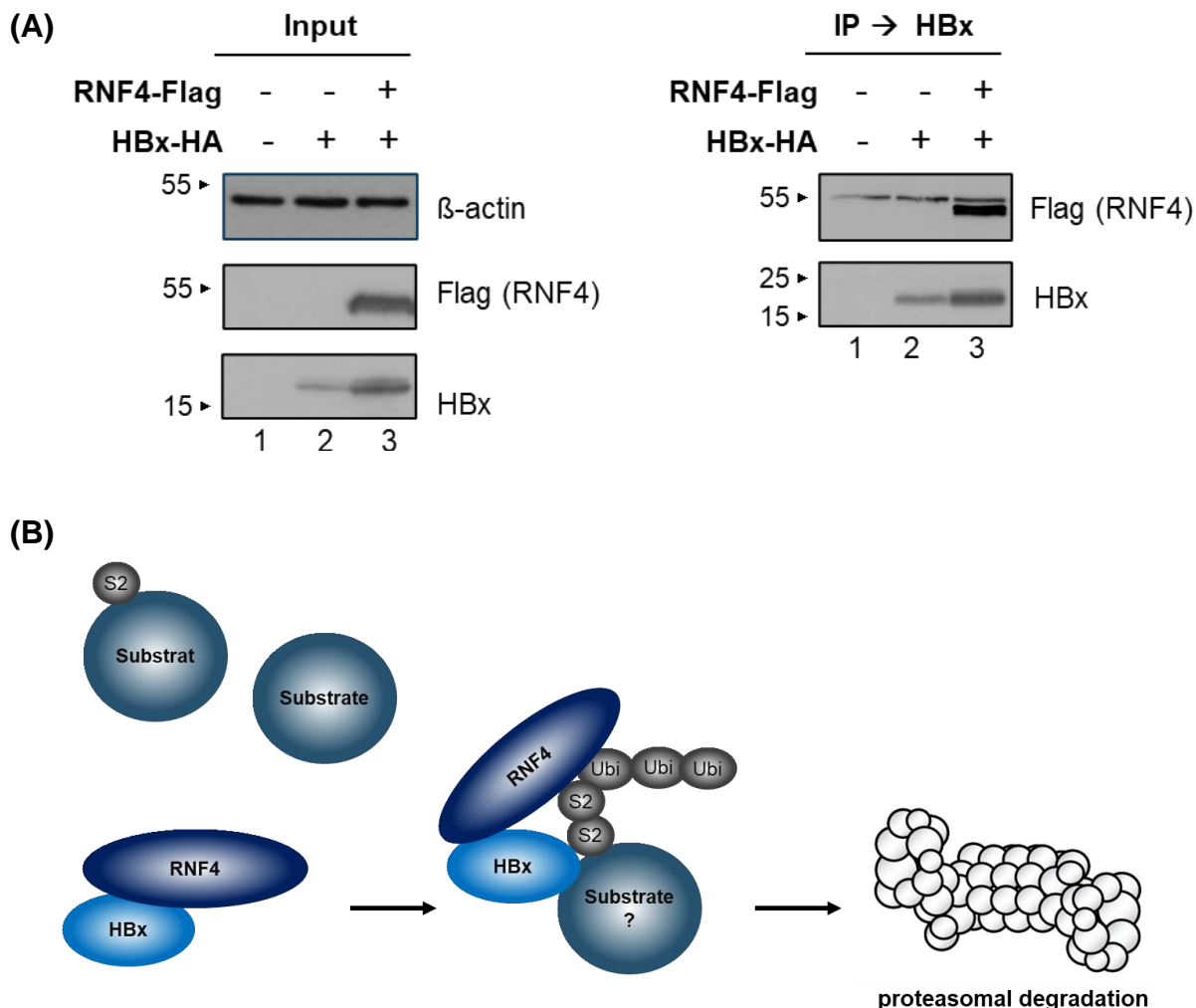


**Figure 23: Interaction of co-transfected HBx with RNF4.** (A) HepG2-NTCP-K7 cells were co-transfected with pcDNA3-HA HBx and pCMX3b-Flag RNF4 and harvested 48 h.p.t.. Protein lysates as well as co-immunoprecipitation (pulled HBx) were implemented, separated by SDS-PAGE and subjected to western blot. Immunodetection was performed by using antibodies for HA (HBx), Flag (RNF4) and β-actin as loading control. Stained proteins are depicted on the right, appendant molecular weights are indicated in kDa on the left, respectively (B) Schematic illustration of our hypothesis based on our previous findings.

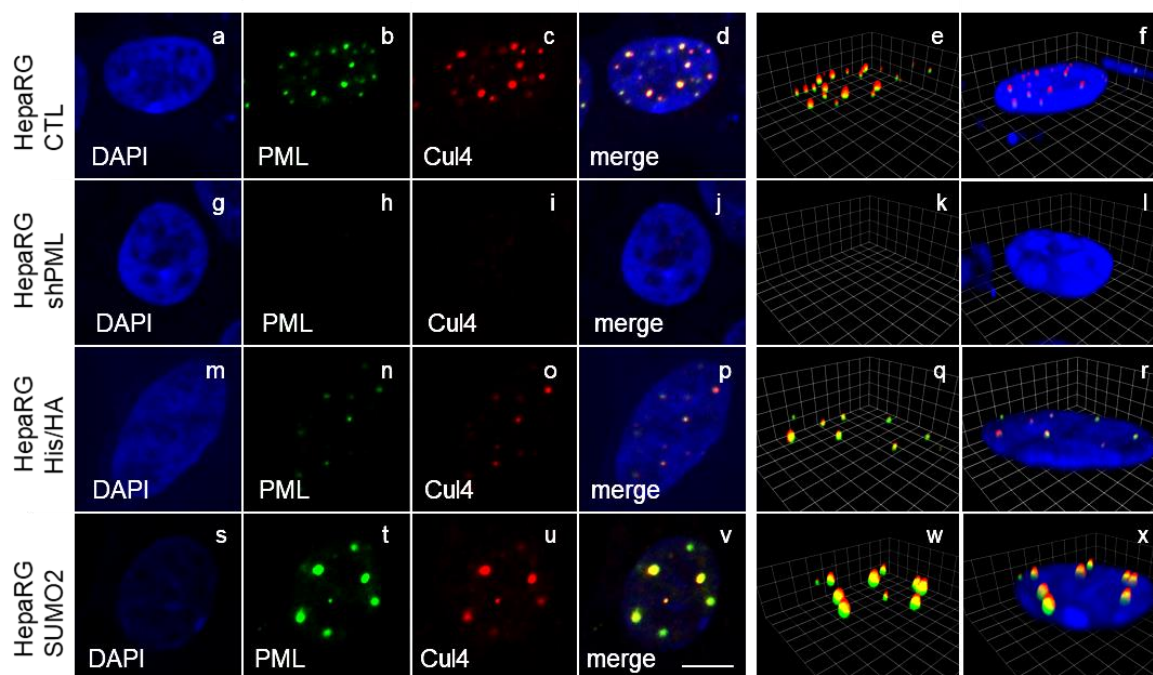
### 3.5.3. Novel interplay between the PML-NBs and the CRL4-HBx complex

To see, whether besides HBx, we also find the HBx associated CRL4 complex located at PML-NBs and whether PML-NBs potentially connect or alter the CRL4-HBx complex those host nuclear foci were further analyzed.

#### 3.5.3.1. Cellular Cul4 proteins are found within PML-NBs

To amplify our findings concerning PML associated proteins, we examined Cul4 being a major component of the HBx-DDB1 CRL4 complex essential for recruitment, ubiquitinylation and proteasomal degradation of substrates [1]. We performed immunofluorescence stainings of endogenous PML and Cul4 in several HepaRG cell lines. Cells were fixed and stained with PML (green, 488 nm), Cul4 (red, 647 nm) and DAPI (nucleus, blue 405 nm). A distinct dot-like co-localization of Cul4 with PML could be displayed in all cells expressing endogenous PML (Fig. 24 A, panel d, p, v; Z-stacks panel e, q, w). Quantification of PC values supported these finding with Pearson coefficient numbers of 0.75 in HepaRG CTL cells, 0.72 in HepaRG His/HA cells and 0.82 HepaRG SUMO2-His/HA cells (Fig. 24 B). Interestingly no Cul4 staining could be detected in HepaRG shPML lacking endogenous PML. Summarized, we found Cul4 to co-localize with PML-NBs, whereupon the dot-like distribution of Cul4 is highly dependent on PML protein expression.

(A)



(B)

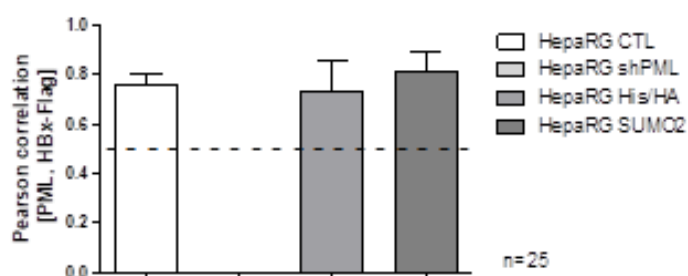
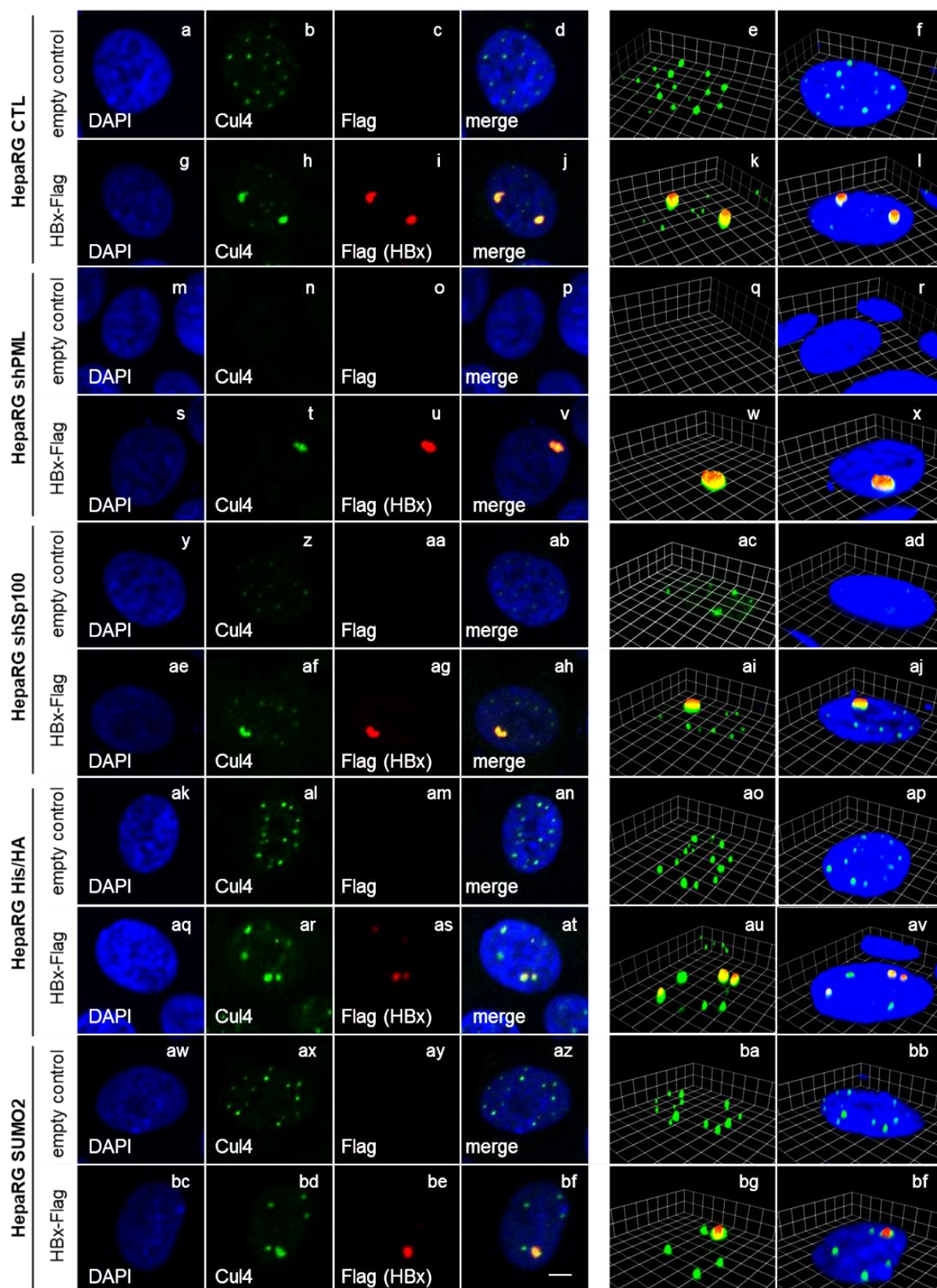


**Figure 24: Co-localization of endogenous PML-NBs and Cul4.** HepaRG CTL, HepaRG shPML, HepaRG His/HA and HepaRG SUMO2-His/HA cells were fixed with 4% PFA and stained with Cul4 and PML primary antibodies detected by conjugated secondary antibodies Alexa488 (PML, green) and Alexa647 (Cul4, red). Nuclei were labeled with DAPI. (A) Representative pictures as well as 3D Z-stack images are depicted. Scale bar indicating 3  $\mu$ m. (B) Pearson coefficients (PC) were quantified by *Volocity*. Depicted bar charts represent the PC values including standard deviations.

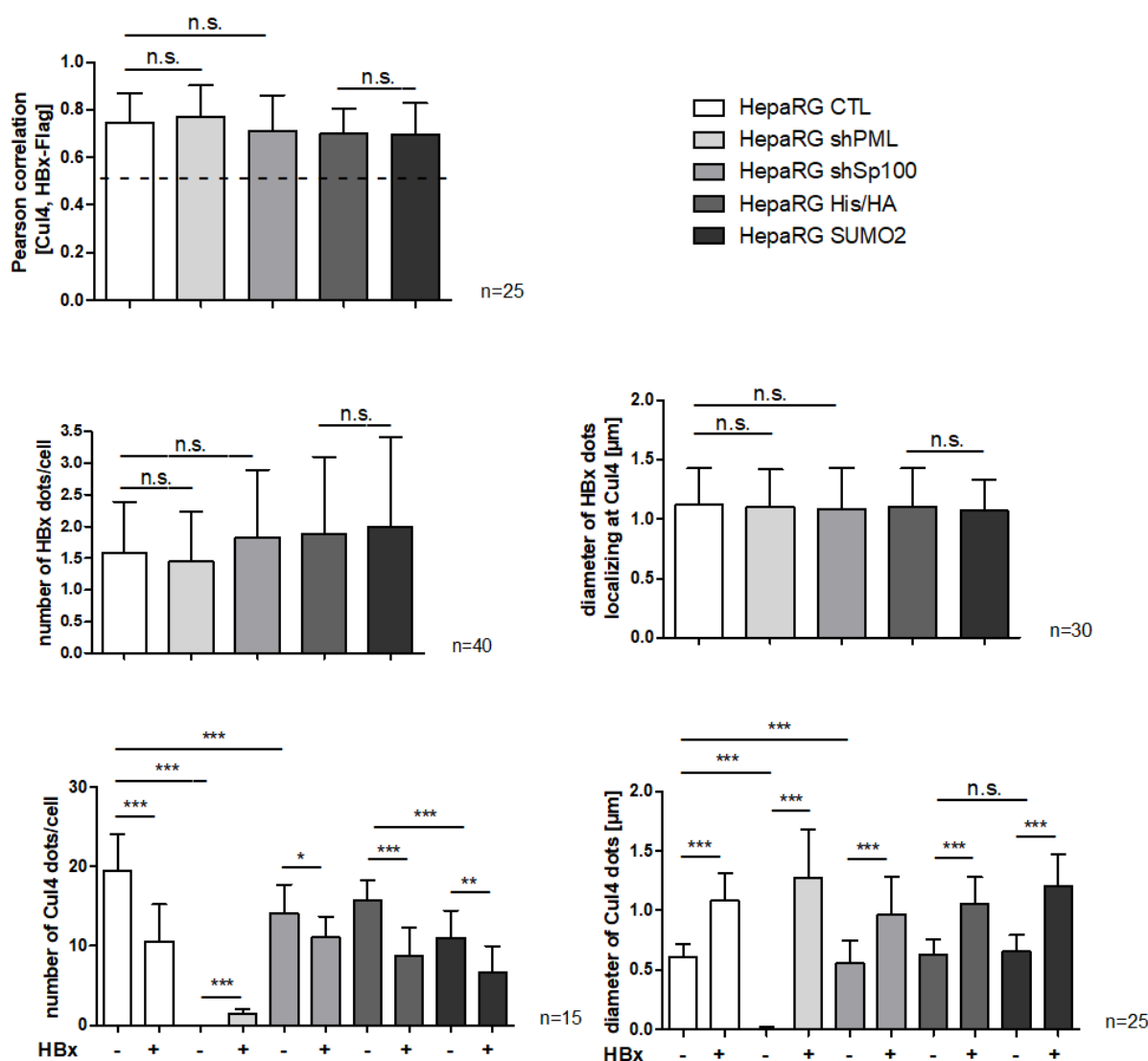
### 3.5.3.2. Transiently expressed HBx modulated Cul4 nuclear localization

As we found Cul4 to localize at PML-NBs, we tested whether HBx/Cul4 cooperation is dependent on PML-NB integrity. HepaRG CTL, HepaRG shPML, HepaRG His/HA and HepaRG SUMO2-His/HA cells were transfected with HBx IVT mRNA and harvested after 24 h. Cells were stained for endogenous Cul4 (green, 488 nm), Flag (HBx, red, 647 nm) and DAPI (nucleus, blue, 405 nm). Representative pictures were taken, and additionally three-dimensional Z-stack images were conducted. We were able to detect a distinct co-localization of HBx with Cul4 in all investigated cell lines (Fig. 25 A, panel j, v, ah, at, bf), which was confirmed by Z-stack images (panel k, w, ai, au, bg) as well as PC values higher 0.5 (Fig. 25 B). Moreover, the number and size of PML-NBs and HBx dots were quantified, revealing no significant changes between cell lines. Nevertheless, we observed that HBx expression induced a significant reduction of Cul4 dots within the cells and simultaneously a significant increase regarding diameters of in Cul4 dots. This impact was found to be similar for all investigated HepaRG cell lines. Consistent with data shown in Fig. 24, no Cul4 staining could be detected in HepaRG shPML. However, transfection of HBx resulted in a recruitment and co-localization of Cul4 to HBx, independent of PML-NBs. Moreover, in HepaRG shSp100 cells significantly less Cul4 dots were detected, compared to HepaRG CTL cells, however the size was significantly larger. HepaRG SUMO2-His/HA cells displayed significantly less Cul4 dots compared to HepaRG His/HA, whereas the diameter of Cul4 dots remained comparable in both cell lines. All these findings disclosed HBx to modulate Cul4 protein distribution within the cell, causing less but bigger Cul4 foci. Besides Cul4 being re-localized to HBx once the viral factor is present, we showed the cellular protein to be dependent on PML, Sp100 and SUMO2.

(A)



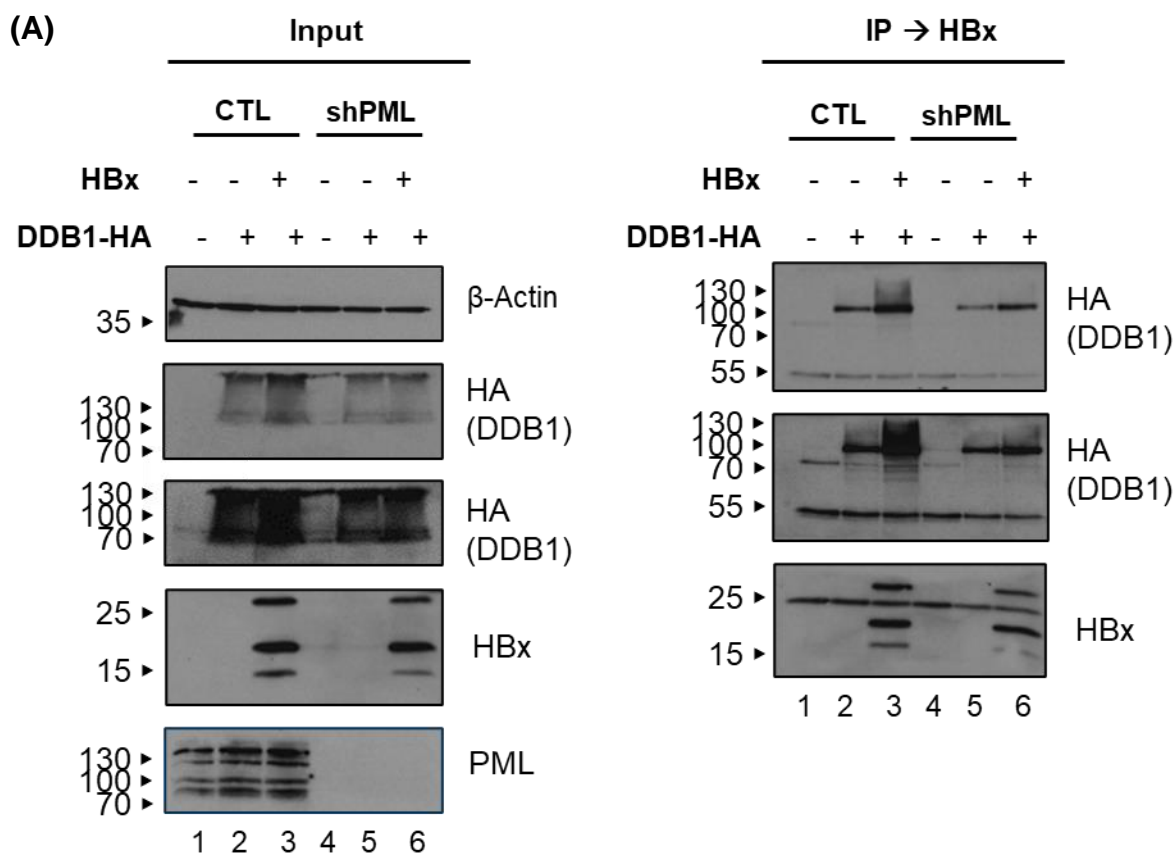
(B)



**Figure 25: Cul4 number and size altered in the presence of transfected HBx.** HepaRG CTL, HepaRG shPML, HepaRG His/HA and HepaRG SUMO2-His/HA cells were transfected with HBx-Flag IVT mRNA. Cells were fixed 24 h.p.t. with 4% PFA and stained with Cul4 and Flag (HBx) primary antibodies detected by conjugated secondary antibodies Alexa488 (Cul4, green) and Alexa647 (Flag (HBx), red). Nuclei were labeled with DAPI. Representative pictures as well as 3D Z-stack images are depicted. Scale bar indicating 3 µm. Pearson correlation coefficients (PC) were quantified via *Volocity*. Depicted bar charts represent the PC values, Cul4 size, HBx size or number of Cul4 or HBx per cell including standard deviations. Statistically significant differences were determined using Welch-corrected Student's t-test. \*:  $p \leq 0.05$ , \*\*:  $p \leq 0.01$ , \*\*\*:  $p \leq 0.001$ , \*\*\*\*:  $p \leq 0.0001$ .

### 3.5.3.3. PML modulates HBx binding with DDB1

Due to the fact, that all previous experiments revealed a strong impact of HBx on PML and *vice versa* we were curious to investigate a possible role of PML for the HBx-DDB1 interaction of the CRL4 complex. Parental HepG2-NTCP-K7 and HepG2-NTCP-K7 shPML cells were transfected with pCMX3b-Flag HBx-V5 and harvested 48 h.p.t.. Whole-protein lysates and co-immunoprecipitation (pulled with HBx) were performed, followed by SDS-PAGE, western blot and immunoblotting for PML, DDB1, HBx, and  $\beta$ -actin. Input levels displayed all expected bands, including the slightly lower HBx protein expression in shPML cells as shown in Fig. 26. Moreover, transiently expressed DDB1 was found to be stabilized in the presence of co-expressed HBx. Co-immunoprecipitation assays showed that pulling HBx give a DDB1 signal at ~100 kDa (Fig. 26, lane 3, 6), indicating binding between both proteins in HepG2-NTCP-K7 CTL cells. In shPML cells we exhibited a weaker signal, concluding that the interaction between HBx and DDB1 is PML dependent.



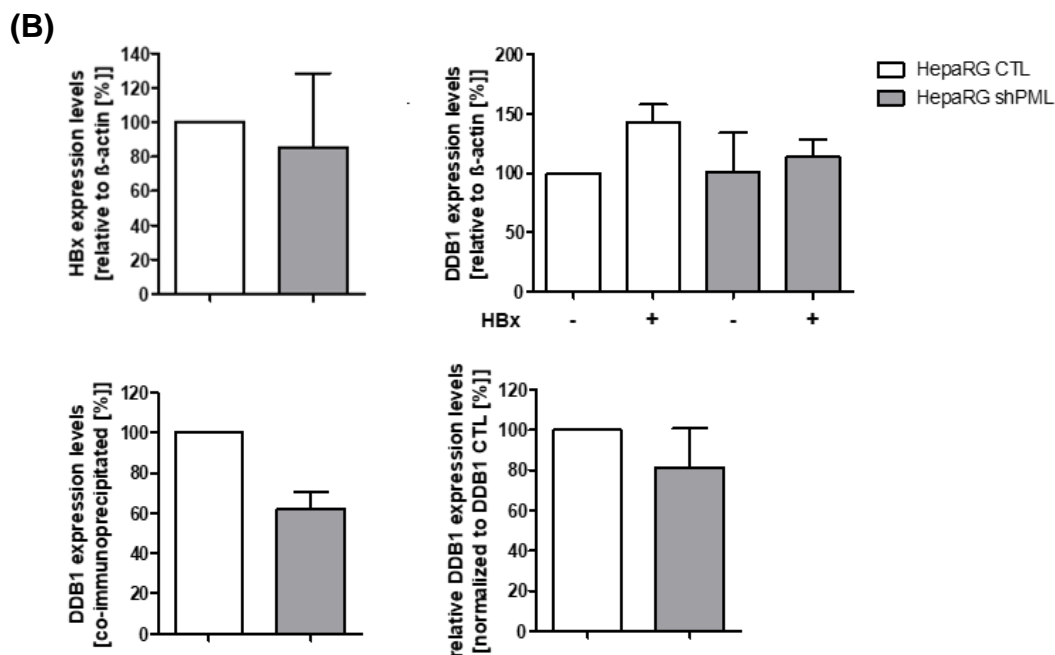
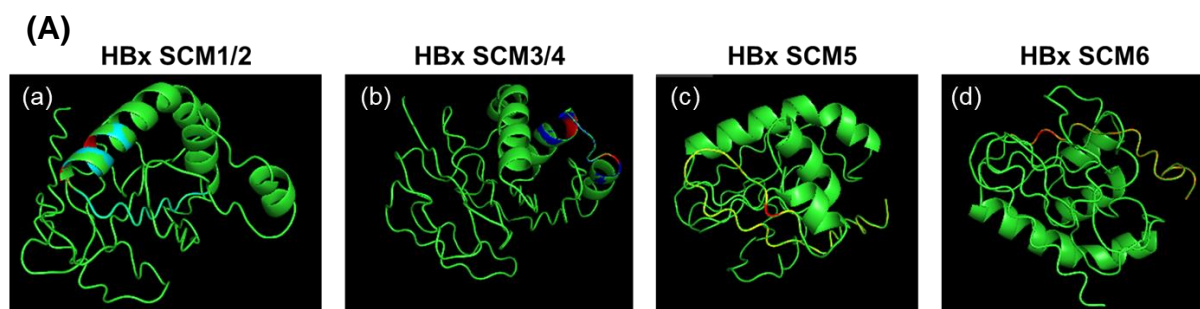


**Figure 26: Interaction of HBx with DDB1 is PML dependent.** HepG2-NTCP-K7 and HepG2-NTCP-K7 shPML cells were co-transfected with pCMX3b-Flag HBx-V5 and harvested 48 h.p.t.. (A) Protein lysates as well as co-immunoprecipitation (pulled HBx) were implemented, separated by SDS-PAGE and subjected to western blot. Immunodetection was performed for PML, DDB1, HBx as well as  $\beta$ -actin as loading control. Stained proteins are depicted on the right, appendant molecular weights are indicated in kDa on the left, respectively. (B) Corresponding protein expression levels were quantified by densitometric analysis of the detected bands via *ImageJ*. Protein expression levels were normalized to the loading control  $\beta$ -actin. Depicted bar charts represent the average values including standard deviations. Statistically significant differences were determined (n=2).

### 3.6. Identification of the relevant HBx SUMO conjugation motif

#### 3.6.1. Structure comparison of predicted HBx SUMO conjugation motif within HBx

Since we were able to disclose HBx SUMOylation and DDB1 crosstalk with PML-NBs, we further characterized the HBx SUMOylation site(s) and the impact of HBx SCM mutants on protein functions. In a first step, structure comparison of HBx wt and SCM mutants were conducted. The exchanged lysine to arginine was indicated in red. Tertiary structure prediction showed no obvious changes between HBx wt (green) and SCM1/2 (light blue, panel a), SCM3/4 (dark blue, panel b), SCM5 (yellow, panel c) and SCM6 (orange, panel d) (Fig. 27 A). Indeed, surface structure analysis displayed minor changes for HBx wt compared to the respective SCM mutants (Fig. 27 B, panel i-l). Thus, all HBx SCM mutants maintained their predicted structure and all SCM were accessible for potential SUMO modifications.



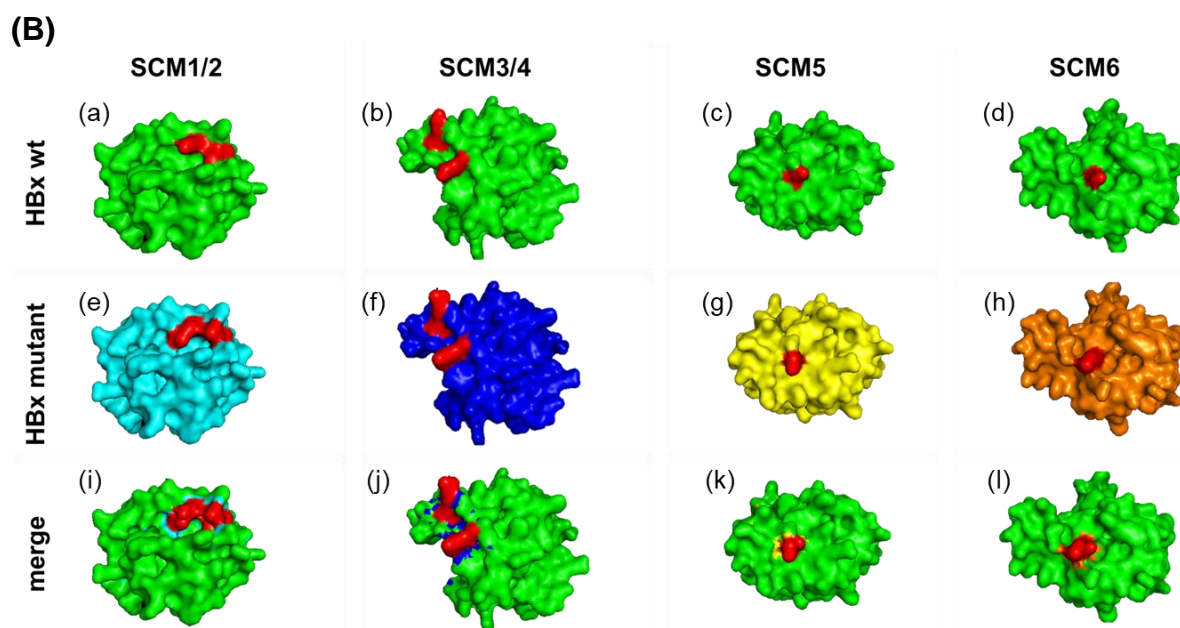


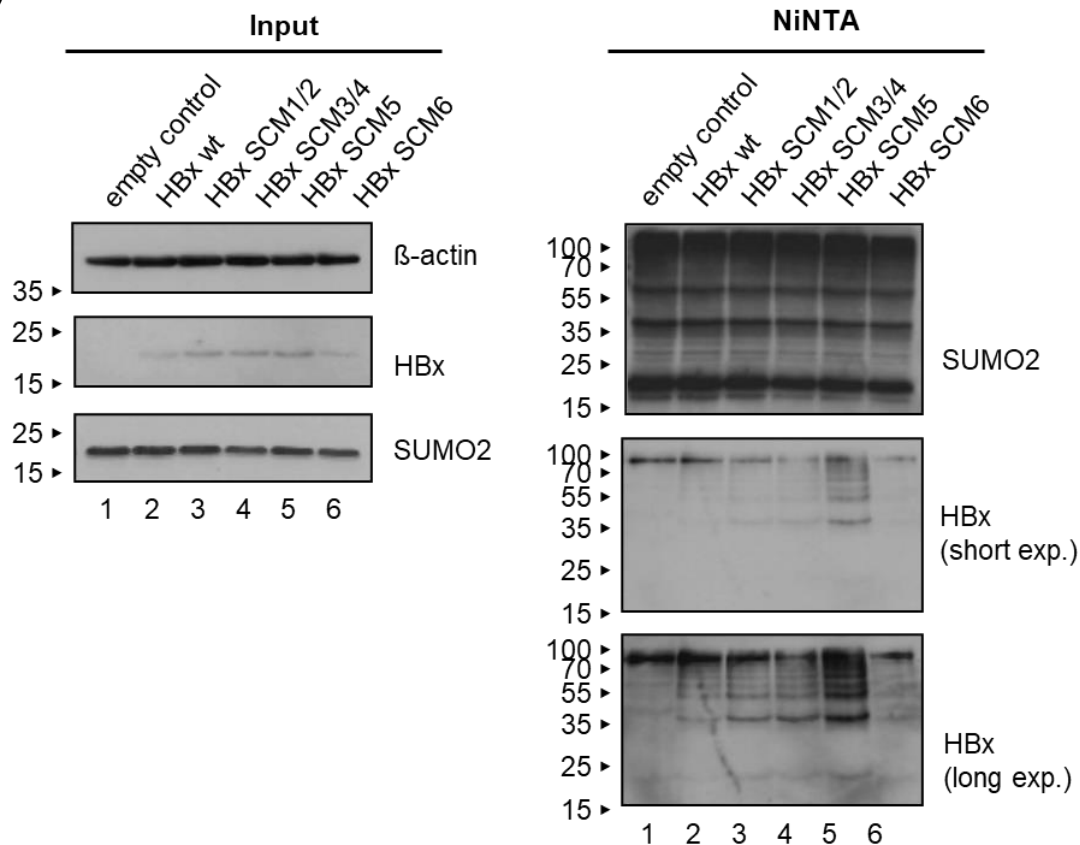
**Figure 27: Structure comparison of HBx wt and SCM mutants.** (A) Schematic overlay depiction of the tertiary structure of HBx wt (green) and HBx SCM1/2 mutant (light blue), HBx SCM3/4 mutant (dark blue), HBx SCM5 mutant (yellow), HBx SCM6 mutant (orange) including the indicated SCM (red). (B) Schematic comparison of the surface structure of HBx wt (green) and HBx SCM1/2 mutant (light blue), HBx SCM3/4 mutant (dark blue), HBx SCM5 mutant (yellow), HBx SCM6 mutant (orange). Merge depicted in i-l.

### 3.6.2. HBx is efficiently SUMOylated at the SCM1/2

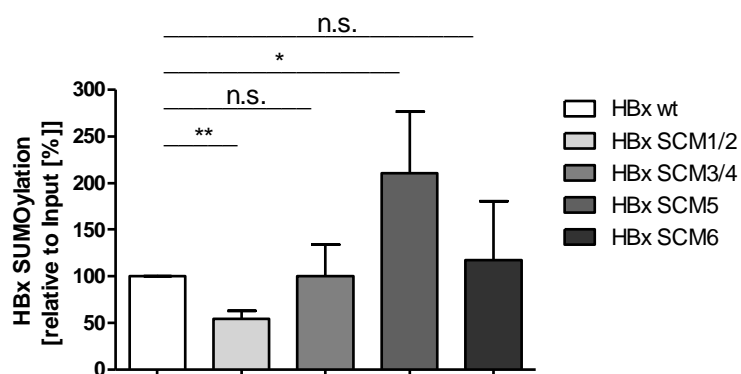
Next, we investigated SUMO conjugation of the respective HBx SCM mutants by SUMO2. HepaRG cells over-expressing 6xHis-tagged SUMO2 were transfected with HBx wt and SCM mutant IVT mRNA and harvested after 24 h. Whole-protein lysis and NiNTA assay were conducted, analyzed using SDS PAGE, western blot as well as immunoblotting for SUMO2/3, HBx and  $\beta$ -actin were performed. Protein input levels showed protein expression for all transfected HBx constructs, however the HBx wt showed weaker expression compared to SCM mutants (Fig. 28 A). The NiNTA assay pulled SUMO2 and thus, SUMOylation of HBx could be detected for all SCM mutants, but with diverse intensities. To visualize the SUMO modification of each protein, the protein expression was quantified relatively to the respective protein input (Fig. 28 B). These data demonstrated a significant reduction of ~54% for the HBx SCM1/2 SUMO modification as well as a significant increase of HBx SUMOylation in SCM5 mutant by

two-fold. SUMO conjugation to HBx SCM3/4 and SCM6 proteins were comparable to the wt protein. Based on these findings, the main SCM of HBx could be revealed at position 1/2.

(A)



(B)



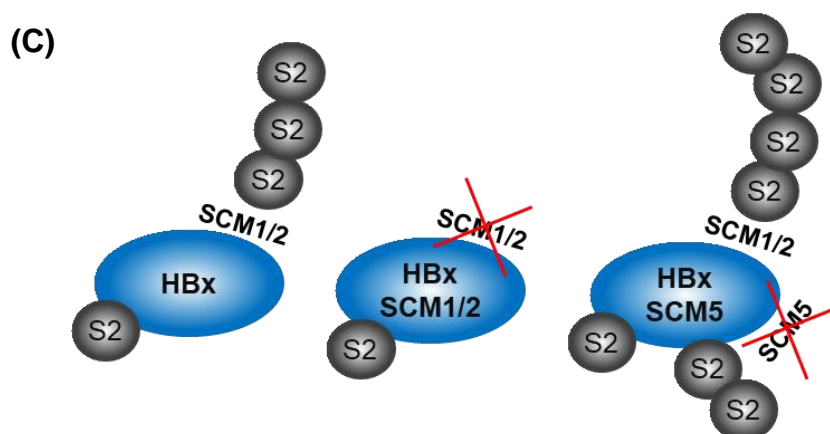


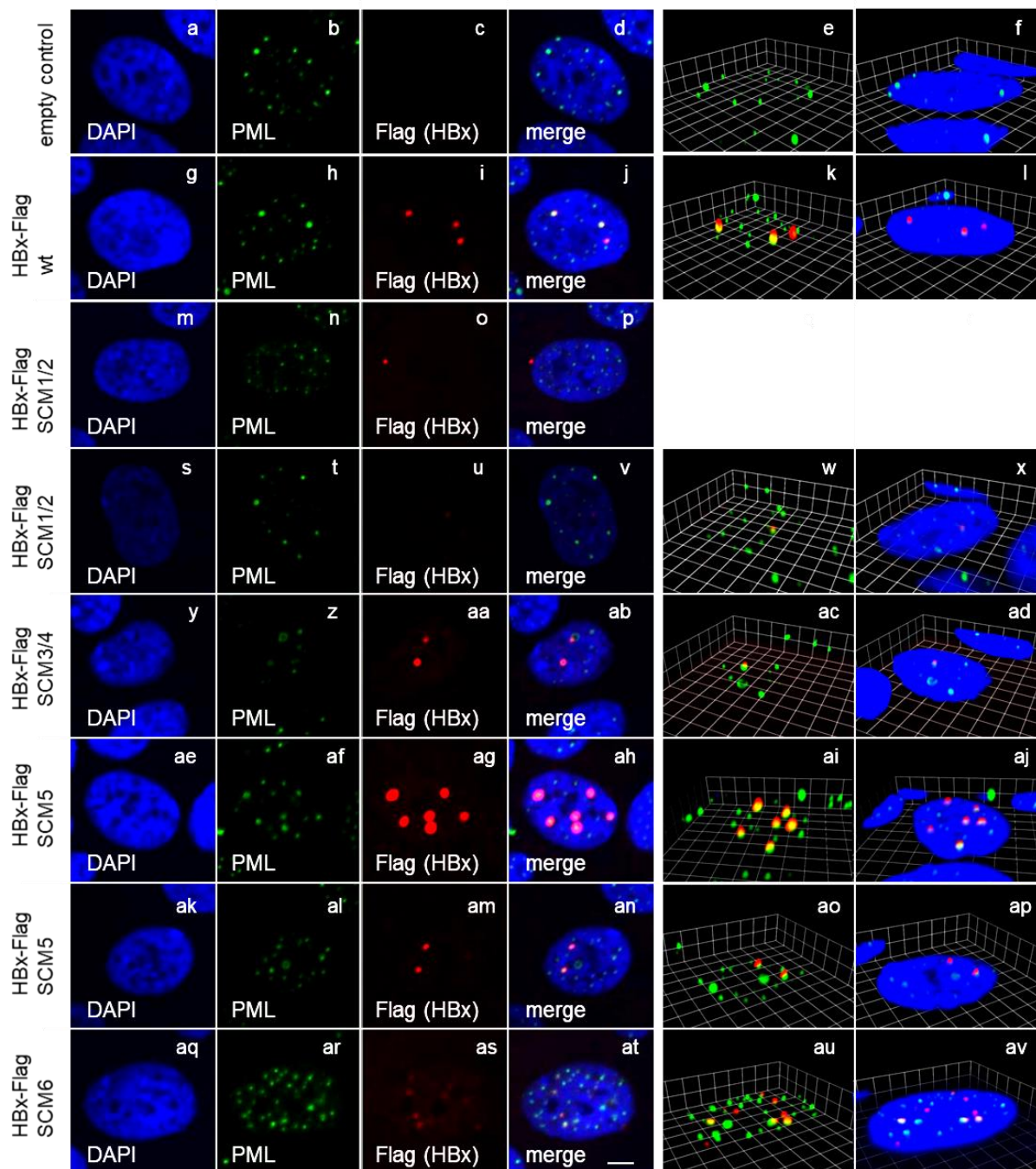
**Figure 28: Reduced SUMOylation of HBx SCM1/2 mutant.** (A) HepaRG SUMO2-His/HA cells were transfected with HBx IVT mRNA and harvested 24 h.p.t.. Protein lysates and the corresponding NiNTA assay were prepared, separated by SDS-PAGE, subjected to western blot and immunodetection using SUMO2/3, HBx and  $\beta$ -actin antibodies. Stained proteins are depicted on the right, appendant molecular weights are indicated in kDa on the left, respectively. (B) HBx SUMOylation levels were quantified by densitometric analysis of the detected bands via *ImageJ* relatively to HBx input levels. HBx wt and SCM mutant SUMOylation levels were quantified relatively to the loading control  $\beta$ -actin and normalized to the HBx input. Depicted bar charts represent these values including standard deviations. Statistically significant differences were determined using Welch-corrected Student's t-test. \*:  $p \leq 0.05$ , \*\*:  $p \leq 0.01$ , \*\*\*:  $p \leq 0.001$ , \*\*\*\*:  $p \leq 0.0001$  ( $n=3$ ) (C) Schematic representation of our previous findings.

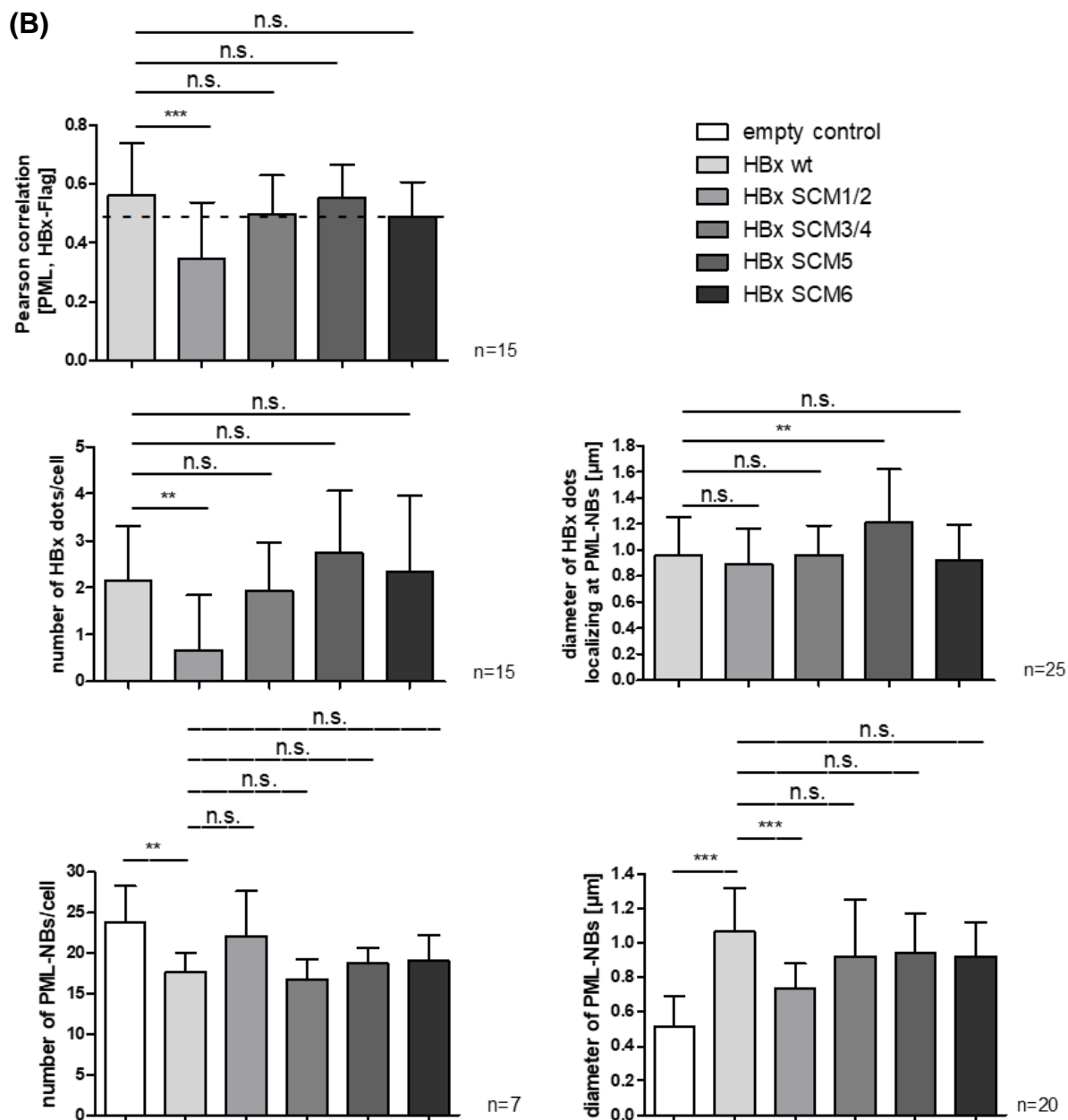
### 3.6.3. Re-localization of HBx SCM1/2 mutant from PML-NBs

To further characterize the HBx SCM mutants, immunofluorescence analysis was conducted to determine intracellular localization of the viral factor. In the course of this experiment, IVT mRNA for HBx wt and all SCM mutants were transfected into HepaRG cells and fixed with 4% PFA after 24 h. Cells were stained with PML (green, 488 nm), Flag (HBx, red, 647 nm) and DAPI (nucleus, blue 405 nm). Representative mono-layer pictures were taken and additional 3D Z-stack images were generated (Fig. 29). HBx wt co-localized in the nucleus at PML-NBs as previously observed (panel j, k). Besides, HBx SCM3/4 (panel ab, ac), SCM5 (panel ah, ai) and SCM6 (panel at, au) co-localized at endogenous PML-NBs, in contrast to HBx SCM1/2. These data were additionally quantified for PC coefficient, supporting the co-localization of all HBx constructs apart from SCM1/2 mutant (PC-value 0.35). This low co-localization rate of HBx SCM1/2 dots *inter alia* resulted from the low number (panel v, w) in the nucleus and particularly from the extranuclear localization of the major HBx SCM1/2 proportion. The remaining HBx constructs shared similar numbers of HBx dots within the nucleus and rare

extranuclear localization. Furthermore, the diameter of nuclear HBx dots was measured, highlighting significantly bigger HBx SCM5 dots in comparison to all other constructs. Finally, the number and size of PML-NBs was determined. PML-NB number was decreased in the presence of HBx wt, SCM3/4, SCM5 and SCM6 whereas SCM1/2 displayed levels comparable to the empty control. Regarding the size of PML-NBs all HBx constructs significantly increased PML-NB diameters except SCM1/2. Taken together, the previously identified SUMOylation mutant HBx SCM1/2 elicited contrary effects on PML-NB localization, number, and size than all other HBx constructs. Additionally, the hyper-SUMOylated HBx SCM5 was found to express especially large nuclear HBx dots, concluding a SUMO dependent nuclear accumulation of HBx.

(A)

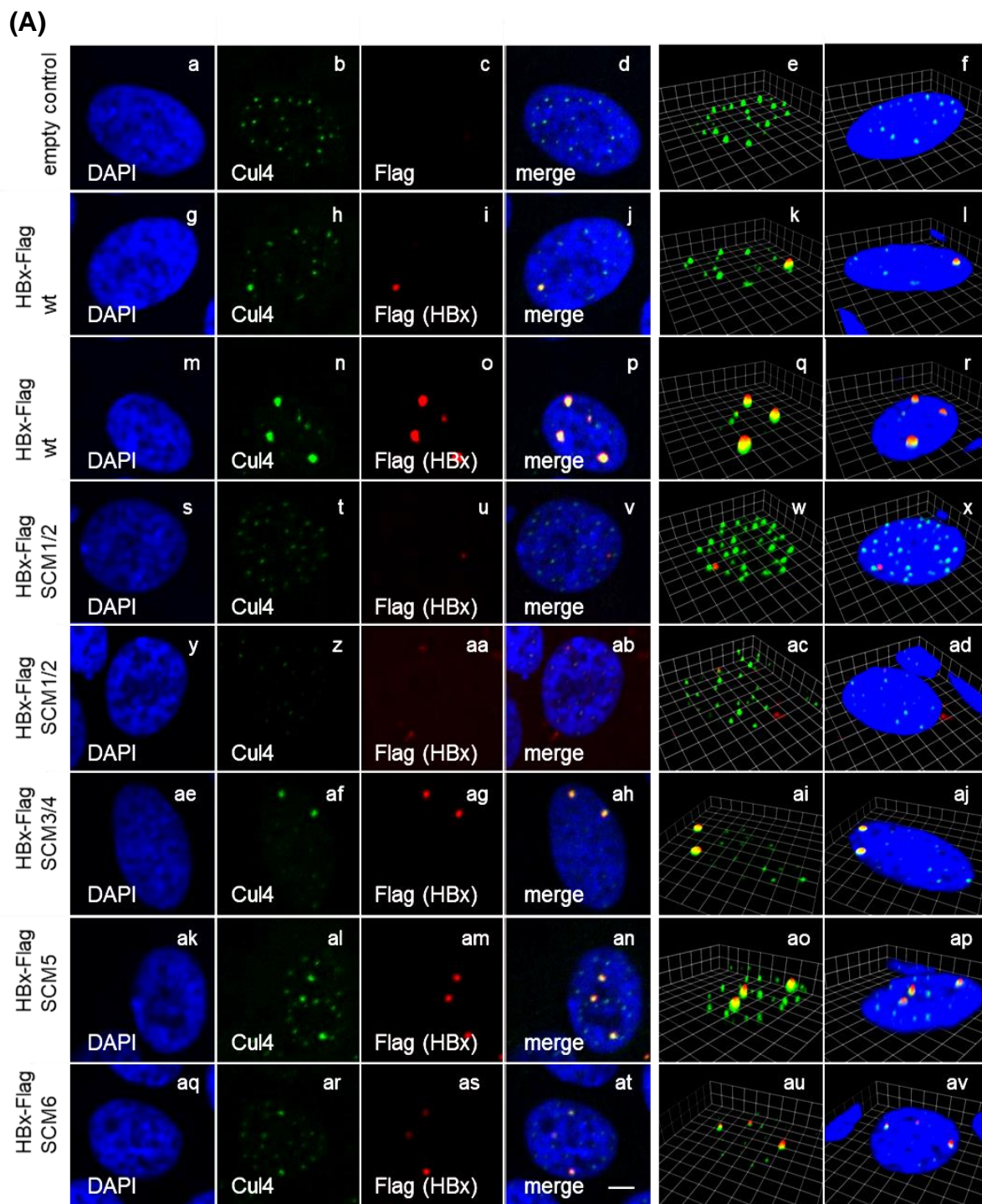




**Figure 29: Co-localization of all HBx SCM mutants with PML-NBs except SCM1/2.** HepaRG cells were transfected with HBx IVT mRNA (wt and SCM mutants) and fixed 24 h.p.t. with 4% PFA. Cells were stained with PML and Flag (HBx) primary antibodies detected by conjugated secondary antibodies Alexa488 (PML, green) and Alexa647 (Flag (HBx), red). Nuclei were labeled with DAPI. Representative pictures as well as 3D Z-stack images are depicted. Scale bar indicating 3 µm. Pearson correlation coefficient (PC) and diameters of PML-NB as well HBx dots were quantified via *Volocity* software. Depicted bar charts represent the average values including standard deviations. Statistically significant differences were determined using Welch-corrected Student's t-test. \*:  $p \leq 0.05$ , \*\*:  $p \leq 0.01$ , \*\*\*:  $p \leq 0.001$ , \*\*\*\*:  $p \leq 0.0001$ .

#### 3.6.4. Cul4 only co-localizes with SUMO conjugated HBx variants

Since our prior investigations already revealed co-localization of endogenous Cul4 and HBx, we tested any crosstalk once SUMOylation is blocked. HBx wt and all SCM mutant IVT mRNAs were transfected into HepaRG cells and fixed with 4% PFA after 24 h. Cells were stained with Cul4 (green, 488 nm), Flag (HBx, red, 647 nm) and DAPI (nucleus, blue, 405 nm). Representative pictures were taken and additional 3D Z-stack images were generated (Fig. 30). These results exemplify co-localization of HBx wt (panel j, k, p, q), SCM3/4 (panel ab, ac), SCM5 (panel ah, ai) and SCM6 (panel at, au), but not SCM1/2 (panel v, w) with endogenous Cul4. In addition, PC values were calculated and supported these observations. All PCs accounted values above 0.5 indicating co-localization, except the significantly lower HBx SCM1/2 with PC=0.35. Moreover, calculations of nuclear HBx numbers as well as size were significantly lower for HBx SCM1/2. In addition, the number of nuclear Cul4 dots was significantly reduced in the presence of all HBx constructs apart from HBx SCM1/2. Simultaneously, HBx wt, SCM3/4, SCM5 and SCM6 led to increased sizes of Cul4 dots. Again, HBx SCM1/2 displayed the opposite pattern, similar to empty vector controls. These findings correspond with Figure 29, revealing less and smaller HBx SCM1/2 dots in the nucleus as well as no co-localization with Cul4. Furthermore, Cul4 foci number and size were altered by all HBx expression apart from HBx SCM1/2. Concluding SUMOylation to play an essential role in HBx localization and aggregation since the SUMO-reduced HBx SCM1/2 mutant showed altered properties than the remaining HBx variants.



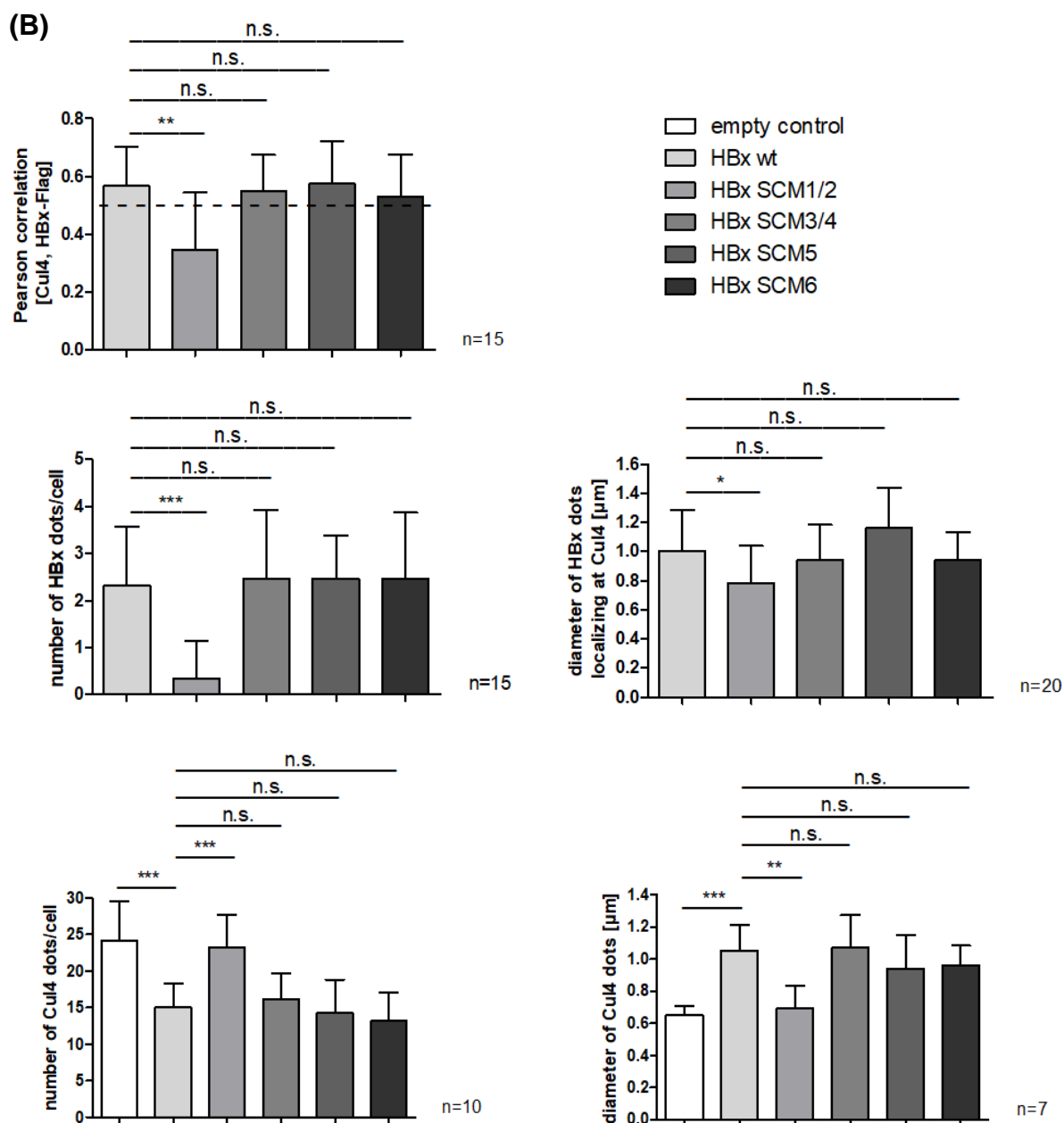


**Figure 30: No co-localization of HBx SCM1/2 with endogenous Cul4.** HepaRG cells were transfected with HBx IVT mRNA and fixed 24 h.p.t. with 4% PFA. Cells were stained with Cul4 and Flag (HBx) primary antibodies detected by conjugated secondary antibodies Alexa488 (Cul4, green) and Alexa647 (Flag (HBx), red). Nuclei were labeled with DAPI. Representative pictures as well as 3D Z-stack images are depicted. Scale bar indicating 3  $\mu\text{m}$ . Pearson correlation coefficient (PC) and diameters of PML-NB as well HBx dots were quantified via *Volocity* software. Depicted bar charts represent these values including standard deviations. Statistically significant differences were determined using Welch-corrected Student's t-test. \*:  $p \leq 0.05$ , \*\*:  $p \leq 0.01$ , \*\*\*:  $p \leq 0.001$ , \*\*\*\*:  $p \leq 0.0001$ .

### 3.6.5. HBx-DDB1 interaction is promoted by less SUMOylated HBx proteins

Since HBx interacts with DDB1 to induce Smc5/6 degradation via ubiquitinylation, we analyzed the impact of HBx SCM mutants in this process. Since co-transfection experiments with pCMX3b-Flag HBx-V5 and pcDNA3-DDB1-HA2 could not distinguish any binding difference between HBx wt and SCM mutants (data not shown here), we decided to investigate endogenous DDB1 and transfected pCMX3b-Flag HBx-V5. Cells were harvested 48 h.p.t., and whole-protein lysates as well as co-immunoprecipitation (pulled by HBx) were performed. SDS-PAGE, western blot and immunoblotting stained for DDB1, HBx as well as  $\beta$ -actin were conducted. Input levels showed similar DDB1 expression levels, whereas transfected HBx SCM5 (Fig. 31, input, lane 5) was weaker expressed compared to the remaining HBx constructs. Co-immunoprecipitation revealed an interaction between HBx and DDB1. Also, HBx SCM3/4, SCM5 and SCM6 displayed interaction with DDB1. For HBx SCM1/2 no interaction could be detected (Fig. 31, IP, lane 3). Since the HBx protein expression levels differ, DDB1 levels were normalized to the pulled HBx levels. Calculated co-immunoprecipitated DDB1 levels depicted no interaction between HBx SCM1/2, a slightly reduced interaction with SCM3/4, a strongly increased interaction with HBx SCM5 and interaction levels for HBx SCM6 comparable to HBx wt. Here, we showed that DDB1 does not interact with the SUMO-reduced HBx mutant SCM1/2, but even stronger with the hyper-SUMOylated HBx mutant SCM5.

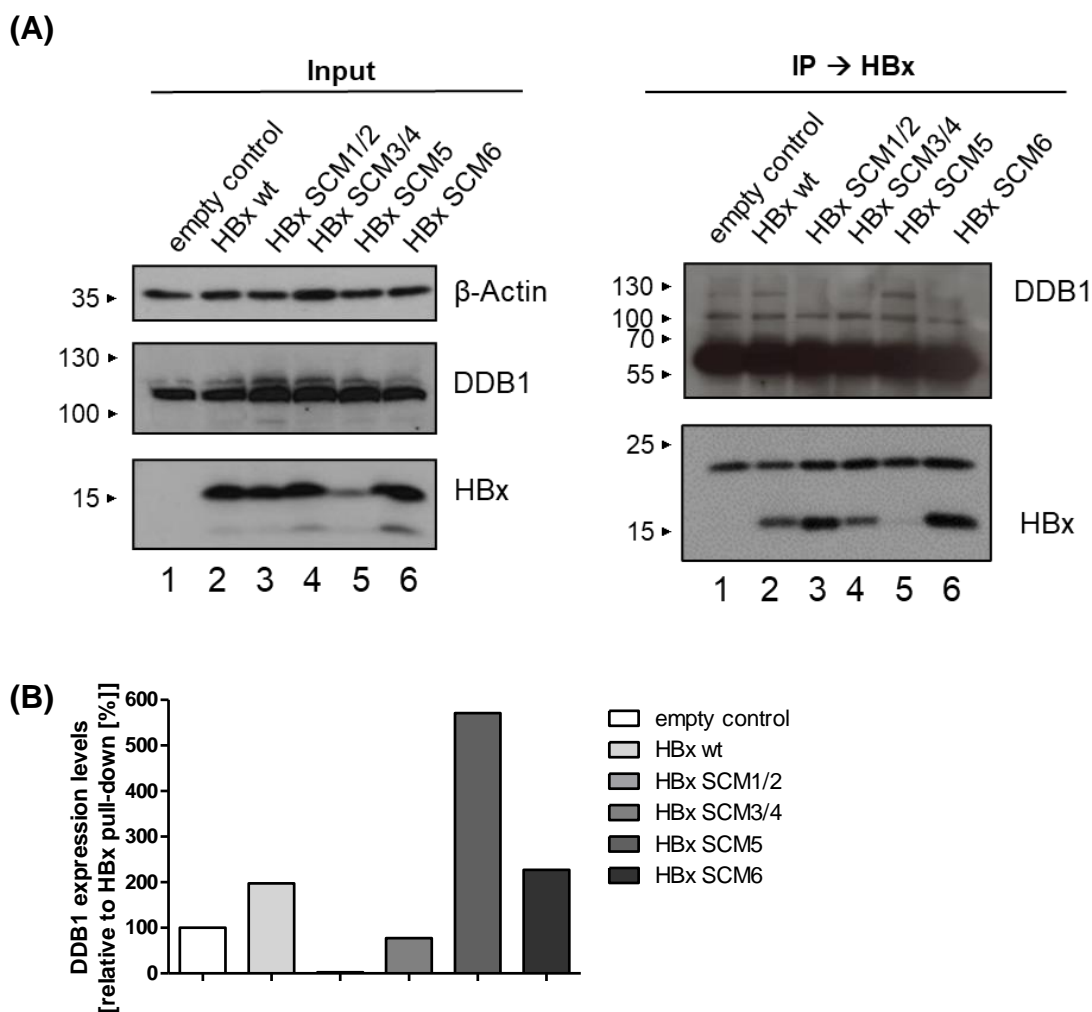


**Figure 31: Interaction between HBx and DDB1 lost in HBx SM1/2 mutant.** HepaRG cells were co-transfected with pCMX3b-Flag HBx-V5 and pcDNA3-DDB1-HA2 and harvested 48 h.p.t.. Protein lysates as well as co-immunoprecipitation (pulled HBx) were implemented, separated by SDS-PAGE and subjected to western blot. Immunodetection was performed using antibodies for DDB1, HBx as well as  $\beta$ -actin as loading control. Stained proteins are depicted on the right, appendant molecular weights are indicated in kDa on the left, respectively. Immunoprecipitated DDB1 bands were quantified relatively to the corresponding HBx protein pull-down via *ImageJ*. Depicted bar charts represent the average protein expression.

### 3.6.6. HBx SUMOylation status irrelevant for alteration of endogenous protein expression levels

Since the interaction between HBx and DDB1 is SUMO dependent, we further analyzed the impact of HBx SUMO conjugation on Smc5/6 degradation. Therefore, HepG2-NTCP-K7 cells were transfected with pCMX3b-Flag HBx-V5 mutants and harvested 48 h.p.t.. SDS-PAGE, western blotting and immunoblotting with PML, Smc6, HBx, as well as  $\beta$ -actin were conducted, and protein expression levels were quantified via *ImageJ*. Endogenous Smc6 levels were decreased in the presence of all HBx constructs compared to the empty control dependent on the amount of expressed HBx protein amount (Fig. 32). Here, stronger expression of HBx triggered a stronger degradation of Smc6. Moreover, HBx induced the elevation or stabilization of endogenous PML. The depicted immunoblot indicated even stronger increase with transfected HBx wt, SCM3/4 and SCM6 (Fig. 32, lane 2 4, 6). Explicitly, the HBx variants SCM1/2 and SCM5 could be revealed during our previous experiments since both have an altered SUMOylation pattern in contrast to HBx wt. Nevertheless, HBx was stronger expressed in all lanes, which revealed even higher PML levels (Fig. 32, lane 2, 4, 6). Concluding the amount of HBx within the cell but not the SUMOylation status of HBx is important for PML stabilization or elevation. Summarized, the degradation process of endogenous Smc6 was unaffected by HBx mutations, while endogenous PML was elevated by all HBx variants.

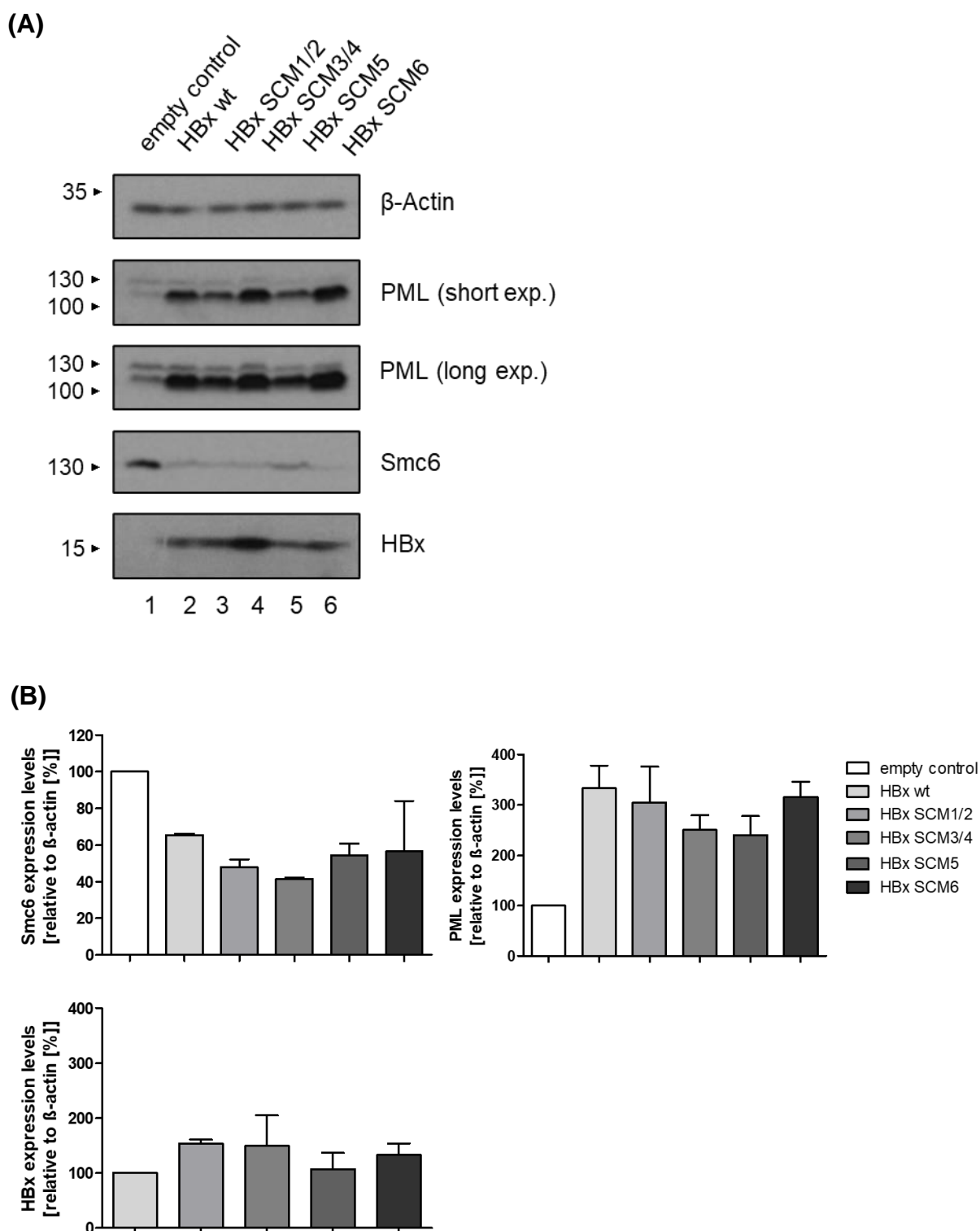


**Figure 32: Alteration of endogenous protein expression levels in the presence of HBx SCM mutants.** (A) HepG2-NTCP-K7 cells were transfected with pCMX3b-Flag HBx-V5 wt and mutants and harvested 48 h.p.t.. Protein lysates were implemented, separated by SDS-PAGE, subjected to western blot and immunodetection for PML, Smc6, HBx as well as  $\beta$ -actin. Stained proteins are depicted on the right-hand side, appendant molecular weights are indicated in kDa on the left-hand side, respectively. ►

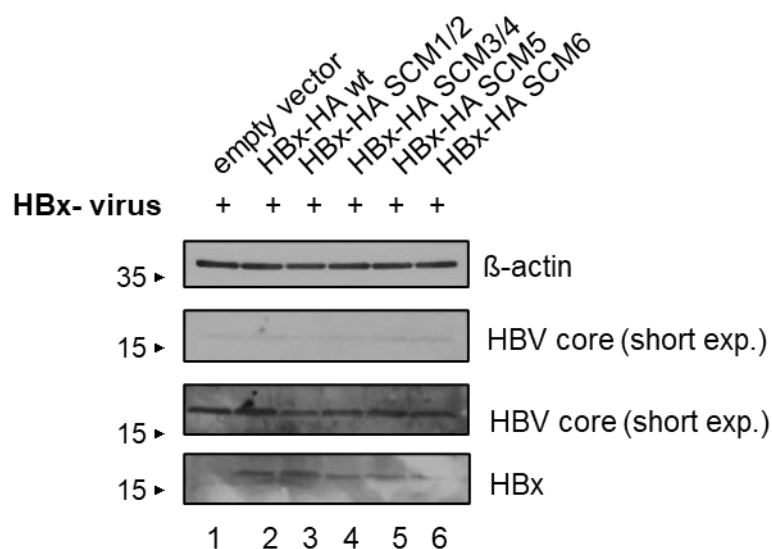
◀ (B) Corresponding protein expression levels were quantified by densitometric analysis of the detected bands via *ImageJ*. Protein expression levels were normalized to  $\beta$ -actin. Depicted bar charts represent the average protein expression values including standard deviations. Statistically significant differences were determined (n=2).

### **3.6.7. HBx SUMOylation is a prerequisite for cccDNA conversion and maintenance**

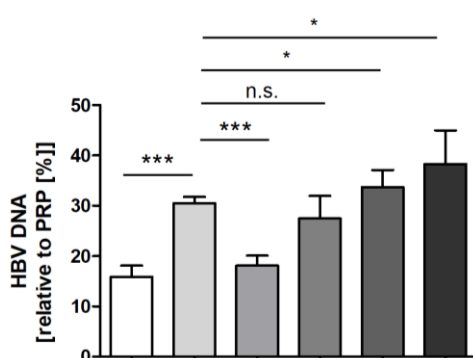
Since we revealed HBx SCM1/2 as a SUMOylation mutant characterized by lacking localization at PML-NBs and association with Cul4 we were highly interested towards the effect of HBx SCM mutants on HBV cccDNA synthesis. Differentiated HepG2-NTCP-K7 cells were transfected with pcDNA-HA HBx wt, SCM1/2, SCM3/4, SCM5 and SCM6 followed by the infection of an HBx- virus. Cells were harvested for whole-protein lysates and DNA extraction 4 d.p.i.. SDS-PAGE, western blot and immunoblotting for core, HBx and  $\beta$ -actin were performed (Fig. 33 A). HBV core served as an infection control. Transfected HBx protein levels were still expressed 4 d.p.i., even though protein levels were relatively low.

Extracted DNA was utilized for qPCR analysis of total HBV DNA and HBV cccDNA (Fig. 33 B). We found that total HBV DNA was significantly increased with transient expression of HBx wt compared to the empty control. HBx SCM1/2 exhibited similar HBV DNA levels as the empty vector control. All further HBx SCM mutants displayed comparable or even higher HBV DNA levels than HBx wt. Additionally, HBV cccDNA levels were investigated, revealing significantly increased levels transfecting HBx wt compared to empty control. All remaining HBx SCM constructs induced similar cccDNA levels like wt HBx. Interestingly, for HBx SCM5 cccDNA levels were again slightly higher than determined for the other constructs. These data revealed, a significant reduction of the viral cccDNA, when HBx is not efficiently SUMOylated as seen with the HBx SCM1/2.

(A)



(B)



(C)

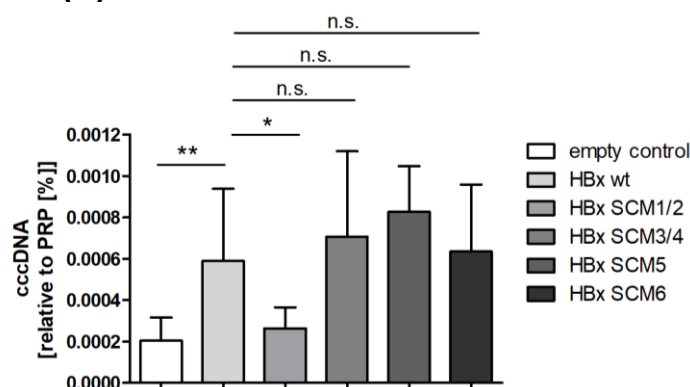


**Figure 33: HBx SCM1/2 promotes reduced HBV DNA and cccDNA levels.** Differentiated HepG2-NTCP cells were transfected with pcDNA-HA HBx wt, SCM1/2, SCM3/4, SCM5 and SCM6, subsequently infected with HBV HBx- virus (MOI 200) and harvested 4 d.p.i.. (A) Protein lysates were implemented, separated by SDS-PAGE, subjected to western blot and immunodetection for core, HBx and  $\beta$ -actin as loading control. Stained proteins are depicted on the right, appendant molecular weights are indicated in kDa on the left, respectively. (B) Total DNA was isolated and qPCR was implemented utilizing specific primers for HBV DNA and PRP as internal control. (C) Quantification of HBV cccDNA was performed by qPCR analysis utilizing specific primers for HBV cccDNA and PRP as housekeeping control. All values were quantified relatively to PrP ( $n=3$ ,  $m=3$ ). Depicted bar charts represent the average values including standard deviations. Statistically significant differences were determined using Welch-corrected Student's t-test. \*:  $p \leq 0.05$ , \*\*:  $p \leq 0.01$ , \*\*\*:  $p \leq 0.001$ , \*\*\*\*:  $p \leq 0.0001$ .

### 3.7. ATO is a potential treatment candidate to reduce HBV chronic cccDNA reservoirs

#### 3.7.1. ATO represses expression of Hepatitis B virus proteins

##### 3.7.1.1. Cell viability assay during ATO administration

Since HBx could be proven to be SUMO2 modified, localize at PML-NBs and target HBV cccDNA, we were interested in the effect of ATO treatment on HBV infections. ATO was chosen as a promising treatment option, due to the fact, that this compound directly affects PML, inducing hyper-SUMOylation followed by ubiquitinylation by RNF4. In a first step, cell viability of HBV infected HepG2-NTCP-K7 cells during ATO treatment was determined. Therefore, cells were differentiated, infected with HBV (MOI 200) and treated with a dilution row (0-4  $\mu\text{M}$ ) of ATO 4 d.p.i. and 7 d.p.i. (Fig. 34). No cytotoxic effect could be observed for ATO concentrations up to 4  $\mu\text{M}$ . Based on these preliminary data, we decided to compare dosages of 2  $\mu\text{M}$  and 4  $\mu\text{M}$  ATO for all future experiments.

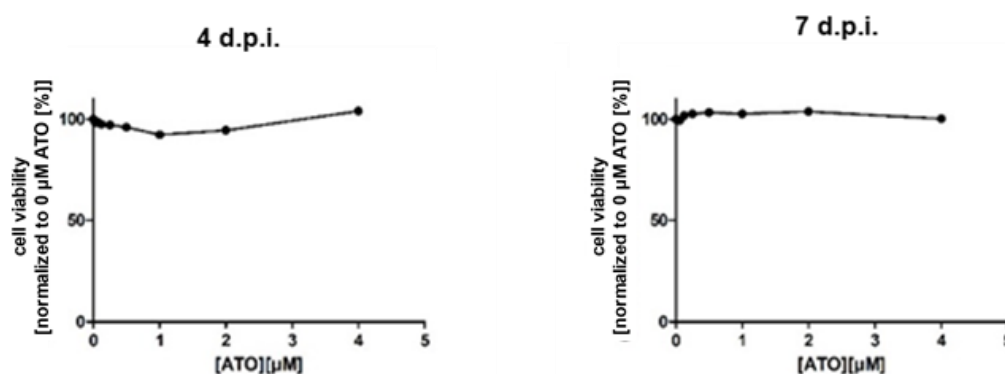


**Figure 34: ATO cell viability unaffected up to 4  $\mu\text{M}$ .** Differentiated HepG2-NTCP-K7 cells were treated with the indicated concentration of ATO for 4 and 7 days. Cell viability of HBV infected cells during ATO treatment was assessed via the Promega CellTiter-Blue Cell Viability Assay.

### 3.7.1.2. Dose-dependent elevation of HBx by ATO

As a primary attempt for ATO treatment, pCMX3b-Flag HBx-V5 was transfected in HepG2-NTCP-K7 cells, subsequently treated with 2  $\mu$ M and 4  $\mu$ M ATO and harvested 48 h.p.t.. Whole-protein lysates, SDS-PAGE, western blot as well as immunoblotting for PML, HBx and  $\beta$ -actin were conducted. PML served as a treatment control since it is proteasomal degraded by ATO treatment [310, 439-441]. Interestingly, endogenous PML expression levels were slightly lower in the presence of HBx without ATO, whereas ATO administration was not as efficient in PML degradation when HBx was present. Moreover, ATO could be shown to dose-dependently increase HBx levels. Hereby, 2  $\mu$ M ATO induced elevation of HBx signal intensities  $\sim$ 3.4-fold and 4  $\mu$ M ATO  $\sim$ 6.2-fold compared to untreated controls (Fig. 35).

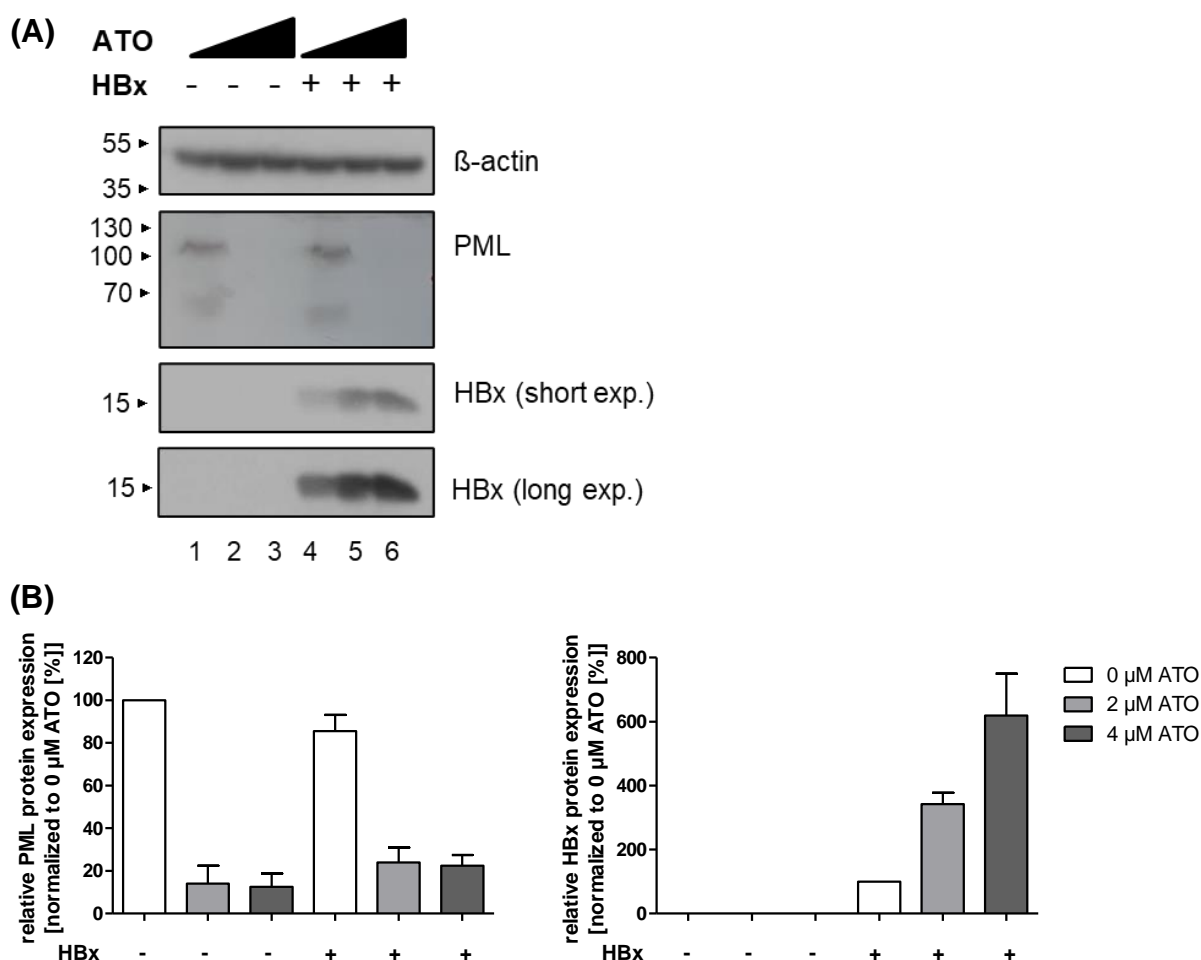


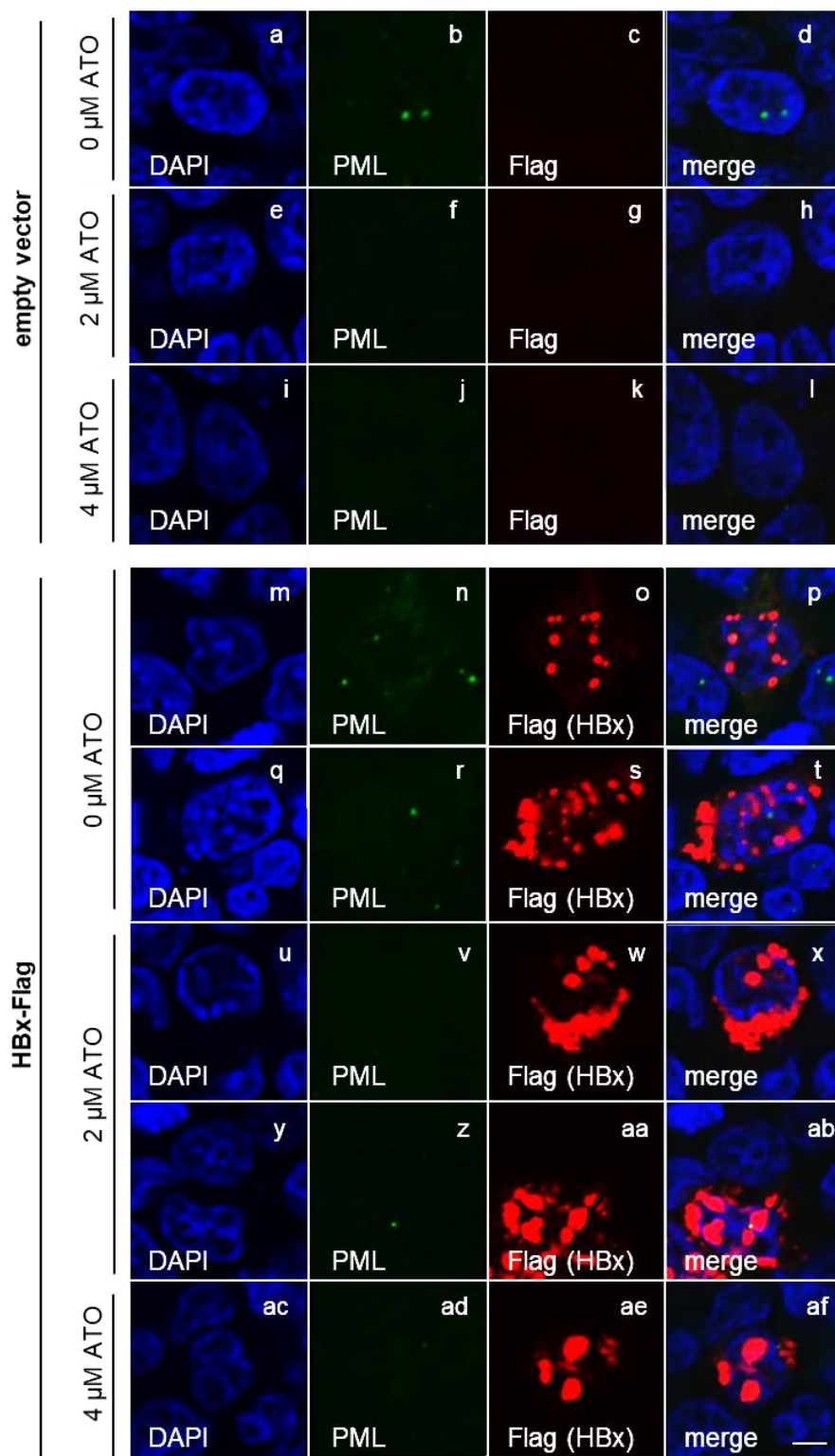
**Figure 35: ATO administration increases transfected HBx protein levels dose-dependently.** (A) HepG2-NTCP-K7 cells were transfected with pCMX3b-Flag HBx-V5, subsequently treated with the indicated concentration of ATO and harvested 48 h.p.t.. Protein lysates were implemented, separated by SDS-PAGE, subjected to western blot and immunodetection using antibodies for PML, HBx and  $\beta$ -actin as loading control. ►

◀ Stained proteins are depicted on the right, appendant molecular weights are indicated in kDa on the left, respectively. (B) Corresponding PML and HBx protein expression levels were quantified by densitometric analysis of the detected bands via *ImageJ*. Protein expression levels were quantified to the loading control  $\beta$ -actin and normalized to the untreated controls. Depicted bar charts represent the average protein expression values including standard deviations (n=2).

### 3.7.1.3. Accumulation of nuclear HBx during ATO administration

To further validate our previous findings, immunofluorescence stainings were performed to determine the HBx phenotype in the presence of ATO. Cells were transfected with pCMX3b-Flag HBx, treated with 2  $\mu$ M and 4  $\mu$ M ATO, fixed with 4% PFA 48 h.p.t. and stained for PML (green, 488 nm), Flag (HBx, red, 647 nm) and DAPI (nucleus, blue, 405 nm). Endogenous PML was stained as ATO control. HBx was detected in the nucleus and in the cytoplasm (Fig. 36, panel p, t), as already observed during previous experiments. ATO administration induced a gradual increase in nuclear HBx staining (panel x, ab, af). To confirm this impact of ATO, the diameter of nuclear HBx dots were calculated (Fig. 36 B). In detail, the size of nuclear HBx dots was significantly as well as dose-dependently increased by ATO application.

(A)



(B)

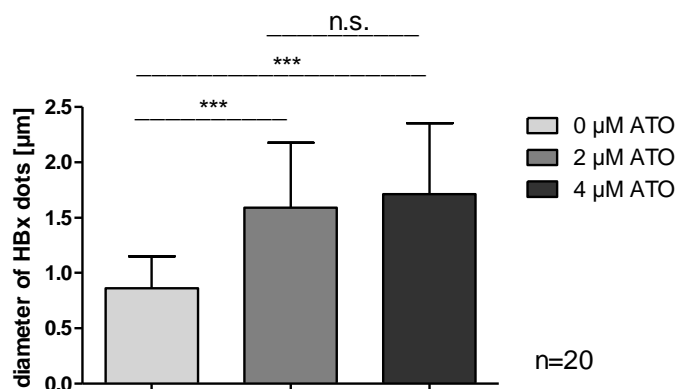


**Figure 36: ATO administration promotes nuclear enrichment of HBx during immunofluorescence staining.** (A) HepG2-NTCP-K7 cells were transfected with pCMX3b-Flag HBx, subsequently treated with the indicated concentration of ATO and fixed 48 h.p.t. with 4% PFA. Cells were stained with Flag (HBx) and PML primary antibodies, detected by conjugated secondary antibodies Alexa488 (PML, green) and Alexa647 (Flag (HBx), red). Nuclei were labeled with DAPI. Scale bar indicating 3 μm. (B) Diameter of HBx dots were quantified via *VoLOCITY*. Depicted bar charts represent the average nuclear HBx diameter including standard deviations. Statistically significant differences were determined using Welch-corrected Student's t-test. \*:  $p \leq 0.05$ , \*\*:  $p \leq 0.01$ , \*\*\*:  $p \leq 0.001$ , \*\*\*\*:  $p \leq 0.0001$ .

#### 3.7.1.4. ATO treatment induces dose-dependent reduction of transfected core

Besides the HBx protein, also transfected HBV core was analyzed, since the HBx protein cannot be used for future experiments as a viral marker, as the HBx detection during HBV infections is currently unfeasible. Therefore, cells were transfected with pcDNA3-HA core, subsequently treated with the indicated concentration of ATO. Cells were harvested 48 h.p.t., whole-cell lysates, SDS-PAGE, western blotting and immunoblotting for HA (core), PML and  $\beta$ -actin were performed (Fig. 37 A). ATO administration successfully degraded PML and also induced a dose-dependent diminution of transfected core levels. These findings were additionally quantified via *ImageJ*, revealing 4 μM induced diminution levels down to 17% in comparison to the untreated control (Fig. 37 B).

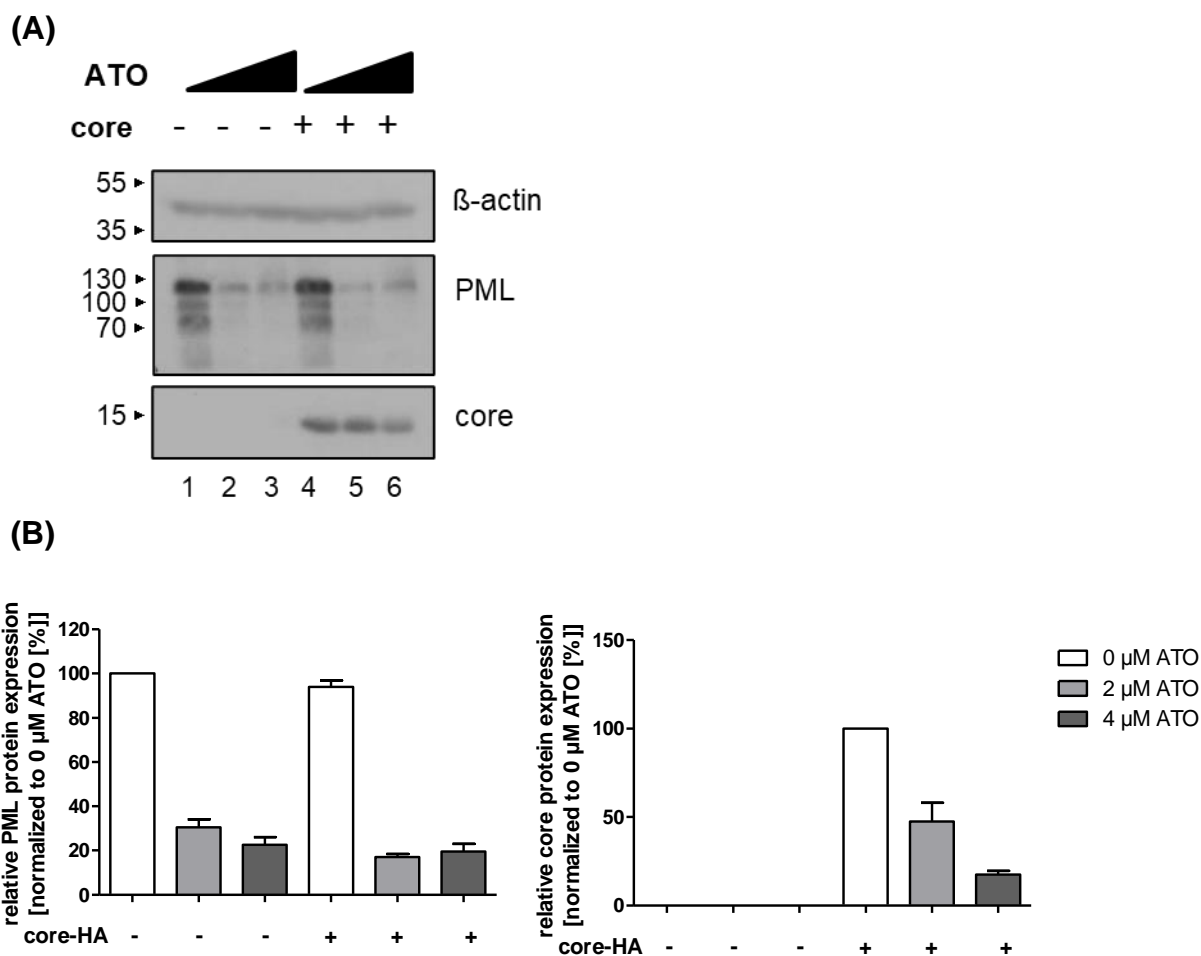


**Figure 37: Dose-dependent decrease of transfected core protein expression levels during ATO administration.** (A) HepG2-NTCP-K7 cells were transfected with pcDNA3-HA core, subsequently treated with the indicated concentration of ATO and harvested 48 h.p.t.. Protein lysates were implemented, separated by SDS-PAGE, subjected to western blot and immunodetection using antibodies for HA (core), PML and  $\beta$ -actin as loading control. Stained proteins are depicted on the right, appendant molecular weights are indicated in kDa on the left, respectively. (B) Corresponding PML and HA (core) protein expression levels were quantified by densitometric analysis of the detected bands via *ImageJ* ( $n=2$ ). Protein expression levels were quantified to the loading control  $\beta$ -actin and normalized to the untreated controls. Depicted bar charts represent these values including standard deviations.

### 3.7.1.5. Re-localization of core during ATO application

To visualize the ATO induced PML and core reduction, immunofluorescence stainings were executed. After pcDNA3-HA core was transfected, treated with ATO and fixed with 4% PFA, cells were stained with PML (green, 488 nm), HA (core, red, 647 nm) and DAPI (nucleus, blue, 405 nm) (Fig. 38). Endogenous PML was completely degraded by ATO treatment. Untreated core was dot-like localized within the nucleus (panel p), whereas ATO administration led to reduced and diffuse nuclear re-localization of core (panel t, x).

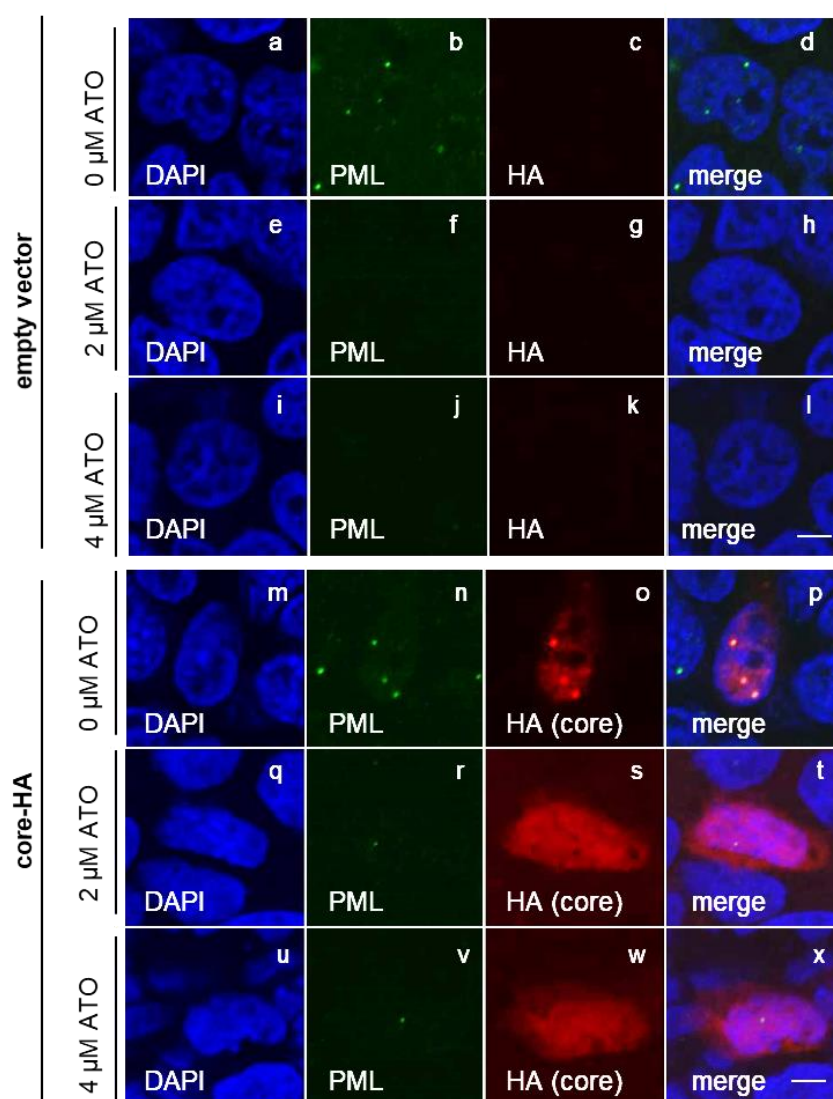
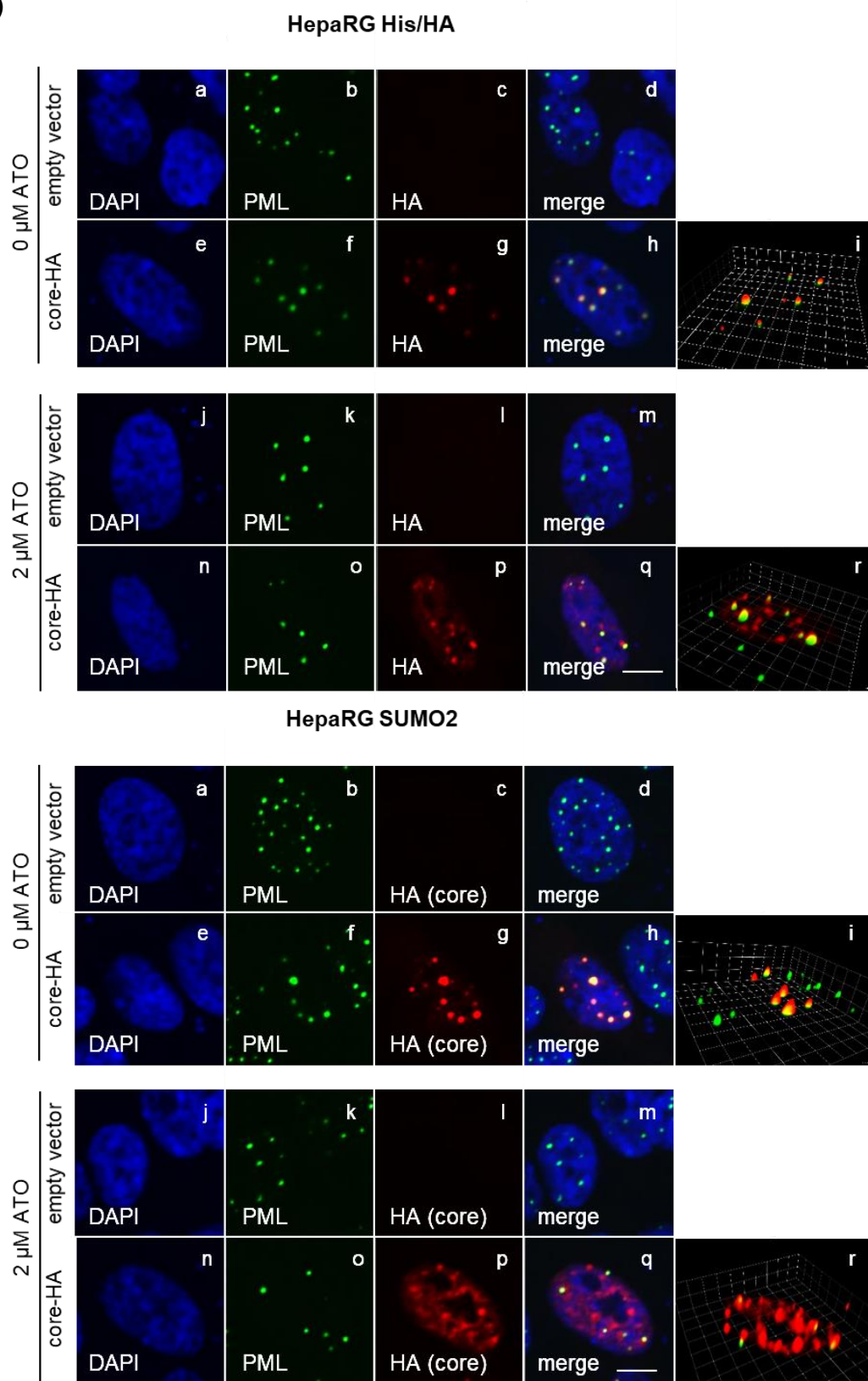


**Figure 38: ATO administration induced re-localization of core dots/expression from PML-NBs.** HepG2-NTCP-K7 cells were transfected with pcDNA3-HA core, subsequently treated with the indicated concentration of ATO and fixed 48 h.p.t. with 4% PFA. Cells were stained with HA (core) and PML primary antibodies detected by conjugated secondary antibodies Alexa488 (PML, green) and Alexa647 (HA (core), red). Nuclei were labeled with DAPI. Scale bar indicating 3  $\mu$ m.

### 3.7.1.6. Efficient core reduction by ATO in SUMO2 overexpressing cells

To amplify our previous data concerning the impact of SUMO on ATO, HepaRG His/HA and HepaRG SUMO2-His/HA cells were analyzed. As previously postulated by our group, the core protein was found to be also modified by SUMO2 proteins (data not shown here). Cells were transfected with pcDNA3-HA core, treated with 2  $\mu$ M ATO and fixed 48 h.p.t.. Immunofluorescence staining was performed utilizing PML (green, 488 nm), HA (core, red, 647) and DAPI (nucleus, blue 405 nm) (Fig. 39). Representative pictures were taken and additional 3D Z-stack images were generated. The number of PML-NBs within (un)treated and (un)transfected cells as well as the PC coefficient were calculated. PML-NBs served as a treatment control. Interestingly, untreated HepaRG His/HA disclosed significantly more PML-NBs within the nucleus than SUMO2 overexpressing cells, whereas this effect was vanished in core transfected cells. Moreover, the number of PML-NBs was found to be significantly reduced in the presence of core. Besides this, PML could be shown again to be reduced during ATO administration. Core co-localized was detectable in both untreated cell lines with PML-NBs (Fig. 39 panel h, i), whereupon this co-localization was significantly lost during ATO treatment (HepaRG His/HA cells PC=0.4, HepaRG SUMO2-His/HA cell PC=0.3) (panel q, r). ATO administration finally induced core re-localization from PML-NBs to a diffuse nuclear staining.

(A)



(B)

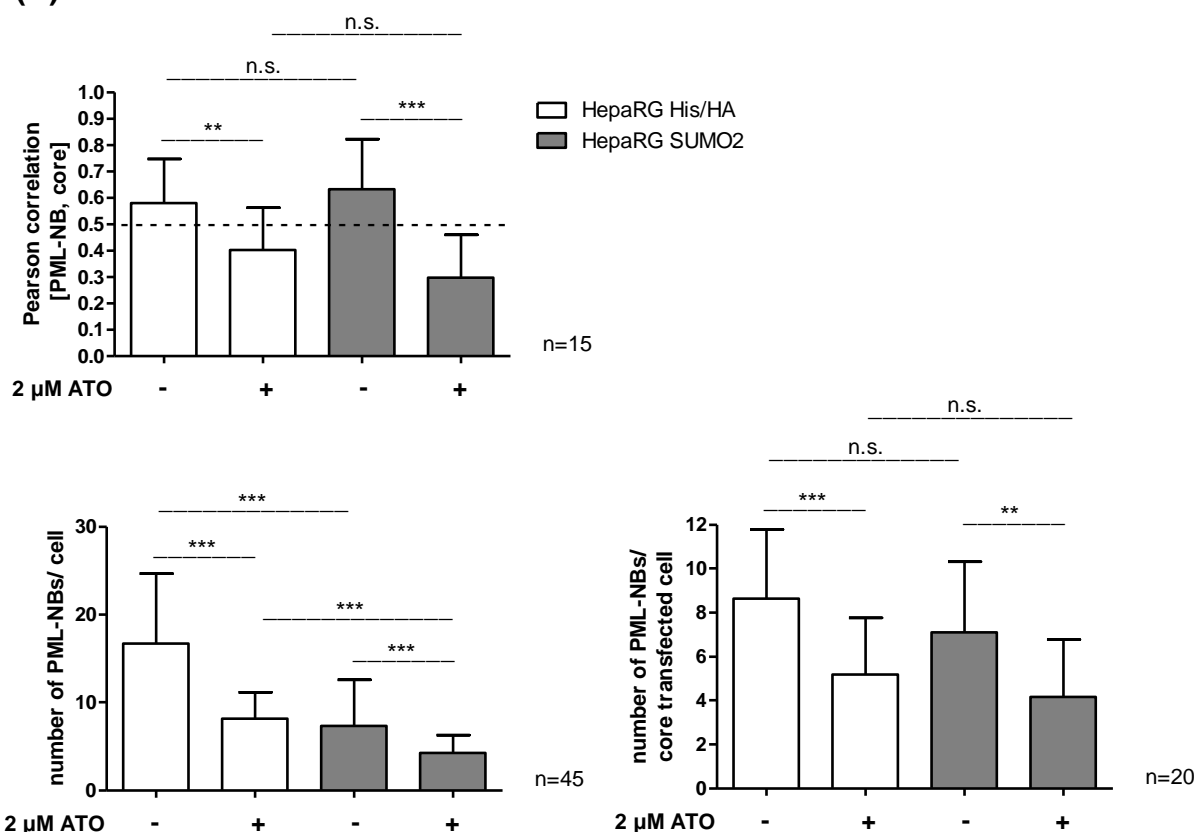


**Figure 39: ATO treatment terminates the SUMO dependent co-localization of transfected core and endogenous PML-NBs.** (A) HepaRG His/HA and HepaRG SUMO2-His/HA cells were transfected with pcDNA3-HA core and subsequently treated with 2 μM ATO. Cells were fixed 48 h.p.t. with 4% PFA and stained with HA (core) and PML primary antibodies detected by conjugated secondary antibodies Alexa488 (PML, green) and Alexa647 (HA (core), red). Nuclei were labeled with DAPI. Scale bar indicating 7 μm. Representative pictures as well as 3D Z-stack images are depicted. (B) Pearson correlation coefficients (PC) and diameters of dots were quantified via *Volocity*. Depicted bar charts represent the average these values including standard deviations. Statistically significant differences were determined using Welch-corrected Student's t-test. \*:  $p \leq 0.05$ , \*\*:  $p \leq 0.01$ , \*\*\*:  $p \leq 0.001$ , \*\*\*\*:  $p \leq 0.0001$ .

### 3.7.2. ATO counteracts acute HBV infections

#### 3.7.2.1. ATO efficiently inhibits HBV core expression

Since our prior experiments revealed varying impact of ATO on single HBV proteins, we were highly interested in the effect of ATO treatment towards HBV infections. To address this question, differentiated cells were infected with HBV, subsequently treated with ATO and HBV core fluorescence intensity were measured 4 d.p.i. and 7 d.p.i.. Core levels were reduced to less than 50% when treated with 4  $\mu\text{M}$  ATO compared to untreated controls. Resulting in a half maximal inhibitory concentration ( $\text{IC}_{50}$ ) of 4.64  $\mu\text{M}$ . HBV core expression levels 7 d.p.i. declined to ~30% when treated with 4  $\mu\text{M}$  ATO compared to untreated controls, corresponding to  $\text{IC}_{50}$ =2.88  $\mu\text{M}$  (Fig. 40).

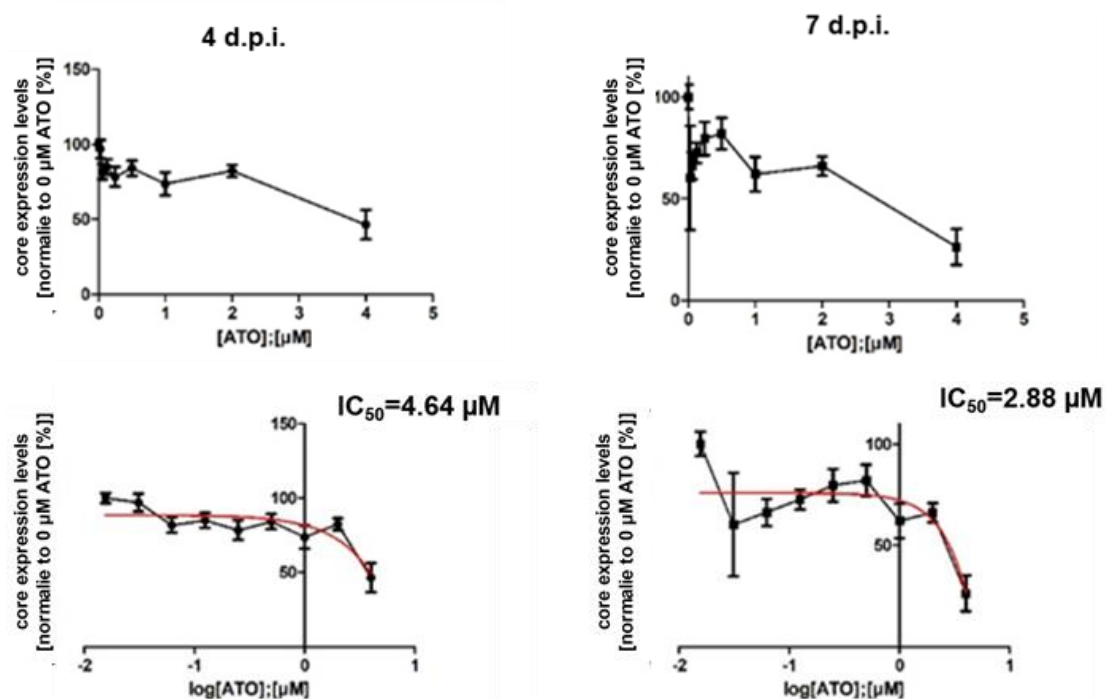
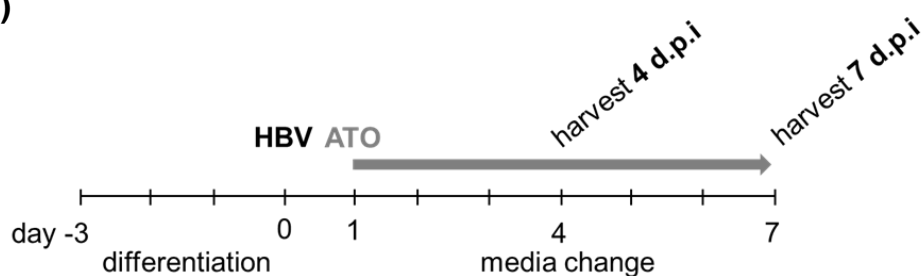


**Figure 40: Determination of ATO  $\text{IC}_{50}$  values.** Differentiated HepG2-NTCP-K7 cells were infected with HBV (MOI 200) treated with the indicated concentration of ATO for 4 and 7 days. Cells were fixed with 4 % PFA, stained with core primary antibody and conjugated to the secondary antibody Alexa488. HBV core fluorescence intensity was measured by a Tecan Infinite 200M plate reader and normalized to untreated, infected cells. Half maximal inhibitory concentrations ( $\text{IC}_{50}$ ) values were determined by a logarithmic data representation.

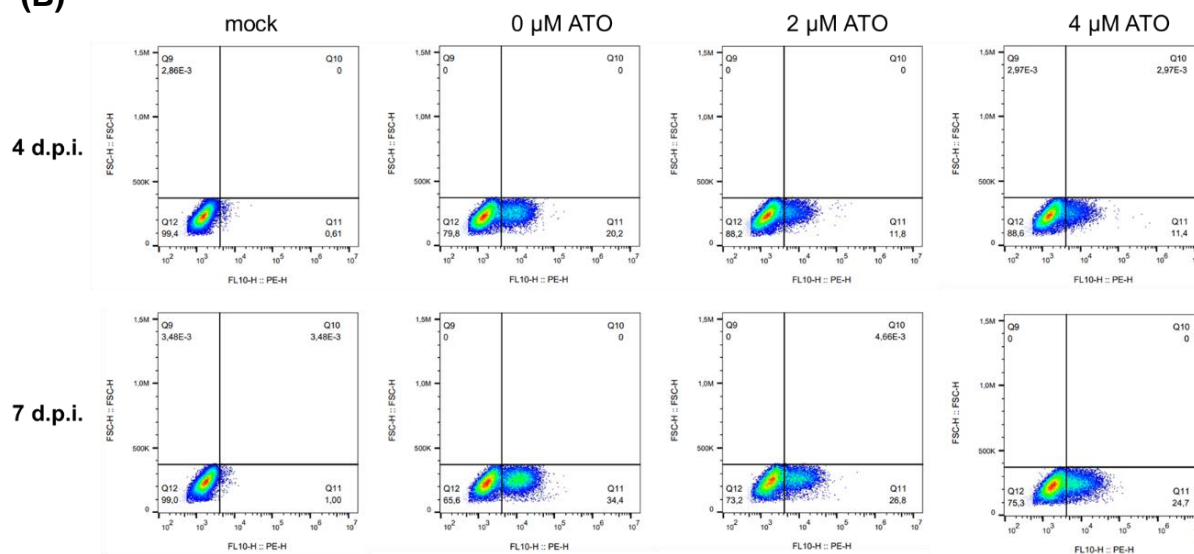
### 3.7.2.2. ATO administration induces diminution of HBV core<sup>+</sup> cells and mean fluorescence intensity

To confirm our first observations, we repeated the experiment and analyzed the impact of ATO on core expression by flow cytometry. Therefore, HepG2-NTCP-K7 cells were differentiated, infected with HBV and treated with ATO the next day. Cells were fixed 4 d.p.i. and 7 d.p.i. and stained with core for flow cytometry analysis (Fig. 41 A, B). The number of core positive (+) cells and the mean fluorescence intensities of core<sup>+</sup> cells were analyzed by *FlowJo*. Core<sup>+</sup> frequency was significantly reduced after 2  $\mu$ M and 4  $\mu$ M ATO administration 4 d.p.i, compared to untreated controls. 7 d.p.i. ATO also induced decreased numbers of core cells, even though this effect was not significant. The mean fluorescent intensity of core expressing cells was significantly reduced after ATO application 4 d.p.i. and 7 d.p.i. (Fig. 41 C). Taken together, our experiments showed for the first time an ATO dependent reduction of HBV core protein during HBV infection.

(A)



(B)



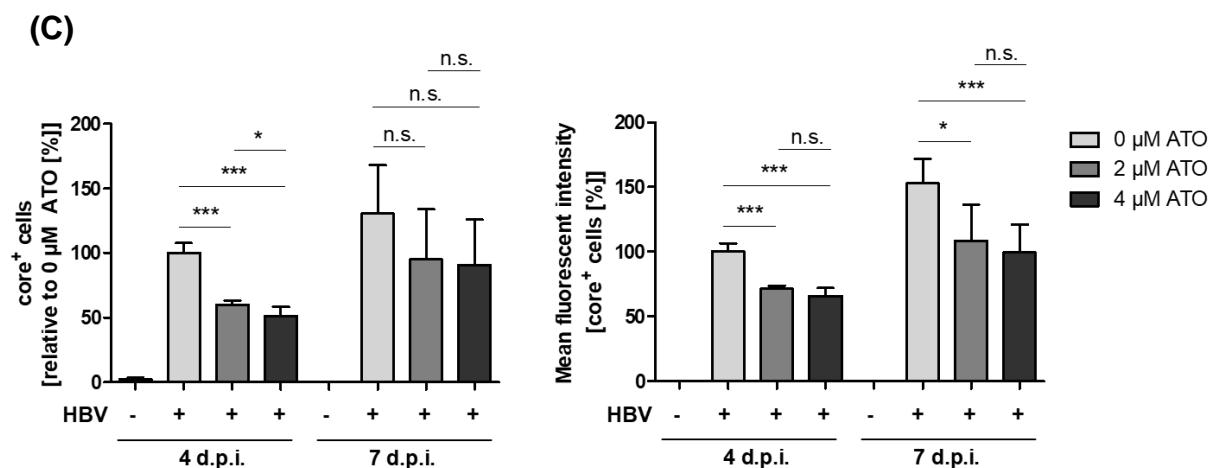


**Figure 41: ATO application reduces HBV core<sup>+</sup> cells and mean fluorescence intensity.** Differentiated HepG2-NTCP-K7 cells were infected with HBV (MOI 200), subsequently treated with the indicated concentrations of ATO and analyzed 4 d.p.i. and 7 d.p.i.. (A) Schematic representation of the implemented experimental setup. (B) Cells were fixed, stained with rAb core primary antibody and PE F(ab')<sub>2</sub> IgG followed by flow cytometry analysis as represented in dot plot graphs. (C) Quantification of core positive cells was calculated by *FlowJo* relative to untreated, infected cells. (D) Mean fluorescent intensity of core<sup>+</sup> cells were calculated relative to untreated, HBV infected cells. Bar charts represent the quantified values including standard deviations. Statistically significant differences were determined using Welch-corrected Student's t-test. \*:  $p \leq 0.05$ , \*\*:  $p \leq 0.01$ , \*\*\*:  $p \leq 0.001$ , \*\*\*\*:  $p \leq 0.0001$  ( $n=6$ ).

### 3.7.2.3. Decreased core protein expression levels during ATO administration

To further validate our findings on HBV core reduction by ATO, cells were differentiated, HBV infected, and treated with the indicated concentration of ATO. Followed by SDS-PAGE, western blot analysis and immunoblotting for HBV core, PML, and  $\beta$ -actin. In addition, protein expression levels were quantified relatively to  $\beta$ -actin. PML reduction during ATO administration confirmed a successful treatment. Consistent with our previous results, core protein expression levels were dose-dependently reduced 4 d.p.i. as well as 7 d.p.i. by ATO (Fig. 42).

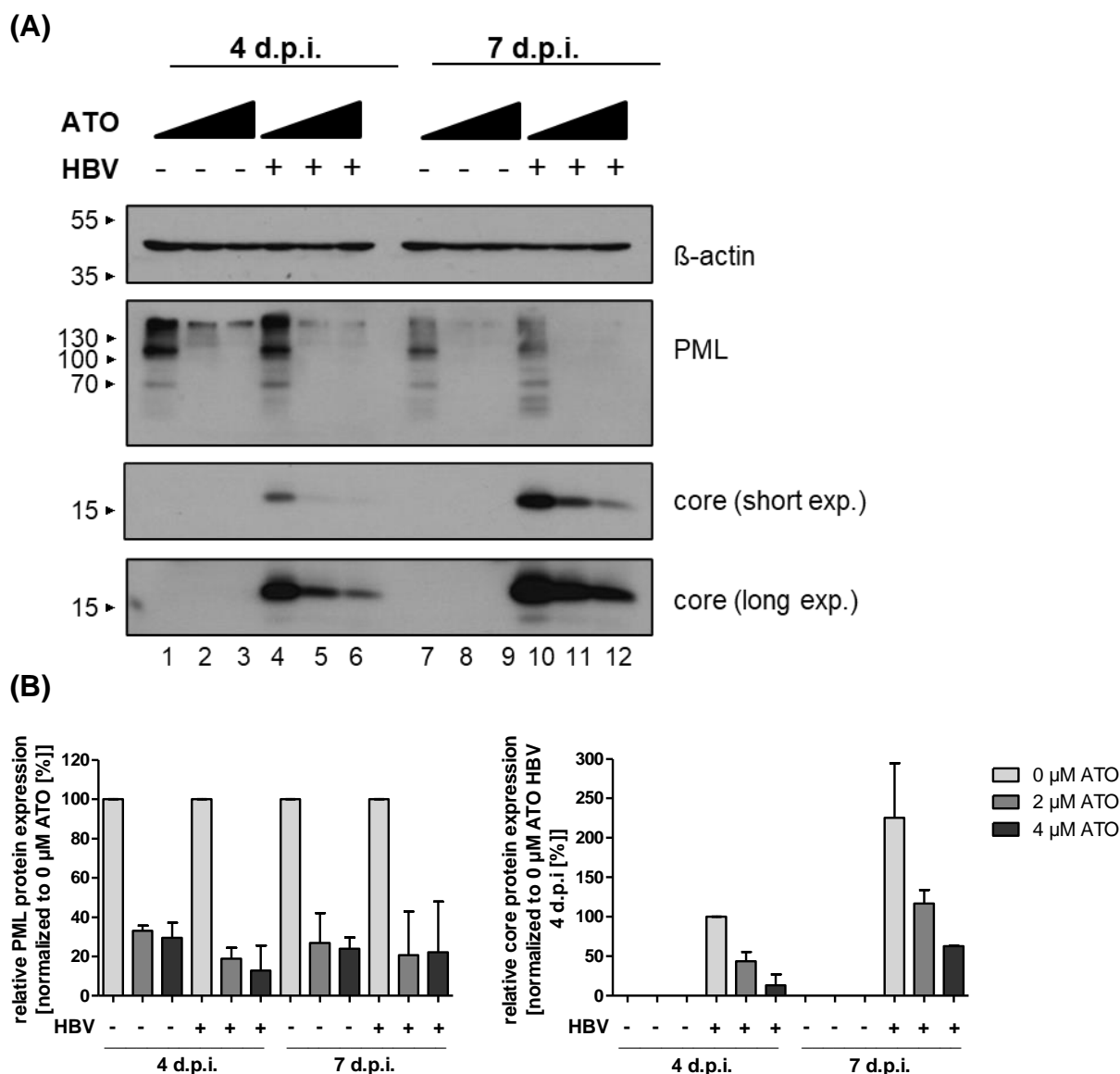


**Figure 42: Decreased core protein levels during ATO treatment early and late after HBV infection.** (A) HepG2-NTCP-K7 cells were infected with HBV (MOI 200) harvested, subsequently treated with the indicated concentration of ATO and harvested 4 d.p.i and 7 d.p.i. Protein lysates were implemented, separated by SDS-PAGE, subjected to western blot and immunodetection for core, PML, and  $\beta$ -actin. Stained proteins are depicted on the right-hand side, appendant molecular weights are indicated in kDa on the left-hand side, respectively. (B) Corresponding PML and core protein expression levels were quantified by densitometric analysis of the detected bands via *ImageJ*. Protein expression levels were normalized to the loading control  $\beta$ -actin (n=2). Depicted bar charts represent the average protein expression values including standard deviations. Statistically significant differences were determined using Welch-corrected Student's t-test. \*:  $p \leq 0.05$ , \*\*:  $p \leq 0.01$ , \*\*\*:  $p \leq 0.001$ , \*\*\*\*:  $p \leq 0.0001$ .

### 3.7.2.4. Nuclear HBV core vanished during ATO application

These data could be confirmed by co-immunofluorescence stainings of HBV core and endogenous PML. Cells were infected and treated like indicated in Figure 41 A, fixed with 4% PFA 4 d.p.i. as well as 7 d.p.i. and stained for PML (green, 488 nm), HBV core (red, 648 nm) and DAPI (nucleus, blue, 405 nm). ATO treatment was again verified by the reduction of PML-NBs. Untreated HBV core was found to localize diffusely in the nucleus early as well as late (panel h) after infection, whereas 2  $\mu$ M and 4  $\mu$ M ATO administration strongly diminished the core staining (panel p, x). Interestingly, 7 d.p.i. HBV core was even found to accumulate in cytoplasmic dots when treated with 4  $\mu$ M (Fig. 43 B, panels u-x). Taken these findings together, ATO application induced HBV core diminution, nuclear re-localization as well as accumulation in the cytoplasm.

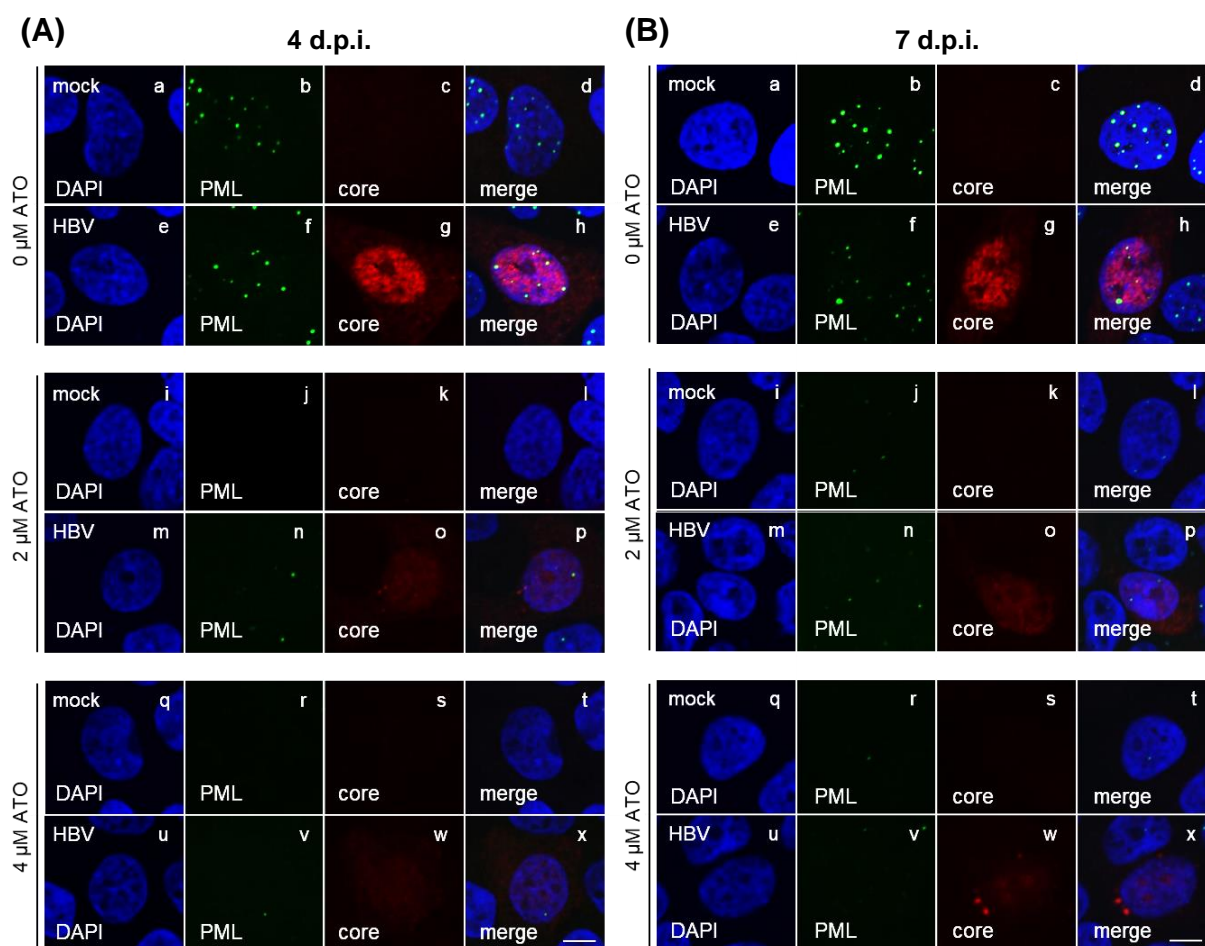


**Figure 43: Core protein staining vanished during ATO treatment early and late after HBV infection.** Differentiated HepG2-NTCP-K7 cells were infected with HBV (MOI 200), subsequently treated with the depicted amount of ATO and fixed 4 d.p.i and 7 d.p.i with 4% PFA. ►

◀ Cells were stained with primary antibodies for core and PML detected by conjugated secondary antibodies Alexa488 (PML, green) and Alexa647 (core, red). Nuclei were labeled with DAPI. Scale bar indicating 7  $\mu\text{m}$ .

### **3.7.2.5. Dose-dependent loss of HBV mRNA, DNA, cccDNA and HBeAg levels by ATO early and late after HBV infection**

Since we disclosed ATO to induce diminution of HBV core protein expression, we were inquisitive concerning the impact of ATO upon HBV total transcripts, total DNA as well as cccDNA. For this purpose, differentiated cells were infected with HBV and treated with 2  $\mu\text{M}$  or 4  $\mu\text{M}$  ATO. 4 d.p.i. and 7 d.p.i. total mRNA and DNA was isolated and qPCR analysis was conducted. Early after infection (4 d.p.i.) total HBV transcripts were significantly reduced after ATO treatment, whereas a significant reduction could only be shown for 4  $\mu\text{M}$  ATO 7 d.p.i. (Fig. 44 A). However, ATO administration induced highly significant reductions of HBV independent of the investigated timepoint or treatment concentration (Fig. 44 B). In line with this, the analysis of cccDNA levels 4 d.p.i. demonstrated significantly reduced levels using 4  $\mu\text{M}$  ATO, whereas a moderate diminution could be detected 7 d.p.i. (Fig. 44 C). In addition, cell supernatant was collected 4 d.p.i. and 7 d.p.i for HBeAg measurement (Fig. 44 D). ATO administration induced a significant and dose-dependent reduction of HBeAg levels early as well as late after infection. Based on these data, ATO could be proven to efficiently counteract viral mRNA, DNA levels as well as HBeAg secretion during HBV infections. Taken together, all examined viral parameters could be declined in the presence of ATO, indicating a strong inhibitory effect of Arsenic trioxide concerning HBV.

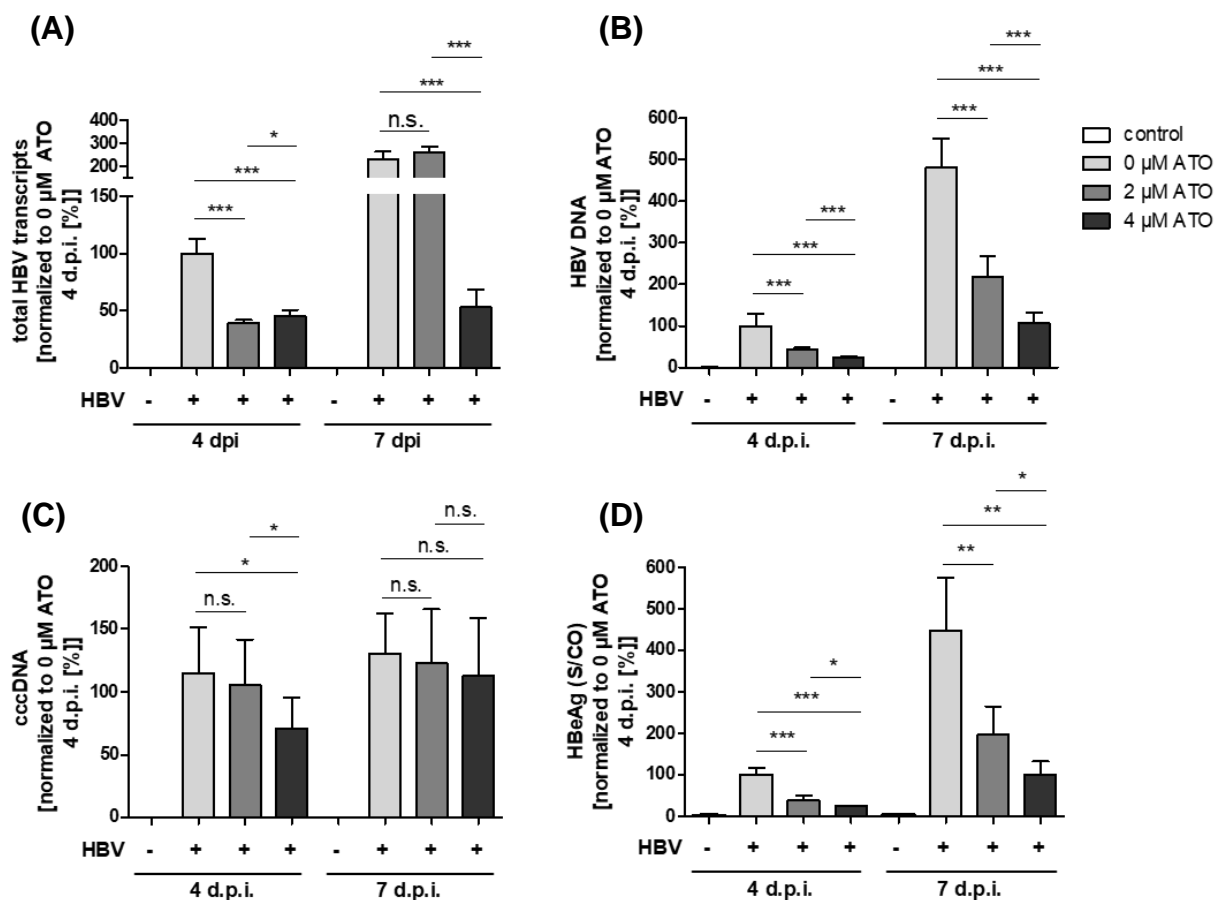


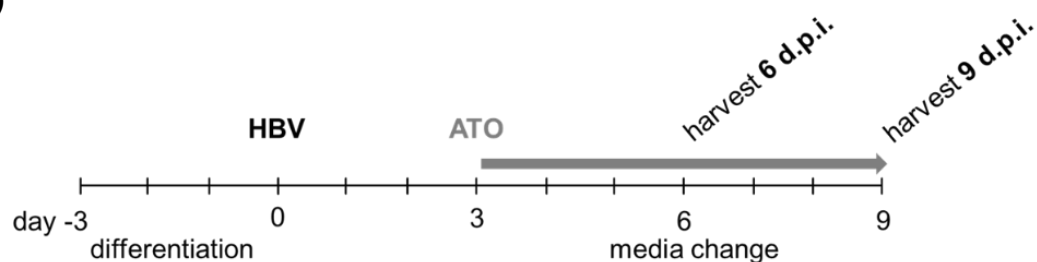
**Figure 44: ATO administration induces dose-dependent loss of HBV parameters early and late after HBV infection.** Differentiated HepG2-NTCP-K7 cells were infected with HBV (MOI 200) and subsequently treated with the indicated concentration of ATO. Total DNA was isolated 4 d.p.i. and 7 d.p.i.. (A) qPCR was implemented utilizing specific primers for HBV DNA, (B) HBV cccDNA, (C) total HBV transcripts and PRP as internal control. All values were quantified relatively to PrP and normalized to untreated, HBV infected control 4 d.p.i.. (D) Cell culture supernatant was collected 4 d.p.i. and 7 d.p.i. and HBeAg measured. Values were normalized to untreated, infected cells. Depicted bar charts represent these values including standard deviations (n=6). Statistically significant differences were determined using Welch-corrected Student's t-test. \*:  $p \leq 0.05$ , \*\*:  $p \leq 0.01$ , \*\*\*:  $p \leq 0.001$ , \*\*\*\*:  $p \leq 0.0001$ .

### 3.7.3. Established HBV infections suppressed during ATO administration

#### 3.7.3.1. Dose-dependent reduction of established core protein by ATO administration

Since the finale goal of ATO treatment would be the eradication of stable cccDNA pool from hepatocytes of chronically infected HBV patients, we analyzed the treatment efficiency towards an established HBV infection during the next experiments. Therefore, HepG2-NTCP-K7 cells were differentiated and infected with HBV (MOI 200). 3 days post infection, cells were treated with 2  $\mu$ M or 4  $\mu$ M ATO and finally analyzed 6 d.p.i. and 9 d.p.i. (Fig. 45 A). Primary, whole-protein lysates, SDS-PAGE, western blot and immunoblotting for HBV core, PML and  $\beta$ -actin was conducted. Protein expression levels were additionally quantified via *Fiji*. As previously mentioned PML degradation served as a successful ATO treatment control. HBV core levels were strongly and dose-dependently decreased by the administration of ATO 6 d.p.i.. This effect was particularly emphasized 9 d.p.i. as 4  $\mu$ M ATO administration induced a 6-fold reduction of core protein levels compared to untreated cells. Based on these data, we received the first indication, that ATO also affects established HBV infections.

(A)



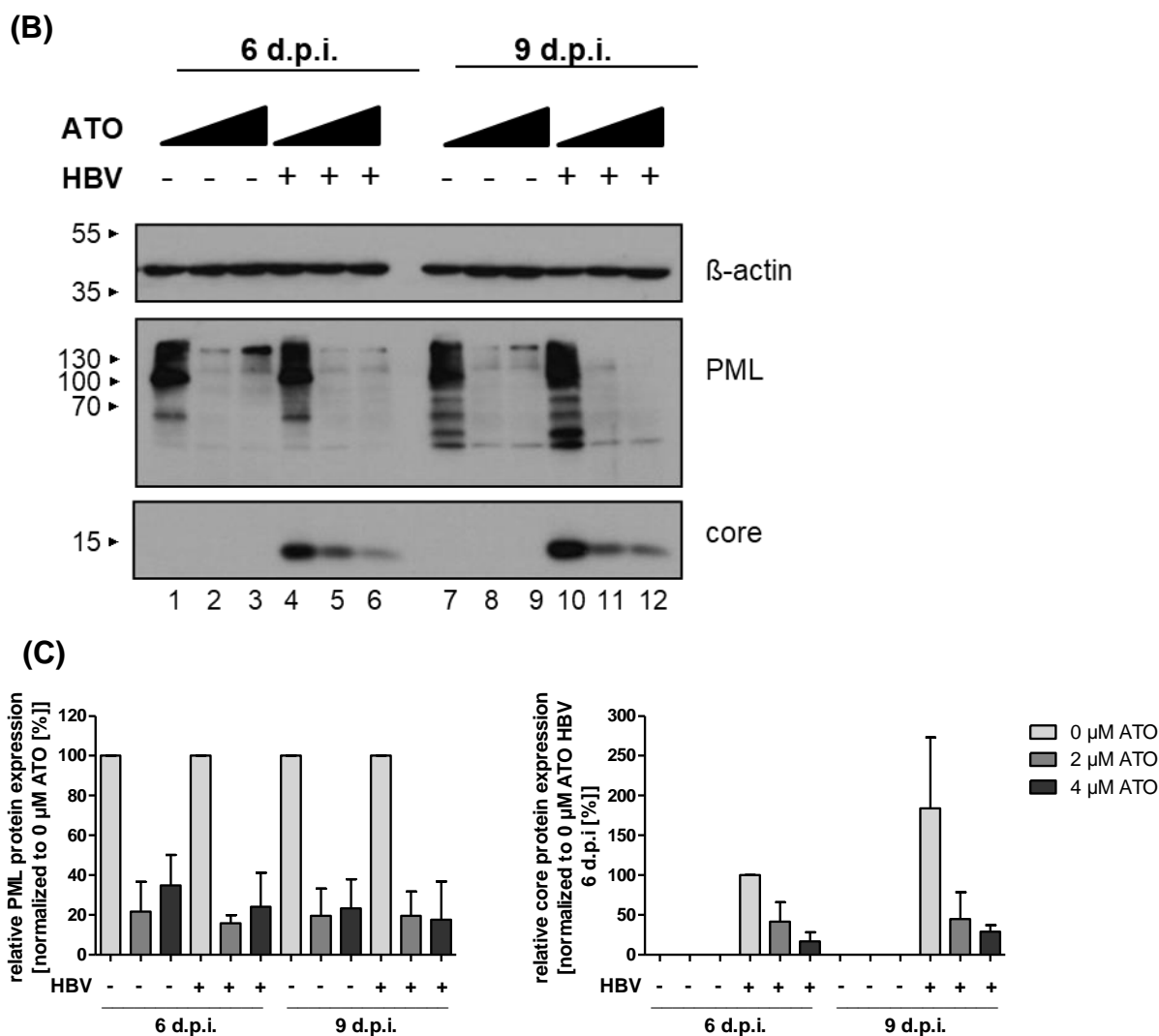


**Figure 45: Efficient diminution of intracellular core protein during established HBV infections.** (A) Schematic representation of the experimental setup. (B) Differentiated HepG2-NTCP-K7 cells were infected with HBV (MOI 200) and treated 3 d.p.i. with the depicted concentration of ATO until harvesting 6 d.p.i. and 9 d.p.i.. Protein lysates were implemented, separated by SDS-PAGE, subjected to western blot and immunodetection for HBV using core, PML and  $\beta$ -actin as loading control. Stained proteins are depicted on the right-hand side, appendant molecular weights are indicated in kDa on the left-hand side, respectively. (C) Corresponding PML and core protein expression levels were quantified by densitometric analysis of the detected bands via *ImageJ*. Protein expression levels were normalized to the loading control  $\beta$ -actin and untreated control. Depicted bar charts represent the average protein expression values including standard ( $n=2$ ).

### 3.7.3.2. Re-localization of HBV core during ATO treatment

To substantiate our prior observations, core protein localization during established HBV infections was analyzed. Cells were handled as indicated (Fig. 45 A) and fixed with 4% PFA 6 and 9 d.p.i. followed by immunofluorescence staining of PML (green, 488 nm), HBV core (red, 647 nm) and DAPI (nucleus, blue, 405 nm). HBV core of established infections was mainly diffusely distributed in the nucleus but also in the cytoplasm of untreated controls (Fig. 46 A, B, panel h). ATO administration induced a severe diminution as well as re-localization of HBV core 6 d.p.i. and 9 d.p.i. compared to untreated controls (panel p, x). Interestingly, core was found to accumulate in the cytoplasm when treated with ATO. Taken together, Arsenic trioxide administration gave first evidence to also negatively altered established HBV infections by affecting the HBV core protein.

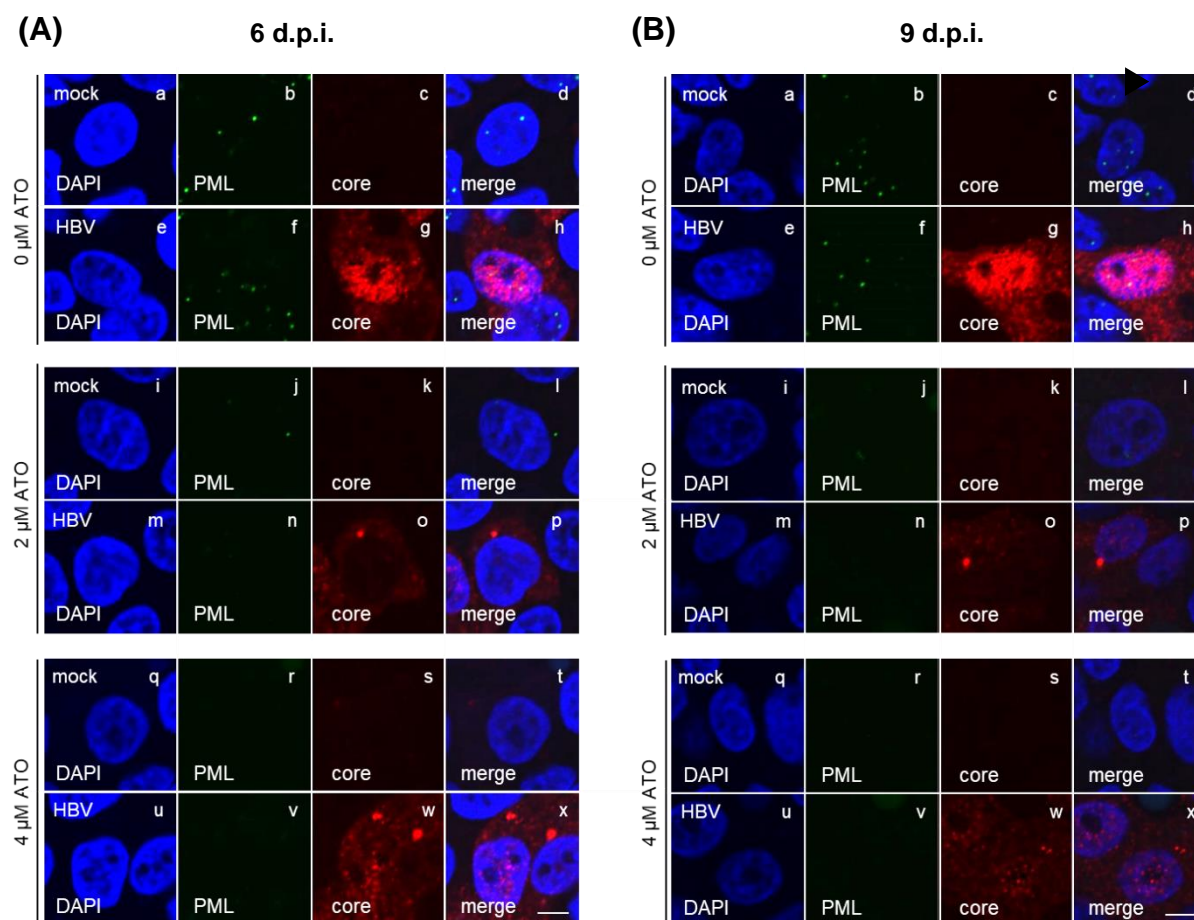


**Figure 46: Intracellular HBV core substantially reduced by ATO administration during established HBV infection.** Differentiated HepG2-NTCP-K7 cells were infected with HBV (MOI 200) and treated 3 d.p.i. with the indicated concentration of ATO until cell were fixed with 4% PFA 3 d.p.i. treatment and 6 d.p.i.. ►

◀ Cells were stained with primary antibodies core and PML conjugated by secondary antibodies Alexa488 (PML, green) and Alexa647 (core, red). Nuclei were labeled with DAPI. Representative pictures as well as 3D Z-stack images are depicted. Scale bar indicating 7  $\mu$ m.

### **3.7.3.3. ATO induced reduction of HBV mRNA, DNA, cccDNA and HBeAg secretion**

To finally investigate the ATO mediated inhibition of established HBV infections, qPCR analysis was conducted for total HBV transcripts, DNA as well as cccDNA. Differentiated cells were infected and treated with ATO prior to mRNA and DNA isolation 6 d.p.i. and 9 d.p.i.. Total HBV transcripts (Fig. 47 A) were efficiently decreased by ATO. This effect was especially pronounced 6 d.p.i. but could also be determined using 4  $\mu$ M ATO 9 d.p.i. revealing a significant diminution of HBV transcripts. Additionally, quantification of total HBV DNA and cccDNA levels exhibited dose-dependently decreased levels in the presence of both ATO dosages independent of the depicted time point (Fig. 47 B, C). In addition, also the HBeAg secretion of established HBV infections during ATO application was disclose (Fig. 47 D). HBeAg levels were measured and quantified relatively to untreated controls. Secreted HBeAg was significantly concentration-dependently reduced by ATO administration 6 d.p.i. findings, concluding a strong impact of ATO towards acute as well as established HBV infections. Taken all these results together, ATO was identified as novel treatment compound efficiently reducing HBV core protein, HBV transcripts, DNA and cccDNA levels as well as HBeAg secretion.

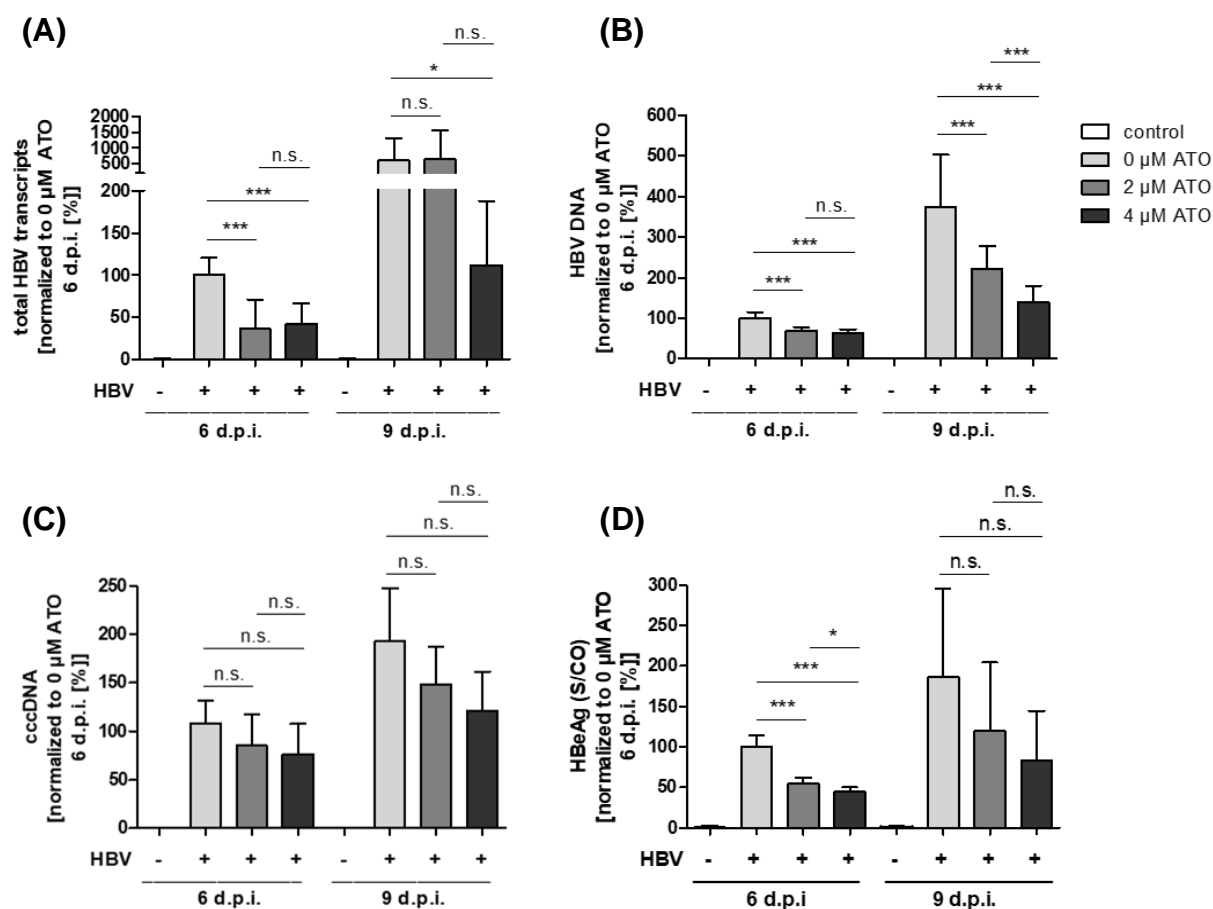


**Figure 47: Administration of ATO stimulated dose-dependent loss of HBV parameters during established HBV infections.** Differentiated HepG2-NTCP-K7 cells were infected with HBV (MOI 200) and treated 3 d.p.i. with the indicated concentration of ATO until total DNA was isolated 6 d.p.i. as well as 9 d.p.i.. (A) Quantification of (A) HBV DNA, (B) HBV cccDNA, (C) total HBV transcripts and PRP as internal control was performed by qPCR analysis utilizing specific primers. All values were quantified relatively to PrP and normalized to untreated, HBV infected control 6 d.p.i.. (D) Cell culture supernatant was collected 6 d.p.i. and 9 d.p.i. and HBeAg was measured. Depicted bar charts represent these values including standard deviations (n=6). Statistically significant differences were determined using Welch-corrected Student's t-test. \*:  $p \leq 0.05$ , \*\*:  $p \leq 0.01$ , \*\*\*:  $p \leq 0.001$ , \*\*\*\*:  $p \leq 0.0001$ .

## 4. Discussion

The generation of effective drugs against HBV remains problematic, due to a lack of knowledge in the HBV infection cycle. Since the cccDNA functions as a highly stable viral persistence reservoir and is mandatory for HBV transcription as replication template, eradication of HBV cccDNA is considered to be the holy grail for a curative treatment [478]. The inability to form new viral particles or undergo genomic recycling can thus result in the eradication of HBV [2, 133, 134]. Nevertheless, all current therapeutic approaches fail to efficiently target HBV cccDNA [41, 157, 265, 267, 268, 276, 277]. Interestingly, Chung *et al.* revealed PML-NBs to be linked to HBV replication [143]. Since PML-NBs are multifunctional complexes, these structures harbor a major number of various proteins such as DNA damage response factors, which are implicated in the regulation of cccDNA formation [143, 308, 469, 479, 480]. PML-NBs are highly dynamic molecular hubs, whereas the recruitment of PML-NB components mainly depends on SUMOylation [300, 302, 304, 305]. As the viral HBx protein is recruited to the cccDNA, inducing its opening and transcription, we were interested in the interplay between PML-NBs, HBx and SUMO as possible treatment targets for chronic HBV [2, 69].

### 4.1. *In silico* prediction and examination of HBx SUMO consensus motifs

Since various viral proteins are known to be SUMO modified *in silico* analysis for HBx SUMOylation was performed [411, 481]. Here, six potential SCMs of HBx were predicted with similar probability scores, whereas SCM5 was more SUMO modified (Fig. 9). Structural analysis of all predicted SCMs confirmed the accessibility for a putative SUMO binding to the indicated HBx sites. Interestingly, HBx SCM1 and SCM2 are located in the DDB1 binding region of HBx, whereas the remaining SCMs reside in the p53 binding region [166, 168, 176, 200, 207, 208, 211-215].

The interaction between HBx and DDB1 was published to induce active gene expression from the HBV cccDNA, by ubiquitinylation and subsequent degradation of

the inhibitor Smc5/6 complex in human hepatocytes and humanized mice [1, 177]. Nevertheless, this interaction is required but not mandatory for HBV replication, as DDB1 is also able to stimulate HBV transcription independent of HBx [207, 482]. The tumor suppressor protein p53 binding region within HBx is known to induce direct interaction between both proteins, resulting in HBx degradation [483]. In return, HBx is able to inhibit p53 functions as the transcriptional activation, DNA binding or apoptosis which might contribute to the molecular pathogenesis of hepatocellular carcinogenesis [166, 167, 484, 485].

#### **4.2. Generation of expression plasmids encoding SUMOylation deficient HBx- variants**

To investigate the HBx wt protein as well as the predicted SCMs, several constructs were generated and characterized. In a first attempt, HBx wt was cloned in various vectors containing different tags, followed by the generation of HBx SCM mutants. Staining of HBx and all appropriate tags could be conducted, however HBx was observed to run slightly higher during SDS-PAGE with tags than compared to untagged HBx (Fig. 10 A). pCMX3b-Flag HBx-V5 could be shown to express the highest amount of HBx, in addition two bands were found to migrate either at a higher or at a lower molecular weight. The lower band presumably represented a splice or degradation product. However, the upcoming band at ~25 kDa might be dimerization or a post-translationally modified version of HBx. Dimerization of HBx could be excluded, since the expected band would run higher (~34 kDa) and was not detected for the later cloned HBx SCM1/2 mutant, although the dimerization region of HBx (21-50 aa) was not changed [486]. As HBx is known to interact with the ubiquitin proteasome, this mass shift might have arisen from an additional mono-ubiquitin (~8.5 kDa) on HBx [487]. However, the detection of ubiquitinated proteins is rather improbable, since most ubiquitinated proteins are immediately degraded by the proteasome [162, 487-489]. Further PTMs such as methylation (14 Da), acetylation (42 Da), formylation (28 Da) or phosphorylation (95 Da) could be also dismissed due to their sizes [490, 491]. The most likely post-translation modification responsible for this shift, is probably

a SUMO modification, with a size of ~11 kDa, which was already predicted previously [492].

Since HBV is a hepatotropic virus, liver derived cell lines were preferentially used in our experiments, as they support the full viral life cycle [134]. However, plasmid transfection efficiency in HepG2 and HepaRG cells is quite low [493-495]. To evade this problem for certain experiments IVT mRNAs encoding for HBx were generated to achieve higher transfection rates. As expected, HBx IVT mRNA demonstrated considerably increased transfection efficiency, protein expression (Fig. 10 C, D) as well as low cytotoxicity [471]. These advantages over plasmid DNA could be explained by the smaller size, comprising only regulatory elements and the coding sequence, in contrast to plasmid DNA harboring additional elements such as antibiotic resistances, causing potential adverse effects for instance triggering immune responses [495-497]. In addition, IVT mRNA can be already translated within the cytoplasm, whereas nuclear entry is indispensable for plasmid DNA expression [495, 497]. Besides differences in HBx protein expression, also the intracellular localization between HBx derived from plasmid DNA and IVT mRNA transfection varied. IVT mRNA transfected HBx was found to localize exclusively in nuclear dot-like in patterns, whereas plasmid DNA transfected HBx was distributed in the nucleus as well as cytoplasm. In general, HBx compartmentalization is known to be associated within the nucleus, cytoplasm, and mitochondria [217, 498]. However, HBx localization was published to be highly dependent on the overall expression level as well as its abundance [217, 498]. Thereby, nuclear localization of HBx is detected during low levels of HBx within the cell, whereas elevated levels correlated with an accumulation of HBx in the cytoplasm and abnormal mitochondrial distribution [217, 498]. These findings led to the suggestion, that the cellular nuclear capacity for HBx might be limited.

### 4.3. Post-translational modification of HBx by SUMO2 moieties

Since SUMOylation represents an essential key regulatory mechanism for eukaryotic cells but also viruses, we investigated the post-translational modification of HBx by SUMO [393, 411, 481, 499]. Our investigations on the interplay between HBx and SUMO revealed nuclear co-localization of HBx with all three SUMO paralogous (Fig. 11). These findings could be confirmed by a NiNTA assay, showing mono- as well as poly-SUMOylation of HBx introduced by the SUMO2 protein (Fig. 12). This SUMO2 modification of HBx could be further proven to either support or induce the proteasomal degradation of HBx via its impact on proteostasis through the regulation of the ubiquitin proteasome system at multiple levels [500]. Since SUMO can be bound to the RING finger ubiquitin ligase like RNF4, SUMOylation was discovered to function as a signal for poly-ubiquitylation inducing proteasomal degradation (Fig. 13) [304, 417, 423, 473].

### 4.4. Interplay between viral HBx proteins and PML

As we identified HBx to be SUMO modified, we were interested to further investigate the interplay between HBx and PML-NBs, which are known to be hotspots for SUMOylation. PML-NBs represent dynamic cellular complexes representing an assembly of PML and PML-NB associated proteins crucial for responses to cellular stress, DNA damage and viral infections [302, 327]. As HBV cccDNA synthesis requires DNA repair factors and is supposed to locate at PML-NBs, the hypothesis arose, that the SUMOylated HBx, essential for viral transcription, is also associated with PML-NBs [2, 69, 84, 135, 144, 145].

Co-immunoprecipitation could confirm a direct interaction between HBx and PML. Immunofluorescence stainings supported this assumption, as co-localization of HBx with endogenous PML-NBs could be visualized (Fig. 14). Moreover, the number of PML-NBs decreased in the presence of transfected HBx, whereas their size enlarged, indicating for a redistribution of PML within the nucleus (Fig. 15). Interestingly, the number of PML-NBs was reduced in Sp100 depleted and SUMO2 overexpressing cells, accompanied with subsequent growth in diameter. Also, the diameters of HBx

dots were affected by PML and Sp100, as they decreased in size in the absence of both proteins. Taken together, these findings supported the already published importance of Sp100 and SUMO2 for PML-NBs, concluding an important role of PML and Sp100 for HBx localization, recruitment and cccDNA de-condensation [302, 305, 344, 441].

With regards to the single PML isoforms, further experiments were conducted to identify the specific PML isoforms for the interplay with the HBx protein. HBx levels were increased by all co-transfected PML isoforms within the soluble cell fraction (Fig. 17, 18). Moreover, HBx and all PML isoforms induced at mutual shift or increase in the insoluble membranous fraction, independent of endogenous PML background. The insoluble nuclear matrix fraction harbors numerous components which participate in several cellular processes, such as DNA replication, DNA repair, cell signaling or carcinogenesis as well as PML-NBs [501-504]. Since, PML-NBs by themselves are matrix associated domains, this finding led to the conclusion, that increased amounts of HBx and PML isoforms were re-located and integrated into PML-NBs [302]. Thereby, the correct localization of PML associated proteins is known to depend on PML, whereas SUMO proteins, account for re-localization and recruitment of proteins to PML-NBs [303, 304, 505].

Furthermore, investigations of single transfected PML isoforms with HBx solely displayed juxtaposed localization, whereas a distinct interaction between HBx and all PML isoforms could be shown (Fig. 16). However, no preferential PML isoform could be determined for HBx functionality or interaction (Fig. 19), concluding either a composition of various PML isoforms to be mandatory for HBx localization at PML-NBs or a PML associated linker protein to be required.

#### 4.5. Crosstalk between viral HBx proteins and PML-NB associated host proteins

As PML-NBs contain many transcriptional and chromatin regulatory factors one major key factor is represented by Sp100 [300, 302-306, 332-336]. This cellular regulator was recently described to affect viral infections like human Papilloma virus, Epstein-Barr virus or Cytomegalovirus infections [506]. Sp100 is spliced into four different isoforms, which were identified to differentially regulate transcriptional processes [300, 302-306, 332-336]. Sp100B, C, and HMG act as transcriptional repressors, whereas Sp100A is the only isoform known to increase chromatin de-condensation and promote transcription [337, 506]. Our investigations revealed a direct interaction of the HBx with Sp100A isoform (Fig. 20). Since HBx is known to induce cccDNA de-condensation for HBV transcription, HBx might cooperate with Sp100A to promote and enhance the viral HBV infection. As HBx was already found to interfere with other endogenous transcription factor, promoting the progression of HCC, a similar mechanism would be supposable for Sp100 A [507].

Another PML-NB associated factor is the RNF4 protein, which is known to induce ubiquitylation and proteasomal degradation of the cellular key organizer PML [423, 427]. As PML-NBs are also essential regulators during viral infection, RNF4 was also found to be a major component during the viral life cycle for example in HAdV [426]. More in detail, RNF4 binds SUMOylated proteins, thereby inducing ubiquitylation and subsequent proteasomal degradation of the SUMO-modified target protein [304, 417, 423]. Since we newly identified the viral HBx protein to be post-translationally modified by SUMO2, we were highly interested in a putative link to RNF4.

Co-transfection of HBx with RNF4 revealed a mutual stabilization as well as re-localization to the insoluble membranous fraction (Fig. 21, 22). The sequestration of RNF4 to the insoluble nuclear matrix fraction was already observed during HAdV infection [426]. Here, the early viral protein together with RNF4 induces PTM and thus proteasomal degradation of a detrimental PML-NB associated endogenous protein, leading to increased viral gene expression and replication [426]. Moreover, the RNF4 protein was described to stabilize a selected group of oncoproteins via phosphorylation [508]. Since HBx represent a viral oncoprotein, this mechanism is presumably

responsible for the HBx stabilization [508-510]. In addition, the HBx protein is known to stabilize proteins, which are beneficial for HBV infections, like transcription factors or centrosome associated proteins [507, 511]. This knowledge supports our hypothesis, that HBx and RNF4 stabilize and recruit each other to the nuclear matrix associated PML-NBs, which were previously found to be mandatory for HBx and HBV infections.

In addition, our data disclosed RNF4 as a novel interaction partner of HBx (Fig. 23). Leading to the idea, that RNF4 targets specific substrates for ubiquitylation followed by proteasomal degradation, which is supported by HBx. HBx here might either function as a E3 ligase, inducing substrate SUMOylation for RNF4 or recruit RNF4 and specific substrate to PML-NBs for proteasomal degradation, supporting HBV transcription and replication. In conclusion, our data indicated that RNF4 represents an important factor for HBV infections.

A further possible linker between HBx and PML-NBs might be the DDB1 protein since it was already published to interact with HBx. Moreover, DDB1 is already known to function as a linker protein, recruiting various proteins to the Cul4-Roc1 (CRL4) complex [512]. Interestingly, certain CRL4s containing specific components, were already identified as PML ubiquitin ligases, supporting the idea of an interplay between PML-NBs and CRL4 [513]. Since DDB1 immunofluorescence stainings were not feasible in our hands, most likely due to a defective antibody, Cul4 was stained as representative of the CRL4 complex [1, 177]. Our investigations revealed co-localization of endogenous PML-NBs with the CRL4 component Cul4 in various cell lines (Fig. 24). Interestingly, no Cul4 dots could be detected in PML depleted cells, concluding PML dependent nuclear localization of Cul4. Consequently, also HBx co-localized to Cul4, which is in line with our previous findings concerning the co-localization of HBx and PML (Fig. 25). HBx decreased the number of Cul4 dots but subsequently elevated their size. In the absence of PML in HepaRG shPML cells, HBx recruited the diffuse distributed Cul4, empathizing their PML-independent interplay. The number and size of Cul4 stainings revealed comparable results as the prior PML-NB staining. Furthermore, endogenous Cul4 dots are altered by the PML-NB components PML, Sp100 and SUMO2, displaying the impact of PML-NBs on Cul4.

This result confirmed the interaction between HBx and the CRL4 complex as well as the associated DDB1 [1, 201, 212, 216, 239-242].

The interplay between PML, HBx and the CRL4 complex could be further demonstrated via the interaction with DDB1 (Fig. 26). In the absence of PML, the interaction between HBx and DDB1 was drastically reduced in comparison to the control cells, supporting the idea of PML-NBs as important spots for functional HBx. Moreover, DDB1 protein levels displayed increased amounts in the control as well as shPML cells in the presence of HBx, whereas the stabilization was stronger in the control cells. This effect could be explained by the fact that HBx and DDB1 are known to exert a mutual stabilization upon binding, empathizing the impact on PML [207, 482, 514-517].

#### **4.6. Identification of the relevant HBx SUMO conjugation motif**

In a next step, the impact of HBx SCM mutations was investigated. At first, comparative structural analysis for all mutants were conducted. SCM1 (aa 91) and SCM2 (aa 95) as well as SCM3 (aa 113) and SCM4 (aa 118) were combined in one construct, as they located in close proximity within the HBx sequence. Structural depictions did not demonstrate major alterations, but only minor changes within the surface prediction for all mutants. Here, the exchange of lysine to arginine should not affect SUMO accessibility, since protein structures are usually very robust towards small sequence variations [518].

Our investigation on the SUMOylation of HBx variants revealed comparable SUMO2 modification for HBx wt, SCM3/4 as well as SCM6 (Fig. 28). In contrast, HBx SCM1/2 (aa 91/95) was significantly less SUMO2 modified, whereas the mutation of SCM5 (aa 130) led to increased SUMOylation. Interestingly, HBx aa 95 was already identified to be responsible for HBx ubiquitinylation [519]. Moreover, Liu *et al.* showed that HBx K91 and K95 affect protein stability, chromatin localization as well as transcriptional regulation, by acting as key sites for NEDDylation [520]. This process represents another highly dynamic PTM of the ubiquitin family involved in the regulation of diverse components of oncogenic and tumor suppressor pathways [521, 522]. Similar to ubiquitin and SUMO, NEDD8 is covalently conjugated to a target lysine residue [523].

SUMO was further discovered to negatively modulate conjugation of NEDD8, which we could not confirm here, as SCM1/2 was stabilized like all HBx variants [524, 525]. In contrast, HBx NEDDylation occurred at the same sites as SUMOylation, indicating a mutual dependency of each other for PTM or a competition for the same lysine site resulting in different functional states for HBx. The elevation of HBx SUMOylation by the mutation of SCM5 can probably be explained by an abrogated interaction or interplay of HBx with an unknown protein. This might result in an increased accessibility for SUMO proteins either facilitating binding of SUMO to another SCM site of HBx or enabling enhanced and prolonged SUMO modification of HBx at multiple other SCM positions.

Interestingly, the HBx variants with altered SUMOylation pattern also disclosed changes in their intracellular localization (Fig. 29, 30). Here the HBx SCM1/2 mutant displayed very low amounts in the nucleus, resulting in no co-localization with PML-NBs or Cul4. Moreover, the endogenous proteins PML and Cul4 were not affected by this HBx mutant, however all other HBx variants induced reduced numbers and increased sizes of both cellular proteins. The hyper-SUMOylated HBx SCM5 even revealed bigger nuclear HBx dots in contrast to all other variants.

The interaction of HBx and DDB1 could be shown to be also SUMO dependent since the mutation of the HBx at SCM1/2 lacks this interaction (Fig. 31). Here, SUMO might either act as a direct linker between both proteins or affect the re-localization of both proteins. These data support the findings from Hodgson *et al.* as they proposed that the HBx double mutant at position 90/91 aa no longer interacts with DDB1 [177, 198, 207, 517, 526]. In contrast, the increased SUMOylation pattern of HBx SCM5 strengthened the interaction with DDB1 compared to wt HBx.

Although, the DDB1-HBx interaction was changed according to its SUMO state, the DDB1-HBx dependent reduction of Smc6 was unaffected by SCM mutation. Smc6 could be shown to be strongly degraded by all HBx variants whereupon PML levels were increased in the presence of HBx in a dose-dependent manner (Fig. 32). Leading to the conclusion, that even extremely low levels of (SUMOylated) HBx, which is representative of HBV infections, are sufficient for Smc5/6 degradation [1, 212, 242, 527-530]. Summarized, we discovered HBx SUMOylation to be important for HBx localization and interaction but not for Smc5/6 degradation, resulting in the question whether there is a DDB1 independent pathway for HBx directed targeting Smc5/6

within the cell. The interaction between DDB1 and HBx was already found to be largely dispensable for the viral DNA replication [207, 482].

Even though, Smc6 was equally reduced by all HBx mutants, differences towards HBV DNA as well as cccDNA levels could be observed. The stable episome-like cccDNA is organized into minichromosomes by chromatin remodelers, histones and non-histones, viral, and cellular proteins, as well as various PTMs like methylation or acetylation [2, 201]. The HBx protein is known to recruit and interact with various of these co-activators (*inter alia* CBP, p300, and PCAF) and transcription factors to epigenetically regulate the viral cccDNA [69, 150, 201, 230, 530, 531]. Our work on the HBx SUMO-reduced mutants displayed significantly reduced levels of HBV DNA and cccDNA for SCM1/2, whereas the hyper-SUMOylated HBx SCM5 was concomitantly accountable for slightly elevated cccDNA levels (Fig. 33). Indicating a HBx SUMOylation dependent transcription of the viral cccDNA for replication.

This hyper-SUMOylated HBx SCM5 mutant (aa 130) was already discovered to be one of the most frequent aa mutations in HBx (at position 5, 38, 94, 130 and 131) found for HCC patients [532]. In general, hyper-SUMOylation of proteins is known to be associated with augmented cell growth and cancer [533, 534]. Moreover, HBx mutations from patients in Europe and Africa revealed a higher incidence of mutation at 130 and 131 aa for mild hepatitis patients and accumulation of HBx in HCC peritumor tissues [159, 535-539]. The clinical double mutation K130M/V131I, even occurs in ~66% of patients with HBV-related HCC and increases the risk in chronic HBV patients for HCC 3.75-fold [532, 540, 541]. This HBx double mutant was also associated with severe liver damage as well as HCC in patients from China and Africa [542]. Moreover, this variant was reported to alter cell proliferation, cell cycle regulatory genes, and intracellular reactive oxygen species production [543]. Nevertheless, this mutant still interacts with the tumor suppressor protein p53 like wt HBx, but it inhibits the p53-mediated gene transcriptions, suggesting this to be the cause for the oncogenic potential of K130M/V131I [544]. Since our generated HBx SCM5 mutant, displayed significantly higher SUMOylated rates as well as cccDNA levels compared to the wt HBx, we conclude a stronger and higher persistent HBV infection with hyper-SUMOylated HBx. Supporting the findings, that mutations of HBx position 130 and 131 in chronic HBV patients are more likely to cause HCC.

Summarized, SUMOylation is known as major regulator of protein functions, which is important for a wide range of cellular processes like nuclear transport, chromosome segregation or transcriptional regulation [353, 355, 360, 382, 393, 545-547]. Here (de)SUMOylation of HBx was likely to regulate HBx functions concerning efficient opening of the cccDNA less SUMOylated HBx elicited significantly less cccDNA and HBV DNA. The altered functionality could be induced directly by SUMO modifications and/or could result from the nuclear re-localization of SUMO deficient mutants from PML-NBs. Both explanations could be supported by the HBx SCM5, which is more strongly SUMO modified as the wt, causing increased PML-NB localization, DDB1 interaction as well as cccDNA levels, probably inducing chronic HBV infections leading to HCC.

#### **4.7. Discovery of ATO as a novel treatment against HBV**

Since we discovered the HBx protein to be associated with PML-NBs, to be SUMO modified and to interact with the RNF4 protein, we were highly interested in the impact of ATO treatment on HBV infections. ATO directly binds to PML proteins, causes hyper-SUMOylation as well as subsequent ubiquitylation via RNF4, followed by proteasomal degradation [310, 428, 429, 439-442]. Leading to reduced PML-NBs numbers within the cell as well as altered composition of the remaining bodies due to de-regulation of the SUMO pool [310, 435, 439-441, 448].

The antiviral activity of ATO was described for the first time in HCV infections, whereby the strong inhibitory effect was proposed to be induced by reactive oxygen species and not by the reductive effect of ATO on PML [548]. Moreover, our group recently discovered ATO as an efficient component against HAdV infections, which are closely connected to PML-NBs [448]. This effect is mainly caused by the ATO-dependent re-localization and disruption of PML-NB as well as by the de-regulation of the intracellular SUMO pool [448]. Furthermore, several studies on the effect of so-called “arsenicals” on HBV and HCC were conducted. Two conflicting studies investigated the impact of increased arsenic exposure in drinking water contaminations, since this affects more than 200 million people worldwide [450, 452, 549]. Zhang *et al.* analyzed the urinary arsenic concentration of inhabitants as a measure for arsenic exposure

[452]. Here, a correlation between elevated arsenic levels with incidence of chronic HBV infection could be found. However, also a connection of urinary arsenic concentration and ethnicity as well as birthplace could be detected [452]. In contrast, the second study on contaminated drinking water by Hsu *et al.* reported increased arsenic intake due to contaminated drinking water reduced the incidence for HCC in HBV patients [450]. Moreover, even the number of inactive HBV carriers declined during the examinations [450]. In summary, it has to be mentioned, that both studies on contaminated drinking water displayed wanting experimental setups, due to the fact, that no specific or constant arsenic exposure could be proven [450, 452]. Furthermore, healthy as well as sick people received arsenic water independent of their health and environmental conditions [450, 452]. A more selected phase II trial of ATO, examined a partial response in an HBV positive patient suffering from HCC [550]. Another study on ATO in HBsAg positive mice indicated a decreased incidence and size of HCC, however, no effect on the survival rates could be shown [449]. As our previous data observed impact of RNF4, SUMO and PML on HBx we hypothesized, that treatment of HBV with ATO also interferes with HBV infection levels and might even affect cccDNA formation and stability.

In a first step, cell viability for all further ATO administrations was assessed. 2  $\mu$ M and 4  $\mu$ M ATO were determined to be sufficient for all experiments since no impact on cell viability could be detected with these concentrations (Fig. 34). Prior to HBV infection studies, transfected HBx was investigated during ATO administration. ATO induced a dose-dependent increase in HBx protein expression as well as elevated dot-like accumulation of HBx in the nucleus (Fig. 35, 36). In addition, the nuclear dot-like distribution at PML-NBs was also re-localized in cells treated with ATO [551-553]. These findings confirmed our former results, demonstrating that HBx was not reduced but stabilized by RNF4. The enhanced HBx levels might be caused by the hyper-SUMOylation of PML-NBs during ATO administration, what could induce increased re-localization of HBx to PML. This hypothesis could be supported by the fact, that our previous experiments revealed increased localization of HBx at PML-NBs when HBx was stronger SUMO modified (HBx SCM5), whereas the SUMO deficient HBx was re-located from PML-NBs. Hyper-SUMOylated PML was subsequently degraded in contrast to the co-localizing HBx, what might be explained by a SUMO shift from HBx to PML-NBs, since decreased HBx SUMO modification, could be shown

to reduce its proteasomal degradation (Fig. 13) [310, 428, 429, 439-442]. Another possible explanation could be that the accumulation of HBx acts as a counteract-reaction against the PML-NBs loss, which we found to be essential for HBV maintenance. Thereby, HBx could attempt to elevate the remaining cccDNA pool by more efficiently opening the cccDNA, inducing HBV transcription [2]. This effect can also be observed within HCC tissues, where HBx is also accumulated within the nucleus [169, 554].

Besides the HBx protein, we further investigated the HBV core proteins, since HBx could not be used as a viral marker for HBV infection experiments, as the HBx protein detection during HBV infections is very challenging. In contrast to HBx, transfected core protein levels were reduced during ATO application (Fig. 37, 38, 39). This effect presumably arose due to an altered SUMOylation pattern, accompanied with PML-NB loss, which therefore disrupts the association of HBV core protein with PML. This could be supported by the fact, that co-localization of core with PML-NBs was stronger reduced in cells overexpressing SUMO2 compared to the control cells.

In a next step, the impact of ATO on core protein levels during HBV infections was examined.  $IC_{50}$  values of 4.64  $\mu$ M 4 d.p.i. and 2.88  $\mu$ M 7 d.p.i. displayed a distinct decrease of HBV core expression (Fig. 40). This finding was further confirmed by western blot and FACS analysis quantifying the number of core positive cells as well as the mean fluorescence intensity (Fig. 41, 42). To verify our data, immunofluorescence stainings were performed, revealing subcellular localization towards nuclear exclusion of HBV core protein upon treatment with ATO comparable to our previous transfection experiments (Fig. 43). In addition, accumulation in the cytoplasm, juxtaposed to the nucleus could be detected in cells treated with ATO indicating either the deactivation of HBV core or a defect in nuclear entry of the nucleocapsid. Next, qPCR analysis confirmed the significant decrease of total HBV transcripts and HBV DNA as well as a strong decrease of the cccDNA. The stable cccDNA pool was reduced to levels of around 50% 4 d.p.i. and 20% 7 d.p.i.. In line with these findings, also HBeAg secretion could be observed to be significantly lowered by ATO administration. Taken together, an efficient suppression of HBV infection parameters could be detected when cells were treated directly with ATO after removal of the inoculum (Fig. 44).

Furthermore, established HBV infections harboring a stable HBV cccDNA pool were investigated concerning delayed treatment with ATO 3 d.p.i. [134]. Again, a diminution of HBV core protein expression as well as re-localization of core could be determined (Fig. 45, 46). Besides these findings, total HBV transcripts as well as total HBV DNA could be examined to be significantly and dose-dependently decreased during HBV treatment. Moreover, HBV cccDNA as well as HBeAg secretion declined during ATO application in correlation to the compound concentration (Fig. 47).

All these effects might can be explained by the loss of PML-NBs, representing a key regulator within the cell and during HBV infections as well as by the loss or re-distribution of PML-NB associated factors like HBV core. Additionally, the inhibition of the nuclear entry of mature rcDNA-containing nucleocapsids hinders re-infection, leading to impaired intracellular cccDNA pool and transcription [91, 134, 148]. In line with our findings, ATO treatment was already described to decrease DNA topoisomerase II levels and activity, resulting in stalled cccDNA conversion [555, 556]. Summarized, these results depicted a distinct and strong suppression of newly synthesized as well as established HBV infections. These promising new data might lead the way for the development of novel antiviral approaches against HBV.

#### 4.8. Summary and concluding remarks

In summary, the HBx protein represents a mandatory factor for efficient HBV infections by enabling viral transcription from cccDNA [2, 69, 149, 156, 201]. We suggest the rcDNA to cccDNA conversion to take place at the SUMOylation hotspot PML-NBs, associated with host DDR proteins, since these factors are mandatory for cccDNA synthesis [467, 468]. This work could reveal the localization of HBx at PML-NBs as well as the PTM of the HBx by SUMO2. All single PML isoforms induced increased HBx protein levels, as well as a shift to the insoluble membranous fraction, supporting the beneficial function of PML for HBx. Furthermore, we found the PML-NB associated Sp100A protein to interact with the HBx protein. Due to the fact, that Sp100A induces chromatin de-condensation like HBx, we proposed a complementary function regarding cccDNA opening for HBV transcription [337, 506]. Additionally, the CRL4 harboring *inter alia* Cul4 and DDB1 were discovered to locate at PML-NBs, whereat Cul4 recruitment to PML-NBs was discovered to even be regulated by PML [1]. Moreover, the interaction between HBx and DDB1 was revealed to be PML dependent. Besides the important role of PML-NBs for HBx, also SUMOylation of the HBx protein was further analyzed. Here, we could examine HBx SCM1/2 as the main SUMOylation site for HBx, since its mutation resulted in significantly less SUMO modification of HBx. Moreover, HBx SCM5 was discovered to highly induce PTM by SUMO, which may support the development of clinical HCC [169, 532, 540, 541, 543]. Finally, this study could also examine the impact of HBx SUMOylation on HBV DNA as well as cccDNA. HBV DNA and cccDNA levels were significantly reduced using the HBx deficient SCM1/2 mutant, revealing the importance of this PTM for the HBV life cycle. This impact of post-translationally modified HBx can be caused by either alteration of HBx localization or its functionality towards cccDNA de-condensation, opening and transcription. Since we newly identified HBx to be located at PML-NBs and to be proteasomally degraded in a SUMO dependent manner, we analyzed whether this process is RNF4 driven, as RNF4 is able to bind SUMOylated proteins thereby inducing ubiquitinylation and subsequent proteasomal degradation [416, 557]. Our data on RNF4 and HBx revealed a mutual stabilization and furthermore interaction of both proteins. These results conclude a novel function for HBx either as a SUMO E3 ligase or as a recruiter of SUMOylated proteins for RNF4.

As we discovered HBx to be SUMO2 modified, localized at PML-NBs and interacting with RNF4, we were highly interested in the impact of ATO treatment on HBV infections. ATO treatment induces hyper-SUMOylation of PML, followed by RNF4 directed ubiquitylation and proteasomal degradation, which reduced PML-NBs numbers and probably altered PML-NB compositions [310, 435, 439-441, 448]. We examined several parameters of HBV including the stable cccDNA to be reduced during ATO treatment. The loss of HBV parameters might therefore be caused by the diminution of the PML protein itself as well as by the loss or re-distribution of PML-NB associated factors like HBV core, whereas HBx unsuccessfully attempted to counteract these antiviral effects.

In conclusion, the results of this study revealed a more detailed understanding of the persistent HBV form, the cccDNA. Our investigations of the underlying mechanisms identified the PTM of the HBx protein by SUMO as sufficient for cccDNA synthesis or maintenance, thereby opening potential for implementation in therapy of chronic HBV infections. Most importantly, the present study substantially extended the current knowledge concerning ATO as a powerful treatment for chronic HBV infections, as viral parameters as well as the HBV cccDNA decline *in vitro*. Our previous findings concerning this therapy approach allow us to pursue this project with future experiments in mouse models and clinical trials, since ATO represents an already approved medication. Taking all our findings together, ATO represents a promising novel antiviral therapy against acute and chronic HBV infections, which is urgently required since no specific compound targeting the viral cccDNA is available and still 257 million individuals worldwide suffer from HBV causing more than 800.000 deaths per year [WHO 2017].

## 5. Addendum

### 5.1. Figure legend

Figure 1: Molecular characteristics of Hepatitis B virus. ....	20
Figure 2: Replication cycle of Hepatitis B virus infection. ....	23
Figure 3: Schematic representation of rcDNA to cccDNA conversion .....	25
Figure 4: Overview of multiple HBx functions. ....	26
Figure 5: Schematic representation of HBx regions. ....	27
Figure 6: Epigenetic modulation of cccDNA. ....	28
Figure 7: HBx dependent SMC5/6 degradation via CRL4 E3 ubiquitin ligase complex. .....	30
Figure 8: The small ubiquitin like modifier (SUMO) Conjugation pathway. ....	35
Figure 9: <i>In silico</i> analysis of predicted HBx SUMO consensus motifs. ....	83
Figure 10: Generation of a HBx plasmid toolbox. ....	87
Figure 11: Co-localization of transfected HBx with all SUMO paralogues. ....	90
Figure 12: HBx is post-translationally SUMO2 modified. ....	91
Figure 13: Proteasomal degradation of HBx depends on SUMO2. ....	92
Figure 14: Interaction between transfected HBx and endogenous PML. ....	94
Figure 15: Transfected HBx modulated PML-NB number and size. ....	97
Figure 16: HBx localizes juxtaposed to all PML isoforms in HepG2-NTCP-K7 shPML cells. ....	99
Figure 17: Increased protein expression levels and mutual shift to the insoluble membranous fraction of transfected HBx in the presence of PML isoforms. ....	102
Figure 18: Increased protein HBx expression levels as well as mutual shift to the insoluble membranous fraction of HBx in the presence of PML isoforms in HepG2-NTCP-K7 shPML cells. ....	104
Figure 19: HBx interacts with all co-transfected PML isoforms. ....	105
Figure 20: Interaction of Sp100 isoform A with HBx. ....	107
Figure 21: Mutual re-localization of HBx and RNF4 to the insoluble membranous fraction. ....	109
Figure 22: RNF4 localization shifted to the nuclear membrane by co-transfected HBx. .....	110
Figure 23: Interaction of co-transfected HBx with RNF4. ....	111
Figure 24: Co-localization of endogenous PML-NBs and Cul4. ....	113
Figure 25: Cul4 number and size altered in the presence of transfected HBx. ....	116
Figure 26: Interaction of HBx with DDB1 is PML dependent. ....	118
Figure 27: Structure comparison of HBx wt and SCM mutants. ....	120
Figure 28: Reduced SUMOylation of HBx SCM1/2 mutant. ....	122
Figure 29: Co-localization of all HBx SCM mutants with PML-NBs except SCM1/2. .....	125
Figure 30: No co-localization of HBx SCM1/2 with endogenous Cul4. ....	128

---

Figure 31: Interaction between HBx and DDB1 lost in HBx SM1/2 mutant.....	130
Figure 32: Alteration of endogenous protein expression levels in the presence of HBx SCM mutants.....	132
Figure 33: HBx SCM1/2 promotes reduced HBV DNA and cccDNA levels. ....	134
Figure 34: ATO cell viability unaffected up to 4 $\mu$ M. ....	135
Figure 35: ATO administration increases transfected HBx protein levels dose-dependently.....	136
Figure 36: ATO administration promotes nuclear enrichment of HBx during immunofluorescence staining. ....	139
Figure 37: Dose-dependent decrease of transfected core protein expression levels during ATO administration.....	140
Figure 38: ATO administration induced re-localization of core dots/expression from PML-NBs.....	141
Figure 39: ATO treatment terminates the SUMO dependent co-localization of transfected core and endogenous PML-NBs.....	144
Figure 40: Determination of ATO IC <sub>50</sub> values. ....	145
Figure 41: ATO application reduces HBV core <sup>+</sup> cells and mean fluorescence intensity. ....	147
Figure 42: Decreased core protein levels during ATO treatment early and late after HBV infection.....	148
Figure 43: Core protein staining vanished during ATO treatment early and late after HBV infection.....	149
Figure 44: ATO administration induces dose-dependent loss of HBV parameters early and late after HBV infection.....	151
Figure 45: Efficient diminution of intracellular core protein during established HBV infections. ....	153
Figure 46: Intracellular HBV core substantially reduced by ATO administration during established HBV infection.....	154
Figure 47: Administration of ATO stimulated dose-dependent loss of HBV parameters during established HBV infections.....	156

## 5.2. Table legend

Table 1: Worldwide geographic incidences of HBV genotypes. [19-27].	18
Table 2: Used cell lines with database number, genotype, and reference.	39
Table 3: Media composition for H1299 and HeLa-SUMO2-His cell lines.	40
Table 4: Media composition for all HepG2 cell lines.	41
Table 5: Media composition for all HepaRG cell lines.	41
Table 6: Bacterial strain with phenotype and reference.	42
Table 7: Used viral strains with database number, genotype and reference.	42
Table 8: Plasmids including database number, description, and reference.	42
Table 9: Primers including database number, sequence, and purpose.	47
Table 10: Primary antibodies including database number, properties, and company.	49
Table 11: Secondary antibodies for western blot analysis including dilution, properties, and company.	50
Table 12: Secondary antibodies for immunofluorescence stainings including dilution, properties, and company.	50
Table 13: Enzymes and buffers including the indicated company.	51
Table 14: Chemicals and reagents including the indicated company.	52
Table 15: Laboratory equipment including the indicated supplier.	55
Table 16: Laboratory equipment including the indicated company.	58
Table 17: Softwares and programs with including the indicated publisher and purpose.	59
Table 18: Composition of the utilized buffers for NiNTA pull down.	67
Table 19: Composition of 10 ml stacking and 2 ml separating gel.	69
Table 20: PCR cycling parameters.	73
Table 21: qPCR cycling parameters for HBV DNA, HBV cDNA and PrP.	80
Table 22: qPCR cycling parameters for HBV cccDNA.	81

## 6. References

1. Murphy, C.M., et al., *Hepatitis B Virus X Protein Promotes Degradation of SMC5/6 to Enhance HBV Replication*. Cell Rep, 2016. **16**(11): p. 2846-2854.
2. Nassal, M., *HBV cccDNA: viral persistence reservoir and key obstacle for a cure of chronic hepatitis B*. Gut, 2015. **64**(12): p. 1972-84.
3. Blumberg, B.S., et al., *A serum antigen (Australia antigen) in Down's syndrome, leukemia, and hepatitis*. Ann Intern Med, 1967. **66**(5): p. 924-31.
4. Huang, S.N., et al., *Virus-Like Particles in Australia Antigen-Associated Hepatitis An Immunoelectron Aficroscopic Study of Human Lirer*. American Journal of Pathology, 1972. **67**(3): p. 453-462.
5. Okamoto, I., et al., *Nucleotide Sequence of a Cloned Hepatitis B Virus Genome, Subtype ayr: Comparison with Genomes of the Other Three Subtypes*. J gen Virol, 1986. **67**: p. 2305-231.
6. Gerlich, W.H., *Medical virology of hepatitis B: how it began and where we are now*. Virol J, 2013. **10**: p. 239.
7. Dane, D.S., C.H. Cameron, and M. Briggs, *Virus-like particles in serum of patients with Australia-antigen-associated hepatitis*. Lancet, 1970. **1**(7649): p. 695-8.
8. Schaefer, S., *Hepatitis B virus taxonomy and hepatitis B virus genotypes*. World J Gastroenterol, 2007. **13**(1): p. 14-21.
9. Hu, J. and K. Liu, *Complete and Incomplete Hepatitis B Virus Particles: Formation, Function, and Application*. Viruses, 2017. **9**(3).
10. Mason WS, B.C., Casey J, Gerlich WH, Howard CR, Kann M, Newbold J, Schaefer S, Taylor JM, Will H Hepadnaviridae. In: Fauquet CM, Mayo MA, Maniloff J, Desselberger U, Ball LA *Virus Taxonomy. Eighth Report of the International Committee on Taxonomy of Viruses*. 2005, Amsterdam: Elsevier.
11. Bonvicino, C.R., M.A. Moreira, and M.A. Soares, *Hepatitis B virus lineages in mammalian hosts: Potential for bidirectional cross-species transmission*. World J Gastroenterol, 2014. **20**(24): p. 7665-7674.
12. Modrow, S., Falke, D., Truyen, U. and Schätzl, H. , *Molekulare Virologie*. 3 ed. 2010, Heidelberg: Spektrum Akademischer Verlag 461-483.
13. Mason, W.S., G. Seal, and J. Summers, *Virus of Pekin ducks with structural and biological relatedness to human hepatitis B virus*. J Virol, 1980. **36**(3): p. 829-36.
14. Chang, S.F., et al., *A new avian hepadnavirus infecting snow geese (Anser caerulescens) produces a significant fraction of virions containing single-stranded DNA*. Virology, 1999. **262**(1): p. 39-54.
15. Marion, P.L., et al., *A virus in Beechey ground squirrels that is related to hepatitis B virus of humans*. Proc Natl Acad Sci U S A, 1980. **77**(5): p. 2941-5.
16. Minuk, G.Y., et al., *Ground squirrel hepatitis virus (GSHV) infection and hepatocellular carcinoma in the Canadian Richardson ground squirrel (Spermophilus richardsonii)*. Liver, 1986. **6**(6): p. 350-6.
17. Lanford, R.E., et al., *Isolation of a hepadnavirus from the woolly monkey, a New World primate*. Proc Natl Acad Sci U S A, 1998. **95**(10): p. 5757-61.
18. Warren, K.S., et al., *A new group of hepadnaviruses naturally infecting orangutans (Pongo pygmaeus)*. J Virol, 1999. **73**(9): p. 7860-5.
19. Velkov, S., et al., *The Global Hepatitis B Virus Genotype Distribution Approximated from Available Genotyping Data*. Genes (Basel), 2018. **9**(10).
20. Kramvis, A., *Genotypes and genetic variability of hepatitis B virus*. Intervirology, 2014. **57**(3-4): p. 141-50.
21. Tatematsu, K., et al., *A genetic variant of hepatitis B virus divergent from known human and ape genotypes isolated from a Japanese patient and provisionally assigned to new genotype J*. J Virol, 2009. **83**(20): p. 10538-47.

22. Kramvis, A., M. Kew, and G. Francois, *Hepatitis B virus genotypes*. Vaccine, 2005. **23**(19): p. 2409-23.
23. Sunbul, M., *Hepatitis B virus genotypes: global distribution and clinical importance*. World J Gastroenterol, 2014. **20**(18): p. 5427-34.
24. Lin, S., et al., *HBV serum markers of 49164 patients and their relationships to HBV genotype in Fujian Province of China*. J Clin Lab Anal, 2013. **27**(2): p. 130-6.
25. Zhang, H.W., et al., *Risk factors for acute hepatitis B and its progression to chronic hepatitis in Shanghai, China*. Gut, 2008. **57**(12): p. 1713-20.
26. Kobayashi, M., et al., *Infection with hepatitis B virus genotype A in Tokyo, Japan during 1976 through 2001*. J Gastroenterol, 2004. **39**(9): p. 844-50.
27. Wai, C.T., et al., *Clinical outcome and virological characteristics of hepatitis B-related acute liver failure in the United States*. J Viral Hepat, 2005. **12**(2): p. 192-8.
28. Pourkarim, M.R., et al., *Molecular identification of hepatitis B virus genotypes/subgenotypes: revised classification hurdles and updated resolutions*. World J Gastroenterol, 2014. **20**(23): p. 7152-68.
29. Aspinall, E.J., et al., *Hepatitis B prevention, diagnosis, treatment and care: a review*. Occup Med (Lond), 2011. **61**(8): p. 531-40.
30. Franco, E., et al., *Hepatitis B: Epidemiology and prevention in developing countries*. World J Hepatol, 2012. **4**(3): p. 74-80.
31. Hou, J., Z. Liu, and F. Gu, *Epidemiology and Prevention of Hepatitis B Virus Infection*. Int J Med Sci, 2005. **2**(1): p. 50-57.
32. Scott, R.M., et al., *Experimental transmission of hepatitis B virus by semen and saliva*. J Infect Dis, 1980. **142**(1): p. 67-71.
33. Bancroft, W.H., et al., *Transmission of hepatitis B virus to gibbons by exposure to human saliva containing hepatitis B surface antigen*. J Infect Dis, 1977. **135**(1): p. 79-85.
34. Borg, M.A., *Hepatitis B transmission through blood and body fluids exposure of school personnel*. Occup Med (Lond), 2005. **55**(2): p. 133-5.
35. Liang, T.J., *Hepatitis B: the virus and disease*. Hepatology, 2009. **49**(5 Suppl): p. S13-21.
36. Barker, L.F. and R. Murray, *Relationship of virus dose to incubation time of clinical hepatitis and time of appearance of hepatitis--associated antigen*. Am J Med Sci, 1972. **263**(1): p. 27-33.
37. Shepard, C.W., et al., *Hepatitis B virus infection: epidemiology and vaccination*. Epidemiol Rev, 2006. **28**: p. 112-25.
38. Beasley, R.P., et al., *Hepatocellular carcinoma and hepatitis B virus. A prospective study of 22 707 men in Taiwan*. Lancet, 1981. **2**(8256): p. 1129-33.
39. McMahon, B.J., et al., *Hepatitis B-related sequelae. Prospective study in 1400 hepatitis B surface antigen-positive Alaska native carriers*. Arch Intern Med, 1990. **150**(5): p. 1051-4.
40. Berk, P.D. and H. Popper, *Fulminant hepatic failure*. Am J Gastroenterol, 1978. **69**(3 Pt 2): p. 349-400.
41. Trepo, C., H.L. Chan, and A. Lok, *Hepatitis B virus infection*. Lancet, 2014. **384**(9959): p. 2053-63.
42. Tang, L.S.Y., et al., *Chronic Hepatitis B Infection: A Review*. JAMA, 2018. **319**(17): p. 1802-1813.
43. Schweitzer, A., et al., *Estimations of worldwide prevalence of chronic hepatitis B virus infection: a systematic review of data published between 1965 and 2013*. Lancet, 2015. **386**(10003): p. 1546-55.
44. (RKI), R.K.-I., *Virus Hepatitis B und D im Jahr 2014*. Epidemiologisches Bulletin, Aktuelle Daten und Informationen zu Infektionskrankheiten und Public Health.
45. (WHO), W.H.O. *Fact sheet, Hepatitis B*. 27.07.2020 01.02.2021]; Available from: [www.who.int/en/news-room/fact-sheets/detail/hepatitis-b](http://www.who.int/en/news-room/fact-sheets/detail/hepatitis-b).

46. Tong, M.J., et al., *Death From Liver Disease and Development of Hepatocellular Carcinoma in Patients With Chronic Hepatitis B Virus Infection: A Prospective Study*. Gastroenterol Hepatol (N Y), 2006. **2**(1): p. 41-47.
47. Iwarson, S., et al., *Successful postexposure vaccination against hepatitis B in chimpanzees*. J Med Virol, 1988. **25**(4): p. 433-9.
48. Beasley, R.P., et al., *Efficacy of hepatitis B immune globulin for prevention of perinatal transmission of the hepatitis B virus carrier state: final report of a randomized double-blind, placebo-controlled trial*. Hepatology, 1983. **3**(2): p. 135-41.
49. Winsnes, R. and J.C. Siebke, *Efficacy of post-exposure prophylaxis with hepatitis B immunoglobulin in Norway*. J Infect, 1986. **12**(1): p. 11-21.
50. Seeger, C. and W.S. Mason, *Molecular biology of hepatitis B virus infection*. Virology, 2015. **479-480**: p. 672-86.
51. Lamontagne, R.J., S. Bagga, and M.J. Bouchard, *Hepatitis B virus molecular biology and pathogenesis*. Hepatoma Res, 2016. **2**: p. 163-186.
52. Chisari, F.V., *Hepatitis B virus biology and pathogenesis*. Mol Genet Med, 1992. **2**: p. 67-104.
53. Chisari, F.V., *Rous-Whipple Award Lecture. Viruses, immunity, and cancer: lessons from hepatitis B*. Am J Pathol, 2000. **156**(4): p. 1117-32.
54. Ueda, K., T. Tsurimoto, and K. Matsubara, *Three Envelope Proteins of Hepatitis B Virus: Large S, Middle S, and Major S Proteins Needed for the Formation of Dane Particles*. J Virol, 1991. **65**(7): p. 3521-3529.
55. Crowther, R.A., et al., *Three-dimensional structure of hepatitis B virus core particles determined by electron cryomicroscopy*. Cell, 1994. **77**(6): p. 943-50.
56. Guo, H., et al., *Characterization of the intracellular deproteinized relaxed circular DNA of hepatitis B virus: an intermediate of covalently closed circular DNA formation*. J Virol, 2007. **81**(22): p. 12472-84.
57. Gerlich, W.H. and W.S. Robinson, *Hepatitis Virus Contains Protein Attached to the 5' Terminus of Its Complete DNA Strand*. Cell, 1980. **21**: p. 801-809.
58. Kidd-Ljunggren, K., Y. Miyakawa, and A.H. Kidd, *Genetic variability in hepatitis B viruses*. J Gen Virol, 2002. **83**(Pt 6): p. 1267-80.
59. Echevarria, J.M. and A. Avellon, *Hepatitis B virus genetic diversity*. J Med Virol, 2006. **78 Suppl 1**: p. S36-42.
60. Churin, Y., M. Roderfeld, and E. Roeb, *Hepatitis B virus large surface protein: function and fame*. Hepatobiliary Surg Nutr, 2015. **4**(1): p. 1-10.
61. Gerlich, W., *Hepatitis B surface proteins*. J Hepatol, 1991. **13 Suppl 4**: p. S90-2.
62. Vanlandschoot, P., T. Cao, and G. Leroux-Roel, *The nucleocapsid of the hepatitis B virus: a remarkable immunogenic structure*. Antiviral Research, 2003. **60**: p. 67-74.
63. Birnbaum, F. and M. Nassal, *Hepatitis B virus nucleocapsid assembly: primary structure requirements in the core protein*. J Virol, 1990. **64**(7): p. 3319-30.
64. Bock, C.T., et al., *Hepatitis B virus genome is organized into nucleosomes in the nucleus of the infected cell*. Virus Genes, 1994. **8**(3): p. 215-29.
65. Walsh, R. and S. Locarnini, *Hepatitis B precore protein: pathogenic potential and therapeutic promise*. Yonsei Med J, 2012. **53**(5): p. 875-85.
66. Milich, D.R., et al., *The secreted hepatitis B precore antigen can modulate the immune response to the nucleocapsid: a mechanism for persistence*. J Immunol, 1998. **160**(4): p. 2013-21.
67. Chen, M., et al., *Immune tolerance split between hepatitis B virus precore and core proteins*. J Virol, 2005. **79**(5): p. 3016-27.
68. Radziwill, G., W. Tucker, and H. Schaller, *Mutational Analysis of the Hepatitis B Virus P Gene Product: Domain Structure and RNase H Activity*. J Virol, 1990. **64**(2): p. 613-620.
69. Lucifora, J., et al., *Hepatitis B virus X protein is essential to initiate and maintain virus replication after infection*. J Hepatol, 2011. **55**(5): p. 996-1003.

70. Moolla, N., M. Kew, and P. Arbutnot, *Regulatory elements of hepatitis B virus transcription*. J Viral Hepat, 2002. **9**(5): p. 323-31.
71. Seeger, C., D. Ganem, and H.E. Varmus, *Biochemical and genetic evidence for the hepatitis B virus replication strategy*. Science, 1986. **232**(4749): p. 477-84.
72. Habig, J.W. and D.D. Loeb, *Sequence identity of the direct repeats, DR1 and DR2, contributes to the discrimination between primer translocation and in situ priming during replication of the duck hepatitis B virus*. J Mol Biol, 2006. **364**(1): p. 32-43.
73. Yee, J.K., *A liver-specific enhancer in the core promoter region of human hepatitis B virus*. Science, 1989. **246**(4930): p. 658-61.
74. Schadler, S. and E. Hildt, *HBV life cycle: entry and morphogenesis*. Viruses, 2009. **1**(2): p. 185-209.
75. Watashi, K., et al., *NTCP and beyond: opening the door to unveil hepatitis B virus entry*. Int J Mol Sci, 2014. **15**(2): p. 2892-905.
76. Schulze, A., P. Gripon, and S. Urban, *Hepatitis B virus infection initiates with a large surface protein-dependent binding to heparan sulfate proteoglycans*. Hepatology, 2007. **46**(6): p. 1759-68.
77. Yan, H., et al., *Sodium taurocholate cotransporting polypeptide is a functional receptor for human hepatitis B and D virus*. eLife, 2012. **1**.
78. Glebe, D., et al., *Mapping of the hepatitis B virus attachment site by use of infection-inhibiting preS1 lipopeptides and tupaia hepatocytes*. Gastroenterology, 2005. **129**(1): p. 234-45.
79. Gripon, P., I. Cannie, and S. Urban, *Efficient inhibition of hepatitis B virus infection by acylated peptides derived from the large viral surface protein*. J Virol, 2005. **79**(3): p. 1613-22.
80. Barrera, A., et al., *Mapping of the hepatitis B virus pre-S1 domain involved in receptor recognition*. J Virol, 2005. **79**(15): p. 9786-98.
81. Engelke, M., et al., *Characterization of a hepatitis B and hepatitis delta virus receptor binding site*. Hepatology, 2006. **43**(4): p. 750-60.
82. Schulze, A., et al., *Fine mapping of pre-S sequence requirements for hepatitis B virus large envelope protein-mediated receptor interaction*. J Virol, 2010. **84**(4): p. 1989-2000.
83. Huang, H.C., et al., *Entry of hepatitis B virus into immortalized human primary hepatocytes by clathrin-dependent endocytosis*. J Virol, 2012. **86**(17): p. 9443-53.
84. Kann, M., A. Schmitz, and B. Rabe, *Intracellular transport of hepatitis B virus*. World J Gastroenterol, 2007. **13**(1): p. 39-47.
85. Li, H.C., et al., *Nuclear export and import of human hepatitis B virus capsid protein and particles*. PLoS Pathog, 2010. **6**(10): p. e1001162.
86. Eckhardt, S.G., D.R. Milich, and A. McLachlan, *Hepatitis B virus core antigen has two nuclear localization sequences in the arginine-rich carboxyl terminus*. J Virol, 1991. **65**(2): p. 575-82.
87. Ning, B. and C. Shih, *Nucleolar localization of human hepatitis B virus capsid protein*. J Virol, 2004. **78**(24): p. 13653-68.
88. Schmitz, A., et al., *Nucleoporin 153 arrests the nuclear import of hepatitis B virus capsids in the nuclear basket*. PLoS Pathog, 2010. **6**(1): p. e1000741.
89. Bock, C.T., et al., *Structural organization of the hepatitis B virus minichromosome*. J Mol Biol, 2001. **307**(1): p. 183-96.
90. Newbold, J.E., et al., *The covalently closed duplex form of the hepadnavirus genome exists in situ as a heterogeneous population of viral minichromosomes*. J Virol, 1995. **69**(6): p. 3350-7.
91. Tuttleman, J.S., C. Pourcel, and J. Summers, *Formation of the pool of covalently closed circular viral DNA in hepadnavirus-infected cells*. Cell, 1986. **47**(3): p. 451-60.
92. Nguyen, D.H., L. Ludgate, and J. Hu, *Hepatitis B virus-cell interactions and pathogenesis*. J Cell Physiol, 2008. **216**(2): p. 289-94.

93. Beck, J. and M. Nassal, *Hepatitis B virus replication*. World J Gastroenterol, 2007. **13**(1): p. 48-64.
94. Fouillot, N., et al., *Translation of the hepatitis B virus P gene by ribosomal scanning as an alternative to internal initiation*. J Virol, 1993. **67**(8): p. 4886-95.
95. Datta, S., et al., *Molecular biology of the hepatitis B virus for clinicians*. J Clin Exp Hepatol, 2012. **2**(4): p. 353-65.
96. Cattaneo, R., H. Will, and H. Schaller, *Hepatitis B virus transcription in the infected liver*. EMBO J, 1984. **3**(9): p. 2191-6.
97. Nassal, M., *Hepatitis B viruses: reverse transcription a different way*. Virus Res, 2008. **134**(1-2): p. 235-49.
98. Zlotnick, A., et al., *Core protein: A pleiotropic keystone in the HBV lifecycle*. Antiviral Res, 2015. **121**: p. 82-93.
99. Zlotnick, A., et al., *Dimorphism of hepatitis B virus capsids is strongly influenced by the C-terminus of the capsid protein*. Biochemistry, 1996. **35**(23): p. 7412-21.
100. Wynne, S.A., R.A. Crowther, and A.G. Leslie, *The crystal structure of the human hepatitis B virus capsid*. Mol Cell, 1999. **3**(6): p. 771-80.
101. Rieger, A. and M. Nassal, *Specific hepatitis B virus minus-strand DNA synthesis requires only the 5' encapsidation signal and the 3'-proximal direct repeat DR1*. J Virol, 1996. **70**(1): p. 585-9.
102. Loeb, D.D., R.C. Hirsch, and D. Ganem, *Sequence-independent RNA cleavages generate the primers for plus strand DNA synthesis in hepatitis B viruses: implications for other reverse transcribing elements*. EMBO J, 1991. **10**(11): p. 3533-40.
103. Tavis, J.E. and E. Lomonosova, *The hepatitis B virus ribonuclease H as a drug target*. Antiviral Res, 2015. **118**: p. 132-8.
104. Chen, Y. and P.L. Marion, *Amino acids essential for RNase H activity of hepadnaviruses are also required for efficient elongation of minus-strand viral DNA*. J Virol, 1996. **70**(9): p. 6151-6.
105. Radziwill, G., W. Tucker, and H. Schaller, *Mutational analysis of the hepatitis B virus P gene product: domain structure and RNase H activity*. J Virol, 1990. **64**(2): p. 613-20.
106. Summers, J. and W.S. Mason, *Replication of the genome of a hepatitis B-like virus by reverse transcription of an RNA intermediate*. Cell, 1982. **29**(2): p. 403-15.
107. Lien, J.M., C.E. Aldrich, and W.S. Mason, *Evidence that a capped oligoribonucleotide is the primer for duck hepatitis B virus plus-strand DNA synthesis*. J Virol, 1986. **57**(1): p. 229-36.
108. Molnar-Kimber, K.L., J.W. Summers, and W.S. Mason, *Mapping of the cohesive overlap of duck hepatitis B virus DNA and of the site of initiation of reverse transcription*. J Virol, 1984. **51**(1): p. 181-91.
109. Haines, K.M. and D.D. Loeb, *The sequence of the RNA primer and the DNA template influence the initiation of plus-strand DNA synthesis in hepatitis B virus*. J Mol Biol, 2007. **370**(3): p. 471-80.
110. Will, H., et al., *Replication strategy of human hepatitis B virus*. J Virol, 1987. **61**(3): p. 904-11.
111. Loeb, D.D., K.J. Gulya, and R. Tian, *Sequence identity of the terminal redundancies on the minus-strand DNA template is necessary but not sufficient for the template switch during hepadnavirus plus-strand DNA synthesis*. J Virol, 1997. **71**(1): p. 152-60.
112. Staprans, S., D.D. Loeb, and D. Ganem, *Mutations affecting hepadnavirus plus-strand DNA synthesis dissociate primer cleavage from translocation and reveal the origin of linear viral DNA*. J Virol, 1991. **65**(3): p. 1255-62.
113. Patzer, E.J., et al., *Intracellular assembly and packaging of hepatitis B surface antigen particles occur in the endoplasmic reticulum*. J Virol, 1986. **58**(3): p. 884-92.
114. Selzer, L. and A. Zlotnick, *Assembly and Release of Hepatitis B Virus*. Cold Spring Harb Perspect Med, 2015. **5**(12).
115. Bruss, V., *Hepatitis B virus morphogenesis*. World J Gastroenterol, 2007. **13**(1): p. 65-73.

116. Bruss, V. and D. Ganem, *The role of envelope proteins in hepatitis B virus assembly*. Proc Natl Acad Sci U S A, 1991. **88**(3): p. 1059-63.
117. Eble, B.E., et al., *Multiple topogenic sequences determine the transmembrane orientation of the hepatitis B surface antigen*. Mol Cell Biol, 1987. **7**(10): p. 3591-601.
118. Watanabe, T., et al., *Involvement of host cellular multivesicular body functions in hepatitis B virus budding*. Proc Natl Acad Sci U S A, 2007. **104**(24): p. 10205-10.
119. Prange, R., *Host factors involved in hepatitis B virus maturation, assembly, and egress*. Med Microbiol Immunol, 2012. **201**(4): p. 449-61.
120. Huovila, A.P., A.M. Eder, and S.D. Fuller, *Hepatitis B surface antigen assembles in a post-ER, pre-Golgi compartment*. J Cell Biol, 1992. **118**(6): p. 1305-20.
121. Patient, R., et al., *Hepatitis B virus subviral envelope particle morphogenesis and intracellular trafficking*. J Virol, 2007. **81**(8): p. 3842-51.
122. Jiang, B., et al., *Subviral Hepatitis B Virus Filaments, like Infectious Viral Particles, Are Released via Multivesicular Bodies*. J Virol, 2015. **90**(7): p. 3330-41.
123. Chai, N., et al., *Properties of subviral particles of hepatitis B virus*. J Virol, 2008. **82**(16): p. 7812-7.
124. Milich, D.R., et al., *Is a function of the secreted hepatitis B e antigen to induce immunologic tolerance in utero?* Proc Natl Acad Sci U S A, 1990. **87**(17): p. 6599-603.
125. Carman, W.F., et al., *Mutation preventing formation of hepatitis B e antigen in patients with chronic hepatitis B infection*. Lancet, 1989. **2**(8663): p. 588-91.
126. Ganem, D. and A.M. Prince, *Hepatitis B virus infection--natural history and clinical consequences*. N Engl J Med, 2004. **350**(11): p. 1118-29.
127. Ganem, D., *Assembly of hepadnaviral virions and subviral particles*. Curr Top Microbiol Immunol, 1991. **168**: p. 61-83.
128. Patient, R., C. Hourieux, and P. Roingeard, *Morphogenesis of hepatitis B virus and its subviral envelope particles*. Cell Microbiol, 2009. **11**(11): p. 1561-70.
129. Glebe, D. and S. Urban, *Viral and cellular determinants involved in hepadnaviral entry*. World J Gastroenterol, 2007. **13**(1): p. 22-38.
130. Gudima, S., et al., *Assembly of hepatitis delta virus: particle characterization, including the ability to infect primary human hepatocytes*. J Virol, 2007. **81**(7): p. 3608-17.
131. Heermann, K.H., et al., *Large surface proteins of hepatitis B virus containing the pre-s sequence*. J Virol, 1984. **52**(2): p. 396-402.
132. Pastor, F., et al., *Direct interaction between the hepatitis B virus core and envelope proteins analyzed in a cellular context*. Sci Rep, 2019. **9**(1): p. 16178.
133. Yang, H.C. and J.H. Kao, *Persistence of hepatitis B virus covalently closed circular DNA in hepatocytes: molecular mechanisms and clinical significance*. Emerg Microbes Infect, 2014. **3**(9): p. e64.
134. Ko, C., et al., *Hepatitis B virus genome recycling and de novo secondary infection events maintain stable cccDNA levels*. J Hepatol, 2018. **69**(6): p. 1231-1241.
135. Lucifora, J. and U. Protzer, *Attacking hepatitis B virus cccDNA--The holy grail to hepatitis B cure*. J Hepatol, 2016. **64**(1 Suppl): p. S41-8.
136. Koniger, C., et al., *Involvement of the host DNA-repair enzyme TDP2 in formation of the covalently closed circular DNA persistence reservoir of hepatitis B viruses*. Proc Natl Acad Sci U S A, 2014. **111**(40): p. E4244-53.
137. Cui, X., et al., *Does Tyrosyl DNA Phosphodiesterase-2 Play a Role in Hepatitis B Virus Genome Repair?* PLoS One, 2015. **10**(6): p. e0128401.
138. Hu, J., U. Protzer, and A. Siddiqui, *Revisiting Hepatitis B Virus: Challenges of Curative Therapies*. J Virol, 2019. **93**(20).
139. Guo, J.T. and H. Guo, *Metabolism and function of hepatitis B virus cccDNA: Implications for the development of cccDNA-targeting antiviral therapeutics*. Antiviral Res, 2015. **122**: p. 91-100.
140. Stahl, M., et al., *Chaperone activation of the hepadnaviral reverse transcriptase for template RNA binding is established by the Hsp70 and stimulated by the Hsp90 system*. Nucleic Acids Res, 2007. **35**(18): p. 6124-36.

141. Sohn, J.A., S. Litwin, and C. Seeger, *Mechanism for CCC DNA synthesis in hepadnaviruses*. PLoS One, 2009. **4**(11): p. e8093.
142. Seeger, C. and W.S. Mason, *Hepatitis B virus biology*. Microbiol Mol Biol Rev, 2000. **64**(1): p. 51-68.
143. Chung, Y.L. and T.Y. Tsai, *Promyelocytic leukemia nuclear bodies link the DNA damage repair pathway with hepatitis B virus replication: implications for hepatitis B virus exacerbation during chemotherapy and radiotherapy*. Mol Cancer Res, 2009. **7**(10): p. 1672-85.
144. Kock, J. and H.J. Schlicht, *Analysis of the earliest steps of hepadnavirus replication: genome repair after infectious entry into hepatocytes does not depend on viral polymerase activity*. J Virol, 1993. **67**(8): p. 4867-74.
145. Gao, W. and J. Hu, *Formation of hepatitis B virus covalently closed circular DNA: removal of genome-linked protein*. J Virol, 2007. **81**(12): p. 6164-74.
146. Qi, Y., et al., *DNA Polymerase kappa Is a Key Cellular Factor for the Formation of Covalently Closed Circular DNA of Hepatitis B Virus*. PLoS Pathog, 2016. **12**(10): p. e1005893.
147. Ashour, M.E., R. Atteya, and S.F. El-Khamisy, *Topoisomerase-mediated chromosomal break repair: an emerging player in many games*. Nat Rev Cancer, 2015. **15**(3): p. 137-51.
148. Kock, J., et al., *Generation of covalently closed circular DNA of hepatitis B viruses via intracellular recycling is regulated in a virus specific manner*. PLoS Pathog, 2010. **6**(9): p. e1001082.
149. Pollicino, T., et al., *Hepatitis B virus replication is regulated by the acetylation status of hepatitis B virus cccDNA-bound H3 and H4 histones*. Gastroenterology, 2006. **130**(3): p. 823-37.
150. Levvero, M., et al., *Control of cccDNA function in hepatitis B virus infection*. J Hepatol, 2009. **51**(3): p. 581-92.
151. Guo, Y.H., et al., *HBc binds to the CpG islands of HBV cccDNA and promotes an epigenetic permissive state*. Epigenetics, 2011. **6**(6): p. 720-6.
152. Yang, F., *Post-translational Modification Control of HBV Biological Processes*. Front Microbiol, 2018. **9**: p. 2661.
153. Hong, X., E.S. Kim, and H. Guo, *Epigenetic regulation of hepatitis B virus covalently closed circular DNA: Implications for epigenetic therapy against chronic hepatitis B*. Hepatology, 2017. **66**(6): p. 2066-2077.
154. Kouzarides, T., *Chromatin modifications and their function*. Cell, 2007. **128**(4): p. 693-705.
155. Riviere, L., et al., *HBx relieves chromatin-mediated transcriptional repression of hepatitis B viral cccDNA involving SETDB1 histone methyltransferase*. J Hepatol, 2015. **63**(5): p. 1093-102.
156. Tessarz, P. and T. Kouzarides, *Histone core modifications regulating nucleosome structure and dynamics*. Nat Rev Mol Cell Biol, 2014. **15**(11): p. 703-8.
157. Tropberger, P., et al., *Mapping of histone modifications in episomal HBV cccDNA uncovers an unusual chromatin organization amenable to epigenetic manipulation*. Proc Natl Acad Sci U S A, 2015. **112**(42): p. E5715-24.
158. Kew, M.C., *Hepatitis B virus x protein in the pathogenesis of hepatitis B virus-induced hepatocellular carcinoma*. J Gastroenterol Hepatol, 2011. **26 Suppl 1**: p. 144-52.
159. Geng, M., et al., *Molecular mechanism of hepatitis B virus X protein function in hepatocarcinogenesis*. World J Gastroenterol, 2015. **21**(38): p. 10732-8.
160. Murakami, S., *Hepatitis B virus X protein: a multifunctional viral regulator*. J Gastroenterol, 2001. **36**(10): p. 651-60.
161. Funk, A., et al., *Avian hepatitis B viruses: molecular and cellular biology, phylogenesis, and host tropism*. World J Gastroenterol, 2007. **13**(1): p. 91-103.
162. Minor, M.M. and B.L. Slagle, *Hepatitis B virus HBx protein interactions with the ubiquitin proteasome system*. Viruses, 2014. **6**(11): p. 4683-702.

163. Fung, J., C.L. Lai, and M.F. Yuen, *Hepatitis B and C virus-related carcinogenesis*. Clin Microbiol Infect, 2009. **15**(11): p. 964-70.
164. Feitelson, M.A., et al., *Hepatitis B x antigen and p53 are associated in vitro and in liver tissues from patients with primary hepatocellular carcinoma*. Oncogene, 1993. **8**(5): p. 1109-17.
165. Wang, X.W., et al., *Abrogation of p53-induced apoptosis by the hepatitis B virus X gene*. Cancer Res, 1995. **55**(24): p. 6012-6.
166. Elmore, L.W., et al., *Hepatitis B virus X protein and p53 tumor suppressor interactions in the modulation of apoptosis*. Proc Natl Acad Sci U S A, 1997. **94**(26): p. 14707-12.
167. Wang, X.W., et al., *Hepatitis B virus X protein inhibits p53 sequence-specific DNA binding, transcriptional activity, and association with transcription factor ERCC3*. Proc Natl Acad Sci U S A, 1994. **91**(6): p. 2230-4.
168. Diao, J., R. Garces, and C.D. Richardson, *X protein of hepatitis B virus modulates cytokine and growth factor related signal transduction pathways during the course of viral infections and hepatocarcinogenesis*. Cytokine Growth Factor Rev, 2001. **12**(2-3): p. 189-205.
169. Ali, A., et al., *Hepatitis B virus, HBx mutants and their role in hepatocellular carcinoma*. World J Gastroenterol, 2014. **20**(30): p. 10238-48.
170. Wu, Z.J., et al., *Constructing the HBV-human protein interaction network to understand the relationship between HBV and hepatocellular carcinoma*. J Exp Clin Cancer Res, 2010. **29**: p. 146.
171. Tian, Y., et al., *HBx promotes cell proliferation by disturbing the cross-talk between miR-181a and PTEN*. Sci Rep, 2017. **7**: p. 40089.
172. Wang, Q., et al., *The viral oncoprotein HBx of Hepatitis B virus promotes the growth of hepatocellular carcinoma through cooperating with the cellular oncoprotein RMP*. Int J Biol Sci, 2014. **10**(10): p. 1181-92.
173. Rossner, M.T., *Hepatitis B Virus X-Gene Product: A Promiscuous Transcriptional Activator*. Journal of Medical Virology, 1992. **36**: p. 101-117.
174. Murakami, S., *Hepatitis B virus X protein: structure, function and biology*. Intervirology, 1999. **42**(2-3): p. 81-99.
175. Nakatake, H., et al., *Effect of X protein on transactivation of hepatitis B virus promoters and on viral replication*. Virology, 1993. **195**(2): p. 305-14.
176. Tang, H., et al., *The transcriptional transactivation function of HBx protein is important for its augmentation role in hepatitis B virus replication*. J Virol, 2005. **79**(9): p. 5548-56.
177. Minor, M.M., et al., *Hepatitis B Virus HBx Protein Mediates the Degradation of Host Restriction Factors through the Cullin 4 DDB1 E3 Ubiquitin Ligase Complex*. Cells, 2020. **9**(4).
178. Benhenda, S., et al., *Hepatitis B virus X protein molecular functions and its role in virus life cycle and pathogenesis*. Adv Cancer Res, 2009. **103**: p. 75-109.
179. Feitelson, M.A. and J. Lee, *Hepatitis B virus integration, fragile sites, and hepatocarcinogenesis*. Cancer Lett, 2007. **252**(2): p. 157-70.
180. Slagle, B.L. and M.J. Bouchard, *Hepatitis B Virus X and Regulation of Viral Gene Expression*. Cold Spring Harb Perspect Med, 2016. **6**(3): p. a021402.
181. Williams, J.S. and O.M. Andrisani, *The hepatitis B virus X protein targets the basic region-leucine zipper domain of CREB*. Proc Natl Acad Sci U S A, 1995. **92**(9): p. 3819-23.
182. Lin, Y., et al., *Hepatitis B virus X protein is a transcriptional modulator that communicates with transcription factor IIB and the RNA polymerase II subunit 5*. J Biol Chem, 1997. **272**(11): p. 7132-9.
183. Waris, G., K.W. Huh, and A. Siddiqui, *Mitochondrially associated hepatitis B virus X protein constitutively activates transcription factors STAT-3 and NF-kappa B via oxidative stress*. Mol Cell Biol, 2001. **21**(22): p. 7721-30.

184. Lee, Y.H. and Y. Yun, *HBx protein of hepatitis B virus activates Jak1-STAT signaling*. J Biol Chem, 1998. **273**(39): p. 25510-5.
185. Arbuthnot, P., A. Capovilla, and M. Kew, *Putative role of hepatitis B virus X protein in hepatocarcinogenesis: effects on apoptosis, DNA repair, mitogen-activated protein kinase and JAK/STAT pathways*. J Gastroenterol Hepatol, 2000. **15**(4): p. 357-68.
186. Benn, J. and R.J. Schneider, *Hepatitis B virus HBx protein activates Ras-GTP complex formation and establishes a Ras, Raf, MAP kinase signaling cascade*. Proc Natl Acad Sci U S A, 1994. **91**(22): p. 10350-4.
187. Tarn, C., et al., *Hepatitis B virus X protein differentially activates RAS-RAF-MAPK and JNK pathways in X-transforming versus non-transforming AML12 hepatocytes*. J Biol Chem, 2001. **276**(37): p. 34671-80.
188. Klein, N.P., et al., *Src kinases involved in hepatitis B virus replication*. EMBO J, 1999. **18**(18): p. 5019-27.
189. Bouchard, M.J., L.H. Wang, and R.J. Schneider, *Calcium signaling by HBx protein in hepatitis B virus DNA replication*. Science, 2001. **294**(5550): p. 2376-8.
190. Lubber, B., et al., *The hepatitis B virus transactivator HBx causes elevation of diacylglycerol and activation of protein kinase C*. Res Virol, 1993. **144**(4): p. 311-21.
191. Kekule, A.S., et al., *Hepatitis B virus transactivator HBx uses a tumour promoter signalling pathway*. Nature, 1993. **361**(6414): p. 742-5.
192. Mukherji, A., V.C. Janbandhu, and V. Kumar, *HBx protein modulates PI3K/Akt pathway to overcome genotoxic stress-induced destabilization of cyclin D1 and arrest of cell cycle*. Indian J Biochem Biophys, 2009. **46**(1): p. 37-44.
193. Gearhart, T.L. and M.J. Bouchard, *Replication of the hepatitis B virus requires a calcium-dependent HBx-induced G1 phase arrest of hepatocytes*. Virology, 2010. **407**(1): p. 14-25.
194. Lara-Pezzi, E., et al., *The hepatitis B virus X protein promotes tumor cell invasion by inducing membrane-type matrix metalloproteinase-1 and cyclooxygenase-2 expression*. J Clin Invest, 2002. **110**(12): p. 1831-8.
195. Kim, J.H. and H.M. Rho, *Activation of the human transforming growth factor alpha (TGF-alpha) gene by the hepatitis B viral X protein (HBx) through AP-2 sites*. Mol Cell Biochem, 2002. **231**(1-2): p. 155-61.
196. Gearhart, T.L. and M.J. Bouchard, *The hepatitis B virus HBx protein modulates cell cycle regulatory proteins in cultured primary human hepatocytes*. Virus Res, 2011. **155**(1): p. 363-7.
197. Benn, J. and R.J. Schneider, *Hepatitis B virus HBx protein deregulates cell cycle checkpoint controls*. Proc Natl Acad Sci U S A, 1995. **92**(24): p. 11215-9.
198. Becker, S.A., et al., *Hepatitis B virus X protein interferes with cellular DNA repair*. J Virol, 1998. **72**(1): p. 266-72.
199. Cheng, B., et al., *The effects of HBx gene on the expression of DNA repair enzymes hOGG1 and hMYHalpha mRNA in HepG2 cells*. J Huazhong Univ Sci Technolog Med Sci, 2009. **29**(2): p. 187-92.
200. Wei, C., et al., *The hepatitis B virus X protein disrupts innate immunity by downregulating mitochondrial antiviral signaling protein*. J Immunol, 2010. **185**(2): p. 1158-68.
201. Belloni, L., et al., *Nuclear HBx binds the HBV minichromosome and modifies the epigenetic regulation of cccDNA function*. Proc Natl Acad Sci U S A, 2009. **106**(47): p. 19975-9.
202. Sidhu, K., et al., *Mass spectrometric determination of disulfide bonds in the biologically active recombinant HBx protein of hepatitis B virus*. Biochemistry, 2014. **53**(28): p. 4685-95.
203. Lee, Y.I., et al., *Phosphorylation of purified recombinant hepatitis B virus-X protein by mitogen-activated protein kinase and protein kinase C in vitro*. J Virol Methods, 2001. **95**(1-2): p. 1-10.

204. Hernandez, S., et al., *The viral transactivator HBx protein exhibits a high potential for regulation via phosphorylation through an evolutionarily conserved mechanism*. *Infect Agent Cancer*, 2012. **7**(1): p. 27.
205. Luo, L., et al., *Hepatitis B virus X protein modulates remodelling of minichromosomes related to hepatitis B virus replication in HepG2 cells*. *Int J Mol Med*, 2013. **31**(1): p. 197-204.
206. Neuveut, C., Y. Wei, and M.A. Buendia, *Mechanisms of HBV-related hepatocarcinogenesis*. *J Hepatol*, 2010. **52**(4): p. 594-604.
207. Hodgson, A.J., et al., *Hepatitis B virus regulatory HBx protein binding to DDB1 is required but is not sufficient for maximal HBV replication*. *Virology*, 2012. **426**(1): p. 73-82.
208. Livingston, C.M., et al., *Identifying and Characterizing Interplay between Hepatitis B Virus X Protein and Smc5/6*. *Viruses*, 2017. **9**(4).
209. Diao, J., et al., *X protein of hepatitis B virus inhibits Fas-mediated apoptosis and is associated with up-regulation of the SAPK/JNK pathway*. *J Biol Chem*, 2001. **276**(11): p. 8328-40.
210. Tang, H., et al., *Molecular functions and biological roles of hepatitis B virus x protein*. *Cancer Sci*, 2006. **97**(10): p. 977-83.
211. Murakami, S., J.H. Cheong, and S. Kaneko, *Human hepatitis virus X gene encodes a regulatory domain that represses transactivation of X protein*. *J Biol Chem*, 1994. **269**(21): p. 15118-23.
212. Li, T., et al., *A promiscuous alpha-helical motif anchors viral hijackers and substrate receptors to the CUL4-DDB1 ubiquitin ligase machinery*. *Nat Struct Mol Biol*, 2010. **17**(1): p. 105-11.
213. Li, S.K., et al., *Identification of functionally important amino acid residues in the mitochondria targeting sequence of hepatitis B virus X protein*. *Virology*, 2008. **381**(1): p. 81-8.
214. Kwun, H.J. and K.L. Jang, *Natural variants of hepatitis B virus X protein have differential effects on the expression of cyclin-dependent kinase inhibitor p21 gene*. *Nucleic Acids Res*, 2004. **32**(7): p. 2202-13.
215. Tao, S., et al., *Characterization and engineering of broadly reactive monoclonal antibody against hepatitis B virus X protein that blocks its interaction with DDB1*. *Sci Rep*, 2019. **9**(1): p. 20323.
216. Slagle, B.L. and M.J. Bouchard, *Role of HBx in hepatitis B virus persistence and its therapeutic implications*. *Curr Opin Virol*, 2018. **30**: p. 32-38.
217. Henkler, F., et al., *Intracellular localization of the hepatitis B virus HBx protein*. *J Gen Virol*, 2001. **82**(Pt 4): p. 871-882.
218. Hoare, J., et al., *Subcellular localisation of the X protein in HBV infected hepatocytes*. *J Med Virol*, 2001. **64**(4): p. 419-26.
219. J. Lucifora, U.P., *Hepatitis B Virus X Protein: A Key Regulator of the Virus Life Cycle*, in *Viral Genomes - Molecular Structure, Diversity, Gene Expression Mechanisms and Host-Virus Interactions*, M. Garcia, Editor. 2012, InTech.
220. Bouchard, M.J. and R.J. Schneider, *The enigmatic X gene of hepatitis B virus*. *J Virol*, 2004. **78**(23): p. 12725-34.
221. Weil, R., et al., *Direct association and nuclear import of the hepatitis B virus X protein with the NF-kappaB inhibitor I kappa B alpha*. *Mol Cell Biol*, 1999. **19**(9): p. 6345-54.
222. Su, Q., et al., *Expression of hepatitis B virus X protein in HBV-infected human livers and hepatocellular carcinomas*. *Hepatology*, 1998. **27**(4): p. 1109-20.
223. Doria, M., et al., *The hepatitis B virus HBx protein is a dual specificity cytoplasmic activator of Ras and nuclear activator of transcription factors*. *EMBO J*, 1995. **14**(19): p. 4747-57.
224. Rahmani, Z., et al., *Hepatitis B virus X protein colocalizes to mitochondria with a human voltage-dependent anion channel, HVDAC3, and alters its transmembrane potential*. *J Virol*, 2000. **74**(6): p. 2840-6.

225. Lee, Y.I., et al., *Human hepatitis B virus-X protein alters mitochondrial function and physiology in human liver cells*. J Biol Chem, 2004. **279**(15): p. 15460-71.
226. Cho, H.K., et al., *Endoplasmic reticulum stress induced by hepatitis B virus X protein enhances cyclo-oxygenase 2 expression via activating transcription factor 4*. Biochem J, 2011. **435**(2): p. 431-9.
227. Cho, H.K., et al., *HBx induces the proliferation of hepatocellular carcinoma cells via AP1 over-expressed as a result of ER stress*. Biochem J, 2015. **466**(1): p. 115-21.
228. Tsuge, M., et al., *HBx protein is indispensable for development of viraemia in human hepatocyte chimeric mice*. J Gen Virol, 2010. **91**(Pt 7): p. 1854-64.
229. Seeger C, M.W., Zoulim F. , *Fields Virology*, ed. H.P. Knipe DM. 2007, Philadelphia.
230. Cougot, D., et al., *The hepatitis B virus X protein functionally interacts with CREB-binding protein/p300 in the regulation of CREB-mediated transcription*. J Biol Chem, 2007. **282**(7): p. 4277-87.
231. Park, I.Y., et al., *Aberrant epigenetic modifications in hepatocarcinogenesis induced by hepatitis B virus X protein*. Gastroenterology, 2007. **132**(4): p. 1476-94.
232. Jung, J.K., et al., *Expression of DNA methyltransferase 1 is activated by hepatitis B virus X protein via a regulatory circuit involving the p16INK4a-cyclin D1-CDK 4/6-pRb-E2F1 pathway*. Cancer Res, 2007. **67**(12): p. 5771-8.
233. Lee, J.O., et al., *Hepatitis B virus X protein represses E-cadherin expression via activation of DNA methyltransferase 1*. Oncogene, 2005. **24**(44): p. 6617-25.
234. Tian, Y., et al., *Hepatitis B virus X protein-induced aberrant epigenetic modifications contributing to human hepatocellular carcinoma pathogenesis*. Mol Cell Biol, 2013. **33**(15): p. 2810-6.
235. Herceg, Z. and A. Paliwal, *Epigenetic mechanisms in hepatocellular carcinoma: how environmental factors influence the epigenome*. Mutat Res, 2011. **727**(3): p. 55-61.
236. Chen, T. and E. Li, *Structure and function of eukaryotic DNA methyltransferases*. Curr Top Dev Biol, 2004. **60**: p. 55-89.
237. Herman, J.G. and S.B. Baylin, *Gene silencing in cancer in association with promoter hypermethylation*. N Engl J Med, 2003. **349**(21): p. 2042-54.
238. Ducroux, A., et al., *The Tudor domain protein Spindlin1 is involved in intrinsic antiviral defense against incoming hepatitis B Virus and herpes simplex virus type 1*. PLoS Pathog, 2014. **10**(9): p. e1004343.
239. Protzer, U., *Hepatitis: Epigenetic control of HBV by HBx protein--releasing the break?* Nat Rev Gastroenterol Hepatol, 2015. **12**(10): p. 558-9.
240. Lee, T.H., S.J. Elledge, and J.S. Butel, *Hepatitis B virus X protein interacts with a probable cellular DNA repair protein*. J Virol, 1995. **69**(2): p. 1107-14.
241. Sitterlin, D., et al., *Interaction of the UV-damaged DNA-binding protein with hepatitis B virus X protein is conserved among mammalian hepadnaviruses and restricted to transactivation-proficient X-insertion mutants*. J Virol, 1997. **71**(8): p. 6194-9.
242. Decorsiere, A., et al., *Hepatitis B virus X protein identifies the Smc5/6 complex as a host restriction factor*. Nature, 2016. **531**(7594): p. 386-9.
243. Abramic, M., A.S. Levine, and M. Protic, *Purification of an ultraviolet-inducible, damage-specific DNA-binding protein from primate cells*. J Biol Chem, 1991. **266**(33): p. 22493-500.
244. Sitterlin, D., et al., *Correct binding of viral X protein to UVDDDB-p127 cellular protein is critical for efficient infection by hepatitis B viruses*. Oncogene, 2000. **19**(38): p. 4427-31.
245. Lee, J. and P. Zhou, *DCAFs, the missing link of the CUL4-DDB1 ubiquitin ligase*. Mol Cell, 2007. **26**(6): p. 775-80.
246. Higa, L.A. and H. Zhang, *Stealing the spotlight: CUL4-DDB1 ubiquitin ligase docks WD40-repeat proteins to destroy*. Cell Div, 2007. **2**: p. 5.
247. Jeppsson, K., et al., *The maintenance of chromosome structure: positioning and functioning of SMC complexes*. Nat Rev Mol Cell Biol, 2014. **15**(9): p. 601-14.

248. Jacome, A., et al., *NSMCE2 suppresses cancer and aging in mice independently of its SUMO ligase activity*. EMBO J, 2015. **34**(21): p. 2604-19.
249. Martin-Lluesma, S., et al., *Hepatitis B virus X protein affects S phase progression leading to chromosome segregation defects by binding to damaged DNA binding protein 1*. Hepatology, 2008. **48**(5): p. 1467-76.
250. Gallego-Paez, L.M., et al., *Smc5/6-mediated regulation of replication progression contributes to chromosome assembly during mitosis in human cells*. Mol Biol Cell, 2014. **25**(2): p. 302-17.
251. Wu, N. and H. Yu, *The Smc complexes in DNA damage response*. Cell Biosci, 2012. **2**: p. 5.
252. Laguette, N., et al., *SAMHD1 is the dendritic- and myeloid-cell-specific HIV-1 restriction factor counteracted by Vpx*. Nature, 2011. **474**(7353): p. 654-7.
253. Ahn, J., et al., *HIV-1 Vpr loads uracil DNA glycosylase-2 onto DCAF1, a substrate recognition subunit of a cullin 4A-ring E3 ubiquitin ligase for proteasome-dependent degradation*. J Biol Chem, 2010. **285**(48): p. 37333-41.
254. Precious, B., et al., *Simian virus 5 V protein acts as an adaptor, linking DDB1 to STAT2, to facilitate the ubiquitination of STAT1*. J Virol, 2005. **79**(21): p. 13434-41.
255. van de Klundert, M.A., et al., *Hepatitis B Virus Protein X Induces Degradation of Talin-1*. Viruses, 2016. **8**(10).
256. Kanwal, F., et al., *Treatment alternatives for hepatitis B cirrhosis: a cost-effectiveness analysis*. Am J Gastroenterol, 2006. **101**(9): p. 2076-89.
257. Zoulim, F., *Hepatitis B virus resistance to antiviral drugs: where are we going?* Liver Int, 2011. **31 Suppl 1**: p. 111-6.
258. Suk-Fong Lok, A., *Hepatitis B Treatment: What We Know Now and What Remains to Be Researched*. Hepatol Commun, 2019. **3**(1): p. 8-19.
259. Lieveld, F.I., et al., *Patient adherence to antiviral treatment for chronic hepatitis B and C: a systematic review*. Ann Hepatol, 2013. **12**(3): p. 380-91.
260. Ford, N., et al., *Adherence to Nucleos(t)ide Analogue Therapies for Chronic Hepatitis B Infection: A Systematic Review and Meta-Analysis*. Hepatol Commun, 2018. **2**(10): p. 1160-1167.
261. Tillmann, H.L., et al., *Mutational pattern of hepatitis B virus on sequential therapy with famciclovir and lamivudine in patients with hepatitis B virus reinfection occurring under HBIg immunoglobulin after liver transplantation*. Hepatology, 1999. **30**(1): p. 244-56.
262. Ayoub, W.S., P. Martin, and K.R. Bhamidimarri, *Hepatitis B Virus Infection and Organ Transplantation*. Gastroenterol Hepatol (N Y), 2018. **14**(1): p. 33-40.
263. Lerut, J.P., et al., *Liver transplantation and HBsAg-positive postnecrotic cirrhosis: adequate immunoprophylaxis and delta virus co-infection as the significant determinants of long-term prognosis*. J Hepatol, 1999. **30**(4): p. 706-14.
264. Beckebaum, S., et al., *Recurrence of Hepatitis B Infection in Liver Transplant Patients Receiving Long-Term Hepatitis B Immunoglobulin Prophylaxis*. Ann Transplant, 2018. **23**: p. 789-801.
265. Rajbhandari, R. and R.T. Chung, *Treatment of Hepatitis B: A Concise Review*. Clin Transl Gastroenterol, 2016. **7**(9): p. e190.
266. Westin, J., et al., *Management of hepatitis B virus infection, updated Swedish guidelines*. Infect Dis (Lond), 2020. **52**(1): p. 1-22.
267. Belloni, L., et al., *IFN-alpha inhibits HBV transcription and replication in cell culture and in humanized mice by targeting the epigenetic regulation of the nuclear cccDNA minichromosome*. J Clin Invest, 2012. **122**(2): p. 529-37.
268. Allweiss, L., et al., *Immune cell responses are not required to induce substantial hepatitis B virus antigen decline during pegylated interferon-alpha administration*. J Hepatol, 2014. **60**(3): p. 500-7.
269. Zoulim, F., F. Lebosse, and M. Levvero, *Current treatments for chronic hepatitis B virus infections*. Curr Opin Virol, 2016. **18**: p. 109-16.

270. Bonino, F., et al., *Predicting response to peginterferon alpha-2a, lamivudine and the two combined for HBeAg-negative chronic hepatitis B*. Gut, 2007. **56**(5): p. 699-705.
271. Marcellin, P., et al., *Comparing the safety, tolerability and quality of life in patients with chronic hepatitis B vs chronic hepatitis C treated with peginterferon alpha-2a*. Liver Int, 2008. **28**(4): p. 477-85.
272. Tang, C.M., T.O. Yau, and J. Yu, *Management of chronic hepatitis B infection: current treatment guidelines, challenges, and new developments*. World J Gastroenterol, 2014. **20**(20): p. 6262-78.
273. Fung, S.K. and A.S. Lok, *Treatment of chronic hepatitis B: who to treat, what to use, and for how long?* Clin Gastroenterol Hepatol, 2004. **2**(10): p. 839-48.
274. Group, C.H.C., *Treatment of chronic viral hepatitis with alpha-interferon: A consensus conference report*. Can J Infect Dis, 1994. **5**(3): p. 107-12.
275. Janssen, H.L., et al., *Pegylated interferon alfa-2b alone or in combination with lamivudine for HBeAg-positive chronic hepatitis B: a randomised trial*. Lancet, 2005. **365**(9454): p. 123-9.
276. Doo, E. and T.J. Liang, *Molecular anatomy and pathophysiologic implications of drug resistance in hepatitis B virus infection*. Gastroenterology, 2001. **120**(4): p. 1000-8.
277. Klein, C., et al., *Inhibition of hepatitis B virus replication in vivo by nucleoside analogues and siRNA*. Gastroenterology, 2003. **125**(1): p. 9-18.
278. Boni, C., et al., *HBV Immune-Therapy: From Molecular Mechanisms to Clinical Applications*. Int J Mol Sci, 2019. **20**(11).
279. Grimm, D., R. Thimme, and H.E. Blum, *HBV life cycle and novel drug targets*. Hepatol Int, 2011. **5**(2): p. 644-53.
280. Lampertico, P., *Discontinuation of nucleoside analogues in hepatitis B virus infection*. Gastroenterol Hepatol (N Y), 2013. **9**(10): p. 656-8.
281. Fischer, K.P., K.S. Gutfreund, and D.L. Tyrrell, *Lamivudine resistance in hepatitis B: mechanisms and clinical implications*. Drug Resist Updat, 2001. **4**(2): p. 118-28.
282. Bartholomew, M.M., et al., *Hepatitis-B-virus resistance to lamivudine given for recurrent infection after orthotopic liver transplantation*. Lancet, 1997. **349**(9044): p. 20-2.
283. Pallier, C., et al., *Dynamics of hepatitis B virus resistance to lamivudine*. J Virol, 2006. **80**(2): p. 643-53.
284. Lai, C.L., et al., *Telbivudine versus lamivudine in patients with chronic hepatitis B*. N Engl J Med, 2007. **357**(25): p. 2576-88.
285. Hadziyannis, S.J., et al., *Long-term therapy with adefovir dipivoxil for HBeAg-negative chronic hepatitis B for up to 5 years*. Gastroenterology, 2006. **131**(6): p. 1743-51.
286. van Bommel, F., et al., *Long-term efficacy of tenofovir monotherapy for hepatitis B virus-monoinfected patients after failure of nucleoside/nucleotide analogues*. Hepatology, 2010. **51**(1): p. 73-80.
287. Chang, T.T., et al., *A comparison of entecavir and lamivudine for HBeAg-positive chronic hepatitis B*. N Engl J Med, 2006. **354**(10): p. 1001-10.
288. Lai, C.L., et al., *Entecavir versus lamivudine for patients with HBeAg-negative chronic hepatitis B*. N Engl J Med, 2006. **354**(10): p. 1011-20.
289. Yuen, M.F. and C.L. Lai, *Treatment of chronic hepatitis B: Evolution over two decades*. J Gastroenterol Hepatol, 2011. **26 Suppl 1**: p. 138-43.
290. Standring, D.N., et al., *Antiviral beta-L-nucleosides specific for hepatitis B virus infection*. Antivir Chem Chemother, 2001. **12 Suppl 1**: p. 119-29.
291. Revill, P., et al., *Global strategies are required to cure and eliminate HBV infection*. Nat Rev Gastroenterol Hepatol, 2016. **13**(4): p. 239-48.
292. Nijampatnam, B. and D.C. Liotta, *Recent advances in the development of HBV capsid assembly modulators*. Curr Opin Chem Biol, 2019. **50**: p. 73-79.
293. Dawood, A., et al., *Drugs in Development for Hepatitis B*. Drugs, 2017. **77**(12): p. 1263-1280.
294. Blank, A., et al., *The NTCP-inhibitor Myrcludex B: Effects on Bile Acid Disposition and Tenofovir Pharmacokinetics*. Clin Pharmacol Ther, 2018. **103**(2): p. 341-348.

295. Chien, R.N. and Y.F. Liaw, *Nucleos(t)ide analogues for hepatitis B virus: strategies for long-term success*. Best Pract Res Clin Gastroenterol, 2008. **22**(6): p. 1081-92.
296. Chisari, F.V., M. Isogawa, and S.F. Wieland, *Pathogenesis of hepatitis B virus infection*. Pathol Biol (Paris), 2010. **58**(4): p. 258-66.
297. Wieland, S.F., et al., *Expansion and contraction of the hepatitis B virus transcriptional template in infected chimpanzees*. Proc Natl Acad Sci U S A, 2004. **101**(7): p. 2129-34.
298. Zeisel, M.B., et al., *Towards an HBV cure: state-of-the-art and unresolved questions--report of the ANRS workshop on HBV cure*. Gut, 2015. **64**(8): p. 1314-26.
299. Lutgehetmann, M., et al., *In vivo proliferation of hepadnavirus-infected hepatocytes induces loss of covalently closed circular DNA in mice*. Hepatology, 2010. **52**(1): p. 16-24.
300. Bernardi, R. and P.P. Pandolfi, *Structure, dynamics and functions of promyelocytic leukaemia nuclear bodies*. Nat Rev Mol Cell Biol, 2007. **8**(12): p. 1006-16.
301. Salomoni, P. and P.P. Pandolfi, *The role of PML in tumor suppression*. Cell, 2002. **108**(2): p. 165-70.
302. Lallemand-Breitenbach, V. and H. de The, *PML nuclear bodies*. Cold Spring Harb Perspect Biol, 2010. **2**(5): p. a000661.
303. Shen, T.H., et al., *The mechanisms of PML-nuclear body formation*. Mol Cell, 2006. **24**(3): p. 331-9.
304. Van Damme, E., et al., *A manually curated network of the PML nuclear body interactome reveals an important role for PML-NBs in SUMOylation dynamics*. Int J Biol Sci, 2010. **6**(1): p. 51-67.
305. Ishov, A.M., et al., *PML is critical for ND10 formation and recruits the PML-interacting protein daxx to this nuclear structure when modified by SUMO-1*. J Cell Biol, 1999. **147**(2): p. 221-34.
306. Rivera-Molina, Y.A., F.P. Martinez, and Q. Tang, *Nuclear domain 10 of the viral aspect*. World J Virol, 2013. **2**(3): p. 110-22.
307. Xu, Z.X., et al., *PML colocalizes with and stabilizes the DNA damage response protein TopBP1*. Mol Cell Biol, 2003. **23**(12): p. 4247-56.
308. Dellaire, G. and D.P. Bazett-Jones, *PML nuclear bodies: dynamic sensors of DNA damage and cellular stress*. Bioessays, 2004. **26**(9): p. 963-977.
309. Everett, R.D., et al., *PML contributes to a cellular mechanism of repression of herpes simplex virus type 1 infection that is inactivated by ICP0*. J Virol, 2006. **80**(16): p. 7995-8005.
310. Sahin, U., et al., *Oxidative stress-induced assembly of PML nuclear bodies controls sumoylation of partner proteins*. J Cell Biol, 2014. **204**(6): p. 931-45.
311. Terris, B., et al., *PML nuclear bodies are general targets for inflammation and cell proliferation*. Cancer Res, 1995. **55**(7): p. 1590-7.
312. Everett, R.D., *DNA viruses and viral proteins that interact with PML nuclear bodies*. Oncogene, 2001. **20**(49): p. 7266-73.
313. Jensen, K., C. Shiels, and P.S. Freemont, *PML protein isoforms and the RBCC/TRIM motif*. Oncogene, 2001. **20**(49): p. 7223-33.
314. Nisole, S., et al., *Differential Roles of PML Isoforms*. Front Oncol, 2013. **3**: p. 125.
315. Fagioli, M., et al., *Alternative splicing of PML transcripts predicts coexpression of several carboxy-terminally different protein isoforms*. Oncogene, 1992. **7**(6): p. 1083-91.
316. Alcalay, M., et al., *Expression pattern of the RAR alpha-PML fusion gene in acute promyelocytic leukemia*. Proc Natl Acad Sci U S A, 1992. **89**(11): p. 4840-4.
317. de The, H., et al., *The PML-RAR alpha fusion mRNA generated by the t(15;17) translocation in acute promyelocytic leukemia encodes a functionally altered RAR*. Cell, 1991. **66**(4): p. 675-84.
318. Goddard, A.D., et al., *Characterization of a zinc finger gene disrupted by the t(15;17) in acute promyelocytic leukemia*. Science, 1991. **254**(5036): p. 1371-4.

319. Kakizuka, A., et al., *Chromosomal translocation t(15;17) in human acute promyelocytic leukemia fuses RAR alpha with a novel putative transcription factor, PML*. Cell, 1991. **66**(4): p. 663-74.
320. Kastner, P., et al., *Structure, localization and transcriptional properties of two classes of retinoic acid receptor alpha fusion proteins in acute promyelocytic leukemia (APL): structural similarities with a new family of oncoproteins*. EMBO J, 1992. **11**(2): p. 629-42.
321. Fagioli, M., et al., *Cooperation between the RING + B1-B2 and coiled-coil domains of PML is necessary for its effects on cell survival*. Oncogene, 1998. **16**(22): p. 2905-13.
322. Borden, K.L., *Pondering the promyelocytic leukemia protein (PML) puzzle: possible functions for PML nuclear bodies*. Mol Cell Biol, 2002. **22**(15): p. 5259-69.
323. Everett, R.D. and M.K. Chelbi-Alix, *PML and PML nuclear bodies: implications in antiviral defence*. Biochimie, 2007. **89**(6-7): p. 819-30.
324. Maroui, M.A., M. Pampin, and M.K. Chelbi-Alix, *Promyelocytic leukemia isoform IV confers resistance to encephalomyocarditis virus via the sequestration of 3D polymerase in nuclear bodies*. J Virol, 2011. **85**(24): p. 13164-73.
325. Bernardi, R., A. Papa, and P.P. Pandolfi, *Regulation of apoptosis by PML and the PML-NBs*. Oncogene, 2008. **27**(48): p. 6299-312.
326. Pearson, M., et al., *PML regulates p53 acetylation and premature senescence induced by oncogenic Ras*. Nature, 2000. **406**(6792): p. 207-10.
327. Everett, R.D., *Interactions between DNA viruses, ND10 and the DNA damage response*. Cell Microbiol, 2006. **8**(3): p. 365-74.
328. Yang, S., et al., *Promyelocytic leukemia activates Chk2 by mediating Chk2 autophosphorylation*. J Biol Chem, 2006. **281**(36): p. 26645-54.
329. Park, S.W., et al., *SUMOylation of Tr2 orphan receptor involves Pml and fine-tunes Oct4 expression in stem cells*. Nat Struct Mol Biol, 2007. **14**(1): p. 68-75.
330. Song, M.S., et al., *The deubiquitylation and localization of PTEN are regulated by a HAUSP-PML network*. Nature, 2008. **455**(7214): p. 813-7.
331. St-Germain, J.R., J. Chen, and Q. Li, *Involvement of PML nuclear bodies in CBP degradation through the ubiquitin-proteasome pathway*. Epigenetics, 2008. **3**(6): p. 342-9.
332. Stubbe, M., et al., *Viral DNA Binding Protein SUMOylation Promotes PML Nuclear Body Localization Next to Viral Replication Centers*. mBio, 2020. **11**(2).
333. Grotzinger, T., et al., *Interferon-modulated expression of genes encoding the nuclear-dot-associated proteins Sp100 and promyelocytic leukemia protein (PML)*. Eur J Biochem, 1996. **238**(2): p. 554-60.
334. Guldner, H.H., et al., *Splice variants of the nuclear dot-associated Sp100 protein contain homologies to HMG-1 and a human nuclear phosphoprotein-box motif*. J Cell Sci, 1999. **112** ( Pt 5): p. 733-47.
335. Negorev, D.G., et al., *Differential role of Sp100 isoforms in interferon-mediated repression of herpes simplex virus type 1 immediate-early protein expression*. J Virol, 2006. **80**(16): p. 8019-29.
336. Berscheminski, J., et al., *Sp100 isoform-specific regulation of human adenovirus 5 gene expression*. J Virol, 2014. **88**(11): p. 6076-92.
337. Newhart, A., et al., *Sp100A promotes chromatin decondensation at a cytomegalovirus-promoter-regulated transcription site*. Mol Biol Cell, 2013. **24**(9): p. 1454-68.
338. Wilcox, K.W., et al., *SP100B is a repressor of gene expression*. J Cell Biochem, 2005. **95**(2): p. 352-65.
339. Negorev, D.G., O.V. Vladimirova, and G.G. Maul, *Differential functions of interferon-upregulated Sp100 isoforms: herpes simplex virus type 1 promoter-based immediate-early gene suppression and PML protection from ICP0-mediated degradation*. J Virol, 2009. **83**(10): p. 5168-80.

- 
340. Isaac, A., K.W. Wilcox, and J.L. Taylor, *SP100B, a repressor of gene expression preferentially binds to DNA with unmethylated CpGs*. *J Cell Biochem*, 2006. **98**(5): p. 1106-22.
341. Bottomley, M.J., et al., *The SAND domain structure defines a novel DNA-binding fold in transcriptional regulation*. *Nat Struct Biol*, 2001. **8**(7): p. 626-33.
342. Seeler, J.S., et al., *Interaction of SP100 with HP1 proteins: a link between the promyelocytic leukemia-associated nuclear bodies and the chromatin compartment*. *Proc Natl Acad Sci U S A*, 1998. **95**(13): p. 7316-21.
343. Muller, S. and A. Dejean, *Viral immediate-early proteins abrogate the modification by SUMO-1 of PML and Sp100 proteins, correlating with nuclear body disruption*. *J Virol*, 1999. **73**(6): p. 5137-43.
344. Seeler, J.S., et al., *Common properties of nuclear body protein SP100 and TIF1alpha chromatin factor: role of SUMO modification*. *Mol Cell Biol*, 2001. **21**(10): p. 3314-24.
345. Lehming, N., et al., *Chromatin components as part of a putative transcriptional repressing complex*. *Proc Natl Acad Sci U S A*, 1998. **95**(13): p. 7322-6.
346. Schultz, D.C., et al., *SETDB1: a novel KAP-1-associated histone H3, lysine 9-specific methyltransferase that contributes to HP1-mediated silencing of euchromatic genes by KRAB zinc-finger proteins*. *Genes Dev*, 2002. **16**(8): p. 919-32.
347. Cho, S., J.S. Park, and Y.K. Kang, *Dual functions of histone-lysine N-methyltransferase Setdb1 protein at promyelocytic leukemia-nuclear body (PML-NB): maintaining PML-NB structure and regulating the expression of its associated genes*. *J Biol Chem*, 2011. **286**(47): p. 41115-24.
348. Li, Y., et al., *Effects of tethering HP1 to euchromatic regions of the Drosophila genome*. *Development*, 2003. **130**(9): p. 1817-24.
349. Niu, C., et al., *The Smc5/6 Complex Restricts HBV when Localized to ND10 without Inducing an Innate Immune Response and Is Counteracted by the HBV X Protein Shortly after Infection*. *PLoS One*, 2017. **12**(1): p. e0169648.
350. Zhong, S., et al., *Role of SUMO-1-modified PML in nuclear body formation*. *Blood*, 2000. **95**(9): p. 2748-52.
351. Bayer, P., et al., *Structure Determination of the Small Ubiquitin-related Modifier SUMO-1*. *J Mol Biol*, 1998. **280**: p. 275-286.
352. Gill, G., *SUMO and ubiquitin in the nucleus: different functions, similar mechanisms?* *Genes Dev*, 2004. **18**(17): p. 2046-59.
353. Johnson, E.S., *Protein modification by SUMO*. *Annu Rev Biochem*, 2004. **73**: p. 355-82.
354. Matunis, M.J., E. Coutavas, and G. Blobel, *A novel ubiquitin-like modification modulates the partitioning of the Ran-GTPase-activating protein RanGAP1 between the cytosol and the nuclear pore complex*. *J Cell Biol*, 1996. **135**(6 Pt 1): p. 1457-70.
355. Muller, S., et al., *SUMO, ubiquitin's mysterious cousin*. *Nat Rev Mol Cell Biol*, 2001. **2**(3): p. 202-10.
356. Hannoun, Z., et al., *Post-translational modification by SUMO*. *Toxicology*, 2010. **278**(3): p. 288-93.
357. Wimmer, P. and S. Schreiner, *Viral Mimicry to Usurp Ubiquitin and SUMO Host Pathways*. *Viruses*, 2015. **7**(9): p. 4854-72.
358. Nayak, A. and S. Müller, *SUMO-specific proteases/isopeptidases: SENPs and beyond*. *Genome Biology*, 2014. **15**.
359. Mukhopadhyay, D. and M. Dasso, *Modification in reverse: the SUMO proteases*. *Trends Biochem Sci*, 2007. **32**(6): p. 286-95.
360. Hilgarth, R.S., et al., *Regulation and function of SUMO modification*. *J Biol Chem*, 2004. **279**(52): p. 53899-902.
361. Hay, R.T., *SUMO: a history of modification*. *Mol Cell*, 2005. **18**(1): p. 1-12.
362. Desterro, J.M., et al., *Identification of the enzyme required for activation of the small ubiquitin-like protein SUMO-1*. *J Biol Chem*, 1999. **274**(15): p. 10618-24.

363. Gong, L., et al., *Molecular cloning and characterization of human AOS1 and UBA2, components of the sentrin-activating enzyme complex*. FEBS Lett, 1999. **448**(1): p. 185-9.
364. Johnson, E.S. and G. Blobel, *Ubc9p is the conjugating enzyme for the ubiquitin-like protein Smt3p*. J Biol Chem, 1997. **272**(43): p. 26799-802.
365. Okuma, T., et al., *In vitro SUMO-1 modification requires two enzymatic steps, E1 and E2*. Biochem Biophys Res Commun, 1999. **254**(3): p. 693-8.
366. Olsen, S.K., et al., *Active site remodelling accompanies thioester bond formation in the SUMO E1*. Nature, 2010. **463**(7283): p. 906-12.
367. Schulman, B.A. and J.W. Harper, *Ubiquitin-like protein activation by E1 enzymes: the apex for downstream signalling pathways*. Nat Rev Mol Cell Biol, 2009. **10**(5): p. 319-31.
368. Knipscheer, P., et al., *Ubc9 sumoylation regulates SUMO target discrimination*. Mol Cell, 2008. **31**(3): p. 371-82.
369. Desterro, J.M.P., J. Thomson, and R.T. Hay, *Ubch9 conjugates SUMO but not ubiquitin*. FEBS Letters, 1997. **417**(3): p. 297-300.
370. Tatham, M.H., et al., *Role of an N-terminal site of Ubc9 in SUMO-1, -2, and -3 binding and conjugation*. Biochemistry, 2003. **42**(33): p. 9959-69.
371. Wimmer, P., S. Schreiner, and T. Dobner, *Human pathogens and the host cell SUMOylation system*. J Virol, 2012. **86**(2): p. 642-54.
372. Pichler, A., et al., *SUMO conjugation - a mechanistic view*. Biomol Concepts, 2017. **8**(1): p. 13-36.
373. Gareau, J.R. and C.D. Lima, *The SUMO pathway: emerging mechanisms that shape specificity, conjugation and recognition*. Nat Rev Mol Cell Biol, 2010. **11**(12): p. 861-71.
374. Rodriguez, M.S., C. Dargemont, and R.T. Hay, *SUMO-1 conjugation in vivo requires both a consensus modification motif and nuclear targeting*. J Biol Chem, 2001. **276**(16): p. 12654-9.
375. Sampson, D.A., M. Wang, and M.J. Matunis, *The small ubiquitin-like modifier-1 (SUMO-1) consensus sequence mediates Ubc9 binding and is essential for SUMO-1 modification*. J Biol Chem, 2001. **276**(24): p. 21664-9.
376. Yunus, A.A. and C.D. Lima, *Lysine activation and functional analysis of E2-mediated conjugation in the SUMO pathway*. Nat Struct Mol Biol, 2006. **13**(6): p. 491-9.
377. Ijaz, A., *SUMOhunt: Combining Spatial Staging between Lysine and SUMO with Random Forests to Predict SUMOylation*. ISRN Bioinform, 2013. **2013**: p. 671269.
378. Nayak, A. and S. Muller, *SUMO-specific proteases/isopeptidases: SENPs and beyond*. Genome Biol, 2014. **15**(7): p. 422.
379. Kunz, K., T. Piller, and S. Muller, *SUMO-specific proteases and isopeptidases of the SENP family at a glance*. J Cell Sci, 2018. **131**(6).
380. Yeh, E.T., L. Gong, and T. Kamitani, *Ubiquitin-like proteins: new wines in new bottles*. Gene, 2000. **248**(1-2): p. 1-14.
381. Hickey, C.M., N.R. Wilson, and M. Hochstrasser, *Function and regulation of SUMO proteases*. Nat Rev Mol Cell Biol, 2012. **13**(12): p. 755-66.
382. Schwartz, D.C. and M. Hochstrasser, *A superfamily of protein tags: ubiquitin, SUMO and related modifiers*. Trends Biochem Sci, 2003. **28**(6): p. 321-8.
383. Xu, J., et al., *A novel method for high accuracy sumoylation site prediction from protein sequences*. BMC Bioinformatics, 2008. **9**: p. 8.
384. Kerscher, O., *SUMO junction-what's your function? New insights through SUMO-interacting motifs*. EMBO Rep, 2007. **8**(6): p. 550-5.
385. Minty, A., et al., *Covalent modification of p73alpha by SUMO-1. Two-hybrid screening with p73 identifies novel SUMO-1-interacting proteins and a SUMO-1 interaction motif*. J Biol Chem, 2000. **275**(46): p. 36316-23.
386. Yuan, H., et al., *Small ubiquitin-related modifier paralogs are indispensable but functionally redundant during early development of zebrafish*. Cell Res, 2010. **20**(2): p. 185-96.

387. Tatham, M.H., et al., *Polymeric chains of SUMO-2 and SUMO-3 are conjugated to protein substrates by SAE1/SAE2 and Ubc9*. J Biol Chem, 2001. **276**(38): p. 35368-74.
388. Saitoh, H. and J. Hinchev, *Functional heterogeneity of small ubiquitin-related protein modifiers SUMO-1 versus SUMO-2/3*. J Biol Chem, 2000. **275**(9): p. 6252-8.
389. Gocke, C.B., H. Yu, and J. Kang, *Systematic identification and analysis of mammalian small ubiquitin-like modifier substrates*. J Biol Chem, 2005. **280**(6): p. 5004-12.
390. Yang, M., et al., *Assembly of a polymeric chain of SUMO1 on human topoisomerase I in vitro*. J Biol Chem, 2006. **281**(12): p. 8264-74.
391. Wang, Y. and M. Dasso, *SUMOylation and deSUMOylation at a glance*. J Cell Sci, 2009. **122**(Pt 23): p. 4249-52.
392. Matic, I., et al., *In vivo identification of human small ubiquitin-like modifier polymerization sites by high accuracy mass spectrometry and an in vitro to in vivo strategy*. Mol Cell Proteomics, 2008. **7**(1): p. 132-44.
393. Wilkinson, K.A. and J.M. Henley, *Mechanisms, regulation and consequences of protein SUMOylation*. Biochem J, 2010. **428**(2): p. 133-45.
394. Bohren, K.M., et al., *A M55V polymorphism in a novel SUMO gene (SUMO-4) differentially activates heat shock transcription factors and is associated with susceptibility to type I diabetes mellitus*. J Biol Chem, 2004. **279**(26): p. 27233-8.
395. Liang, Y.C., et al., *SUMO5, a Novel Poly-SUMO Isoform, Regulates PML Nuclear Bodies*. Sci Rep, 2016. **6**: p. 26509.
396. Peroutka, R.J., et al., *Enhanced protein expression in mammalian cells using engineered SUMO fusions: secreted phospholipase A2*. Protein Sci, 2008. **17**(9): p. 1586-95.
397. Desterro, J.M., M.S. Rodriguez, and R.T. Hay, *SUMO-1 modification of I $\kappa$ B inhibits NF- $\kappa$ B activation*. Mol Cell, 1998. **2**(2): p. 233-9.
398. Zhao, J., *Sumoylation regulates diverse biological processes*. Cell Mol Life Sci, 2007. **64**(23): p. 3017-33.
399. Park, I.S., et al., *SUMOylation regulates nuclear localization and stability of TRAIIP/RNF206*. Biochem Biophys Res Commun, 2016. **470**(4): p. 881-7.
400. Wen, D., et al., *SUMOylation Promotes Nuclear Import and Stabilization of Polo-like Kinase 1 to Support Its Mitotic Function*. Cell Rep, 2017. **21**(8): p. 2147-2159.
401. Tossidou, I., et al., *SUMOylation determines turnover and localization of nephrin at the plasma membrane*. Kidney Int, 2014. **86**(6): p. 1161-73.
402. Yang, Y., et al., *Protein SUMOylation modification and its associations with disease*. Open Biol, 2017. **7**(10).
403. Cubenas-Potts, C. and M.J. Matunis, *SUMO: a multifaceted modifier of chromatin structure and function*. Dev Cell, 2013. **24**(1): p. 1-12.
404. Gomez-del Arco, P., J. Koipally, and K. Georgopoulos, *Ikaros SUMOylation: switching out of repression*. Mol Cell Biol, 2005. **25**(7): p. 2688-97.
405. Gill, G., *Something about SUMO inhibits transcription*. Curr Opin Genet Dev, 2005. **15**(5): p. 536-41.
406. Kotaja, N., et al., *The nuclear receptor interaction domain of GRIP1 is modulated by covalent attachment of SUMO-1*. J Biol Chem, 2002. **277**(33): p. 30283-8.
407. Hofmann, H., S. Floss, and T. Stamminger, *Covalent modification of the transactivator protein IE2-p86 of human cytomegalovirus by conjugation to the ubiquitin-homologous proteins SUMO-1 and hSMT3b*. J Virol, 2000. **74**(6): p. 2510-24.
408. Hong, Y., et al., *Regulation of heat shock transcription factor 1 by stress-induced SUMO-1 modification*. J Biol Chem, 2001. **276**(43): p. 40263-7.
409. Goodson, M.L., et al., *Sumo-1 modification regulates the DNA binding activity of heat shock transcription factor 2, a promyelocytic leukemia nuclear body associated transcription factor*. J Biol Chem, 2001. **276**(21): p. 18513-8.
410. He, X., et al., *Characterization of the loss of SUMO pathway function on cancer cells and tumor proliferation*. PLoS One, 2015. **10**(4): p. e0123882.

411. Su, C.I., et al., *SUMO Modification Stabilizes Dengue Virus Nonstructural Protein 5 To Support Virus Replication*. J Virol, 2016. **90**(9): p. 4308-19.
412. Sohn, S.Y. and P. Hearing, *Adenovirus Early Proteins and Host Sumoylation*. mBio, 2016. **7**(5).
413. Sun, H., J.D. Levenson, and T. Hunter, *Conserved function of RNF4 family proteins in eukaryotes: targeting a ubiquitin ligase to SUMOylated proteins*. EMBO J, 2007. **26**(18): p. 4102-12.
414. Sriramachandran, A.M. and R.J. Dohmen, *SUMO-targeted ubiquitin ligases*. Biochim Biophys Acta, 2014. **1843**(1): p. 75-85.
415. Sriramachandran, A.M., et al., *Arkadia/RNF111 is a SUMO-targeted ubiquitin ligase with preference for substrates marked with SUMO1-capped SUMO2/3 chain*. Nat Commun, 2019. **10**(1): p. 3678.
416. Kumar, R., et al., *The STUbL RNF4 regulates protein group SUMOylation by targeting the SUMO conjugation machinery*. Nat Commun, 2017. **8**(1): p. 1809.
417. Xu, Y., et al., *Structural insight into SUMO chain recognition and manipulation by the ubiquitin ligase RNF4*. Nat Commun, 2014. **5**: p. 4217.
418. Liew, C.W., et al., *RING domain dimerization is essential for RNF4 function*. Biochem J, 2010. **431**(1): p. 23-9.
419. Plechanovova, A., et al., *Mechanism of ubiquitylation by dimeric RING ligase RNF4*. Nat Struct Mol Biol, 2011. **18**(9): p. 1052-9.
420. Plechanovova, A., et al., *Structure of a RING E3 ligase and ubiquitin-loaded E2 primed for catalysis*. Nature, 2012. **489**(7414): p. 115-20.
421. Pickart, C.M., *Mechanisms underlying ubiquitination*. Annu Rev Biochem, 2001. **70**: p. 503-33.
422. Deshaies, R.J. and C.A. Joazeiro, *RING domain E3 ubiquitin ligases*. Annu Rev Biochem, 2009. **78**: p. 399-434.
423. Lallemand-Breitenbach, V., et al., *Arsenic degrades PML or PML-RARalpha through a SUMO-triggered RNF4/ubiquitin-mediated pathway*. Nat Cell Biol, 2008. **10**(5): p. 547-55.
424. Kuo, C.Y., et al., *An arginine-rich motif of ring finger protein 4 (RNF4) oversees the recruitment and degradation of the phosphorylated and SUMOylated Kruppel-associated box domain-associated protein 1 (KAP1)/TRIM28 protein during genotoxic stress*. J Biol Chem, 2014. **289**(30): p. 20757-72.
425. Bruderer, R., et al., *Purification and identification of endogenous polySUMO conjugates*. EMBO Rep, 2011. **12**(2): p. 142-8.
426. Muncheberg, S., et al., *E1B-55K-Mediated Regulation of RNF4 SUMO-Targeted Ubiquitin Ligase Promotes Human Adenovirus Gene Expression*. J Virol, 2018. **92**(13).
427. Percherancier, Y., et al., *Role of SUMO in RNF4-mediated promyelocytic leukemia protein (PML) degradation: sumoylation of PML and phospho-switch control of its SUMO binding domain dissected in living cells*. J Biol Chem, 2009. **284**(24): p. 16595-608.
428. Maroui, M.A., et al., *Requirement of PML SUMO interacting motif for RNF4- or arsenic trioxide-induced degradation of nuclear PML isoforms*. PLoS One, 2012. **7**(9): p. e44949.
429. Weisshaar, S.R., et al., *Arsenic trioxide stimulates SUMO-2/3 modification leading to RNF4-dependent proteolytic targeting of PML*. FEBS Lett, 2008. **582**(21-22): p. 3174-8.
430. HD Sun, L.M., XC Hu, TD Zhang, HDML Sun, *Ai-lin 1 treated 32 cases of acute promyelocytic leukemia*. Chin J Integrat Chin West Med, 1992.
431. Waxman, S. and K.C. Anderson, *History of the development of arsenic derivatives in cancer therapy*. Oncologist, 2001. **6 Suppl 2**: p. 3-10.
432. Emadi, A. and S.D. Gore, *Arsenic trioxide - An old drug rediscovered*. Blood Rev, 2010. **24**(4-5): p. 191-9.

433. A. Cowan Doyle, M.B., C. M. EDIN *Notes of a case of leukocythaemia.* . The Lancet, 1882. **119**(3056).
434. List, A., et al., *Opportunities for Trisenox (arsenic trioxide) in the treatment of myelodysplastic syndromes.* Leukemia, 2003. **17**(8): p. 1499-507.
435. Soignet, S.L., et al., *United States multicenter study of arsenic trioxide in relapsed acute promyelocytic leukemia.* J Clin Oncol, 2001. **19**(18): p. 3852-60.
436. Raelson, J.V., et al., *The PML/RAR alpha oncoprotein is a direct molecular target of retinoic acid in acute promyelocytic leukemia cells.* Blood, 1996. **88**(8): p. 2826-32.
437. Grignani, F., et al., *The acute promyelocytic leukemia-specific PML-RAR alpha fusion protein inhibits differentiation and promotes survival of myeloid precursor cells.* Cell, 1993. **74**(3): p. 423-31.
438. Pandolfi, P.P., et al., *Structure and origin of the acute promyelocytic leukemia myl/RAR alpha cDNA and characterization of its retinoid-binding and transactivation properties.* Oncogene, 1991. **6**(7): p. 1285-92.
439. Jeanne, M., et al., *PML/RARA oxidation and arsenic binding initiate the antileukemia response of As<sub>2</sub>O<sub>3</sub>.* Cancer Cell, 2010. **18**(1): p. 88-98.
440. Zhang, X.W., et al., *Arsenic trioxide controls the fate of the PML-RARalpha oncoprotein by directly binding PML.* Science, 2010. **328**(5975): p. 240-3.
441. de The, H., M. Le Bras, and V. Lallemand-Breitenbach, *The cell biology of disease: Acute promyelocytic leukemia, arsenic, and PML bodies.* J Cell Biol, 2012. **198**(1): p. 11-21.
442. Lallemand-Breitenbach, V., et al., *Role of promyelocytic leukemia (PML) sumolation in nuclear body formation, 11S proteasome recruitment, and As<sub>2</sub>O<sub>3</sub>-induced PML or PML/retinoic acid receptor alpha degradation.* J Exp Med, 2001. **193**(12): p. 1361-71.
443. Niu, C., et al., *Studies on treatment of acute promyelocytic leukemia with arsenic trioxide: remission induction, follow-up, and molecular monitoring in 11 newly diagnosed and 47 relapsed acute promyelocytic leukemia patients.* Blood, 1999. **94**(10): p. 3315-24.
444. Shen, Z.X., et al., *Use of arsenic trioxide (As<sub>2</sub>O<sub>3</sub>) in the treatment of acute promyelocytic leukemia (APL): II. Clinical efficacy and pharmacokinetics in relapsed patients.* Blood, 1997. **89**(9): p. 3354-60.
445. Alimoghaddam, K., et al., *Treatment of relapsed acute promyelocytic leukemia by arsenic trioxide in Iran.* Arch Iran Med, 2011. **14**(3): p. 167-9.
446. Ghavamzadeh, A., et al., *Phase II study of single-agent arsenic trioxide for the front-line therapy of acute promyelocytic leukemia.* J Clin Oncol, 2011. **29**(20): p. 2753-7.
447. Alimoghaddam, K., et al., *Anti-leukemic and anti-angiogenesis efficacy of arsenic trioxide in new cases of acute promyelocytic leukemia.* Leuk Lymphoma, 2006. **47**(1): p. 81-8.
448. Hofmann, S., et al., *ATO (Arsenic Trioxide) Effects on Promyelocytic Leukemia Nuclear Bodies Reveals Antiviral Intervention Capacity.* Adv Sci (Weinh), 2020. **7**(8): p. 1902130.
449. Chung, Y.L. and M.L. Wu, *Dual oncogenic and tumor suppressor roles of the promyelocytic leukemia gene in hepatocarcinogenesis associated with hepatitis B virus surface antigen.* Oncotarget, 2016. **7**(19): p. 28393-407.
450. Hsu, L.I., et al., *Effects of Arsenic in Drinking Water on Risk of Hepatitis or Cirrhosis in Persons With and Without Chronic Viral Hepatitis.* Clin Gastroenterol Hepatol, 2016. **14**(9): p. 1347-1355 e4.
451. Cardenas, A., et al., *Cross sectional association of arsenic and seroprevalence of hepatitis B infection in the United States (NHANES 2003-2014).* Environ Res, 2018. **166**: p. 570-576.
452. Zhang, W.H., et al., *Elevated Arsenic Exposure Is Associated with an Increased Risk of Chronic Hepatitis B Virus Infection: NHANES (2003-2014) in U.S. Adults.* Curr Med Sci, 2018. **38**(4): p. 610-617.

453. Gripon, P., et al., *Infection of a human hepatoma cell line by hepatitis B virus*. Proc Natl Acad Sci U S A, 2002. **99**(24): p. 15655-60.
454. Vertegaal, A.C., et al., *A proteomic study of SUMO-2 target proteins*. J Biol Chem, 2004. **279**(32): p. 33791-8.
455. Sloan, E., et al., *Analysis of the SUMO2 Proteome during HSV-1 Infection*. PLoS Pathog, 2015. **11**(7): p. e1005059.
456. Mitsudomi, T., et al., *p53 gene mutations in non-small-cell lung cancer cell lines and their correlation with the presence of ras mutations and clinical features*. Oncogene, 1992. **7**(1): p. 171-80.
457. Schreiner, S., et al., *Proteasome-dependent degradation of Daxx by the viral E1B-55K protein in human adenovirus-infected cells*. J Virol, 2010. **84**(14): p. 7029-38.
458. Hanahan, D., *Studies on transformation of Escherichia coli with plasmids*. J Mol Biol, 1983. **166**(4): p. 557-80.
459. Ladner, S.K., et al., *Inducible expression of human hepatitis B virus (HBV) in stably transfected hepatoblastoma cells: a novel system for screening potential inhibitors of HBV replication*. Antimicrob Agents Chemother, 1997. **41**(8): p. 1715-20.
460. Cuchet, D., et al., *PML isoforms I and II participate in PML-dependent restriction of HSV-1 replication*. J Cell Sci, 2011. **124**(Pt 2): p. 280-91.
461. Zhao, Q., et al., *GPS-SUMO: a tool for the prediction of sumoylation sites and SUMO-interaction motifs*. Nucleic Acids Res, 2014. **42**(Web Server issue): p. W325-30.
462. Ren, J., et al., *Systematic study of protein sumoylation: Development of a site-specific predictor of SUMOsp 2.0*. Proteomics, 2009. **9**(12): p. 3409-3412.
463. Schneider, C.A., W.S. Rasband, and K.W. Eliceiri, *NIH Image to ImageJ: 25 years of image analysis*. Nat Methods, 2012. **9**(7): p. 671-5.
464. Bradford, M.M., *A rapid and sensitive method for the quantitation of microgram quantities of protein utilizing the principle of protein-dye binding*. Anal Biochem, 1976. **72**: p. 248-54.
465. Grundemann, D. and E. Schomig, *Protection of DNA during preparative agarose gel electrophoresis against damage induced by ultraviolet light*. Biotechniques, 1996. **21**(5): p. 898-903.
466. Xia, Y., et al., *Analyses of HBV cccDNA Quantification and Modification*. Methods Mol Biol, 2017. **1540**: p. 59-72.
467. Schreiner, S. and M. Nassal, *A Role for the Host DNA Damage Response in Hepatitis B Virus cccDNA Formation-and Beyond?* Viruses, 2017. **9**(5).
468. Gomez-Moreno, A. and U. Garaigorta, *Hepatitis B Virus and DNA Damage Response: Interactions and Consequences for the Infection*. Viruses, 2017. **9**(10).
469. Boe, S.O., et al., *Promyelocytic leukemia nuclear bodies are predetermined processing sites for damaged DNA*. J Cell Sci, 2006. **119**(Pt 16): p. 3284-95.
470. van Hemert, F.J., et al., *Protein X of hepatitis B virus: origin and structure similarity with the central domain of DNA glycosylase*. PLoS One, 2011. **6**(8): p. e23392.
471. Oswald, A., *Application of in vitro transcribed mRNA to analyze hepatitis B virus infection and its targeting by CRISPR/Cas9* 2020.
472. S. Bolte, F.P.C., *A guided tour into subcellular colocalization analysis in light microscopy*. Journal of Microscopy, 2006. **224**: p. 213-232.
473. Miteva, M., et al., *Sumoylation as a signal for polyubiquitylation and proteasomal degradation*. Subcell Biochem, 2010. **54**: p. 195-214.
474. Lee, D.H. and A.L. Goldberg, *Proteasome inhibitors: valuable new tools for cell biologists*. Trends Cell Biol, 1998. **8**(10): p. 397-403.
475. Gartner, A. and S. Muller, *PML, SUMO, and RNF4: guardians of nuclear protein quality*. Mol Cell, 2014. **55**(1): p. 1-3.
476. Tatham, M.H., et al., *RNF4 is a poly-SUMO-specific E3 ubiquitin ligase required for arsenic-induced PML degradation*. Nat Cell Biol, 2008. **10**(5): p. 538-46.
477. Guo, Q., et al., *Origin of structural relaxation dependent spectroscopic features of bismuth-activated glasses*. Opt Express, 2014. **22**(13): p. 15924-31.

478. Fanning, G.C., et al., *Therapeutic strategies for hepatitis B virus infection: towards a cure*. Nature Reviews Drug Discovery, 2019.
479. Varadaraj, A., et al., *Evidence for the receipt of DNA damage stimuli by PML nuclear domains*. J Pathol, 2007. **211**(4): p. 471-80.
480. Dellaire, G., et al., *Promyelocytic leukemia nuclear bodies behave as DNA damage sensors whose response to DNA double-strand breaks is regulated by NBS1 and the kinases ATM, Chk2, and ATR*. J Cell Biol, 2006. **175**(1): p. 55-66.
481. Adamson, A.L. and S. Kenney, *Epstein-barr virus immediate-early protein BZLF1 is SUMO-1 modified and disrupts promyelocytic leukemia bodies*. J Virol, 2001. **75**(5): p. 2388-99.
482. Kim, W., et al., *DDB1 Stimulates Viral Transcription of Hepatitis B Virus via HBx-Independent Mechanisms*. J Virol, 2016. **90**(21): p. 9644-9653.
483. Xian, L., et al., *p53 Promotes proteasome-dependent degradation of oncogenic protein HBx by transcription of MDM2*. Mol Biol Rep, 2010. **37**(6): p. 2935-40.
484. Lin, Y., et al., *The transactivation and p53-interacting functions of hepatitis B virus X protein are mutually interfering but distinct*. Cancer Res, 1997. **57**(22): p. 5137-42.
485. Truant, R., et al., *Direct interaction of the hepatitis B virus HBx protein with p53 leads to inhibition by HBx of p53 response element-directed transactivation*. J Virol, 1995. **69**(3): p. 1851-9.
486. Lin, M.H. and S.C. Lo, *Dimerization of hepatitis B viral X protein synthesized in a cell-free system*. Biochem Biophys Res Commun, 1989. **164**(1): p. 14-21.
487. Xu, G. and S.R. Jaffrey, *Proteomic identification of protein ubiquitination events*. Biotechnol Genet Eng Rev, 2013. **29**: p. 73-109.
488. Mann, M. and O.N. Jensen, *Proteomic analysis of post-translational modifications*. Nat Biotechnol, 2003. **21**(3): p. 255-61.
489. Wilkinson, K.D., et al., *Metabolism of the polyubiquitin degradation signal: structure, mechanism, and role of isopeptidase T*. Biochemistry, 1995. **34**(44): p. 14535-46.
490. Parker, C.E., et al., *Mass Spectrometry for Post-Translational Modifications*, in *Neuroproteomics*, O. Alzate, Editor. 2010: Boca Raton (FL).
491. Lanouette, S., et al., *The functional diversity of protein lysine methylation*. Mol Syst Biol, 2014. **10**: p. 724.
492. Verger, A., J. Perdomo, and M. Crossley, *Modification with SUMO. A role in transcriptional regulation*. EMBO Rep, 2003. **4**(2): p. 137-42.
493. de Los Milagros Bassani Molinas, M., et al., *Optimizing the transient transfection process of HEK-293 suspension cells for protein production by nucleotide ratio monitoring*. Cytotechnology, 2014. **66**(3): p. 493-514.
494. Leonhardt, C., et al., *Single-cell mRNA transfection studies: delivery, kinetics and statistics by numbers*. Nanomedicine, 2014. **10**(4): p. 679-88.
495. Rettig, L., et al., *Particle size and activation threshold: a new dimension of danger signaling*. Blood, 2010. **115**(22): p. 4533-41.
496. Hemmi, H., et al., *A Toll-like receptor recognizes bacterial DNA*. Nature, 2000. **408**(6813): p. 740-5.
497. Steinle, H., et al., *Concise Review: Application of In Vitro Transcribed Messenger RNA for Cellular Engineering and Reprogramming: Progress and Challenges*. Stem Cells, 2017. **35**(1): p. 68-79.
498. Cha, M.Y., et al., *Stimulation of hepatitis B virus genome replication by HBx is linked to both nuclear and cytoplasmic HBx expression*. J Gen Virol, 2009. **90**(Pt 4): p. 978-986.
499. Flotho, A. and F. Melchior, *Sumoylation: a regulatory protein modification in health and disease*. Annu Rev Biochem, 2013. **82**: p. 357-85.
500. Liebelt, F. and A.C. Vertegaal, *Ubiquitin-dependent and independent roles of SUMO in proteostasis*. Am J Physiol Cell Physiol, 2016. **311**(2): p. C284-96.
501. van Driel, R., et al., *Nuclear domains and the nuclear matrix*. Int Rev Cytol, 1995. **162A**: p. 151-89.

502. Stuurman, N., et al., *The nuclear matrix from cells of different origin. Evidence for a common set of matrix proteins.* J Biol Chem, 1990. **265**(10): p. 5460-5.
503. Stuurman, N., et al., *A monoclonal antibody recognizing nuclear matrix-associated nuclear bodies.* J Cell Sci, 1992. **101 ( Pt 4)**: p. 773-84.
504. Wasag, P. and R. Lenartowski, *Nuclear matrix - structure, function and pathogenesis.* Postepy Hig Med Dosw (Online), 2016. **70**(0): p. 1206-1219.
505. Fu, C., et al., *Stabilization of PML nuclear localization by conjugation and oligomerization of SUMO-3.* Oncogene, 2005. **24**(35): p. 5401-13.
506. Berscheminski, J., et al., *Sp100A is a tumor suppressor that activates p53-dependent transcription and counteracts E1A/E1B-55K-mediated transformation.* Oncogene, 2016. **35**(24): p. 3178-89.
507. Wang, J., et al., *HBx regulates transcription factor PAX8 stabilization to promote the progression of hepatocellular carcinoma.* Oncogene, 2019. **38**(40): p. 6696-6710.
508. Diefenbacher, M. and A. Orian, *Stabilization of nuclear oncoproteins by RNF4 and the ubiquitin system in cancer.* Mol Cell Oncol, 2017. **4**(1): p. e1260671.
509. Thomas, J.J., et al., *RNF4-Dependent Oncogene Activation by Protein Stabilization.* Cell Rep, 2016. **16**(12): p. 3388-3400.
510. Rajput, P., S.K. Shukla, and V. Kumar, *The HBx oncoprotein of hepatitis B virus potentiates cell transformation by inducing c-Myc-dependent expression of the RNA polymerase I transcription factor UBF.* Virol J, 2015. **12**: p. 62.
511. Yen, C.J., et al., *Hepatitis B virus X protein (HBx) enhances centrosomal P4.1-associated protein (CPAP) expression to promote hepatocarcinogenesis.* J Biomed Sci, 2019. **26**(1): p. 44.
512. He, Y.J., et al., *DDB1 functions as a linker to recruit receptor WD40 proteins to CUL4-ROC1 ubiquitin ligases.* Genes Dev, 2006. **20**(21): p. 2949-54.
513. Wang, Y.T., et al., *Ubiquitination of tumor suppressor PML regulates prometastatic and immunosuppressive tumor microenvironment.* J Clin Invest, 2017. **127**(8): p. 2982-2997.
514. Bontron, S., N. Lin-Marq, and M. Strubin, *Hepatitis B virus X protein associated with UV-DDB1 induces cell death in the nucleus and is functionally antagonized by UV-DDB2.* J Biol Chem, 2002. **277**(41): p. 38847-54.
515. Leupin, O., S. Bontron, and M. Strubin, *Hepatitis B virus X protein and simian virus 5 V protein exhibit similar UV-DDB1 binding properties to mediate distinct activities.* J Virol, 2003. **77**(11): p. 6274-83.
516. Bergametti, F., D. Sitterlin, and C. Transy, *Turnover of hepatitis B virus X protein is regulated by damaged DNA-binding complex.* J Virol, 2002. **76**(13): p. 6495-501.
517. Lin-Marq, N., et al., *Hepatitis B virus X protein interferes with cell viability through interaction with the p127-kDa UV-damaged DNA-binding protein.* Virology, 2001. **287**(2): p. 266-74.
518. Schaefer, C. and B. Rost, *Predict impact of single amino acid change upon protein structure.* BMC Genomics, 2012. **13 Suppl 4**: p. S4.
519. Tan, G., et al., *Type-I-IFN-Stimulated Gene TRIM5gamma Inhibits HBV Replication by Promoting HBx Degradation.* Cell Rep, 2019. **29**(11): p. 3551-3563 e3.
520. Liu, N., et al., *HDM2 Promotes NEDDylation of Hepatitis B Virus HBx To Enhance Its Stability and Function.* J Virol, 2017. **91**(16).
521. Yavuz, A.S., N.B. Sozer, and O.U. Sezerman, *Prediction of neddylation sites from protein sequences and sequence-derived properties.* BMC Bioinformatics, 2015. **16 Suppl 18**: p. S9.
522. Gatel, P., M. Piechaczyk, and G. Bossis, *Ubiquitin, SUMO, and Nedd8 as Therapeutic Targets in Cancer.* Adv Exp Med Biol, 2020. **1233**: p. 29-54.
523. Li, J., et al., *Neddylation, an Emerging Mechanism Regulating Cardiac Development and Function.* Front Physiol, 2020. **11**: p. 612927.

524. Perez Berrocal, D.A., et al., *Hybrid Chains: A Collaboration of Ubiquitin and Ubiquitin-Like Modifiers Introducing Cross-Functionality to the Ubiquitin Code*. *Front Chem*, 2019. **7**: p. 931.
525. El Motiam, A., et al., *Interplay between SUMOylation and NEDDylation regulates RPL11 localization and function*. *FASEB J*, 2019. **33**(1): p. 643-651.
526. Leupin, O., et al., *Hepatitis B virus X protein stimulates viral genome replication via a DDB1-dependent pathway distinct from that leading to cell death*. *J Virol*, 2005. **79**(7): p. 4238-45.
527. Landsberg, C.D., et al., *A Mass Spectrometry-Based Profiling of Interactomes of Viral DDB1- and Cullin Ubiquitin Ligase-Binding Proteins Reveals NF-kappaB Inhibitory Activity of the HIV-2-Encoded Vpx*. *Front Immunol*, 2018. **9**: p. 2978.
528. Riviere, L., et al., *Hepatitis B virus replicating in hepatocellular carcinoma encodes HBx variants with preserved ability to antagonize restriction by Smc5/6*. *Antiviral Res*, 2019. **172**: p. 104618.
529. Abdul, F., et al., *Smc5/6 Antagonism by HBx Is an Evolutionarily Conserved Function of Hepatitis B Virus Infection in Mammals*. *J Virol*, 2018. **92**(16).
530. Wang, Z., W. Wang, and L. Wang, *Epigenetic regulation of covalently closed circular DNA minichromosome in hepatitis B virus infection*. *Biophysics Reports*, 2020. **6**(4): p. 115-126.
531. Guerrieri, F., et al., *Genome-wide identification of direct HBx genomic targets*. *BMC Genomics*, 2017. **18**(1): p. 184.
532. Lee, J.H., et al., *Impact of hepatitis B virus (HBV) x gene mutations on hepatocellular carcinoma development in chronic HBV infection*. *Clin Vaccine Immunol*, 2011. **18**(6): p. 914-21.
533. W. Hanel, L.T., D. Huszar, A. Prouty, X. Zhang, J. Helmig-Mason, B. Mundy-Bosse, Y. Youssef, S. Parekh, K. Maddocks, R. Baiocchi, L. Alinari, *Targeting Hypersumoylation in Mantle Cell Lymphoma*. *Blood*, 2019. **134**.
534. Cox, O.F. and P.W. Huber, *Developing Practical Therapeutic Strategies that Target Protein SUMOylation*. *Curr Drug Targets*, 2019. **20**(9): p. 960-969.
535. Hsia, C.C., H. Yuwen, and E. Tabor, *Hot-spot mutations in hepatitis B virus X gene in hepatocellular carcinoma*. *Lancet*, 1996. **348**(9027): p. 625-6.
536. Takahashi, K., et al., *Hepatitis B virus genomic sequence in the circulation of hepatocellular carcinoma patients: comparative analysis of 40 full-length isolates*. *Arch Virol*, 1998. **143**(12): p. 2313-26.
537. Kim, D.C., et al., *Clinicopathological characteristics of PIK3CA and HBx mutations in Korean patients with hepatocellular carcinomas*. *APMIS*, 2014. **122**(10): p. 1001-6.
538. Baptista, M., A. Kramvis, and M.C. Kew, *High prevalence of 1762(T) 1764(A) mutations in the basic core promoter of hepatitis B virus isolated from black Africans with hepatocellular carcinoma compared with asymptomatic carriers*. *Hepatology*, 1999. **29**(3): p. 946-53.
539. Iavarone, M., et al., *Characterisation of hepatitis B virus X protein mutants in tumour and non-tumour liver cells using laser capture microdissection*. *J Hepatol*, 2003. **39**(2): p. 253-61.
540. Yang, Z., et al., *Naturally occurring basal core promoter A1762T/G1764A dual mutations increase the risk of HBV-related hepatocellular carcinoma: a meta-analysis*. *Oncotarget*, 2016. **7**(11): p. 12525-36.
541. Chiu, A.P., et al., *HBx-K130M/V131I Promotes Liver Cancer in Transgenic Mice via AKT/FOXO1 Signaling Pathway and Arachidonic Acid Metabolism*. *Mol Cancer Res*, 2019. **17**(7): p. 1582-1593.
542. Leon, B., et al., *HBx M130K and V131I (T-A) mutations in HBV genotype F during a follow-up study in chronic carriers*. *Virol J*, 2005. **2**: p. 60.
543. Siddiqui, Z.I., et al., *A comparative study of hepatitis B virus X protein mutants K130M, V131I and KV130/131MI to investigate their roles in fibrosis, cirrhosis and hepatocellular carcinoma*. *J Viral Hepat*, 2017. **24**(12): p. 1121-1131.

- 
544. Iyer, S. and J.D. Groopman, *Interaction of mutant hepatitis B X protein with p53 tumor suppressor protein affects both transcription and cell survival*. Mol Carcinog, 2011. **50**(12): p. 972-80.
545. Melchior, F., M. Schergaut, and A. Pichler, *SUMO: ligases, isopeptidases and nuclear pores*. Trends Biochem Sci, 2003. **28**(11): p. 612-8.
546. Seeler, J.S. and A. Dejean, *SUMO: of branched proteins and nuclear bodies*. Oncogene, 2001. **20**(49): p. 7243-9.
547. Schorova, L. and S. Martin, *Sumoylation in Synaptic Function and Dysfunction*. Front Synaptic Neurosci, 2016. **8**: p. 9.
548. Kuroki, M., et al., *Arsenic trioxide inhibits hepatitis C virus RNA replication through modulation of the glutathione redox system and oxidative stress*. J Virol, 2009. **83**(5): p. 2338-48.
549. Shakoor, M.B., et al., *Human health implications, risk assessment and remediation of As-contaminated water: A critical review*. Sci Total Environ, 2017. **601-602**: p. 756-769.
550. Lin, C.C., et al., *Arsenic trioxide in patients with hepatocellular carcinoma: a phase II trial*. Invest New Drugs, 2007. **25**(1): p. 77-84.
551. Huber, A.D., et al., *The Heteroaryldihydropyrimidine Bay 38-7690 Induces Hepatitis B Virus Core Protein Aggregates Associated with Promyelocytic Leukemia Nuclear Bodies in Infected Cells*. mSphere, 2018. **3**(2).
552. Yeh, C.T., et al., *Cell cycle regulation of nuclear localization of hepatitis B virus core protein*. Proc Natl Acad Sci U S A, 1993. **90**(14): p. 6459-63.
553. Zhang, W., et al., *PRMT5 restricts hepatitis B virus replication through epigenetic repression of covalently closed circular DNA transcription and interference with pregenomic RNA encapsidation*. Hepatology, 2017. **66**(2): p. 398-415.
554. Paterlini, P., et al., *Selective accumulation of the X transcript of hepatitis B virus in patients negative for hepatitis B surface antigen with hepatocellular carcinoma*. Hepatology, 1995. **21**(2): p. 313-21.
555. Sheraz, M., et al., *Cellular DNA Topoisomerases Are Required for the Synthesis of Hepatitis B Virus Covalently Closed Circular DNA*. J Virol, 2019. **93**(11).
556. Zhao, D., et al., *Arsenic trioxide reduces drug resistance to adriamycin in leukemic K562/A02 cells via multiple mechanisms*. Biomed Pharmacother, 2011. **65**(5): p. 354-8.
557. Kumar, R. and K. Sabapathy, *RNF4-A Paradigm for SUMOylation-Mediated Ubiquitination*. Proteomics, 2019. **19**(21-22): p. e1900185.

---

## Patent, publications and meetings

**Patent pending:** Schreiner, Plank, Hofmann: **Internationale Patentanmeldung PCT/EP2020/080299**; New Means and Methods for Therapy and Diagnosis of DNA Virus Infections

### I. Articles in peer-reviewed journals

V. Plank, S. Hofmann, A. Oswald, U. Protzer, S. Schreiner (2021) **Regulation of Hepatitis B virus X protein function by host SUMOylation processes** (prepared manuscript)

V. Plank\*, S. Hofmann\*, A. Oswald, U. Protzer, S. Schreiner (2021) **ATO (Arsenic Trioxide) efficiently interferes with HBV infection** (prepared manuscript)

V. Plank, A. König, J. McKeating, U. Protzer, S. Schreiner (2021) **SAMHD1 is a novel restriction factor impairing human adenovirus infection** (prepared manuscript)

S. Hofmann, V. Plank, P. Groitl, N. Skvorc, L. Tübel, C. Ko, P. Zimmerman, D. Stadler, M. Nassal, U. Protzer, S. Schreiner (2021) **HBV core SUMOylation represents a novel functional switch to promote HBV cccDNA conversion at PML bodies** (in revision)

\* shared first authorship

---

## **II. National conferences**

### **2018 - 28th annual Meeting of the Society of Virology**

March 14-17, 2018, Würzburg, Germany

### **2018 – Joined retreat of the Institute of Virology, Immunology and Experimental Oncology 2018**

June 18-19, 2018, Herrsching, Germany

Poster presentation: Hepatitis B virus X (HBx) SUMOylation by the host cell regulates cccDNA establishment

### **2018 - TRR179 Determinants and dynamics of elimination versus persistence of hepatitis virus infection Retreat 2018**

November, 19-20, 2018, Heidelberg, Germany

Poster presentation, Hepatitis B virus X (HBx) SUMOylation by the host cell regulates cccDNA establishment

### **2019 - 29<sup>th</sup> annual Meeting of the Society of Virology**

March, 20-23, 2019, Düsseldorf, Germany

Oral presentation: Hepatitis B virus X (HBx) SUMOylation by the host cell regulates cccDNA establishment; **Travel grant award**

### **2019 - SFB IRTG retreat PhD and Post-Doc Retreat, DFG TRR 179**

May, 27-29, 2019, Freiburg, Germany

Oral presentation: Hepatitis B virus X (HBx) SUMOylation by the host cell regulates cccDNA establishment

### **2019 - Retreat of the Institute of Virology 2019**

June 17-18, 2019, Herrsching, Germany

Oral presentation: HBx first, make SUMO great again

---

## **2021 - 30th annual Meeting of the Society of Virology**

March 24-26, 2021, Hannover, Germany

Poster presentation: **SAMHD1 is a novel restriction factor impairing human adenovirus infection (planned)**

### **III. International conferences**

#### **2018 International HBV Meeting – The Molecular Biology of Hepatitis B Viruses**

October 03-06, 2018, Taormina, Italy

Poster presentation: Hepatitis B virus X (HBx) SUMOylation by the host cell regulates cccDNA establishment

#### **2019 International HBV Meeting – The Molecular Biology of Hepatitis B Viruses**

October 01-05, 2016, Melbourne, Australia

Oral presentation: HBx SUMOylation promotes DDB1 binding and efficient host substrate degradation; **Travel grant award**

#### **2020 International HBV Meeting – The Molecular Biology of Hepatitis B Viruses**

Toronto, Canada postponed to September, 13-17, 2021, **Registration**

### **IV. Participation in courses/workshops**

October 09-10, 2018 **Erfolgreiche Kommunikation im Arbeitsalltag**

November 27-28, 2018 **Graphic design and life science figures**

December 06, 2018 **Erste-Hilfe Ausbildung**

May 09, 2019 **Biostatistik mit Graphpad Prism**

September 18, 2019 **Zitieren statt plagieren**

December 12, 2019 **Advanced training seminar in accordance with §15 GenTSV for project managers and assigned persons for biological security**

November 26 and December 10, 2020 **Self-positioning and systematic career development**

---

## Acknowledgement

First of all, I would like to thank my first supervisor Prof. Dr. Sabrina Schreiner for giving me the opportunity to do my PhD thesis in her research group and that I could work on such an interesting, challenging and important project. I'm especially thankful for her guidance and support and during the whole time and giving me the chance to present my work at several national and international conferences. Likewise, I am grateful to Prof. Dr. Percy Knolle for his disposability as second supervisor and his valuable input during my thesis committee meetings. Further, I would like to thank Prof. Dr. Andreas Pichlmair for being part of my thesis committee and offering precious help on the project. Additionally, I want to acknowledge Prof. Dr. Ulrike Protzer and for her support and constructive discussions and suggestions.

Moreover, I would like to thank the Jürgen Manchot Stiftung for giving me the facility to conduct my PhD thesis, by funding my work. Special thanks go to my lab colleagues from the Munich lab for support and help in the lab as well as the good scientific discussions: Peter Groitl, Christina Weiß, Lilian Göttig, Miona Stubbe Anna Hofferek, Maryam Karimi and Ute Finkel. Furthermore, I also want to thank all the current and former members of the Institute of Virology for supporting me during my PhD thesis, especially Daniela Stadler, Chunkyu Ko and Andreas Oswald. Not to forget also the Hannover team: Samuel Hofmann, Sawinee Masser, Julia Mai and Ilka Simons.

Of course, I want to thank my family, especially my wonderful mother, for the constant support. You always helped me without asking as a matter of course. Finally, I especially thank Andi for his tremendous support concerning IVT mRNA but particularly my well-being. I am deeply grateful for all your support, inspiration, motivation and faith in me!